Università degli Studi di Firenze

DIPARTIMENTO DI MECCANICA E TECNOLOGIE INDUSTRIALI

DOTTORATO DI RICERCA IN PROGETTO E SVILUPPO DI PRODOTTI E PROCESSI INDUSTRIALI

SETTORE SCIENTIFICO DISCIPLINARE ING-IND/14

CICLO XXV

CONCEPT MODELING TECHNIQUES FOR THE DESIGN OF AUTOMOTIVE STRUCTURES

DOTTORANDA:

ING. PAVLINA GEORGIEVA BRANDISKA

TUTOR:

DOTT. ING. NICCOLÒ BALDANZINI

CONTRORELATORE:

DOTT. ING. LUC CREMERS

COORDINATORE DEL DOTTORATO:

PROF. ING. MARCO PIERINI

ANNI 2010/2012

"Simplicity is the ultimate sophistication."

Leonardo da Vinci

To Kosta – my inspiration and love

Abstract

During the last decades the overall trend in the automotive industry has been to shorten the design cycles and decrease the production costs while increasing the product quality with respect to competitors. In such a context there is an ever growing need for analysis that leads the design process from the concept phase onward. On the other hand, a conventional Finite Element (FE) model of a vehicle can be created only when its detailed Computer-Aided Design (CAD) model is available, which automatically excludes obtaining early stage simulation results. In this sense novel Computer-Aided Engineering (CAE) methodologies are required to support the concept modeling and optimization of vehicles.

This challenge defines the main framework of the research in the present dissertation. The leading motivation is to introduce new improvements and developments in the field of CAE concept approaches. The focus is put on the design of the car structure. The main objective is to obtain in an efficient way accurate early stage predictions of its static and low frequency dynamic behavior by means of FE concept models. Predecessor-based concept modeling methods, which start from the reference FE model of an existing car and aim at achieving variant or incremental improvements of it, are addressed. Developments in regard to two main groups of techniques are introduced: methods based on simplified FE models of the vehicle structure and methods based on mesh morphing.

The related achievements are presented in this dissertation. To begin with, the current challenges of 1D beam concept modeling have been thoroughly investigated. Guidelines have been given on good practices to overcome the intrinsic limitations of the existing techniques and to make them more accurate and reliable. Beam Bounding Box has been proposed as a novel approach for 1D beam concept modeling and optimization handling, which is accurate, computationally beneficial, easy to implement and to apply. Furthermore superelement joints have been introduced as means for the creation of more accurate simplified FE models. A major breakthrough has been achieved in the field of sizing optimization by identifying, improving, implementing and validating successfully Differential Evolution (DE) as an advanced alternative to the state-of-the-art gradient-based methods. Finally, surrogate modeling based on mesh morphing of predecessor FE models has been introduced as another option to enable fast modification and optimization studies in the concept stage. The added value of all these contributions in the automotive engineering practice has been demonstrated by their application on a number of realistic industrial case-studies throughout the dissertation.

Table of contents

List of figures

List of tables

List of symbols

$\approx$	Is approximately equal to
$\bullet^{-1}$	Inverse of $\bullet$
$\bullet^{T}$	Transpose of $\bullet$
$\exists$	Exists
$\forall$	For all
ν	Poisson's ratio
ϕ	Eigenvector
ρ	Mass density
σ	Standard deviation
$\vee$	Disjunction (or)
$\wedge$	Conjunction (and)
$\widehat{\bullet}$	Approximation of $\bullet$
C_w	Warping constant
$f_{1^{\mathbf{st}}b}$	Eigenfrequency of the first bending mode
$f_{1^{\mathbf{st}}t}$	Eigenfrequency of the first torsional mode
I_{XX}, I_{YY}, I_{ZZ}	Principal moments of inertia
J_{xx}, J_{yy}	Area moments of inertia
J_{xy}	Cross-product of inertia
J_{zz}	Torsional stiffness parameter
K_b	Static bending stiffness
K_t	Static torsional stiffness
$max\bullet$	Maximum of $\bullet$

$min\bullet$	Minimum of $\bullet$
R^2	Coefficient of determination
R^2_{adj}	Adjusted coefficient of determination
A	Cross-sectional area
C	Constant
d	Diameter
E	Young's modulus
F	F-statistic
F	Force
G	Shear modulus
h	Height
M	Moment
m	Mass
t	Thickness
w	Width

List of abbreviations

1D	One-Dimensional
2D	Two-Dimensional
3B	Beam Bounding Box
3D	Three-Dimensional
ABCS(s)	ArBitrary Cross-Section(s)
ACO	Ant Colony Optimization
ALGA	Augmented Lagrangian Genetic Algorithm
ANN(s)	Artificial Neural Network(s)
ANOVA	ANalysis Of VAriance
ARMOGA	Adaptive Range Multi-Objective Genetic Algorithm
BIW	Body-In-White
BJP	Beam, Joint and Panel
CAD	Computer-Aided Design
CAE	Computer-Aided Engineering
CMS	Component Mode Synthesis
COMAC	CO-ordinate Modal Assurance Criterion
CS	Cross-Section
DE	Differential Evolution
DOE	Design Of Experiment
DOF(s)	Degree(s) Of Freedom
EA(s)	Evolutionary Algorithm(s)
EBBT	Euler-Bernoulli Beam Theory
EC	Evolutionary Computation
ES	Evolution Strategy
FE	Finite Element
FEA	Finite Element Analysis
FEM	Finite Element Method
FRAC	Frequency Response Assurance Criterion

FRF(s)	Frequency Response Function(s)
GA(s)	Genetic Algorithm(s)
GB	Gradient-Based
GNCS(s)	GeNeric Cross-Section(s)
IAPP	Industry-Academia Partnerships and Pathways
ICDM	In-plane Cross-section Deformation Measure
ITN	Initial Training Network
KBE	Knowledge-Based Engineering
LHS	Latin Hypercube Sampling
MAC	Modal Assurance Criterion
MBS	Multi-Body Simulation
MC	Marie Curie
MDO	Multi-Disciplinary Optimization
MMA	Method of Moving Asymptotes
MMFD	Modified Method of Feasible Directions
MOGA	Multi-Objective Genetic Algorithm
MOI	Moment(s) Of Inertia
MPC(s)	Multi-Point Constraint(s)
NCAC	National Crash Analysis Center
NLP	NonLinear Programming
NN(s)	Neural Network(s)
NPGA	Niched Pareto Genetic Algorithm
NSGA	Non-dominated Sorting Genetic Algorithm
NURBS	Non-Uniform Rational B-Splines
NVH	Noise, Vibration and Harshness
OEM(s)	Original Equipment Manufacturer(s)
OF(s)	Objective Function(s)
OFAT	One-Factor-At-a-Time
PSO	Particle Swarm Optimization
QA	Quantum Annealing
RPC	Remote Parameter Control
RS(s)	Response Surface(s)
RSM	Response Surface Methodology
RVAC	Response Vector Assurance Criterion

SA	Simulated Annealing
SE(s)	SuperElement(s)
SLP	Sequential Linear Programming
SOP	Start Of Production
SQP	Sequential Quadratic Programming
SSS	Simple Structural Surface
STCS(s)	STandard Cross-Section(s)
TBT	Timoshenko Beam Theory
TS	Tabu Search
VAM	Variational Asymptotic Method
VCM	Vehicle Concept Modeling
VDP	Vehicle Development Process
WBS	Wave-Based Substructuring

Chapter 1

Introduction

1.1 The vehicle development process

1.1.1 Overview

Nowadays the vehicle development process (VDP) constitutes a complex set of activities which employ significant amount of resources for long periods of time. It has to respond to the steadily increasing customer demands while facing often conflicting design criteria and legislations. Because of the higher number of requirements, more and more functional performance attributes have to be addressed during the VDP. Consequently, various engineering disciplines are subject to in-depth study such as crashworthiness, driving dynamics, durability, structural statics and dynamics, interior and exterior acoustics, aerodynamics, electromagnetic compatibility, and many others. The car itself becomes more and more complex, with a higher number of features and functions. On the other hand, the market has a competitive nature – innovative designs must be developed and brought to market before a competitor does. Moreover, improved product quality must be reached at lower costs and possibly with minimized risk.

All this would not have been possible without the aid of the virtual prototyping. Computer-aided design (CAD) and computer-aided engineering (CAE) systems are an integral part of the modern automotive product development. In the recent years they have not only helped to shorten the time-to-market and improve the vehicle quality, but also to reduce the number of physical prototypes to an ever growing extent. Containing both geometric and functional data, virtual cars enable fast prototype build and increase the efficiency of the VDP, the latter being one of its main driving factors. In regard to virtual engineering three major phases can be distinguished in function of the available product knowledge [1–3] (Fig. 1.1):

- **Concept stage (pre-CAD engineering).** In this stage the detailed CAD data is still not available, so the amount of information is limited. On the other hand, the degrees of freedom (DOFs) for decisions are high (Fig. 1.1) and large design changes can be realized. As design alternatives must be evaluated under uncertainties and lack of knowledge, it is sufficient if a principle structure is identified, which gives the right balance between all aspects.

This can be achieved either on the basis of engineering experience, or, preferably, by the use of concept CAE techniques.

- **Detailed stage (in-process CAD engineering).** This phase comprises the development of the detailed CAD model of the full vehicle and its validation through CAE simulations. As it can be seen from Fig. 1.1, while the model complexity increases, the design space becomes smaller. In addition, each change in the CAD model can affect various functional performance attributes and thus the CAE model must be continuously updated. These iterations between design and simulation must be as fast as possible.
- **Refinement stage (post-CAD engineering).** This stage comprises the design validation after freezing the detailed CAD model, when only slight modifications are possible. Any changes in this phase are performed on an already improved design. On one hand, the first experimental results become available and can be used to correct the CAE models accordingly, if needed. On the other hand, CAE can be helpful for problem solving and in-depth study of the issues identified during testing.

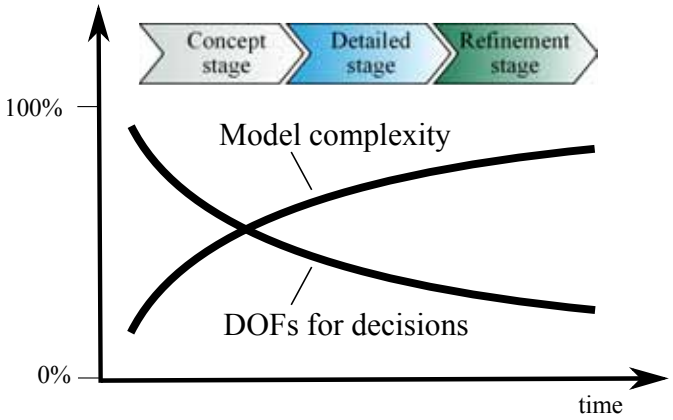

Figure 1.1: Model complexity and DOFs for decisions versus time.

1.1.2 The V-cycle

In addition to the horizontal time line division by stages, the VDP can be represented as a V-shape process (Fig. 1.2). Having its origins in software development, this kind of representation is commonly used also in the automotive industry [1, 4]. The vertical dimension of this so-called V-cycle is divided by levels, which from top to bottom correspond to vehicle, subsystem and component level. First the overall vehicle targets are defined on the basis of the requirements analysis (at the top of the "V"). The final performance targets are then cascaded down into targets for subsystem and subsequently for component design (left branch of the "V"). This process is complex as functional targets at component level are not always independent. They must be thus handled in a multi-attribute context instead of

chain-like downward cascading. After that virtual and physical validation is performed in hierarchical order of the components, of the subsystems and finally of the full vehicle (right branch of the "V"). Today's vehicles comprise important and complex subsystems such as the driveline, the engine, the chassis and the body. Various functional performance attributes must be considered for each of them. Thus in practice the V-diagram breaks down into a number of development cycles for each of the core subsystems. They are partly parallel and partly in series, with synchronization between them.

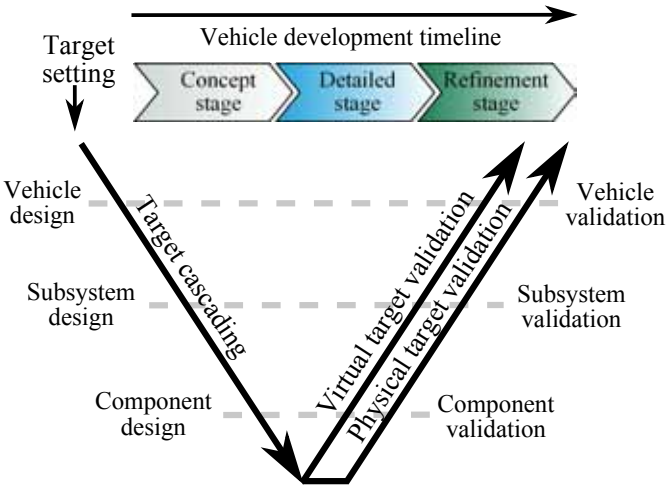

Figure 1.2: The V-cycle.

1.1.3 Traditional versus new paradigm

The trend to shorten the development cycles, to cut the costs and to reduce the number of physical prototypes has led to an ever growing integration of virtual engineering in the VDP. The rapid evolution of both software and hardware has improved the stability, reliability, and the effectiveness of numerical simulation in the field of car design. Nowadays however, it is important that its integration takes place at all stages, starting from the concept one. Simulation-driven product development is needed so that early-stage predictions of the various performance attributes can be made and adequate design decisions can be taken. The sooner this happens, the cheaper their implementation and the bigger their impact on the final design. As stated by the "rule of ten" [5, 6], the costs caused by a design change increase by a factor of 10 from phase to phase. Thus the cost of a change due in the concept phase increases 10 times in the detailed engineering stage, 100 times in the pre-series stage, 1000 times during series development, and 10000 times after start of production (SOP) . To minimize the risk of late changes and the related costs, product maturity must be achieved as early as possible.

Fig. 1.3 illustrates the traditional and the new paradigm of vehicle development. The main differences between these two processes concern above all the

concept and detailed stages.

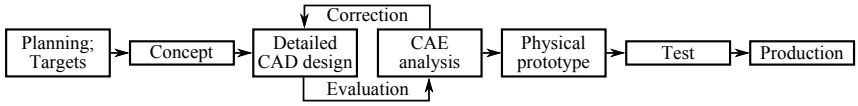

(a) Traditional.

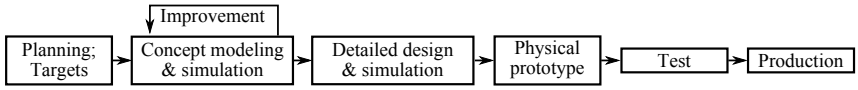

(b) New.

Figure 1.3: VDP paradigms.

The traditional VDP includes various iterations between the detailed CAD and CAE models (Fig. 1.3(a)). After a change in the CAD design, the CAE model must be updated so that the performance attributes under study can be reassessed. However, this transition is not straightforward, because of the historical disconnection between CAD and CAE [7]. While Finite Element Analysis (FEA) in engineering had its origins in the 1950s and 1960s, CAD was developed later – in the 1970s and 1980s. Nowadays CAD is a much bigger industry than CAE, although the major Finite Element (FE) programs were technically mature long before modern CAD was widely adopted. The gap between CAD and CAE resulted in quite different geometric representations. Despite the efforts for automatic meshing and assembly techniques the generation of FE mesh based on the CAD design is costly, time consuming and can create inaccuracies. In addition, the numerical simulation of detailed FE models at full vehicle level typically requires considerable computational efforts. Finally, one integrated software package is almost never used by the Original Equipment Manufacturers (OEMs) for all the activities of the detailed CAD-CAE phase. A heterogeneous environment is more common in which geometry creation, mesh generation, pre-processing, analysis and post-processing are performed by means of different software tools. The main reason is that even if an integrated environment exists, the included software tools are not necessarily the best in class.

Because of all these difficulties and the ever increasing importance of the analysis in the initial concept stage, a paradigm shift has been taking place over the last years from CAD- to CAE-centric product development. This advanced VDP (Fig 1.3(b))) aims at the use of upfront CAE tools in order to perform analysis already in the concept stage, i.e. the idea of "analysis leads design" [1, 8]. As a better product is obtained before the detailed engineering phase, the initial CAD design is also improved. Hence the lengthy iterations between CAD and CAE are reduced as much as possible and the design cycle is shortened. Furthermore, the chances to achieve a "design right first time" and to manufacture only a single prototype increase.

The benefits of CAE front-loading are illustrated in Fig. 1.4. It can increase significantly the product knowledge early in the design process. Moreover, various design alternatives can be evaluated and the optimal one can be selected. Finally,

the product performance can be optimized faster and at lower cost. Although there will be still some changes to make later on in the VDP, the risk is decreased by orders of magnitude.

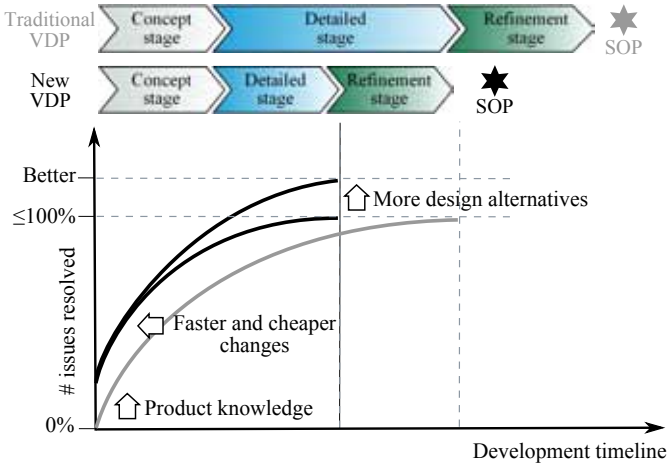

Figure 1.4: Benefits of CAE front-loading.

Although vehicle concept modeling (VCM) is increasingly recognized as an important part of the modern virtual prototyping process, many difficulties are still encountered. The following major bottlenecks must be overcome:

- **Speed-up.** Given the short duration of the initial concept phase, fast exploration of the design space is needed or otherwise the application of VCM will be limited. Computationally efficient methodologies are a must in order to decrease the time and the resources needed to prepare and perform the concept study. Moreover, it is crucial to quickly generate and modify the concept models without CAD availability.
- **Accuracy.** VCM is expected to provide accurate and reliable predictions, so that the risk of unexpected changes later on can be minimized. This requirement is in conflict with the speed-up of the concept phase. In general, the more product knowledge there is and the more detailed the model, the more precise are the simulation results. On the other hand, there is a lack of detailed knowledge during the concept stage and a lot of uncertainties. In addition, it is easier to perform fast concept studies by means of more simplified models. Ideally a compromise must be achieved between accuracy and speed-up.
- **Concept models.** The definition of concept models is a challenge itself. As a standard, FE models are detailed and are based on detailed CAD models of the different components. Thus during the creation of the simplified simulation models the design engineers are compelled to rely mainly on their experience and, if available, on the predecessor data of already existing models.

- **Dedicated software tools.** Each development phase requires modeling and simulation tools having an adequate level of complexity in order to comply with its corresponding targets and the available time frame. In the early design stage software packages are needed that are flexible enough and do not need the complete and detailed data of the vehicle to define its numerical model. Furthermore, this model must be parametric so that it can be easily changed during modification or optimization studies. This is not a simple task, as the traditional CAE tools are based on detailed CAD designs which has impeded their tight integration in the concept stage so far. Another hold-back is that these concept CAE tools must preferably have a wider scope regarding the included concept methodologies and the performance attributes under consideration.

Facing all these challenges and finding a solution for them is still an ongoing process. Being a fundamental change, the new paradigm of vehicle development needs further efforts to be put in the development of fast, accurate and reliable concept methodologies.

1.2 The vehicle structure

1.2.1 Introduction

The structure is one of the fundamental subsystems of a vehicle which contributes significantly to its development and manufacturing cost [9]. Its main goal is to maintain the car shape and to support the various static and dynamic loads applied to it. The vehicle structure consists of chassis frame and body shell. In modern cars the most common type of structure is the unitary (or integral) body [9, 10], in which the chassis parts cannot be physically removed from the upper body parts. The structural integration of both is considered as a mean to obtain good performance at a reduced mass. Moreover, the uni-body is well suited to mass production methods. Most of the panels and body components are still stamped from sheet steel [9, 10] and then fixed together mainly by spot welding [9]. A comprehensive reading related to the vehicle structure can be found in [9–14].

The following functions (not ranked by priority) must be achieved by the completely assembled structure [10, 11]:

- aesthetics;
- appearance;
- ergonomics;
- roominess;
- thermal comfort;
- acoustic comfort;
- vibration comfort;
- dynamic performance;

- handling;
- aerodynamics;
- safety;
- structural integrity;
- durability.

Moreover, the body must have high reliability and at the same time low cost. High recyclability of the materials must be also ensured.

When it comes to the vehicle structural performance the term body-in-white (BIW) is often used. It refers to the main body of the vehicle as assembly of a frame and panels, after the welding of its sheet metal components, but before painting and before adding the powertrain, the suspensions and any non-structural detachable parts such as moving parts (e.g. doors, deck lids, hoods, fenders) and trim (e.g. glass, seats, upholstery, electronics). The main idea is to exclude all parts with small or no stiffness contribution. Some OEMs denote with the term BIW the steel body-in-white together with the windscreens, because of their importance for the car stiffness. Fig. 1.5 shows a vehicle BIW and some commonly used terms. The roof panel is hidden in order to visualize better some of the components.

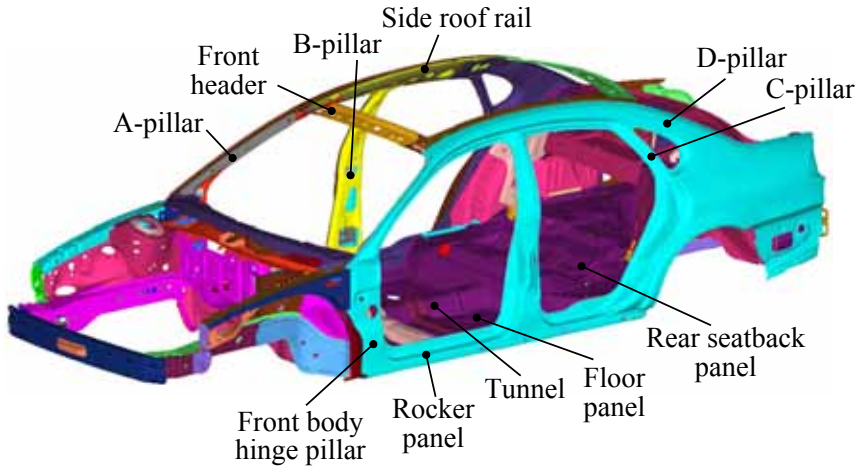

Figure 1.5: Ford Taurus BIW.

1.2.2 Basic performance attributes

The main and most important function of the unitary body is structural. Therefore the following basic performance attributes related to the structure are discussed in this section: the strength, the stiffness and the vibration behavior of the car. They are used to assess the performance of a vehicle structure and choose between different structural concepts under the additional constraints of

mass, cost, method of production, product application and others [9]. Other crucial criteria, such as crashworthiness, are not treated hereby as they are out of the scope of this dissertation.

Strength

The strength of a vehicle structure can be defined as the maximum force that it can withstand. The unitized body must be sufficiently strong independently of the various load cases to which it might be subjected so that no loss of function occurs. If the vehicle structure and all its parts maintain their functions when subjected to road loads, a good strength performance is achieved. There are two factors which can potentially cause loss of function: instantaneous overloads due to extreme load cases and fatigue damage [9]. Therefrom, instantaneous and fatigue strength must be assessed and monitored in the process of vehicle development.

Instantaneous overloads are related to short duration transient events with high amplitudes [15], e.g. driving over large pits, hitting the curbs of side walks, braking suddenly on high friction ground or starting up in low gear [14]. Instantaneous failure may be caused by failure of joints, by overstressing of components beyond the elastic limit or by their buckling when subject to compression or shear [9]. On the other hand, fatigue loads are characterized by complex time histories with lower amplitudes but a greater number of occurrences (a number of cycles in the order of 10^4 to 10^5) [15], e.g. driving on bumpy roads with almost full loads [14].

Fatigue life estimation requires detailed stress analysis and consequently considerable knowledge at component level, which is unavailable in the concept stage. For this reason the assessment of fatigue strength is only performed from the detailed engineering stage onward. In the concept phase it is usually assumed that if the structure can resist the (rare) worst possible loading, then its fatigue life is more likely to be satisfactory [15]. The main interest and efforts are thus focused on instantaneous strength. To ensure that the structure will not fail in service due to instantaneous overload, the vehicle designer needs to know the worst or most damaging loads to which the structure is likely to be subjected [15]. The actual dynamic loading on the vehicle is often replaced by a "factored static loading" multiplied by an optional safety factor [15]:

equivalent dynamic load = (static load) x (dynamic load factor) x (safety factor)

To apply this approach, certain load cases must be defined. This is not an easy task as the loads experienced by the body are variable and sometimes unpredictable. Additionally, each company has its own load factors, based on the experience with successful designs. The load cases in the concept phase are usually gross simplifications of the real complex road loading events [15] and must be updated as soon as more information is available. At a first try global road load cases are defined [15], in which the whole structure is affected. Five basic load cases are usually considered, the first three of which are the most important ones [16]: bending, torsion, combined bending and torsion, lateral and, finally, fore and aft loading. Local load cases are added later on as the design evolves. All these load cases generate stresses throughout the whole vehicle structure. It is thus important

that the stress level under the worst load conditions is kept well beyond the yield stress [16].

Stiffness

Stiffness can be defined as the force needed to achieve certain deformation of the structure [17]. For structures in the elastic range it is actually the slope of the load versus deflection curve [9]. The structural stiffness of the vehicle is fundamental for its handling and vibrational behavior [9, 14]. It must be sufficiently high so that deformations due to extreme loads are limited and do not deteriorate the vehicle operation. Low stiffness might be the cause of various problems such as, for instance, impeded opening or closing of the doors, altered kinematic behavior of the suspensions, unacceptable vibrations (e.g. scuttle shake) [14].

Mainly two load cases are used as benchmarks for the global car body stiffness [9, 11, 14, 18]:

- **Bending stiffness K_b.** The global bending test replicates the load due to passengers, luggage and vertical accelerations [11]. The body is normally constrained at the front and rear shock towers [18]. The forces are applied at the front seats [18] or near the center of the wheelbase [9, 11]. The static bending stiffness is typically defined as the ratio of the applied load to the maximum deflection along the rocker panel and the tunnel beam [18]. It is relatively easy to reach satisfactory values of K_b, except for very long vehicles [14]. According to [14] the targets for K_b are considered reasonable if in the range from $7E6$ to $10E6N/m$.
- **Torsional stiffness K_t.** The global torsion test replicates a vehicle parked with just one wheel on a sidewalk [11, 14]. The body is normally constrained at its rear shock towers [14, 18]. Torque is applied as equal and opposite couples acting on the suspension mounting points at the front [14, 18]. The torsion angle can be determined as the resulting deformation angle between the front and rear shock towers [18]. The static torsional stiffness can be thus defined as the ratio of the applied moment and the torsion angle [11, 18]. In [14] the targets for K_t are considered reasonable if in the range from $7E5$ to $15E5Nm/rad$.

  It is more difficult to achieve high torsional stiffness than high bending one [9, 14]. Consequently, K_t is used as a benchmark for the performance of the vehicle structure. Cars of different size can be compared based on K_t if it is first divided by their wheel base or overall length [11, 14]. Additionally, the quality of a vehicle structure can be assessed based on the ratio between its torsional stiffness and its mass.

K_b and K_t can be evaluated both experimentally and numerically. The experimental setup is based on the same static deformation test bench for both tests, which is easily reconfigured thanks to the similarity between the load cases [11, 14]. In both cases precautions are taken to avoid the influence of local deformations where loads are applied.

The numerical and experimental assessments of K_b and K_t have to face the lack of standardized procedure used by all OEMs. The test setup, load application and constraints for the K_b and the K_t load cases can differ from one car manufacturer to another. On the other hand, the global static stiffness depends strongly on the boundary conditions and the force application, which makes the comparison of K_b and K_t for different vehicles a difficult task.

The evaluation of K_b and K_t is often repeated at different assembly stages – from the BIW to the fully assembled vehicle, including interiors, powertrain and suspensions [11]. In this way the contribution of removable parts, glass and other components to the global vehicle stiffness can be assessed. The parts subjected to higher deformations can be then identified and optimized to increase both the overall stiffness and the reliability of the structure [11].

Vibration behavior

Noise, vibration and harshness (NVH) are becoming more and more important factors in vehicle design as a result of the accelerated development of new and highly refined vehicles. In recent years, the customer expectations for quality and vehicle comfort have increased. Moreover, noise pollution has become a subject to legislation. Finally, the trend towards lighter vehicles (i.e. reduced fuel consumption) has resulted in more potential noise and vibration problems.

Vibration has always been an important issue closely related to reliability and quality. Controlling it is not an easy task as, unlike many machine systems, motor vehicles have several sources of vibration which are interrelated and speed dependent. The vibration in a vehicle arises mainly from continuous periodic or random disturbances, e.g. rotor imbalance, road inputs to suspensions and many others [16]. The main sources of dynamic excitation and thus vehicle vibration are the wheels, the engine and the driveline [13].

The global vibration behavior of a vehicle is directly related to its natural frequencies and mode shapes. The car body modes can be divided in global and local. A local mode concerns only a part of the structure where most of its elastic energy is concentrated, while a global mode involves the whole structure in which the associated elastic energy is uniformly distributed [11]. Because of their nature, local modes are much easier to damp than global ones. Fig. 1.6 illustrates two of the global mode shapes of a Ford Taurus BIW.

Being a continuous structure, the car body has an infinite number of normal modes. Its eigenfrequencies range from several tens of Hz for the global modes to several kHz for the local modes of relatively small and stiff structural parts. Due to the complexity of the structure the resonances can result concentrated in certain frequency ranges. Thus the BIW has from 150 to 250 modes below 200 Hz [11]. The dynamic analysis of a vehicle is traditionally focused on the low frequency range as higher eigenfrequencies are more highly damped.

A better vibration comfort can be achieved if global and local resonances are avoided. Moreover, the worst possible resonance situation must be prevented, in which there is a coincidence of the natural mode shape and the excitation mode shape at the same frequency. For this purpose the eigenfrequencies and the harmful

(a) Global vertical bending at 32.05 Hz.

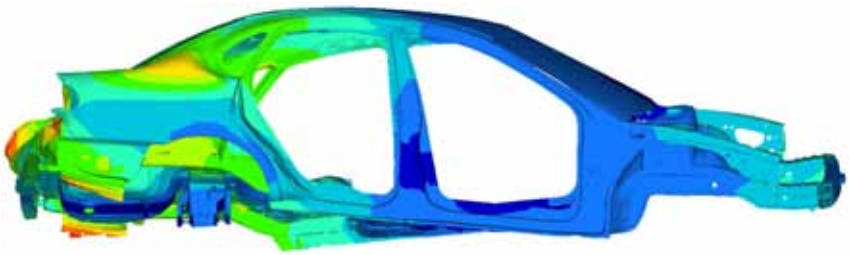

(b) Global torsion at 35.06 Hz.

Figure 1.6: Mode shapes of a Ford Taurus BIW.

excitation frequencies must be kept apart by a factor of $\sqrt{2}$ [4]. If for some reason this is not achieved, possible solutions can be: to increase the global static stiffness with respect to wheelbase and body mass, to shift the resonance frequencies by means of struts or the application of absorbers, or to decrease the total mass with respect to the body size [4]. Local resonances are usually easier to deal with than global ones. There are various countermeasures [13]: increasing the stiffness of the system; increasing its damping; reducing the amplitude of the excitation at the source; adding dampers close to the zones affected by vibration; preventing vibration transmitted from the source to the resonant element.

An important stage in improving the NVH performance is the proper target setting. This process is often based on the benchmark tests of competitor cars of the same or higher category as well as on the test of predecessor products [1, 19]. While obtaining information on the feasible performances, design bottlenecks can be also identified. There are also other ways to define the targets such as concept CAE analysis or customer surveys [1]. The most commonly used structural NVH targets include global and component eigenfrequencies and mode shapes, as well as frequency response functions (FRFs) [1]. They can be defined regarding the structural performance of the BIW, the trimmed body or the full vehicle. The global modes are of primary interest for VCM [1]. Often the eigenfrequencies of the first and second global bending and torsional modes are considered as benchmarks of the vehicle performance during the concept phase. FRFs at customer relevant locations can be also a subject of early stage studies.

1.2.3 FE modeling

The role of virtual prototyping has increased drastically during the last decades. As underlined in Section 1.1.3, CAE methodologies are of leading importance for the VDP. The focus of this dissertation is on the Finite Element Method (FEM), being the state-of-the-art method for structural analysis (e.g. statics, low frequency dynamics, etc.). Therefore some aspects of FE modeling for the car body are discussed further on in this section. Two main categories of FE models of the vehicle structure can be distinguished [1, 16]: simplified and detailed ones.

Detailed FE models

The car body is composed by hundreds of individual components having relatively complex geometry and different properties. They all have to be included in the detailed CAD and then in the detailed FE model. Fig. 1.7 shows a zoomed view of a BIW FE model. As it can be seen, this representation is highly detailed. For example, even the beads on the floor and rear seatback panels are included as they are important for local stiffening.

Figure 1.7: Zoomed exploded view of a Ford Taurus BIW.

It is not appropriate to use solid elements for the mesh of the car body because of the geometrical complexity and the small thickness (normally ranging from 0.6 up to 5 mm) that characterize most of its parts. To reduce the mesh complexity in terms of elements and nodes, the body components are typically meshed with linear and quadratic shell elements. If detailed local stresses must be assessed, higher-order elements can be also used (p-type refinement). Naturally, the decrease of the element size increases the model accuracy too (h-type refinement). Regarding the frequency range of validity, for dynamic analysis the mesh must be such as to have 6 to 10 linear elements per wavelength. For geometry of arbitrary complexity, typically a mixed mesh is generated in which the quadrilateral shell elements are considerably more than the triangular ones [1]. Despite the latest improvements in the automatic mesh generation algorithms, some user interaction is often required to obtain an optimal mesh.

The connections between the different parts must be given special consideration. Spot welds are fundamental as they are the most common connection type in the BIW. A generic model must be selected for use throughout the structure which gives the right balance between computational cost and accuracy. This choice is strongly conditioned by the performance attribute of interest. For example, spot weld models with coarser mesh are preferred for global statics and dynamics, as well as optimization, while they are not suitable for fatigue life assessments. Other common BIW connections include seam welds (modeled with rigid elements) and glue (modeled with hexahedral or linear spring elements) [1].

The correlation between detailed CAD and FE models is very close in terms of geometry, materials and interface conditions between the various components [11]. The high level of detail allows the prediction both of global and local structural characteristics. In addition, detailed models are more reliable than simplified ones as less assumptions and approximations are involved.

On the other hand the structural analysis of such models could be quite time consuming and could impede fast optimization studies. Moreover, the creation of parametric CAD-based FE models is difficult. Even if possible, there could be too many parameters because of the complex geometry, while the design responses are sensitive only to a small set of them [11]. Finally, detailed geometry definition is rarely available during the concept stage, although the use of predecessor models might be of some help.

Simplified FE models

Initially simplified models were used in the VDP, such as beam and joint models representing the main structural members and the nodes between them. With the increase of computer power and the continuous attempts to consider more and more details, the complexity of the FE models grew enormously. Simplified models of the car body were thus replaced by more detailed ones. The number of elements in these detailed models has increased gradually from a few thousands in the beginning up to few millions nowadays. However, during the last years the use of simplified models has been re-emerging, especially in the concept phase [1, 20]. Although some precision can be sacrificed, simplified FE models of the car body can often provide the design engineers more insight in shorter time compared to a complex, highly detailed solution. They require much shorter computational times and are also intrinsically parametric which makes them easier to optimize than their detailed counterparts. Moreover, the trend is to use them increasingly not only at subsystem level but also in the full vehicle context as part of multi-body simulation (MBS) models (e.g. [21]) in which the concept representation of the vehicle is incorporated as flexible body. Thanks to the combination of FE and MBS models it becomes possible to shorten the development cycle and to achieve better accuracy as local body flexibility and global large displacements are taken into account not consecutively but at the same time. The added advantage of using simplified FE models instead of detailed ones is that flexible MBS can be performed at affordable computational cost. As concept models have a much smaller number of DOFs, less effort is required for substructuring (see Section 2.2.5). In this way

fast investigations can be made on how the performance of the full vehicle (e.g. ride and handling) is affected by the body modifications. Moreover, car body optimization under various full vehicle load cases can be performed in a single process where not only the parameters of the structure are considered as design variables, but also the spring damper characteristics of the drive and power train, the mount specifications and others. For all these reasons simplified FE models are one of the central topics of Chapter 2 where an in-depth study of the state-of-the-art methodologies for car body VCM is performed.

1.3 Objectives and main contributions

1.3.1 Objectives of the dissertation

Sections 1.1.3 and 1.2.3 highlighted some of the problems that vehicle structure CAE has to face. In particular, the urgent need of analysis that leads the design process from the concept stage onward was underlined. As it will be discussed in Chapter 2, some of the existing concept methodologies have promising features and good predictability, but an efficient holistic approach suitable both for simpler cases and for industrial applications is still missing. The objective of this dissertation is to answer these needs by providing such generalized methodology and by improving the concept modeling and simulation for the vehicle structure. The focus is on predictions of its static and low frequency dynamic behavior by means of FE concept models. The goal is to address the following specific requirements:

- The predictions must be available as early as possible in the VDP. This can increase the feasibility of reaching various, sometimes conflicting, performance targets. It can also help avoiding costly and less efficient late modifications.
- The predictions of the structural behavior must be as precise as possible, so that reliable results can be obtained and product quality can be increased.
- The concept FE models must be small-sized enough to allow multiple fast modification and optimization studies. They must be as simple as possible, but also as detailed as necessary in order not to compromise the model accuracy. In addition, the concept FE models must be parametric so that optimization can be easily performed.
- The methods for creation of concept FE models must be efficient and applicable both for academic and industrial case-studies. They must be able to work under lack of detailed knowledge about the new structure. It must be also possible to include carry over parts and, if needed, to adapt some of them to the new design.
- The algorithms for structural optimization must assist the design engineers in finding better, possibly global optima in reasonable time. The solutions found must be able to give a better insight on how the optimized detailed FE models would look like.

To be able to manage the existing bottlenecks and to satisfy the requirements listed above, the following practical tasks must be accomplished:

- An in-depth study must be performed on the state-of-the-art VCM approaches, their strengths and limitations.
- Dedicated VCM methodologies for the car body structure must be developed that respond to the current needs and cover the existing gaps.
- Guidelines must be derived on good practices for concept modeling and optimization both with the existing and the newly proposed approaches.
- The proposed methodologies must be first validated on simpler academic problems; afterwards they must be applied on realistic case-studies typical for the automotive industry.

1.3.2 Main contributions of the dissertation

This dissertation comprises both the development of original methodologies as well as the introduction of improvements in the application practice. The main contributions are listed below in decreasing order of importance:

- **Beam Bounding Box** is a novel approach for 1D beam concept modeling and optimization handling which is an improved alternative of the existing methods. It keeps the reference cross-sectional shapes of all 1D beams, but when each of them is rescaled during optimization, the beam is represented by means of generic cross-sectional properties. Thus a lighter and simpler representation of the concept beams is created and at the same time the connection with the detailed FE model is not broken. The proposed method is computationally beneficial, easily implementable and applicable.
- **Advanced sizing optimization** is proposed as alternative to the state-of-the-art gradient-based (GB) approaches. During the concept stage it is decisive to improve the static and dynamic performance of the vehicle structure. In this optimization process it is not only the algorithm speed that counts, but also the quality of the final results and the amount of obtained knowledge. For this purpose, an advanced global search method – Differential Evolution (DE), is identified, improved, implemented and validated. It proves as appropriate for sizing optimization of the vehicle structure, which on its turn can be extremely complex, involving thousands of design variables, highly restricted and discontinuous domain, conflicting objectives. Moreover DE is robust, scalable, easy to tweak and requires reasonable time to converge, so that it can be applied in the industry.
- **Potential error factors in 1D beam concept modeling** are identified, the most important of which comprise cross-section deformations, spot welds, flanges, discontinuities and beam cross-section geometry. A systematic study is performed of their impact on the model precision. A novel cross-section deformation measure is introduced. Consequently, guidelines are given on good practices to overcome the intrinsic limitations of 1D beam concept modeling techniques. They can be easily applied to industrial case-studies. The

achieved better insight of the potential pitfalls and their possible solutions, helps making VCM more accurate and reliable.

- **Surrogate-based optimization of detailed FE models** is introduced as an alternative to the simulation-based optimization of simplified FE models. The structural modifications of the detailed model are performed by means of mesh morphing techniques and local joint modifications. The global static and dynamic performance of the vehicle structure is represented with response surface (RS) models. The considerable time for structural analysis of detailed FE models is thus bypassed as the evaluation of the approximating polynomials is computationally cheap. In this way fast modification and optimization studies can be made, which are crucial for the concept stage. At the same time, some of the problems typical for simplified FE models can be avoided.
- **Superelement joints** are proposed as means to model the structural nodes in the vehicle body and to improve beam-only simplified FE models. The dynamic superelement (SE) reduction of all joints results in more accurate and more realistic simplified models. The proposed approach can be applied for joints with varying geometrical complexity. Furthermore, it is generally valid also for the case of other complex parts of the structure which cannot be substituted appropriately with 1D beams.

These contributions are in line with the goals defined in Section 1.3.1. They aim at achieving a better VDP through CAE front-loading and improved VCM (Fig. 1.4). Moreover, an emphasis is put on the direct applicability of all these advances for realistic cases from the vehicle engineering practice.

1.4 Outline of the dissertation

The rest of the dissertation consists of seven chapters and three appendices. Chapter 2 gives a detailed overview of the state-of-the-art approaches for concept modeling and optimization. This serves as a basis for the proposed improvements and original contributions in the next chapters. From this chapter onward the focus is on simplified beam, joint and panel (BJP) FE models predicting the static and low-frequency dynamic behavior of the vehicle structure. Chapter 3 treats the important aspect of errors introduced due to the use of 1D beams in the concept models. In addition to the systematic study of the most important error factors, guidelines are given to overcome the limitations of the existing modeling techniques. In Chapter 4 a novel approach for 1D beam concept modeling and optimization handling is presented – Beam Bounding Box. Its feasibility is demonstrated, as well as its applicability in the engineering practice and its benefits in terms of computational time. In Chapter 5 a methodology is presented to include structural nodes in the concept model as SE joints. The same structure is modeled with beams only, as well as with beams and joints, so that both models can be compared and the advantages of the proposed approach can be evidenced. DE is chosen and improved for the purposes of advanced sizing optimization of BJP

models in Chapter 6. Its performance in the case of real-world engineering problems with varying complexity is compared to the one of standard GB algorithms. The strengths, weaknesses and possible application areas of these two optimization strategies are discussed. Finally, Chapter 7 presents an alternative to the BJP models in the concept phase, that is based on detailed FE models of predecessor vehicle structures. This approach relies on global mesh morphing and local joint modifications combined with the response surface methodology (RSM). The differences between such surrogate models and the BJP ones are clearly evidenced. In Chapter 8 general conclusions are made. Possible future improvements are also discussed. Appendix A includes some additional figures as supporting information for Chapters 5 and 6. Finally, Appendix B summarizes the Euler-Bernoulli and the Timoshenko beam theories, while Appendix C gives an overview of Genetic Algorithms.

Chapter 2

State-of-the-art

2.1 Introduction

Until late 1970's the design of thin shell structures relied on analytic tools such as the simple structural surface (SSS) method [11]. The main idea of this approach is that the entire body shell structure can be idealized with a set of plane structural surfaces, which approximate its curved surface [14]. The contribution of the beams can be neglected, retaining only their role in avoiding wall instability, while the contribution of the closure panels to the global structural behavior is considered quite important. The SSS are held in equilibrium by forces which arise from vehicle loads and which are transmitted to and from adjacent SSS and eventually to the ground. The SSS approach can be used for concept development involving the general architecture of the body [14]. This simple method can be applied for the initial structure definition and allows many different alternatives to be considered in a short time. It is particularly useful for the assessment of possible load paths.

Although the SSS method can undoubtedly be a helpful preliminary step before FEA, the rough approximations given by it and similar analytic tools can in no way replace CAE in the concept stage. As discussed in Chapter 1, the new VDP paradigm requires CAE front-loading (Fig. 1.3(b)), during which both modeling and optimization techniques are involved. This early design phase can consist of different steps, depending mainly on how the concept model is created. In Fig. 2.1 some examples are given, which will be discussed in detail in Section 2.2. The concept model can be a surrogate (Fig. 2.1(d)), a detailed FE (Fig. 2.1(a) and 2.1(c)) or a simplified FE model (Fig. 2.1(b) and 2.1(e)). The common thing between all sub-figures, is that each concept model is subject to optimization. However, the choice of optimization algorithm can be sometimes influenced by the model itself, e.g. complexity, number of design variables, etc.

In this regard, the current chapter treats the state-of-the-art techniques for FE concept modeling and structural optimization with focus on the static and vibration behavior of the vehicle body. Section 2.2 considers the most advanced methods for the creation of car body concept FE representations. The way to perform structural modifications of these models is also discussed as being directly related to their optimization. Section 2.3 focuses on the state-of-the-art algorithms

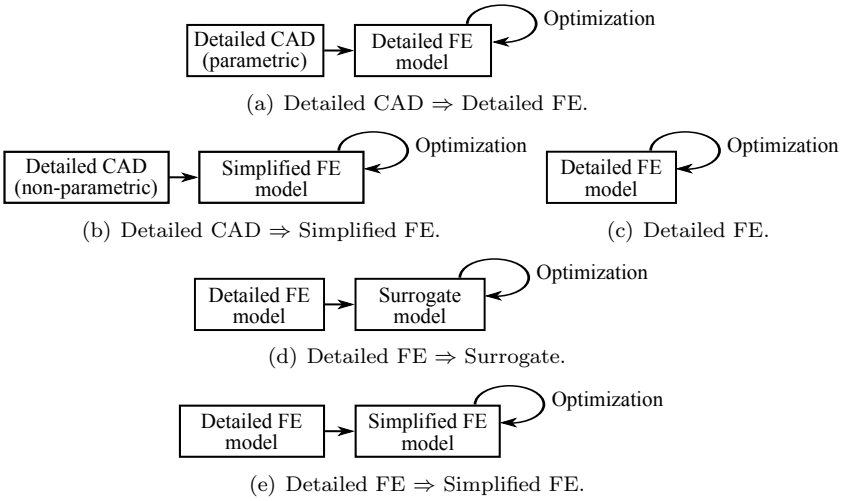

(a) Detailed CAD ⇒ Detailed FE.

(b) Detailed CAD ⇒ Simplified FE.

(c) Detailed FE.

(d) Detailed FE ⇒ Surrogate.

(e) Detailed FE ⇒ Simplified FE.

Figure 2.1: Various types of concept stages.

for structural optimization.

2.2 Concept modeling for the vehicle structure

2.2.1 Overview

Due to the increasing importance of VCM, there has been an active research and development in this field during the last years. A wide multitude of methodologies has been created, which vary in complexity, features, range of validity and field of application. They can range from rough simplifications valid only for simple academic cases to elaborate approaches fully validated at industrial level. In addition to the individual efforts of various researchers, there has been also a number of projects fostering VCM, like for example the Coordination Action project AUTOSIM, the Flemish IWT research project "Analysis Leads Design" (ALD), the European Commission Marie Curie (MC) FP7 Industry-Academia Partnerships and Pathways (IAPP) project "Innovative Concept Modeling Techniques for Multi-Attribute Optimization of Active Vehicles" (INTERACTIVE), the EC MC FP7 Initial Training Network (ITN) project "VEhicle COncept Modeling" (VECOM).

The comprehensive study of the available concept methodologies requires a proper classification to be made. The most intuitive division is based on the type of FE model used:

- Methods using simplified FE models;
- Methods using detailed FE models.

Simplified FE models of the vehicle structure normally involve 1D bar or beam elements, some kind of concept joint representation, as well as concept panels with

less dense 2D shell mesh. On the other hand, detailed FE models are much bigger and with increased level of complexity. They are directly used as concept models only in rare cases, optimization studies excluded. Alternatively, the detailed FE model might be substituted with a surrogate one (Fig. 2.1(d)) which can be the result of a RSM. Another way to reduce the computational efforts involved in solving large FE problems is to employ techniques such as Static Condensation or Component Mode Synthesis (Section 2.2.5) for parts of the model which will not be changed.

Another widely spread classification [1, 8, 21–26] breaks down the concept approaches in the following three groups, mainly depending on the amount and type of design information available:

- Predecessor-based methods;
- Methods "from scratch";
- CAD-CAE integration methods.

These three categories will be discussed into detail in Sections 2.2.2, 2.2.3 and 2.2.4. In the course of their description, reference will be also made to the type of FE models used by the various methods.

2.2.2 Predecessor-based methods

When dealing with the car structure, the predecessor-based concept modeling methods are among the most often used approaches. This can be explained with the fact that rarely the development of a vehicle starts "from scratch" and does not rely on any predecessor information. These approaches are applied to create a variant or incremental improvement of an already existing vehicle. Its validated detailed FE model is used as a basis for subsequent research. The aim is to provide reliable early-stage predictions of various performance attributes and to be able to perform fast modification and optimization studies. Two main groups of methods can be distinguished: methods using simplified structure layout and methods based on mesh morphing.

Methods using simplified structure layout

The methods based on concept FE equivalent of the structure have gained extreme popularity testified by the numerous publications in this field, e.g. [1, 3, 8, 20–24, 26, 26–35, 35–48]. The basic idea is as shown in Fig. 2.1(e). The main phases common for most of these approaches are illustrated in Fig. 2.2(a). Fig. 2.3 illustrates a simplified FE model of a BIW employing beam and shell elements.

The validated FE model of an existing vehicle structure is used as a reference. In this detailed FE model three basic groups of components can be typically identified: beam-like structures (e.g. A-pillar), joints between them (e.g. C-pillar to roof rail) and panel-like structures (e.g. floor). The goal is to create simplified equivalents for the components of each group. The techniques for concept modeling of beams, joints and panels will be explained in the following sections. The resulting BJP concept model is small-sized and parametric representation of the

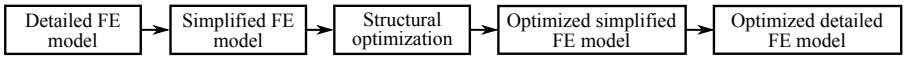

(a) Obtaining optimized detailed FE model.

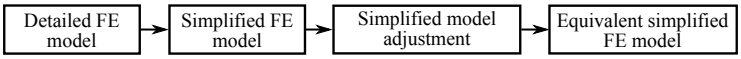

(b) Obtaining equivalent simplified FE model.

Figure 2.2: Methods using simplified structure layout.

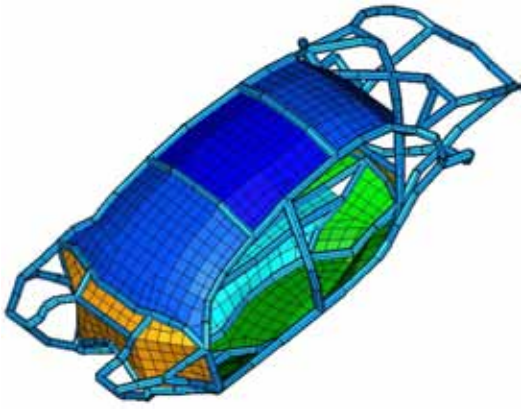

Figure 2.3: Beam and shell BIW FE model [49].

reference FE model and can be thus quickly modified and/or optimized. The final goal is to obtain a better detailed FE and consequently CAD model. Mainly the static and dynamic performance of the vehicle is addressed by these methods.

Another not so often but possible application of the methods using simplified structure layout is shown in Fig. 2.2(b). In the case of errors introduced by the different approximations, the simplified FE model can be adjusted by means of correction factors or updating techniques. The resulting equivalent concept model can substitute the reference one, e.g. in MBS [21, 50]. Naturally, if the modeling errors are negligible, the adjustment step can be skipped. Further considerations in this regard are made in Section 2.2.5.

Beams Beams are an important component group when creating a concept model. They are characterized by a length much greater than the cross-section dimensions. In the detailed FE model of the vehicle body and chassis the beam-like members represent the main load-carrying structure, so they are usually the first to be simplified. They are complex parts of the car, which can be both straight or curved and are characterized by strong geometrical irregularities along the beam length, e.g. varying cross-sections, discontinuities. Their cross-section geometry can be both thin-walled or thick-walled, opened or closed, welded or unwelded [20].

Their simplification is normally done by substituting the beam-like parts built-

up from 2D shell elements with 1D beam elements [1, 3, 8, 22–24, 26, 28–33, 35, 41, 43, 45–48, 51, 52]. Fig. 2.4 shows an example of a BIW modeled with 1D beams. The number of nodes and elements decreases substantially. The simplified model shown in Fig. 2.4 has only 15678 nodes, while the reference one (Fig. 3.20) has 249 640 nodes. The simulation time for simplified models is shorter which is essential for front-loading the analysis phase as early as possible in the VDP.

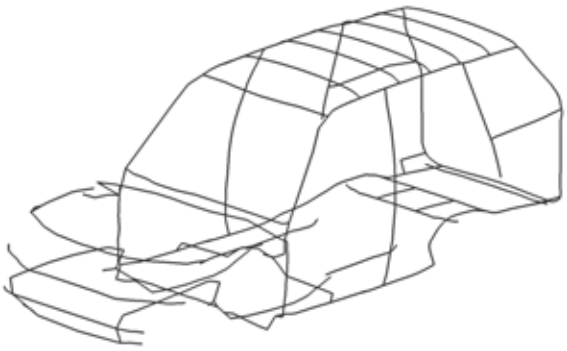

Figure 2.4: BIW simplified with 1D beams.

As consequence of the substitution with 1D beams, the concept models not only become smaller, but automatically parametric and thus all cross-sectional properties can be changed. This makes them particularly suited for sizing optimization, and eventually also for shape optimization. In contrast to that, if sizing optimization is to be performed with a detailed FE model, only the plate thicknesses of the beam-like parts can be directly accessed as design variables, but not the dimensions of the beam cross-sections. As reported by various studies, this often leads to limited improvements because the design space is restricted and the optimization algorithm has less freedom to find good final configurations [53].

Two important aspects must be taken into account when creating a new 1D beam concept model – its structural behavior and its cross-sectional geometry. The first one is directly related to the used beam theory. Because of the advantages of 1D beam models, a number of beam theories has been developed during the years for various engineering applications regarding the static and dynamic analysis of structures [54]. While the classical beam theories of Euler-Bernoulli [55, 56], de Saint-Venant [57, 58], and Timoshenko [59, 60] are still being used, new, refined ones are in process of development. Many methods have been proposed each of which relying on different techniques and resulting in different precision of the concept models. Some improvements which are worth mentioning include the introduction of shear correction factors [61–69], the use of warping functions based on the de Saint-Venant's solution [70–75], the introduction of additional DOF for each node accounting for warping [61, 76], the variational asymptotic solution [77–84], generalized beam theories [85–92] and higher-order beam models [93–99]. More details about the essentials of the most important beam theories, as well as for their assumptions and limitations, are given in Chapter 3 and Appendix B. The book by Carrera et. al. [54] offers an excellent further reading.

The second and equally important aspect to consider is the cross-sectional geometry. Currently three main approaches for its modeling and optimization handling can be distinguished. They are briefly discussed in the next paragraphs. In this dissertation no reference is made to 1D bar elements as they can be considered a simplified version of 1D beams for which the neutral axis and the axis connecting the shear centers of the end cross-sections are coincident. However, if there are bar elements in the concept model, the approaches described below can be applied in a similar manner.

- Standard cross-section approach

  In this approach the 1D beams are assigned standard cross-sections (STCSs) which are simplified versions of the most common cross-section typologies like box, tube, I–, L–, C–shape, etc. These profiles are normally available in the form of a predefined library. For each 1D beam element the STCS shape is chosen that best approximates the projection of the real cross-section on a plane perpendicular to the 1D beam axis. The dimensions and thicknesses of the STCS are directly accessible so they can be adjusted to match as much as possible the detailed beam-like structure. At the same time a parametric model is automatically obtained, which can be used for optimization purposes. Fig. 2.5(a) shows an example of simplifying the A-pillar of a Ford Taurus FE model with 1D beams having box cross-sections (both simple and detailed 1D element display). Concept modeling methods applying this technique can be found in [28–33, 41, 52].

- Arbitrary cross-section approach

  In this approach the projection of the real cross-section on the plane perpendicular to the 1D beam axis is described with points, segments and their corresponding thicknesses. Thus it is possible to control the model precision and the desired degree of details. The description of the cross-section can range from a simple rectangle enclosing the real shape to a very detailed description distinguishing open from closed cross-sections and including also internal shell layers and stiffeners. Thus an arbitrary cross-section (ABCS) that matches the projection of the reference cross-section almost perfectly will have the same geometry and cross-sectional properties. During sizing optimization each ABCS can be rescaled by changing the height and width of an imaginary rectangle around it. The thicknesses of the segments are also available as design variables. This is the most common approach for optimization handling of ABCSs, e.g. [41, 100], as the alternative change of the position of each point could make the whole process unnecessarily complex. Fig. 2.5(b) shows an example of simplifying the A-pillar of a Ford Taurus FE model with 1D beams having ABCSs (both simple and detailed 1D element display). Concept modeling methods applying this technique can be found in [41].

- Generic cross-section approach

  In contrast to the STCS and the ABCS approach, this method keeps no information about the geometry of the cross-section. Instead, each cross-

section is directly substituted with its generic equivalent, i.e. with its equivalent cross-sectional properties such as area, moments of inertia (MOI), etc. These quantities become automatically design variables during sizing optimization. Fig. 2.5(c) shows the A-pillar of a Ford Taurus FE model and its simplification with 1D beams having generic cross-sections (GNCSs). Concept modeling methods applying this technique can be found in [1, 8, 22, 23, 26, 35, 43, 45, 51].

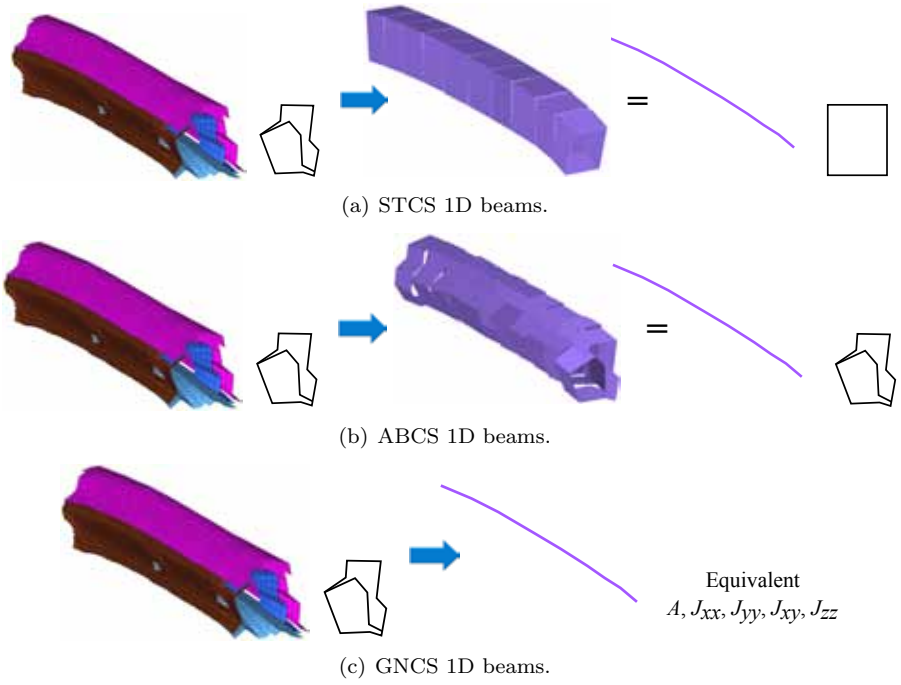

(a) STCS 1D beams.

(b) ABCS 1D beams.

(c) GNCS 1D beams.

Figure 2.5: Techniques for simplifying the detailed FE model of an A-pillar.

Joints A joint is the part of the vehicle structure where two or more load-carrying beams intersect [20, 101]. It can be also defined as a region where an abrupt change in geometric continuity is observed [102]. The joints between beam-like parts in the car body can impact greatly the global vehicle behavior [1, 20, 42, 103–106]. Because of their importance, they are subject to many requirements regarding their stiffness, crash performance, cost, manufacturability and other relevant characteristics [103]. For the same reason their representation in the simplified models can influence the overall approximation and prediction capabilities of the different concept methods. Joints are usually simplified after the concept beam layout has been defined. They have complex geometry and although their basic topology repeats, detailed designs can differ significantly. The vehicle joints are intricate structures with a lot of irregularities, which are difficultly made parametric. Moreover, the

evaluation of their performance by means of analytical formulas is impossible. Fig. 2.6 shows an example of some major BIW joints. Two types can be distinguished – T-type and corner-type joints.

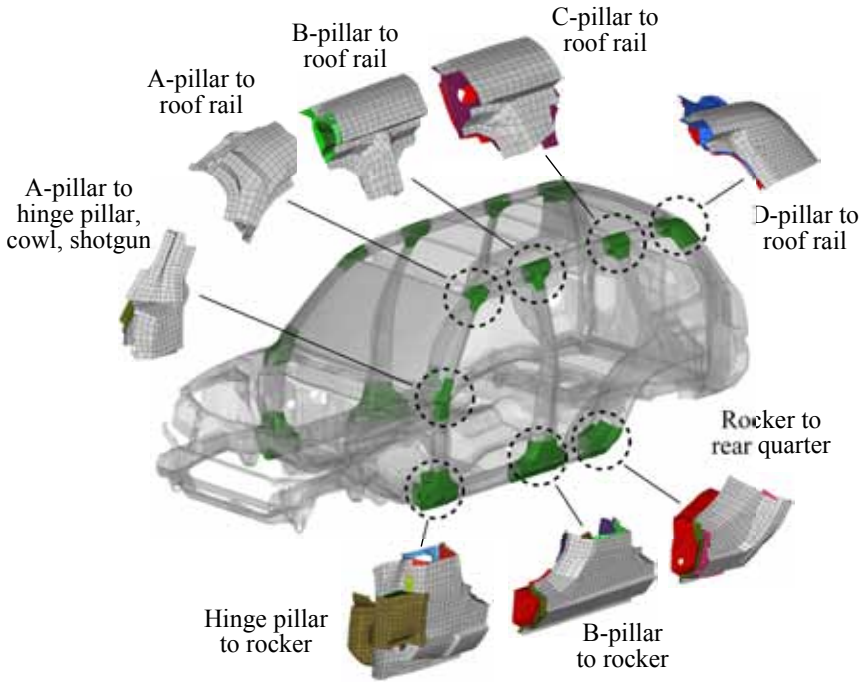

Figure 2.6: Major BIW joints.

In the literature there is a diversity of approaches for the concept modeling of joints. In order to make their overview easier, they can be divided in the following groups:

- Simplified parametric joints.

  These models are small-sized and relatively simple. Usually 1D elements are employed for their creation such as beams, rigids, springs and hinges. Among the variety of methods, the following important contributions can be distinguished:

  – Joints as junction of 1D beams.

    This is one of the most straightforward approaches. It relies on the simple idea that the joint is the part of the structure where two or more beams are connected. Thus it can be modeled by joining 1D beams in the same node [28–31, 41, 43], e.g. like in Fig. 2.4. The joint properties are changed by varying the 1D beam cross-section parameters. In [107] a step further is made. Again beam only models are created but based on a higher order 10 DOF beam theory including 4 additional warping and

distortional DOFs. The aim is to account for cross-section deformations near the joint so its stiffness is not overestimated.

– Joints with spring elements.

The common feature between the approaches in this group is that 1D spring elements are used. In [102] joints with regular geometry are modeled by sets of rotational springs. The spring parameters are determined analytically by making use of experimental data from static load tests. In [43] elastic joint representation is proposed consisting of rigid and spring elements. In [108] a concept joint model with beams, hinges and torsional springs is introduced. The magnitudes of the torsional spring constants, the positions and the orientations of the torsional springs account respectively for the joint flexibility, for the location of the rotation centers, and for coupling effects [108]. Other examples of using springs in joint concept models can be found in [33, 46–48, 52, 101, 109]. In all these approaches usually the spring parameters can be obtained either by means of physical experiments or as result of FEA of the detailed joint model.

– Joints as combination of 2-joints.

The stiffness matrix of a joint connecting N beams can be defined as a $(N*6)$ by $(N*6)$ matrix as there are 6 DOFs for each incoming beam. Such joint can be decomposed into a number of 2-joints connecting all pairs of incoming beams [110]. As the 2-joints have two connection points, they have a 12 by 12 stiffness matrix. The overall stiffness of the concept joint is calibrated to match the real joint either on the basis of experiments or by using detailed FE models. To achieve a good match, the stiffness parameters of each 2-joint are adjusted. After that an area-type design variable is assigned to each 2-joint, which can be also zero, i.e. absence of the structural element. This makes the approach extremely well suited for subsequent topology optimization [110].

- Detailed non-parametric joints.

The techniques from this group aim at keeping the detailed FE model of the joints. Reduction techniques are used to decrease the related computational efforts (see also Section 2.2.5). The representation of joints as SEs impedes modifications of their geometry, so they are non-parametric. Similarly to joints modeled as junction of 1D beams, this approach is quite popular. Up to now, mainly static reduction [111] has been used [1, 8, 22–24, 26, 35, 45, 103, 112–115]. By condensing the stiffness and mass of the joint to its end nodes a simplified small-sized model is achieved. In [24] Guyan reduction has been combined with Wave-Based Substructuring (WBS), so that the local behavior of the joint end cross-sections can be taken into account.

- Detailed parametric joints

Many efforts have been dedicated to the creation of detailed parametric joints [104–106, 108]. This is a long and intricate process, involving a lot of parameters. However, the performance of the joint is not equally sensitive to

all of them. In [42] a simpler alternative is proposed to change detailed FE joints by means of mesh morphing techniques. Morph volumes are defined that include the joint itself as well as small parts of the incoming beams. The dimensions of the morph volumes can be varied, so that the joint becomes parametric.

Finally, there are some less intuitive techniques, relying on correction factors for the joint stiffness [32, 116]. Because of their limited applicability they have not been included in the current classification. In addition to the methods described above, there are some approaches for detailed joint analysis at component level, which are worth mentioning. In [103, 113–115, 117–120] a tool called ADRIAN is developed for the preliminary static and dynamic evaluation of joints. The static stiffness is evaluated using linear static SE reduction. As for dynamic stiffness, modal analysis is performed according to an improved dynamic joint method similar to the one presented in [121]. In [104–106] two translators are developed that link the physical design parameters of a joint to its performance attributes and vice-versa. In order to achieve fast analysis, these relations are established using Neural Networks (NNs) and RS polynomials.

Panels Panels are shell-like parts with large flat or slightly curved surfaces and small wall thicknesses. They play an essential role in the simplified body layout as they are capable of carrying in-plane loads. Even if the global BIW behavior is dominated mainly by its beams and joints, panels have important contribution to the overall structural stiffness. Thus a concept BIW such as the one in Fig. 2.4 will not be complete without its main panels (e.g. roof, floor).

Where as beams and joints represent a challenge for VCM, panels are the easiest to handle among these three groups. They are also the last to be included in the concept model. Most often they are simplified by coarsening the original FE mesh [23, 26, 41–43], while maintaining sufficient accuracy for the concept predictions of interest. Basic geometric features such as panel shape and curvature are preserved [26]. Local geometric features which are not critical for the static and dynamic stiffness can be disregarded. Panels are normally connected to the adjacent beams and/or joints with rigid elements [23, 26, 41–43], thus forming the final concept model. Their thicknesses can be used as design variables for optimization.

Being relatively simple, the concept modeling of panels is not a subject of further research in this dissertation. The commonly adopted conventional techniques [23, 26, 41–43] are directly applied in case concept panels are needed.

Joining dissimilar elements The joining of dissimilar elements can become a particular issue in simplified and hybrid (partly simplified and partly detailed) FE models of the vehicle structure. It might occur when parts having different meshes (e.g. 1D and 2D mesh) must be connected. Possible problems can arise in any combination simplified–detailed FE beam or joint such as the connection between a simplified beam member and a detailed joint, a simplified and a detailed beam member, or a simplified joint and a detailed beam member. The last two

examples are more typical for hybrid models, whereas the first one is common for the classical BJP models.

In this regard, special attention has been dedicated to joining 1D beams with the 2D shell mesh of detailed joints. So far this problem has been approached in the following ways:

- Rigid elements.

  Rigids (Nastran RBE2 elements [122]) are used in many works [10, 33, 42, 112, 123]. The 1D beam end node becomes the independent node of the RBE2 which is connected to the adjacent shell elements of the joint end cross-section. Although such a solution introduces some additional stiffness in the model [23], it is among the popular and recommended approaches because of its simplicity. Moreover, this technique has been validated on a wide range of case studies – both academic and industrial. Some authors [42] have also proposed an advanced connection in which the rigid connects to the 2D shell mesh by means of spring elements. The idea behind is to make the coupling less stiff. However, this approach is still to be further developed and tested.

- Interpolation elements.

  Interpolation elements (Nastran RBE3 elements [122]) are proposed as an alternative to rigids in some papers [1, 8, 21, 22, 26, 33]. In this case the 1D beam end node becomes the dependent node of the RBE3 which is again connected to the adjacent shell elements of the joint end cross-section. As pointed out in [23] such coupling makes the structure more flexible and limits the accuracy of the concept model. It is inappropriate for describing the rotation of the end cross-section. Moreover, the eventual deformation of the end cross-section combined with the flexibility of the RBE3 would further increase the error.

- Mixed rigid-interpolation elements.

  While the rigids make the structure stiffer, the interpolation elements make it more flexible. As neither of these effects is desirable, a new mixed connection RBE2.5 was proposed in [23] that uses both RBE2 and RBE3 elements and combines their advantages. The new coupling describes well the rotation of the end cross-section as rigids are used, and in the same time it does not suffer from end effect issues in contrast to the interpolation element. For an industrial application RBE2.5 resulted in better model precision than the other two connections types (RBE2 and RBE3). Although promising, the solution given in [23] remains purely heuristic and guided by intuition. A sound theoretical justification must be provided for it, together with extensive validation on a wide range of academic and industrial case studies. Precise guidelines for its applications must be given as well.

- Multi-point constraints.

  In [124] consistency between the DOFs of a detailed joint (2D shell mesh) and its incoming 1D beams is enforced by means of multi-point constraints

(MPCs) [122]. The dissimilar elements at the interfaces (joint end cross-sections) are matched with the help of analytically derived MPC equations. This approach can be applied not only for the classical 1D beams with 6 DOFs, but also for those using higher order beam theory. This technique relies on a sound theoretical background and seems promising for future development. However, its application and validation have been quite limited (mainly academic examples, closed STCS beams only). It still not clear what difficulties might be encountered in more realistic case studies. In this regard, the analytic derivation of the MPCs represents a disadvantage, being too cumbersome.

In the presence of dissimilar elements in the concept model, the technique used for their joining becomes an important choice which can influence the accuracy of the concept predictions. As it seems, it is still a challenge to find such a connection that the benefit of using detailed modeling for some vehicle parts is not deteriorated or lost due to their inappropriate integration with the rest of the structure. Although not without deficiencies, the rigid elements can be currently regarded as the most acceptable technique. They are easy to apply for any kind of connection interface and can be considered a good compromise between precision and reliability. For the same reasons their use has been reported in various papers. The appropriateness of the RBE2 coupling has been confirmed also by the comparative study performed in [42] where the performance of the four main types of connections was checked. The rigid connection was chosen among the others as the most suitable one since it turned out that for the typical automotive case studies the rigid deformations of the cross-section are often prevalent with respect to its warping and distortion [42].

In view of the above, RBE2 elements have been adopted as a joining technique throughout the rest of this thesis. The creation of an even better, "error-free" connection without side effects remains an important aspect for future research. However it is not further treated in the dissertation, being outside its scope.

Methods based on mesh morphing

Concept modeling methods based on mesh morphing aim at transforming an existing FE mesh from reference to new target styling information while in the same time keeping the element connectivity [1, 125]. The grid locations in the FE mesh are modified so that the detailed model of the predecessor vehicle is restyled without the need of a CAD model and without re-meshing. This allows subsequent modification or optimization studies, following the patterns from Fig. 2.1(c) and 2.1(d). In Fig. 2.7 an example is given of stretching a BIW in longitudinal direction by using mesh morphing techniques.

Before using the morphed model for analysis, model refinement is usually performed [1]. Weak spots are identified so that various countermeasures can be taken to ensure the quality of the morphed model. Both the element quality (especially important near areas with strong deformation) and the mesh geometry should be checked. Incorrect deformation of the internal components (e.g. steering wheel, seats) should also be prevented. In addition, incorrect cross-section deformation

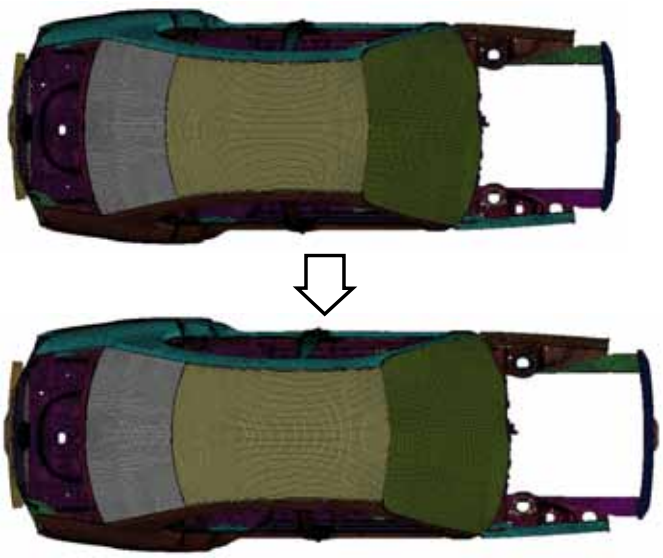

Figure 2.7: Stretching a BIW through mesh morphing.

should be reduced as much as possible, because it strongly influences the global modes, vehicle stiffness and crash performance. Finally, the connection stiffness after morphing should be still realistic and the continuity of the connections should be ensured.

After all these checks have been performed and countermeasures have been applied where needed, the model can be analyzed. As it is a variant of a validated and highly detailed predecessor, it is possible to assess a wide range of performance attributes such as ride and handling, NVH, structural integrity and durability, aerodynamics. However, it must be taken into account that the method is usually limited to small changes. In the case of major shape changes the mesh quality deteriorates significantly and mesh morphing techniques quickly become obsolete or can be used only with extreme limitations [126]. Although according to [126] non-linear analysis and/or analysis with explicit time steps is impossible with morphed models, application of mesh morphing for crash analysis has been reported in [125].

Initially developed for the computer graphics industry [127], nowadays morphing is often used in the automotive field [2, 3, 8, 42, 53, 125, 128–132]. In this regard, there are also various software tools with advanced mesh morphing features such as HyperWorks, ANSA and LMS Virtual.Lab. Different morphing techniques can be distinguished:

- Freehand morphing.

  With this technique meshes are reshaped intuitively without the need for any additional entities such as domains, handles and morph volumes. Morphing is directly applied by moving the nodes. Various operations are possible such as translation, rotation, scaling, projection, etc. Usually not only the

moving nodes but also those which have to stay fixed are defined, as well as all affected elements. In this manner, arbitrary and rapid changes can be manually made. Custom modifications are also possible so that practically any kind of morphing can be accomplished.

- Geometry mapping.

  With this approach parts of the model are morphed in order to fit geometric entities such as lines, planes and surfaces. Likewise, the nodes of the FE mesh can be mapped to elements, node lists or equations. Additional operations can be also performed such as applying line differences, surface differences, and normal offsets to the model.

- Morph volumes.

  This method, also referred to as box morphing, encloses the mesh in one or more deformable six-sided 3D blocks called morph volumes. Each of these blocks governs the movement of the mesh within its boundaries. By changing the shape of a block through the handles placed at its corners and along its edges, the shape of the mesh is automatically modified. This quick and intuitive approach is suitable for simple and/or large-scale changes to complex FE models.

- Morphing with domains and handles.

  With this approach the mesh is divided into domains containing elements or nodes, and handles are placed at the corners of these domains. When the handles are moved, the shape of the mesh changes according to the domain boundaries. This method also allows for parametric morphing of lengths, angles, radii, and arc angles as well as morphing the mesh to match geometric data and other meshes. The domains and handles approach can be intricate but in the same time it provides great flexibility. Not only detailed modifications can be made to any mesh (local domains and handles), but also general changes to space frame type meshes (global domains and handles).

The different approaches can be also classified according to the type of modifications made:

- Global morphing.

  Global structural modifications are made regarding the whole BIW, e.g. length, wheelbase, height, width [128]. Such morphing techniques can thus exert strong influence on the static and dynamic performance of the vehicle.

- Local morphing.

  Local changes are applied that involve only small parts of the body, e.g. rotating the B-pillar [128], changing the roof curvature [125], applying different bead patterns on the floor panel [1].

Finally, some authors [1] divide the morphing techniques in direct and indirect ones:

- Direct morphing.

  This type of morphing acts directly on the FE mesh. For this purpose either the concept of moving/fixed nodes and affected/frozen zones of elements is used, or origin and target curves are employed. This process is not repeatable on multi-attribute meshes of the same vehicle having arbitrary mesh density and topology [1]. In addition, it is time consuming as it requires a lot of manual interactions. Therefore, direct morphing is usually limited to local modifications.

- Indirect morphing.

  With this approach the morphing operations are not carried out directly on the FE mesh. Instead, they are applied by means of volumes, boxes or domains that incorporate different parts of the original FE mesh. Transformations are performed by moving the handles of these control blocks. As the location of the FE nodes inside the control blocks is linked to the location of the handles, they are automatically changed and restyling is achieved. This process is repeatable on multi-attribute meshes and it is suitable both for local and global modifications.

As already pointed out previously, the computational cost of analyzing detailed FE models is high. Even more, when optimization is involved (Fig. 2.1(c)), this cost is often not affordable. Consequently, despite of the employed morphing approach, morphing is applied mainly for simple "what-if" studies [2, 3, 8, 125, 129, 130]. In [53] the crash performance of the car front part is optimized as function of only three design variables. In [42] some of the main vehicle joints are morphed to optimize the global static and dynamic performance. However, the employed model is a hybrid one, i.e. including both simplified (1D beam) and detailed (2D shell) parts. Finally, Danti et al. [128] combined mesh morphing techniques with surrogate models in order to approximate the vehicle static, dynamic, acoustic and ergonomics performance. This concept is similar to the one illustrated in Fig. 2.1(d). An additional mathematical model is created in order to replace the detailed one during optimization.

2.2.3 Methods from scratch

In contrast to transfiguration design (i.e. predecessor-based concept modeling), the methods from scratch do not aim at mere variant or incremental improvements, but at the definition of completely new vehicle structures at the very beginning of the design. Consequently, the requirements that have to be met by this group of methods are much higher and intricate. The initial development of integrated methodologies and dedicated tools is highly complex and involves considerable amount of time, efforts and previous experience. For this reason the approaches from this group are not so numerous as the predecessor-based ones.

Before proceeding with the creation of a radically new concept, the topology of the structure is normally determined. By finding out where material should be located in the existing design space, topology optimization gives a preliminary idea of the BIW and its optimal load path configuration for statics, NVH and

crashworthiness [1, 133]. The member packaging spaces resulting from the load-path analysis can be then transformed into thin-sheet structures [133]. Thus the optimized topology can be directly used as a basis for parametric concept design from scratch.

Novelty design methods can involve both simplified and detailed FE models, the latter being more commonly used. Some typical techniques for designing the layout of the load-carrying components from scratch are discussed hereafter.

It must be noted that methods traditionally classified as predecessor-based are in some cases also able to create concept models from scratch (mainly BJP models). However, the general prediction capabilities of the models created with these approaches must be confirmed in advance, and the expected modeling error must be estimated. Some examples can be found in [31, 41, 42].

In [134, 135] knowledge-based engineering (KBE) techniques are applied for the automated creation of a FE model of the vehicle structure. This concept model is defined by means of a standard library with existing component designs of beams, joints and panels. If new styling lines are available, the BIW structural package is automatically adapted in order to match them.

In [136] a fully parametric template method is presented which can be used to build concept BIW geometry and simplified FE models quickly and easily. Various templates for cars, buses and trucks are initially created and stored. Starting from one of the existing model frameworks, the user can produce new instances with different characteristics by simply adjusting a set of control points to the desired new styling surfaces. Besides the control node positions, the BIW dimensions can be also changed and various constraints can be defined.

The SFE CONCEPT ^{TM}software is based on a holistic approach which deserves special attention [126, 133, 137–145]. The model creation, modification and optimization with SFE CONCEPT ^{TM}is illustrated in Fig. 2.8. It is an advanced, highly automated upfront design tool for fast creation and modification of parametric BIW geometries and their related FE models. It is not only capable of building completely novel concepts, but can also make use of imported and converted predecessor CAD/FE geometry. Simple geometrical description is achieved by means of building blocks such as influence points, base lines, cross-sections, beams and joints, free-form surfaces. Various model parts are available in a predefined modular construction library and can be used during the assembly of a new design. Progressive top-down refinement can be achieved by starting from the base geometry and gradually adding more details (e.g. holes, beads, stamps). After the creation of a fully parametric design, its FE mesh is automatically generated. A robust FE model becomes automatically available for FEA (e.g. NVH, crash, statics) and optimization (e.g. shape, topology or topography optimization, optimization based on surrogate models, multi-disciplinary optimization, optimization of vehicle product families). In general, SFE CONCEPT ^{TM}follows the pattern shown in Fig. 2.1(a). It is being employed by important car manufacturers like BMW [143–145], Porsche [133, 141] and Ford [137, 138].

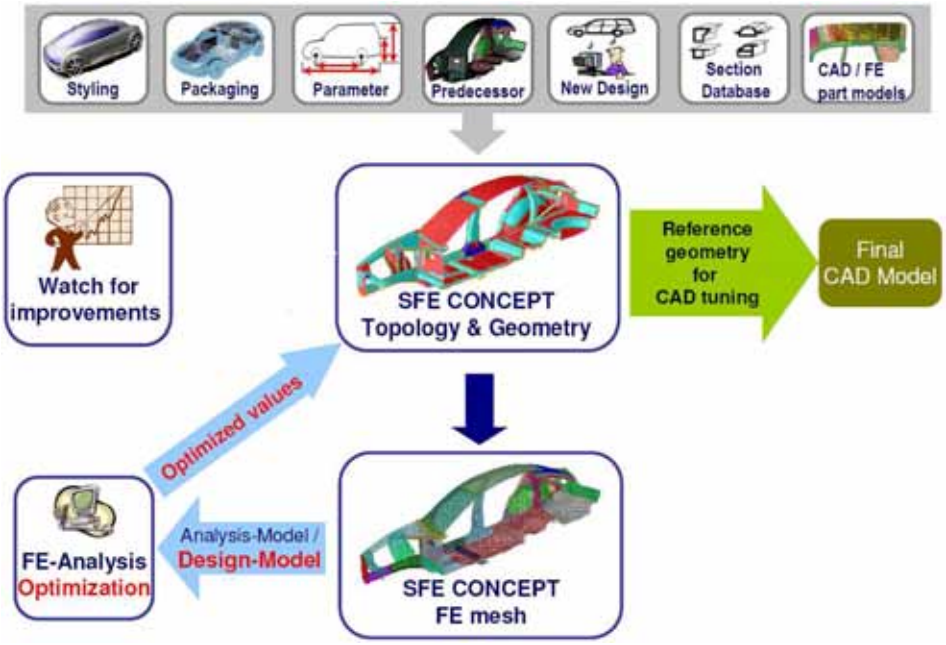

Figure 2.8: Modeling and optimization with SFE CONCEPT ™ [126].

2.2.4 Integrated CAD-CAE methods

FEA has its origins in the 1950s and 1960s, whereas CAD emerged in the 1970s and 1980s. Major FE programs were technically mature long before modern CAD was widely adopted. However, nowadays CAD is a much bigger industry than CAE. This historical disconnection between CAD and FEA resulted in quite different geometric representations in both [7]. In the traditional CAD-centric development designs are encapsulated in CAD systems and meshes are generated from CAD data. The construction of FE geometry (i.e. the mesh) is costly, time consuming and creates inaccuracies. These difficulties have led to a paradigm change. Although nowadays CAE-centric development is recognized as undoubtedly important, a step even further is needed – integrated CAD-CAE systems are required [146].

During the recent years more and more CAD and CAE programs have been coupled – interactive links between them have been created so that if the geometry is changed in one environment, it is automatically updated in the other one. Some examples for such integration in commercially available packages include ANSYS and CATIA, Pro/ENGINEER or SolidWorks, as well as COMSOL and SolidWorks or Pro/ENGINEER [147]. Even more, some CAE companies have literally embedded their analysis software as part of the CAD programs, thus working with native geometry, e.g. Mentor Graphics FloEFD for Pro/ENGINEER or CATIA [147]. Concepts such as bidirectional associations, parametric models, feature-based modeling and design history are being adopted extensively by the

CAD-CAE world.

Despite all these attempts, the CAD-CAE gap has still not been bridged. Thus an alternative idea emerged to extend FEA with something more CAD-like and avoid the approximation in the geometrical problem description. A promising research direction to resolve the problem is isogeometric analysis – a method developed by Hughes et al. [7, 148–155]. An example of meshes for FEA and isogeometric analysis of a bracket is shown in Fig. 2.9. Isogeometric analysis is based on Non-Uniform Rational B-Splines (NURBS), which is a standard technique employed in CAD systems. The exact CAD geometry is matched by NURBS surfaces, then a coarse mesh of NURBS elements is constructed. These would be solid elements in three-dimensions that exactly represent the geometry. If there is some CAD data initially available at least for part of the structure, its concept representation can be created by means of a coarse isogeometric model. Successive refinement is simple and does not require additional interaction with the CAD system. All subsequent meshes retain exact geometry.

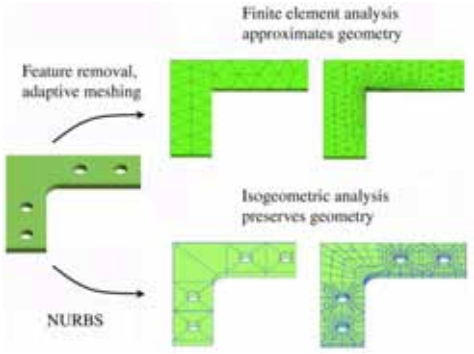

Figure 2.9: FEA versus isogeometric analysis mesh for a bracket [148].

Logically, if design and analysis share the same geometry model, the existing gap between them can be closed. However, isogeometric analysis is still in process of development and has a long way to go before becoming an alternative to FEA.

2.2.5 Complementary techniques

There are two additional techniques often applied in VCM – model updating and SEs. They are not concept modeling approaches by themselves but are in many cases employed to support them. They are briefly discussed in the following sections.

Model updating

Model updating is a technique that is traditionally used to validate and correct FE models of mechanical structures by means of experimental data for the real physical prototypes [156]. This idea inspired a similar approach in VCM – the

updating of simplified FE models with respect to their detailed reference counterparts [27–31]. In some papers the same technique is referred to as correction factors [1, 8, 22, 23]. The motivation of the concept model updating is that often the actual structural behavior (both static and dynamic) is not perfectly matched due to the inevitable simplifications and approximations made. By itself, model updating is an optimization process that minimizes the differences between simplified and detailed FE model by changing the inaccurate simplified model. For this purpose the following main steps must be carried out [156] (Fig. 2.10):

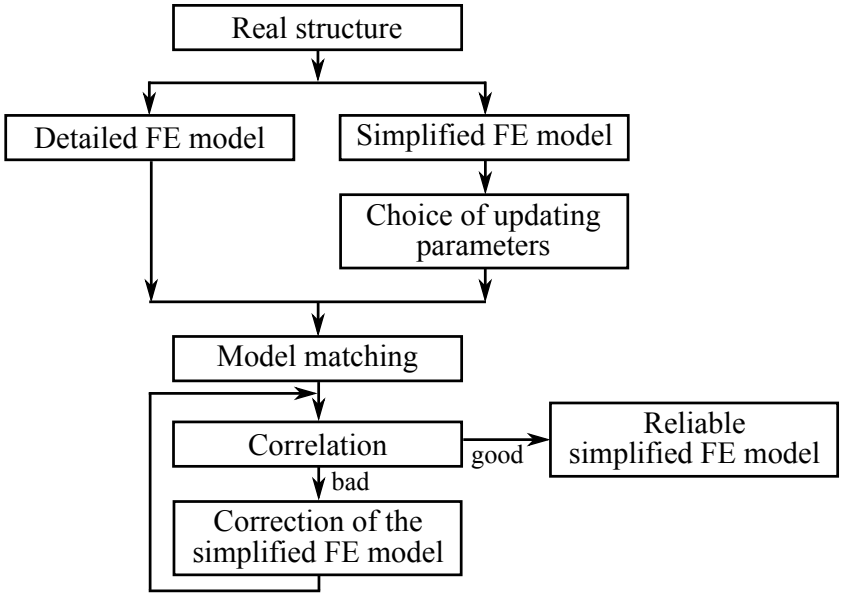

Figure 2.10: Concept model updating.

- Initialization and selection of updating parameters.

  The reference detailed FE model and its concept representation must be available. Updating parameters must be chosen for the simplified model in case that it turns out to be imprecise and has to be corrected. Their proper choice is crucial for the success of the whole process. One can choose between physical parameters of the FE model (e.g. geometry or material properties) or submatrices/individual elements of the global system matrices.

- Model matching.

  As the FE meshes of the simplified and the detailed model are in general incompatible, they must be matched in terms of DOFs. Detailed FE models have times more DOFs than simplified ones. This is unacceptable for most of the subsequent correlation and correction techniques which require a one-to-one correspondence between the DOFs. To tackle this problem, either expansion techniques must be applied for the simplified model, or reduction techniques must be used for the detailed one.

- Correlation check.

  In this step FEA is performed for the simplified and the reference FE model. The degree of agreement between them in terms of static and dynamic performance can be quantified with various criteria: node translations and rotations, total mass, natural frequencies, Modal Assurance Criterion (MAC), Co-ordinate Modal Assurance Criterion (COMAC), Frequency Response Assurance Criterion (FRAC), Response Vector Assurance Criterion (RVAC), cross and mixed orthogonalities, etc. Normally as many as possible of these measures are considered simultaneously during the updating process in order to take into account different aspects of the correlation.

- Correction of the simplified FE model.

  In case of bad correlation, the simplified FE model has to be adjusted by changing its updating parameters accordingly. After that a correlation check is performed again and, if needed, new corrections are made. These iterations continue until good agreement between both models has been achieved.

Model updating can be applied both at local component level and at full body level. In the first case, one simplified part at a time (e.g. beam member) and its detailed counterpart are isolated and updating is performed in order to achieve correspondence between them. In the second case, the updating parameters of all simplified components are simultaneously changed so that the global behavior of the reference FE model can be matched. None of these approaches is ideal. While local updating is tedious and time consuming, error compensation can occur in global updating. Nonetheless, concept model updating remains a useful additional tool for the designer which can find various applications, among which:

- Correction of erroneous concept models in order to make them equivalent to their corresponding detailed FE models in terms of static and dynamic behavior.
- Creation of simplified physical prototypes of the BIW (body fixtures) at lower cost and in shorter time in order to support rolling chassis remote parameter control (RPC) tests.
- Identification of problematic parts in the concept model.
- Finding alternative modeling solutions.

Superelements

With SEs it becomes possible to solve large complex problems, but also to make FEA more efficient and to perform more design iterations. SE analysis can be regarded as a form of substructuring, i.e. the FE model is divided into a number of components (SEs). Each SE is processed independently of the others and is then replaced by a reduced set of matrices (mass, stiffness, damping, loads) describing its behavior as seen from the rest of the structure. A residual structure is formed of all model components that were not assigned to a SE and of the assembly of the reduced SE matrices. Based on the assembled matrices for the residual structure,

the system solution can be obtained. The results can be then used to perform data recovery (e.g. calculation of displacements or stresses) for each SE by expanding the solution at the attachment points.

SEs are widely used not only in the detailed CAE phase, but also in concept modeling [1, 8, 22–24, 26, 35, 45, 103, 112–115]. The following possible application cases need to be mentioned:

- Carry over parts.

  During the creation of a FE model, the carry over parts from predecessor vehicles can be reduced as SEs. They are kept unchanged in case of modeling errors, whereas the residual structure has to be fixed and processed again. Taking into account that this process might require more than one iteration, the development of new models becomes faster.

- Complex parts.

  In the case of highly simplified FE models, SEs are sometimes the only feasible alternative to take into account complex structural parts without deteriorating the model accuracy. The structural joints are a typical example [1, 8, 22–24, 26, 35, 45].

- Optimization.

  SEs are extremely suitable when a FE model is analyzed more than once, i.e. as in the case of optimization. All unchanged parts are modeled as SEs. Only the components that are subject to modifications are processed. Through the avoidance of a complete solution, better efficiency is achieved and a significant time gain might be attained. The computational cost of individual runs is reduced without sacrificing the accuracy of the results. Some examples can be found in [1, 21, 23, 157].

- Distributed model development and security.

  SEs are an appropriate choice when different parts of the structure have to be modeled independently by separate design groups. Each group models its own parts and sends them to a system integrator. He/she assembles the models, performs FEA and sends the results back to the groups for their individual use.

  In the case of proprietary or secure projects, special considerations must be made when information has to be shared between different engineers or design groups. Often the need arises to send a part of the model to others so that they can include it in an assembly and perform analysis. With SEs it is possible to avoid sharing any geometric information, but to send just a set of reduced matrices regarding the mass, stiffness, damping and loads as seen at the boundary.

- Large-scale problems.

  Large-scale FE models can be split into SEs to overcome the limitations of the available hardware. The structural problem is divided into several small

problems on a substructure level, that are more efficiently solved independently, and then recombined to obtain the global behavior. SEs can be used for incremental processing of such problems by means of split databases. As the SEs can be processed separately and at lower computational cost than the complete FE model, they can be handled in parallel on the same or even different computers allowing for more efficient FEA.

In static analysis no approximation is introduced by using SEs. The substructure level solution typically consists of a Guyan reduction [111] (also called static condensation or static reduction). The full static response of the SE is represented by the reduced matrices.

The reduction methods used for SEs in dynamics are less exact. Either static or dynamic reduction can be applied. If static reduction is used, the reduction of the stiffness is exact, but approximations occur during the reduction of the mass and damping matrices. It is assumed that the motion of the exterior DOFs, multiplied by the static transformation matrix can represent the dynamic solution of the SE. It is also assumed that the components are very stiff and that local dynamic effects can be ignored. Although this might be true in some cases, Guyan reduction is often insufficient. Satisfactory results can be obtained for the lowest modes of the system, but the higher frequency or local modes can be wrongly calculated or even entirely missed.

For most problems dynamic reduction is more accurate, but it also has a higher computational cost and requires a certain engineering judgment. A Component Mode Synthesis (CMS) approach [158–161] is typically used to solve the substructures independently and synthesize the results. Each substructure is represented by its component modes. Modal superposition is used to transform each detailed FE part into a reduced modal model based on its normal modes. Including all modes for each SE gives an exact solution but has prohibitive computational cost. Alternatively, if fewer modes are kept (modal truncation), approximations are introduced in the problem and CMS is not exact. Usually the normal modes are enriched with static or dynamic response vectors due to a local input at the interface DOFs of the substructure. A wide variety of CMS methods exists depending on the way compatibility of substructure interfaces is enforced, on the boundary conditions applied to the substructure interface for computation of the normal modes, as well as on the choice of enrichment vectors. The SE quality is strongly influenced both by the number of eigenvectors kept and by the treatment of the exterior DOFs.

2.2.6 Trends and challenges

Based on the previous sections, the following trends and challenges can be observed:

- There is still no approach generally valid for all problem categories. A compromise must be always made between precision, simplicity, model size and similarity to the reference structure. Although a variety of approaches exists, there are no standards. For this reason, the OEMs are usually forced

to rely on their own in-house methodologies and dedicated tools. Nevertheless, the predecessor-based techniques can undoubtedly claim to be the most developed and widely used ones.

- Not only is a holistic, generally valid approach missing, but there is also a lack of comparative studies of the available methodologies and just a few state-of-the-art surveys are available. Even finding the most suitable approach to be applied for a certain problem becomes a not so easy task.
- Simplified FE modeling is a challenge not only for structural joints, but also for beam-like members. The modeling techniques for both component groups have not reached maturity yet. Despite this, methods based on simplified structure layout become increasingly appealing because of their competitive advantages with respect to the other approaches.
- The current trend is oriented towards concept models of the vehicle structure that are as coarse as possible in order to keep their time advantage and shorten the VDP cycles. In the same time the concept models have to be as detailed as needed so that their fidelity is not severely compromised. The extent to which these conflicting requirements are satisfied is one of the fundamental decisions to be made by the design engineer. It predetermines to a great extent the quality of the concept methodology itself.

It is within the scope of this dissertation to follow these trends and appropriately address the current challenges.

2.3 Structural optimization

2.3.1 Overview

A mechanical structure is a body or an assembly of bodies in space intended to sustain the loads applied to it. The aim of structural optimization is thus to improve structures so that they support loads in the best way [162]. This enhancement process is still often performed in an iterative-intuitive way [146, 162], during which a few designs are created and compared based on a small number of performance attributes. Then the best one is selected which is hopefully an acceptable final design. Such an optimization approach is based on expert knowledge and/or CAE techniques for the design evaluation. Being a manual process, it is often limited to selecting alternatives recognized by the expert, and it fails to identify any unknown but potentially better designs. Only a few design variants are usually investigated, and the selection of optimal structural concepts is obtained more or less by chance and thanks to the experience of the design engineers.

To allow for a better exploration of the design space, structural optimization has evolved with time from a totally manual to an increasingly automatic algorithmic process. This mathematical approach to structural optimization relies on rigorous rules and precise problem formulation. In this sense, it is possible to

define a general multi-objective constrained optimization problem as:

$$\begin{aligned} &\text{Find } \mathbf{X} = [x_1, x_2, ..., x_D] \\ &\text{that minimizes } OF_k(\mathbf{X}), k = 1..K \\ &\text{subject to constraints } g_l(\mathbf{X}) \leq 0, l = 1..M \\ &\text{and boundary constraints } x_j^{(LB)} \leq x_j \leq x_j^{(UB)}, j = 1..D \end{aligned} \tag{2.1}$$

where $x_j^{(LB)}$ and $x_j^{(UB)}$ are the lower and upper bounds of each design variable x_j, and OF_k is the k^{th} objective function (OF) used as performance measure. It must be noted that maximization problems are represented as minimization ones by simply inverting the sign of the OF.

Although the existence of numerical methods for optimization dates back to the days of Newton, Lagrange and Cauchy, no considerable progress was made until the era of high-speed digital computers when they were finally implemented as optimization algorithms [163]. The increased computing power together with the availability of CAE systems for structural analysis led to a remarkable growth in structural optimization research and applications. Being relatively new and less mature than FEA, the field of structural optimization is still undergoing rapid changes and cannot be considered fully developed [163, 164]. Hence the numerous journal papers, textbooks, dissertations and other information sources available on this topic. A good understanding of the state-of-the-art optimization algorithms becomes therefore impossible without their proper classification. Section 2.3.2 aims at providing such an overview with focus on automotive engineering. Similar surveys not only facilitate the algorithm choice among the variety of methods available, but can also highlight the existing challenges and potential directions for future research (Section 2.3.5).

2.3.2 Classification

For better understanding and evaluation of the state-of-the-art optimization approaches, first the attributes of a good algorithm must be briefly discussed. The most important of them are as follows:

- Efficiency:

  A good algorithm must have a fast convergence rate [165]. It must employ as few as possible OF (and gradient) evaluations for the design task at hand in order to be an economical alternative for its optimization. Moreover, it should treat efficiently multiple constraints and objectives. Finally, algorithms with parallel computing capabilities are to be preferred.

- Robustness:

  The algorithm must be reliable. Its convergence should not be influenced by the initial conditions. Starting from any initial design (or initial population of randomly generated designs), the performance of the optimization algorithm should be similar.

- Ability to escape from local minima:

  For multimodal problems with more than one minimum it is important that the global one is identified. In engineering, this is equivalent to finding the best possible design. In practice, it can be often sufficient to achieve a significant improvement, especially for complex real-world problems.

- Generality:

  A good algorithm must be able to treat different kinds of constraints (e.g. equality and inequality, linear and non-linear), design variables (e.g. integer and real-valued) and OFs (e.g. continuous and discontinuous).

- Scalability:

  Ideally, the algorithm performance should not be influenced by the number of design variables. The optimization method should be able to work equally well for problems with one to thousands of design variables. Scalability is a crucial point, especially for industrial applications.

- Ability to deal with real-world problems:

  The research in the area of structural optimization methods is increasingly driven by real-life applications in fields like automotive, aerospace and civil engineering [164]. Real-world problems are as a rule extremely complex and large [165], with a high number of design variables and constraints, as well as multiple objectives. Moreover, the evaluation of OF and derivatives is computationally expensive. To answer the demands of the industry, the numerical techniques for structural optimization must cope with these challenges.

- Accuracy:

  The algorithm must be able to converge to an optimum with the desired accuracy [165], i.e. it must be able to reach a solution close enough to the optimum in terms of OF, constraints and design variables. As a precise optimum is seldom meaningful, a near-optimum design can be sufficient for most of the practical cases.

- Ease of use:

  The algorithm should be easy to apply into practice and must require minimum efforts for the adjustment of its various control properties. Both inexperienced and experienced users must be able to use it.

All the above attributes are meaningful, but it is of utmost importance for practical applications that the algorithm is efficient, robust and that it is able to manage real-world problems. Unfortunately, there is no algorithm that fully satisfies all requirements. Even more, no general-purpose universal optimization strategy exists which performs equally well for all types of problems ("no free lunch theorem" [166]). This explains the multitude of methods currently available. It also makes their classification compulsory in order to get a quick but comprehensive overview of the state-of-the-art approaches and to be able to select the right strategy for a given problem. There are many possible division schemes based on

various criteria. Some of the most important ones are given hereafter, partially inspired by the works of Roy et al. [146] and Saitou et al. [167].

- Based on the number of design variables:
  - Single-dimensional optimization;
  - Multi-dimensional optimization.

  As real-world problems have more than one design variable, practically all state-of-the-art optimization techniques must have multi-dimensional capabilities. However, it is also quite common to transform multi-dimensional constrained into multi-dimensional unconstrained problems, which on their turn can be reduced to simple single-dimensional ones. Thus many multi-dimensional optimization techniques generalize to a series of single-dimensional optimizations [168]. Most of the available nonlinear programming (NLP) algorithms are based on the minimization of a function of a single variable without constraints. Some of the most notable one-dimensional optimization approaches include both search and approximation methods [169]: dichotomous search, Fibonacci search, golden-section search, quadratic interpolation method, cubic interpolation method.
- Based on the allowed values of the design variables:
  - Continuous optimization;
  - Discrete optimization;
  - Hybrid optimization.

  Many engineering phenomena have continuous nature and can be represented with real-valued design variables. Consequently, most of the existing algorithms are well suited for continuous optimization, including large groups of methods such as the GB ones [165]. However, either because of the discrete nature of some quantities or for convenience matters, in some practical engineering problems it can become obligatory to work with a finite number of possible values, i.e. discrete variables. Even more, for some engineering problems it could be necessary to use both continuous and discrete values in a hybrid approach. In [165] some of the most often used discrete optimization algorithms are discussed including the Branch and Bound method, sequential linearization methods, the neighborhood search method, rounding-off techniques, Simulated Annealing (SA) and Genetic Algorithms (GAs). Stochastic optimization algorithms are continuously gaining importance as they seem more appropriate than the enumeration techniques in regard to solving discrete variable problems efficiently. Moreover, some stochastic approaches such as GA are capable of performing a hybrid optimization involving both continuous and discrete design variables. This important feature makes GA appealing for complex real-world applications as the structural optimization of composite car bodies [170].
- Based on the existence of constraints:

  - Unconstrained optimization;
  - Constrained optimization.

  Constrained optimization techniques must be able to deal with equality and inequality, as well as linear and nonlinear constraints. Despite that engineering problems are predominantly constrained ones (with few exceptions), many of the available algorithms have been originally designed to perform unconstrained optimization only. A long list of examples can be given: steepest descent, Broyden-Fletcher-Goldfarb-Shanno, Fletcher-Reeves/Polak-Ribiere, Hooke-Jeeves, Nelder-Mead, Powell's method, SA, Tabu search (TS), Evolution Strategy (ES), GA, DE. In the most often case of an algorithm originally not conceived for constrained optimization, it is a common practice to combine it with supporting techniques such as penalty functions, special representations and operators, repair algorithms, separation of objectives and constraints, hybrid methods (e.g. Lagrangian multipliers, fuzzy logic) [171]. Among these techniques, constrained optimization by means of penalties is undoubtedly the most extensively used one, because of its ease of integration in an existing approach. A comprehensive state-of-the-art on the currently employed penalty functions methods is given in [171].

- Based on the number of objective functions:

  - Single-objective optimization;
  - Multiobjective optimization.

  As a multiobjective optimization problem has infinite solutions, the user must choose out of them a trade-off that suits the requirements of his/her application. For this purpose the entire Pareto optimal set or a good representation of it might be needed. The majority of the algorithms consider a single OF in their original formulation. One of the most straightforward ways to make them suitable also for multiobjective optimization is to reduce the multiple objectives into a single one [172]. This transformation is easily achieved by techniques such as the weighted sum method, the weighted global criterion method, the lexicographic method, the ε-constraint method and similar [165]. By varying the parameters of the single composite function and performing a series of single-objective optimization runs, different optimum solutions for the problem can be generated. Some methods always yield Pareto optimal solutions but may not be able to capture all of them. Other methods provide also non-Pareto optimal points together with all points in the Pareto optimal set. Beside these relatively simple aggregating approaches, there are others which treat all OFs in the same time and are able to generate the Pareto optimal set for a given problem. The Multi-Objective GA (MOGA), the Non-dominated Sorting GA (NSGA) and the Niched Pareto GA (NPGA) are a few representative examples of this class [173].

- Based on the calculation of the OF:

  - Optimization over analytic functions;

  - Simulation-based optimization.

  The above separation concerns quantitative OFs only, whereas qualitative ones (involving issues like manufacturability and aesthetics) are not considered. In analytic optimization the algorithm has to deal with a mathematical expression. It might be a well known function used for test and benchmark purposes (e.g. the Rastrigin function, the Rosenbrock function), but it might be as well a surrogate model obtained after a Design of Experiment (DOE) and RSM. In practice, all optimization algorithms are able to handle analytic functions. However few of them can deal efficiently with simulations. The requirements towards simulation-based optimization methods are much higher. While the time needed for the evaluation of an analytic OF is negligible, simulation-based OFs are computationally expensive. This second group of algorithms must be thus able to obtain satisfactory results within a highly limited number of OF calls. Because of their fast convergence, GB approaches are often preferred for simulation-based optimization. In addition, since they iterate by slightly modifying a current design, reanalysis methods can be used to reduce the computational cost and to approximate the analysis result of a new design based on the non-approximated analysis result of the current design [167]. However, due to the deficiencies of these conventional methods, the current trend is oriented towards more advanced techniques – mainly stochastic approaches such as SA, GA and similar.

- Based on the ability to search the design space:
  - Local optimization;
  - Global optimization.

  In case that the problem at hand is multimodal, i.e. has more than one minimum, a distinction is made between local and global optimizers. A local-search algorithm explores the design space around its initial starting point. Although being fast, such a strategy can get easily stuck into the nearest local minimum. Typical representatives for this group of approaches are the classical iterative methods, e.g. Sequential Quadratic Programming (SQP), the steepest descent method, conjugate gradient methods and similar. Fortunately, in some cases it is appropriate and possible to employ a local optimizer also in global search through a multi-start approach. The local optimization algorithm is launched multiple times from different starting points to increase the chances of better design space exploration. This technique is often used [165], being one of the simplest global search approaches. Moreover, it is even implemented in some commercial software programs such as MATLAB®. Undoubtedly, the group of heuristic approaches has the highest success rate when searching for global optima. This is due to their principles inspired mainly by natural phenomena such as evolution and swarms. Whereas these methods were initially regarded as mere academic research, during the last years they have found their way into engineering and into structural optimization in particular [146, 165, 167, 174]. Finally, local and global optimization strategies are sometimes combined in a hybrid

approach, e.g. [44, 170, 175]. First the excellent search capabilities of a global-search algorithm are exploited to get near the global optimum. After that a fast local optimizer is launched from the best final solution in order to speed up the search process. The main difficulty consists in deciding when the global optimum has been approached enough to switch to the local-search algorithm.

- Based on the number of disciplines:
  - Single-disciplinary optimization;
  - Multi-disciplinary optimization.

  In contrast to single-disciplinary optimization, multi-disciplinary optimization (MDO) considers the interaction between several disciplines (e.g. statics, normal modes, buckling). By incorporating all relevant disciplines simultaneously, the system performance can be significantly improved while avoiding iterations between them. In such a total system approach the best compromise between the disciplines can be efficiently detected. Nowadays the VDP is more and more driven by the need for MDO [176]. On the other hand the research in this field is still at its very beginning. While single-disciplinary optimization can be handled by algorithms traditionally employed for the problem at hand, including all disciplines simultaneously increases significantly the complexity of the problem. Different disciplines usually require different FE meshes and solvers, and employ different amount of computational time. The nature of the studied quantities can vary significantly ranging from linear continuous to highly non-linear and discontinuous responses with eventual disturbances by numerical noise. In general the MDO approaches depend strongly on the disciplines involved. Metamodels based on RSs are often employed for structural statics, low frequency dynamics and crashworthiness [177–181]. If the surrogate models manage to represent the actual physical characteristics sufficiently well, the time needed for optimization is negligible and the choice of optimization strategy is of secondary importance. Such MDO optimization is by far the most efficient [176]. Other authors recommend the direct use of stochastic optimization algorithms, given that most MDO problems are non-convex and multimodal [140, 143, 176, 182]. These studies showed that in cases where at least one discipline is characterized by a highly non-regular response, evolutionary algorithms were the best in class [140, 143, 176, 182]. GAs seem to be advantageous if the design is still in the early phases and feasible zones in the total design space have to be identified [44, 176, 182].

Whereas the previous classifications can be generally valid also for other engineering fields, the last two viewpoints are exclusively related to structural optimization and have been extensively used for the literature in this area [146, 165, 167, 183]:

- Based on the coupling with FEA:
  - Gradient-based optimization through approximate design models;

  - "Black box" heuristic optimization.

- Based on the type of geometry parameters:
  - Topology optimization;
  - Shape optimization;
  - Sizing optimization.

Because of their importance, these two classifications will be the subject of Sections 2.3.3 and 2.3.4 respectively.

2.3.3 Gradient-based and heuristic optimization

Gradient-based optimization

The classical algorithms for structural optimization are driven by deterministic mathematical procedures through which the design is iteratively changed until a convergence criterion is reached. They are still regarded as the most straightforward way to tackle structural optimization problems. These traditional methods are based on NLP techniques which use the gradients of the OF and constraints, hence the name gradient-based. Logically, they are suitable for differentiable optimization problems with continuous variables. A considerable amount of literature can be found on GB mathematical programming algorithms [165]. Some of the most prominent NLP approaches include Sequential Linear Programming (SLP), SQP, Modified Method of Feasible Directions (MMFD), Method of Moving Asymptotes (MMA), augmented Lagrangian methods. The interior point methods, developed initially for linear problems, have also been extended for nonlinear problems [165].

Although GB algorithms are fast, only speed by itself does not suffice to achieve excellent performance as their direct coupling with FEA is inefficient. As pointed out in [163, 164], the mechanism by which the structural analysis and optimization programs communicate is critical. Their direct interference as well as the number of FEA runs must be minimized as much as possible. In this regard, Lucien Schmit laid the foundations for the development of many modern structural optimization methods [184]. He pioneered a general new approach of coupling FE structural analysis and non-linear mathematical programming techniques to create automated optimum design capabilities. Schmit's ideas initiated the development of a new class of methods, referred to as sequential approximation algorithms, which are nowadays becoming widely used and are successfully applied to a multitude of structural systems [165]. They exploit the nature of structural optimization problems whose objective and constraints often exhibit near-monotonic behavior within small variations of the design variable vector [167]. First gradient computations of the structural responses with respect to the design variables are incorporated into the FEA code. Based on the gradient information the analysis package is used to define an approximation of the structural design problem (in terms of approximated OF and constraints). Various mathematical optimization techniques are then employed to solve it. The optimum of the approximate problem is then used as a basis for performing one or more structural analyses for the

purpose of updating or refining the approximate design problem. The concept of the approximate design model (2.11) drastically reduces the computational cost of solving the structural optimization problem [163].

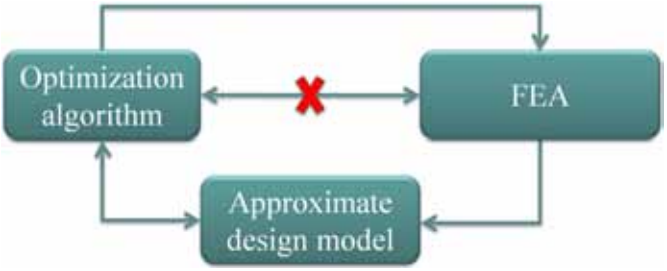

Figure 2.11: The approximate design model.

Thus it is clear that in modern structural optimization the search strategy and FEA are interrelated and go hand in hand. In practice this means that the platform used must have not only optimization but also analysis capabilities. An excellent state-of-the-art example for such integration is provided by the commercially available software MD Nastran [122], which is widely recognized in the automotive, aerospace, maritime and civil engineering communities. Even more, as stated in [185], MD Nastran with its SOL200 [100] is extensively used as a standard for structural optimization in the automotive industry. In a modern GB optimization software first FE structural analysis is performed. Then all constraints are screened, and only the critical ones are considered in the current design cycle. Sensitivity analysis is performed to obtain the derivatives of the OF and the active constraints with respect to the design variables. Based on this information, the original problem is approximated locally about the current point in the design space. Usually Taylor series expansion of OF and constraints is used, truncated up to the first derivative term (linear approximation). The approximate problem is optimized and once a solution is found, a new design cycle can start. FEA is performed again and a new approximation is created. The final solution of the original optimization problem is thus obtained iteratively by solving the sequence of approximate explicit problems. The approximation concept (2.11) acts like an interface between FEA and the optimizer, drastically reducing the number of FEA required. An illustration of the whole process is given in Fig. 2.12.

Because of its wide popularity, GB optimization through approximate design models has found numerous applications in the automotive field from the concept stage onward [1, 41, 42, 53, 170, 185–188]. It is suitable both for a single run local search and for a multi-start global approach, as well as for a hybrid global-local strategy.

Heuristic optimization

The heuristic approach to structural optimization relies on zero-order methods for global search. Population-based metaheuristics such as GA, ES, Particle Swarm Optimization (PSO), Ant Colony Optimization (ACO) and other similar

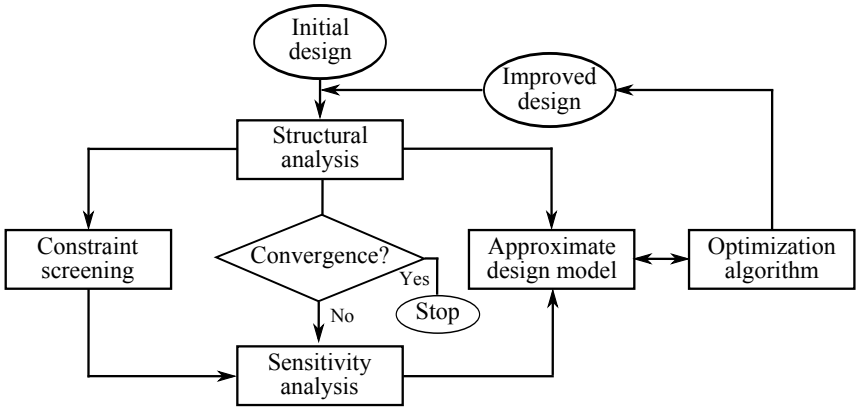

Figure 2.12: Advanced gradient-based structural optimization.

techniques are used. Neighborhood metaheuristics is also employed, e.g. SA, TS, Quantum Annealing (QA).

The use of heuristic approaches in structural optimization emerged as consequence of the deficiencies of the classical methods in complex optimization problems [174]. Stochastic methods make no assumptions about the nature of the problem and are able to explore non-linear, non-convex design spaces with discontinuities. Moreover, very large spaces of candidate solutions can be searched and solutions near the global optimum can be located. The heuristic methods are suitable for problems with continuous and/or discrete variables, and they can be used for MDO. In addition, they are derivative free (i.e. direct search). For some authors relying on arbitrariness (i.e. generation and use of random numbers during the search) instead of making use of gradients can be a serious shortcoming [172]. On the other hand, heuristic algorithms have proved useful in exploring many design alternatives and finding significantly better solutions, especially in regard to topology and shape optimization [167, 174].

Their main drawback is that they communicate directly with FEA (in contrast to Fig. 2.11). Thus each OF evaluation means a completely new structural analysis. If opposed to GB optimization through approximate design models, heuristic optimization can be designated as “black box” approach. If the computational time for the analysis is high, such inefficiency might be unacceptable [163]. Until a decade ago, the cost of repeated analyses has been the main reason for the limited applicability of metaheuristics to practical problems.

Currently, heuristic optimization is a fully recognized structural optimization paradigm [174], which is extensively used not only by researchers but also by practitioners. Despite the computational difficulties encountered, the unceasing interest of the designers towards the heuristic approaches for structural optimization is driven by their potential for creative behavior and radically different designs [172]. Many applications have been reported [146, 174]. Metaheuristics is slowly finding its way also in the concept stage of vehicle development. Structural optimization of concept FE models was performed in various studies mainly by means

of the classical GA [1, 22, 23, 27–31, 44] and some of its improved versions like the Adaptive Range Multi-Objective GA (ARMOGA) [128]. DE was employed for heuristic structural optimization in few studies [1, 8].

According to [146] the GA is so far one of the most popular algorithmic optimization approaches. Moreover, GA seems the most widely used Evolutionary Computation (EC) method in structural optimization [174]. Despite their huge success, today GAs still represent an active area of research [172]. In [146] Roy et al. outlined the emergent computing techniques in engineering design optimization. The most promising algorithms identified included stochastic approaches such as SA, DE, Quantum Computing and Swarm Intelligence (ACO and PSO). As concluded in [174], heuristic algorithms are still far from maturity and are likely to be the subject of intense research and development in the coming years.

2.3.4 Topology, shape and sizing optimization

Based on the type of geometry changes applied during structural optimization, a distinction can be made between sizing, shape and topology optimization algorithms. From sizing through shape to topology optimization, the DOFs for modification increase, but also the problem complexity. The difference between these three types of structural optimization is illustrated in Fig. 2.13 for a mechanical component.

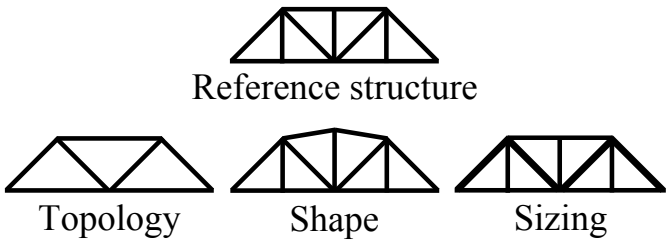

Figure 2.13: Topology, shape and sizing optimization.

Topology optimization is the most general form of structural optimization. It aims at finding the optimal material layout of an engineering system.

In shape optimization the optimal boundary form or contour of a structure is sought. During this process the connectivity of the structure remains unchanged and new boundaries are not formed.

In sizing optimization the structure is modified by a predefined set of dimensions allowed to vary while its topology and shape are fixed. These dimensions are typically cross-section parameters and plate thicknesses.

Topology optimization can work with a less detailed FE model than required by shape or sizing optimization. Taking into account the lack of product knowledge and the high number of DOFs for decisions in the concept phase, topology optimization becomes suitable for layout and load-path studies during the initial design stage [167, 174]. It is good at dealing with global design responses (e.g. structural compliance, eigenvalues, displacements). On the other hand shape and

sizing modifications are more appropriate for detailed designs [174] and are generally focused on local design responses (e.g. stress, strain). The traditional application of these three groups of structural optimization approaches in the VDP is shown in Fig. 2.14.

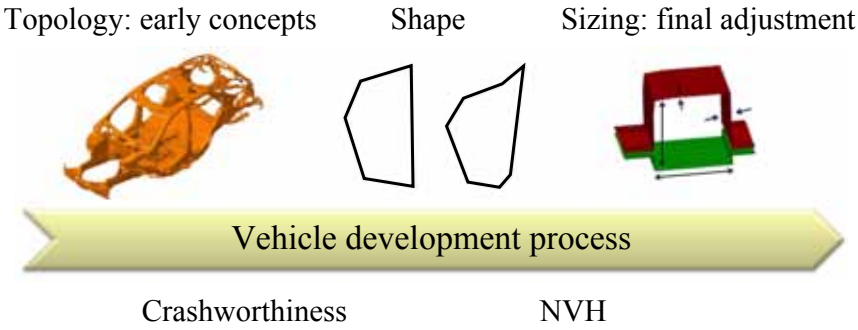

Figure 2.14: Structural optimization in the VDP.

Topology, shape and sizing optimization problems have been addressed in numerous studies by employing both GB and heuristic algorithms [174]. Sizing problems are usually considered as the easiest ones and are successfully handled by mathematical programming methods [167, 174]. Difficulties may arise in the case of large FE models or highly nonlinear phenomena [167]. Some applications of population-based methods such as GA, ES and Evolutionary Algorithm (EA) have also been reported [174].

Whereas in sizing optimization GB algorithms seem to be predominant, in shape optimization they are used to complement the heuristic approaches [174]. Formal methods are well established for continuum structures, but EC approaches are also used. Metaheuristics is extensively employed for the shape optimization of discrete structures.

Having the highest complexity of all three, topology optimization problems are normally solved with stochastic approaches such as SA and EA [174]. In this third group difficulties are often encountered in regard to checkerboard effects, computational cost in case of more variables, design manufacturability and other issues.

2.3.5 Trends and challenges

Future research in the area of structural optimization will continue to address the currently open issues, which can be summarized as follows:

Choice of optimization algorithm

As seen in Section 2.3.2, there are a lot of characteristics that a good optimization method must possess. Since there is no algorithm without any deficiencies, a trade-off must be always found. The main problem is that the number of existing optimization approaches to choose from is immense. Some basic knowledge about

at least the most prominent of them becomes essential. When a certain method is selected, there is no guarantee that it will be the best performing one for the current problem. On the other hand, if the OF is simulation-based, testing even a limited number of different methods becomes impossible. Benchmark tests on well-known analytic functions are often made in order to compare various algorithms. However, a judgment made on such a basis can be misleading as many engineering problems are practically a "black box". Thus no direct link can be made between the performance of an algorithm in a test and in a real-world case study. For all these reasons, the choice of proper optimization approach is a non-trivial task which is in the hands of the design engineer. This difficult decision is mainly experience-based, although benchmarks as well as use cases and results reported in literature can still help to get a preliminary idea of the algorithm performance.

Global versus local search

The aim of mathematical optimization is to find the best solution for a given problem. In practice, a solution can be claimed to be a global optimum either by proving that the problem is convex, or by exhaustive search of the feasible set [165]. As both approaches are computationally expensive for real-world problems, their final solution is usually regarded as local minimum [146]. In an industrial context finding the global optimum is often impossible because of the problem size and complexity, as well as the lack of knowledge [146, 176]. In many cases a solution which is feasible and significantly better than the initial design is sufficient [146, 183]. Hereafter, the best known (hopefully) near-global solution is intended by global optimum.

Most topology, shape and sizing optimization problems can have more than one local optimum and are not convex [162, 164]. In addition, there are real-world structural optimization problems with hundreds or even thousands of design variables [41, 44, 189]. The computational effort to solve the global optimization problem increases enormously and even nowadays it represents a serious challenge [165].

The classical GB algorithms are fast but local optimizers, i.e. the final solution depends on the starting point and can be a local optimum [44, 164, 165, 175, 176]. The possibility that better and/or radically different design alternatives are missed is high, especially for large-scale problems [164]. From this point of view GB algorithms are not without deficiencies for many real-life structural optimization problems [146]. Involving a GB method in a multi-start approach for global optimization can alleviate but not completely overcome its weaknesses in this regard. Heuristic optimization methods are able to locate near-global and/or radically new solutions. However, being inherently slow, they are mainly used for small-scale problems. Thus the choice between local and global optimizers can be roughly considered as a choice between speed at one hand and solution quality on the other.

Detailed versus simplified FE models

The type of FE model employed is of utmost importance in simulation-based optimization. As stated by Roy et al. [146], design optimization is limited by the computational cost of the design evaluation. In this regard, handling large FE models is one of the challenges of simulation-based optimization [146]. The direct use of detailed FE models is traditionally prohibitive for the application of population-based approaches such as EAs and GAs [164]. In fact, until the last few years their high computational cost has been unaffordable in direct heuristic optimization which on its turn limited the development and application of these algorithms for real-world structural problems. Surrogate models based on a combination of DOE and RSM are a possible but not always applicable workaround [146, 190] (e.g. 2.1(d)). Not only are they inappropriate for more than 10-15 design variables, but also in the case of non-linearities and/or discontinuous feasible domain. Being a flexible alternative to detailed FE models and to their surrogate representations, simplified FE models are one of the promising future research trends [167]. In fact, the structural optimization of small-sized concept models is increasingly gaining importance and popularity [8, 31, 41, 42, 44].

Scalability

According to the curse of dimensionality [191] the volume of the design space and the number of OF evaluations required for its exhaustive search grow exponentially with the increase of the problem dimensions (i.e. the number of design variables). A great majority of the optimization algorithms perform well for small dimensions (up to 10 design variables) but suffer scalability issues for medium-scale (10 to 100 design variables) and large-scale problems ($>$ 100 design variables). On the other hand, there are numerous practical applications for which large-scale structural optimization is needed [41, 42, 44, 170, 189]. The development of advanced algorithms to deal with such problems is identified by many authors as one of the future challenges that structural optimization has to face [146, 165, 167]. This is fully valid especially as far as global-search stochastic approaches are concerned.

Other issues

Naturally, there are also many additional challenges. They could give the motivation for further research in the following directions:

- Uncertainty and reliability [146];
- Qualitative design space [146];
- Multiple disciplines [176];
- CAD-FEA interoperability and integration [167];
- Multi-modal and (large-scale) multi-objective optimization [146, 172].

It is thus clear that structural optimization has still a long way to go before being considered completely mature.

Chapter 3

Concept modeling of beams

3.1 Introduction

Undoubtedly the methods based on simplified FE equivalent of the vehicle structure are among the most popular concept modeling approaches and represent an area of active research [1, 3, 8, 20–24, 26, 26–35, 35–37, 39, 41–48] (Section 2.2.2). A simplified BJP representation of a detailed FE model is both small-sized and parametric, thus enabling fast optimization studies. The vehicle static and dynamic performance can be improved efficiently and at low computational cost. The BJP models are extremely suitable for sizing optimization in which the cross-sectional dimensions and plate thicknesses of the beam-like structural parts can be changed, as well as the joint parameters. The big number of design variables accessible to the engineer ensures a higher degree of flexibility. Shape optimization can be also performed and modeling from scratch is not to be excluded either.

The alternative use of detailed FE models of predecessor vehicles is related to various disadvantages. Their main drawback is that they can be times bigger than their concept counterparts and can thus require considerably more time for structural analysis. Furthermore, creating parametric models becomes more difficult. All plate thicknesses are directly available as design variables but this is often insufficient [53]. Mesh morphing gives more freedom to explore the design space but the computational cost of directly involving the parametric morphed models in an optimization process remains high and often not affordable. Being a mathematical abstraction not based on the problem physics, surrogate models are not always appropriate as a workaround technique. Even if they can be used, the initial time for their creation might be unacceptable in an industrial context. Moreover, only a limited number of design variables can be handled by the meta-models.

In comparison to the predecessor-based approaches, the application of the other two groups (Section 2.2.3 and 2.2.4) is much more limited. Although the methods from scratch are quite powerful, they are highly complex and require significant development time and efforts, as well as extensive expert knowledge and previous experience (e.g. for the creation of the library with predefined components). The development of such methodologies is only possible at an OEM or at least in collaboration with one or more OEMs. On the other hand, the approaches aiming at integrated CAD-CAE systems like the isogeometric analysis of Hughes et al.

[7] are still in their very beginning. They offer promising new horizons but are far from maturity. An extensive research, development and validation of this third group is required to achieve at least the current capabilities of the other methods.

The fact that the approaches using simplified structure layout have appealing strengths and enjoy great popularity does not mean that they fully outmatch all other method groups. They still have various deficiencies to overcome. A reasonable way to get a better understanding of the current problems is to take a closer look at the three building groups of the BJP models. As discussed in Section 2.2.2, panels do not represent any particular difficulty as it is quite simple and straightforward to obtain their concept equivalents. However, a major effort is required regarding the other two groups of components. Even the most advanced methods for the creation of concept BJP models introduce some modeling errors with respect to their detailed FE equivalents because of the inevitable simplifications made. For the same reason the transition from the optimized simplified to the optimized detailed FE model is not straightforward. The link between the concept and the detailed FE model can be sometimes lost after optimization. In addition, a well-established, standardized methodology for the concept model creation must be available. Dedicated automation tools are needed or this task can become onerous and error prone. Whereas concept joints will be the topic of Chapter 5, the current and the next chapter focus on concept beams.

As discussed in Section 2.2.2, 1D beam elements are used to simplify all beam-like BIW members in a BJP model. This leads to a significant reduction in the number of elements and nodes with respect to the initial shell mesh. However, it can cause various discrepancies between the detailed FE model and its concept equivalent. Concept models with 1D beams result stiffer than their detailed FE counterparts as they do not take into account local cross-section deformations. Additional differences can occur because of factors such as flanges, spot welds, stiffeners and discontinuities in the reference FE model, which are heavily simplified or not considered in the concept model. The type of the 1D beam cross-section is also important as it influences the accuracy in approximating the real cross-section properties. Various solutions have been proposed to tackle these issues: better modeling alternatives [23, 34, 41, 42], model updating [28–31], correction factors [1, 8, 22, 23]. However, in all these works, the problem is only partially addressed and solved. Still no holistic approach exists.

The aim of this chapter is to perform a systematic study of the error factors in 1D beam concept modeling and of their potential impact on the model precision. Consequently, guidelines are given on good practices for overcoming the intrinsic limitations of models based on 1D beams. By providing a better insight of its major bottlenecks, potential pitfalls and their possible solutions, 1D beam concept modeling can become more accurate and reliable.

This chapter is organized as follows. The used methodology is described in Section 3.2 and it is then applied to various idealized and non-idealized component level case-studies in Section 3.3. In Section 3.4 the derived good modeling practices are applied to a couple of industrial case-studies, both at car body level. A hybrid detailed-concept FE model of a BIW is created and analyzed in Section 3.4.1, while an existing BIW concept model is studied in Section 3.4.2.

3.2 Methodology

This section focuses on the quality of 1D beam models. The main criteria to evaluate it are considered, as well as the major error factors that can deteriorate it.

3.2.1 1D beam concept modeling

To assess the performance of a specific 1D beam concept model, two main aspects must be taken into account. On one hand, its structural behavior must be as close as possible to the one of its corresponding detailed FE model, thus resulting in better prediction capabilities. On the other hand, a geometry match between the detailed and the concept model must be also ensured. The fulfillment of this second condition is especially important for optimization studies so that the optimized concept model could be used to find the optimized detailed FE model. These two important considerations are discussed hereafter.

Beam theories

1D beam models are simpler and computationally more efficient than models with 2D shell or 3D solid meshes. In consequence, beam theories are extensively used for various engineering applications regarding the static and dynamic analysis of structures [54]. Many methods have been proposed each of which relying on different assumptions and simplifications and resulting in different precision of the concept models.

The beam theories of Euler-Bernoulli [55, 56], de Saint-Venant [57, 58], and Timoshenko [59, 60] represent the group of classical approaches. In contrast to its two predecessors, Timoshenko's model accounts also for transverse shear deformations. However, none of the three considers non-classical effects such as in- and out-of-plane cross-section deformations and torsion-bending coupling. The application of the classical methods for cases in which such effects are present can lead to wrongly estimated structural stiffness. This has been the main motivation for the further development of refined beam theories during the last years. Because of their fundamental importance, the Euler-Bernoulli and the Timoshenko beam models are described in Appendix B.

Various solutions have been proposed to overcome the intrinsic limitations of the conventional approaches. They rely on different techniques: the introduction of shear correction factors, the use of warping functions based on the de Saint-Venant's solution, the variational asymptotic solution, generalized beam theories and higher-order beam models. A comprehensive state-of-the-art can be found in [54]. Despite of the attempts to extend the applicability of 1D beam modeling, few of these works have led to a fully functional and tested commercial software to be used by the engineering community. The proposed approaches are often developed and validated for specific academic case-studies, but their performance in more general cases is not guaranteed.

For the purposes of this dissertation Timoshenko's beam theory was used, extended with an additional DOF accounting for warping [61, 76]. Thus 1D beams

have 7 DOFs at each end node – three translations T, three rotations R and one DOF approximating the cross-section deformation due to torsional warping. This 7^{th} DOF is actually the rate of change of the angle of twist with respect to the beam axis, i.e. $\frac{d\theta_z}{dz}$, where θ_z is the angle of rotation at any cross-section and z is the beam axis.

When a beam is transversely loaded in such a manner that the resultant force does not pass through the longitudinal shear center axis, the beam will not only bend but also twist. On its turn, if a torque is applied to non-circular cross-sections, the transverse sections which are plane prior to twisting, warp in the axial direction. Thus the plane sections no longer remain plane after twisting and axial stresses are produced. This out-of-plane distortion is called warping. Thereby, an in-plane distortion of the cross-section also occurs. When the warping deformation is constrained, the member undergoes non-uniform torsion. The total torque T_{tot} can be expressed as:

$$T_{tot} = T_{SV} + T_w = GJ_{zz}\frac{d\theta_z}{dz} - EC_w\frac{d^3\theta_z}{dz^3} \tag{3.1}$$

where T_{SV} is the St. Venant torque, T_w is the warping torque, G is the shear modulus, J_{zz} is the torsional constant, E is the Young?s modulus, and C_w is the warping constant. When the 7^{th} DOF $\frac{d\theta_z}{dz}$ is known, T_{SV} and T_w can be calculated for any cross-section.

For the sake of simplicity only this advanced beam theory has been employed throughout the study. A commercial solution widely used in the automotive industry was chosen – MD Nastran 2010 [100].

Geometrical similarity

As discussed in Section 2.2.2, there are currently three state-of-the-art approaches for geometry description of 1D beam cross-sections – STCSs, ABCSs and GNCSs (Fig. 2.5). Each of these methods has different strengths and weaknesses. Consequently, it is important to be familiar with them so that the right choice of cross-section description can be made.

The creation of 1D concept beams with STCSs is quite straightforward and simple, considering that a library with simplified versions of the most common cross-section typologies is available. STCSs can turn out important in the very early phase of vehicle development if there is a lack of knowledge about the detailed geometry of the cross-sections. Moreover, STCSs are typically used for modeling space frame constructions (e.g. [52]). However, this approach is not always appropriate despite its simplicity, given that many of the beam cross-sections in a vehicle unibody are highly irregular. Their description with standard shapes is an approximation which introduces a modeling error that depends on how close the match is. Moreover, in the case of bad approximation, it can be difficult to link the optimized 1D beam model with its equivalent detailed FE model.

The ABCS approach is extremely suitable for concept modeling as the level of details can be finely controlled. The cross-section description can range from

a simple rectangle enclosing the real shape to a geometry that matches it almost perfectly. In fact, a fully detailed ABCS will have the same geometry and cross-sectional properties as the projection of the reference cross-section. This facilitates the transition from the optimized concept model to the optimized detailed FE model (Fig. 2.2(a)). The drawback of this approach is that the description with points and segments is more complex and requires more effort so dedicated tools and scripts should be used.

The GNCS method is simple and effective. However, in contrast to the previous two methods, the real cross-sectional geometry is lost once the concept model has been changed. Instead of keeping the reference geometry information, it is substituted with its equivalent cross-sectional properties such as area and MOI. Although this equivalent GNCS can be still precise, the direct relation with the detailed FE model is broken. Thus both the application of geometry constraints during optimization and the transition from the optimized concept to the optimized detailed FE model become problematic.

In this study the performances of the ABCS and the STCS approach are compared on a small set of beams. GNCSs are not considered as from the point of view of the analysis ABCSs and STCSs are after all transformed to GNCSs (Fig. 4.1), but a GNCS-only description loses the important link to the actual cross-section geometry. Breaking this relation is undesirable, especially for concept optimization studies.

3.2.2 Potential error factors

There are many factors which could influence the precision of the concept model regarding its structural behavior and geometrical similarity with the reference structure. Those considered as the most important ones are discussed hereafter. They will be subject of a detailed study in Section 3.3.

Cross-section deformations

As out-of-plane deformations are approximated by the employed beam theory [61, 76], they are not a subject of study in this work. Regarding the in-plane cross-section distortion, a new measure is hereby proposed to quantify it. The in-plane cross-section deformation measure ($ICDM$) aims to compare two cross-sections. The first one is a deformed cross-section resulting from static analysis of the detailed FE model. The second one is the undeformed equivalent of this cross-section that mimics the behavior of a 1D beam and can undergo rigid transformations only. The $ICDM$ is obtained as the average of the distances between the corresponding nodes of the deformed and the rigid cross-section. The procedure for its calculation is as follows:

- A control node C is defined for the cross-section under study (reference detailed FE model). It can be positioned in the cross-section centroid or shear center, as well as in any other point. The coordinates $\mathbf{Nds}_{ref}$ of all N nodes belonging to the cross-section are obtained from the FE model. The three translations and rotations of each node are obtained after linear static

analysis is performed. Thus the matrices $\mathbf{T}_{nds}$ and $\mathbf{R}_{nds}$ can be defined, that contain the translations and rotations of all N nodes. Likewise, $\mathbf{T}_C$ and $\mathbf{R}_C$ stay for the translations and rotations of the control node C.

- The coordinates $\mathbf{Nds}_{def}$ of all nodes belonging to the deformed cross-section are obtained as:

$$\mathbf{Nds}_{def} = \mathbf{Nds}_{ref} + \mathbf{T}_{nds} \tag{3.2}$$

- An undeformed counterpart of the distorted cross-section is obtained to mimic 1D beam behavior. It is allowed to undergo rigid transformations only. The coordinates $\mathbf{Nds}_{rgd}$ of all nodes belonging to this rigid cross-section are obtained as:

$$\mathbf{Nds}_{rgd} = Rotate(\mathbf{Nds}_{ref} + \mathbf{T}_C, \mathbf{R}_C) \tag{3.3}$$

  where *Rotate* rotates all nodes of the rigid cross-section at angles $\mathbf{R}_C$ around C. In fact, the control node C can be thought of as the end node of an imaginary 1D beam. The rigid cross-section has the same dimensions as the reference one and can be regarded as the 1D beam section which translates and rotates together with the beam node C while remaining undeformed.

- The plane P' that best fits all reference nodes is found. Both the nodes belonging to the deformed and to the rigid cross-section are projected in this plane. Their new coordinates are found as:

$$\mathbf{Nds}'_{rgd} = Project(\mathbf{Nds}_{rgd}, P') \tag{3.4}$$

$$\mathbf{Nds}'_{def} = Project(\mathbf{Nds}_{def}, P') \tag{3.5}$$

  where *Project* gives the projection respectively of $\mathbf{Nds}_{rgd}$ and $\mathbf{Nds}_{def}$ in P'. This step is needed because normally the reference nodes (consequently those of the deformed and the rigid cross-section as well) will not be in the same plane except for the case of a highly regular mesh.

- $ICDM$ is calculated as:

$$ICDM = \left(\sum Dist(\mathbf{Nds}'_{def}, \mathbf{Nds}'_{rgd})\right)/N \tag{3.6}$$

  where *Dist* gives the vector of all distances between the corresponding nodes of the deformed and the rigid cross-section. It must be noted that the division by N in Eq. 3.6 aims to avoid the dependency on the number of nodes which can vary between the different cross-sections. The unit of $ICDM$ is the same as the length unit of the model.

Fig. 3.1 illustrates the final result of the procedure described above applied to a B-pillar cross-section. In Section 3.3 $ICDM$ is calculated for all beam case-studies.

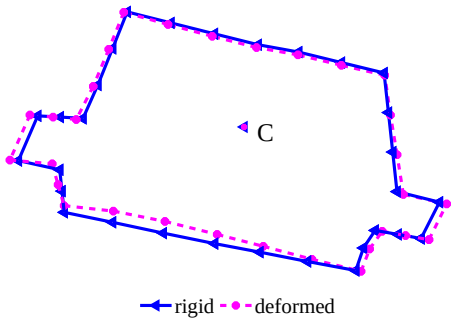

Figure 3.1: B-pillar in-plane cross-section deformation.

Beam cross-section geometry

The approximation of the reference cross-sections in the 1D beam model is decisive not only for the geometrical similarity with the actual structure (Section 3.2.1), but also for the concept precision. In case that the reference geometry can be completely matched by STCSs, the performance will be the same as that of an ABCS model. The difference between these two techniques is clearly pronounced in the frequent case of non-standard cross-sections. The beam-like parts of the BIW are often highly irregular, non-prismatic and with various internal layers and stiffeners. The bigger the discrepancies introduced by STCSs with respect to the true cross-section properties, the bigger is the error not only at local level, but also regarding the structural behavior of the whole concept model. It is preferable to perform the simplification of such reference FE models with ABCSs. They allow the designer to achieve the desired balance between precision and complexity of the concept model by varying the level of detail in the cross-section description. As mentioned in Section 3.2.1, GNCSs are not considered in this work.

To study this error factor three beam structures with non-standard cross-section geometry are presented in Section 3.3.1. Two types of concept models are created for each of them using STCSs and ABCSs respectively and their performance is compared. In Section 3.3.2, more complex structures are studied, made up of several thin metal sheets and internal stiffeners.

Discontinuities

The presence of structural discontinuities in the detailed FE model can be the cause of inaccuracies in the concept one. The error depends on how abrupt the transition is in both models. The more different the cross-section properties of the two adjacent beam structures (e.g. box to C-shape cross-section), the more the error is expected to increase. The usage of STCS modeling could further deteriorate the problem, being a method in general less precise than ABCSs. In many cases the design engineer is forced to increase the discrepancy between the actual and the modeled cross-sections because of the limited typologies available in the predefined library. As a consequence, transitions which are smooth in

the reference FE model become abrupt in a STCS concept model, additionally increasing the modeling error.

To study the influence of this error factor two irregular beam structures with alternating open and closed cross-sections are considered (Section 3.3.1), for which both STCS and ABCS modeling is applied. Furthermore, a B-pillar having discontinuities is studied in Section 3.3.2.

Spot welds and flanges

Spot welds are the predominant joining method in the automotive industry. Thin steel metal sheets are assembled into vehicle components by means of spot welding. Thus a typical vehicle BIW can contain several thousands of spot-welded joints. They have a significant influence on important performance attributes such as global modes, static stiffness, durability and crashworthiness performance [1, 11, 157]. For this reason spot welds have to be considered in the detailed FE model of the vehicle. A state-of-the-use review of the various modeling techniques can be found in [192]. Furthermore, because of its importance, the spot weld layout is often subject to MDO [157].

The beam-like parts of the BIW are not an exception. They are made of formed steel shells, which are joined together by spot welding along their lip flanges (Fig. 3.2(a)). In the concept FE model the segments of the 1D beam cross-section corresponding to the spot welds in the detailed FE model have to be closed (Fig. 3.2(b)). This has to be performed even for the most precise ABCS description in order to ensure the continuity of the concept cross-section and in the same time the connection of the metal sheets. This approximation decreases the precision of the concept model, as the actual distribution of the spot welds is considerably sparser and the real structure is more flexible.

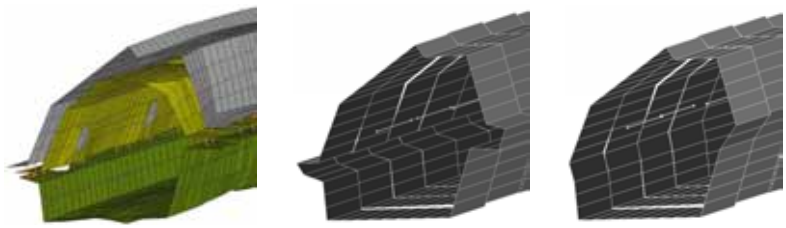

(a) Detailed. (b) Concept. (c) Concept without flanges.

Figure 3.2: Beam structure example.

Furthermore, in industrial problems it is a common practice to neglect the lip flanges in the concept model [41, 131], e.g. Fig. 3.2(c). The reason is that when ABCSs are used, the whole cross-section is rescaled in the optimization process [41, 100, 131]. If the cross-section contains flanges, their size is also changed, which on the other hand is undesirable as their main function is to allow the spot welding of the metal sheets. The resizing of the flanges can make the properties of the 1D

beam cross-sections as well as the mass of the whole structure infeasible and not realistic.

To assess the influence of these two interrelated error factors, several beam-like parts of the BIW are considered (Section 3.3.2). The performance of concept models both with and without flanges is compared. Additionally, modified detailed models are created and compared with the reference ones. Their aim is to mimic the concept modeling of spot welds by adding more connections between the nodes at the flange borders.

3.3 Component level studies

In this section two groups of beam structures are studied at component level: idealized and non-idealized ones. Thanks to its intentional simplicity, the first group serves to distinguish unambiguously the influence of some of the error factors introduced in Section 3.2.2. On its turn, the second group includes more problematic and realistic cases taken directly from the vehicle BIW, for which all studied factors are relevant.

3.3.1 Idealized beams

Case-study definition

Six different 2D shell models were subject to simplification with 1D beams. Because of the simple geometry, there was a perfect match between them. The corresponding detailed models (DM) and concept models (CM) are displayed in Fig. 3.3. The left-most column evidences the reference cross-section shapes. These six cases are a representative but not exhaustive selection of cross-section typologies, given their wide variety in the vehicle shell BIW [131]. All beams are prismatic, 0.5 m long and made of steel with plate thickness of 2 mm. Three of them have standard profile (1 to 3) while the rest have a non-standard one (4 to 6). In addition, they can be divided in closed (1 and 4), open (2 and 5) and mixed open/closed (3 and 6) cases. For the cases with non-standard profile (4 to 6) three additional 1D beam models with STCSs (CM'_4 to CM'_6) were also considered in order to compare their performance with their ABCS counterparts (CM_4 to CM_6). Each of them was created as a bounding box around its corresponding DM. Their masses were kept the same as those of the DM by adjusting the shell thickness of each STCS model accordingly. Such an approach is considered a good practice as having different masses is not desirable for the dynamic load cases. For all 1D beam structures from Fig. 3.3 the origin of each element coordinate system was placed at the shear center of its corresponding cross-section (Fig. 4.3). Moreover, the axes of all these local coordinate systems (x, y and z) were aligned with the axes of the global coordinate system O_{XYZ}.

Finally, for each of the six case-studies the reference cross-section dimensions (width w_{ref} and height h_{ref}) were varied one at a time resulting in four configurations such that $w = 0.5w_{ref}$, $w = 1.5w_{ref}$, $h = 0.5h_{ref}$ and respectively $h = 1.5h_{ref}$. The width w is the size of the side parallel to the X axis and the

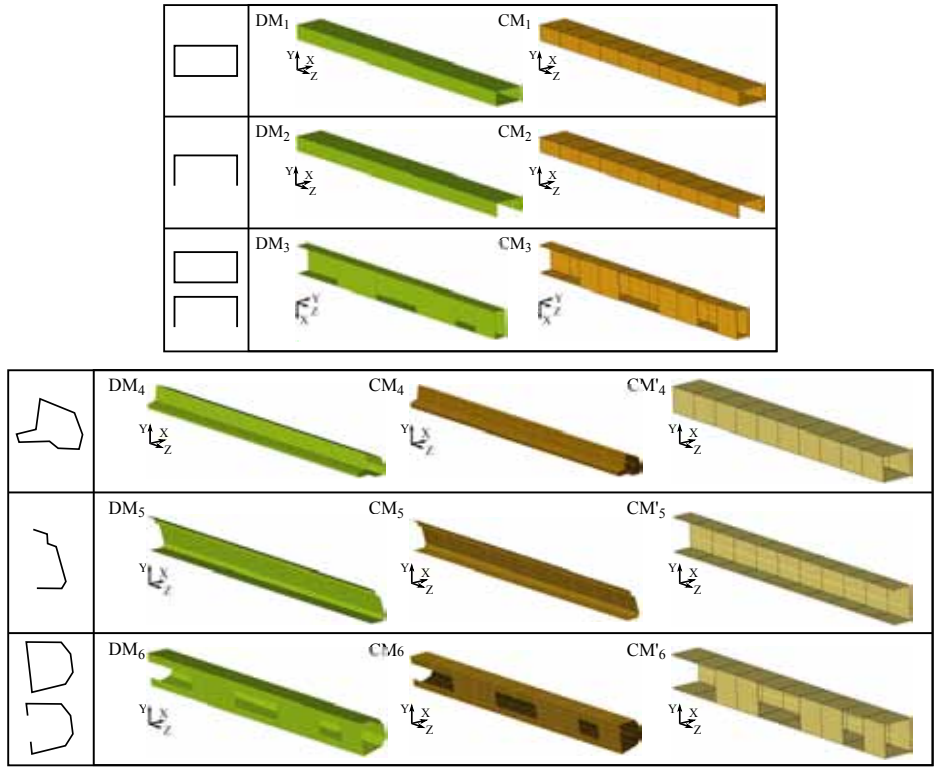

Figure 3.3: Idealized beam case-studies.

height h is the size of the side parallel to the Y axis. An example is given in Fig. 3.4 for DM_5. These additional models were considered in order to study the relation between the modeling error and the size variation of the same beam, which normally occurs during structural optimization. To apply these structural modifications on the detailed FE models, indirect mesh morphing via morph volumes was used (Section 2.2.2). In the concept models, it was sufficient to change the cross-section parameters (STCS) or rescale accordingly the bounding box around the cross-section (ABCS). The shear center offsets were also updated where appropriate.

The area MOI J_{xx} and J_{yy}, and the torsional stiffness parameter J_{zz} of the cross-sections can be considered practically the same in all concept and detailed models except for the STCS approximations CM'_4 to CM'_6. The relative percentage differences $\Delta_{J_{\mathbf{xx}}}$, $\Delta_{J_{\mathbf{yy}}}$ and $\Delta_{J_{\mathbf{zz}}}$ between the cross-sectional properties in the STCS models CM'_4 to CM'_6 and their actual values (CM_4 to CM_6) are summarized in Tables 3.1, 3.2 and 3.3. For CM'_6 the properties of both the open and the closed cross-section (CS) are given. The columns of these tables correspond to the reference (ref) and the resized configurations ($0.5h_{ref}$, $1.5h_{ref}$, $0.5w_{ref}$, $1.5w_{ref}$). The effect of the significant percentage difference which can be observed for most

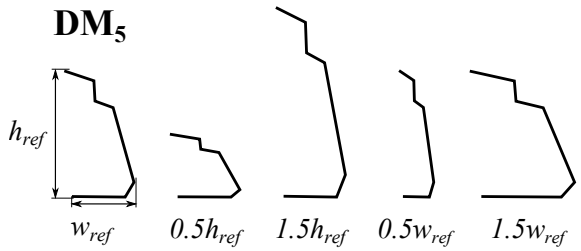

Figure 3.4: Reference and resized cross-sections for **DM5**.

of the cases is discussed in the following section.

Table 3.1: $\Delta_{J_{xx}}$ [%].

CM	ref	$0.5h_{ref}$	$1.5h_{ref}$	$0.5w_{ref}$	$1.5w_{ref}$
$4'$	74.97	89.98	64.74	55.05	82.99
$5'$	32.85	37.95	28.42	27.72	34.72
$6'$ - open CS	27.76	38.08	19.52	14.33	32.88
$6'$ - closed CS	26.25	30.78	22.94	20.99	27.57

Table 3.2: $\Delta_{J_{yy}}$ [%].

CM	ref	$0.5h_{ref}$	$1.5h_{ref}$	$0.5w_{ref}$	$1.5w_{ref}$
$4'$	64.58	44.54	75.15	82.87	52.17
$5'$	47.99	49.28	40.91	42.13	49.06
$6'$ - open CS	-2.68	16.41	-17.45	-24.36	7.66
$6'$ - closed CS	32.76	30.39	32.30	33.23	31.03

Table 3.3: $\Delta_{J_{zz}}$ [%].

CM	ref	$0.5h_{ref}$	$1.5h_{ref}$	$0.5w_{ref}$	$1.5w_{ref}$
$4'$	126.61	132.97	127.54	126.90	129.41
$5'$	-34.49	-34.12	-35.52	-35.56	-34.27
$6'$ - open CS	-7.02	-2.20	-11.39	-14.48	-4.02
$6'$ - closed CS	21.50	23.88	22.35	24.67	21.17

Seven static load cases were defined both for the detailed FE and the concept models. They are schematically presented in Fig. 3.5. For each beam three moments (M_x, M_y, M_z) and three forces (F_x, F_y, F_z) were applied at its neutral axis separately, as well as all together in a generic load case. Various load value configurations were possible according to several plausible criteria. For the purposes of the current study the BIW concept FE model of an existing vehicle was analyzed

for different global static load cases. The loads generated in all 1D beam elements were extracted and the corresponding frequency distributions were obtained. Finally, the values of F_x, F_y, F_z, M_x, M_y and M_z were chosen based on the most frequent values, corresponding approximately to 90% of the 1D elements. The loads showed the following ratios for forces in Newtons and moments in Newton millimeters: 1:1:1:100:100:50.

Each 1D beam structure had 11 control nodes (Fig. 3.5(b)), of which the resulting translations and rotations were measured. As the concept and the detailed model differed in terms of DOFs and FE mesh, model matching was performed by adding rigid (Nastran RBE2) and interpolation (Nastran RBE3) elements in the detailed model. The RBE2 (magenta) connected the nodes of the cross-sections at both beam ends, whereas the RBE3 (black) connected the nodes of the intermediate cross-sections along the beam length (Fig. 3.5(a)). Both the rigid and the interpolation elements were created in correspondence with the cross-sections at the control nodes in the concept model. Moreover, the independent nodes of the RBE2 and the dependent ones of the RBE3 were the same 11 control nodes as in the concept model.

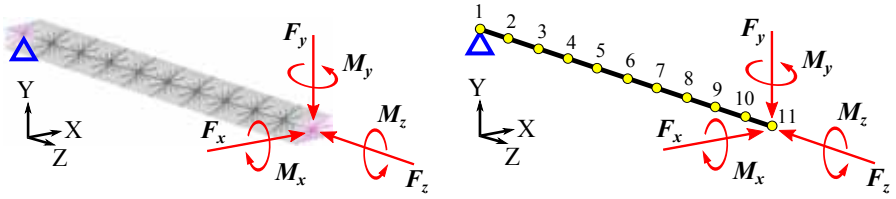

(a) Detailed model. (b) Concept model and node numbering.

Figure 3.5: Beam loading conditions.

Results

Linear static analysis was performed with MD Nastran for all 6 beam cases (DM, CM, CM') – reference and resized configurations. The values of the applied forces and moments (Fig. 3.5) were not changed. The translational and rotational components of the displacement vectors were extracted for the 11 control nodes in each model (Fig. 3.5). $ICDM$ was calculated for the 9 non-rigid cross-sections along the beam length corresponding to the intermediate control nodes.

Figs. 3.6 to 3.11 show the results for the reference configurations 1 to 6 (generic load case). These figures have two Y-axes. The one on the left is for the magnitudes of the translational components T of all control nodes, and the one on the right is for the magnitudes of their rotational components R. As expected, there is a stiffness overestimation in the CM for all six cases, although the difference greatly varies according to the cross-section geometry. The difference with respect to the DM results bigger for R. For the closed cross-section beams (cases 1 and 4) there is almost no error introduced by the CM as the structural behavior of CM and DM practically coincides (Figs. 3.6 and 3.9). The discrepancies increase for the

open cross-section beams (cases 2 and 5), which can be explained with the higher cross-section distortion in the DM, unaccounted for in the CM.

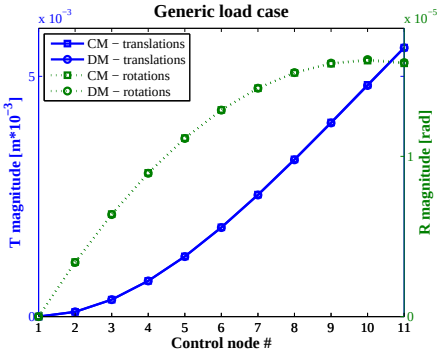

Figure 3.6: T, R – case 1.

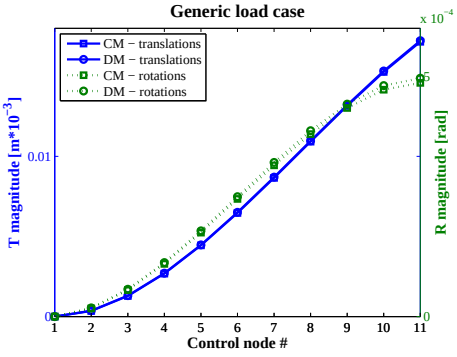

Figure 3.7: T, R – case 2.

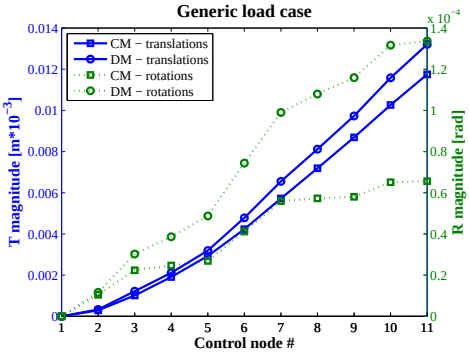

Figure 3.8: T, R – case 3.

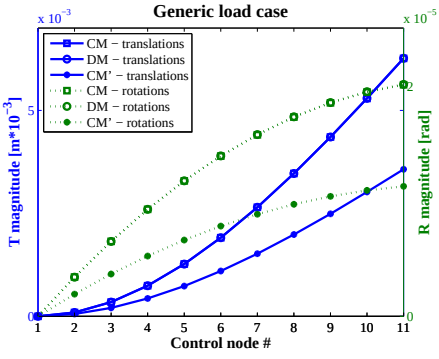

Figure 3.9: T, R – case 4.

However, the highest errors are observed for cases 3 and 6 which have both open and closed cross-sections (Figs. 3.8 and 3.11). The results can be partially attributed to the abrupt change in the cross-sectional properties at each transition node. Figs. 3.12, 3.13 and 3.14 show the $ICDM$ along the beam length for cases 1, 2 and 3 respectively (reference configurations). $ICDM$ is zero for the first cross-section corresponding to the constraint, as well as for the last cross-section because of the rigid element connecting its nodes (Nastran RBE2). While in Figs. 3.12 and 3.13 there is a gradual change in the $ICDM$, various peaks can be noted in Fig. 3.14. They correspond to the nodes in which there is a transition open/closed cross-section, i.e. 3, 5, 7, 9, 10 (Fig. 3.3). Moreover, the less different the cross-section geometries at the transition, the smaller the modeling error. Thus CM_6 (Fig. 3.11) performs better than CM_3 (Fig. 3.8).

Finally, CM'_4, CM'_5 and CM'_6 resulted in an even bigger overestimation of the structural stiffness (Figs. 3.9, 3.10 and 3.11) with respect to their ABCS

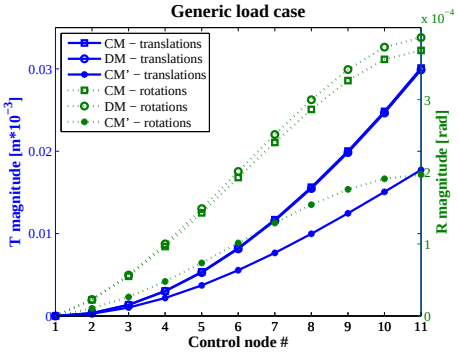

Figure 3.10: **T**, **R** – case 5.

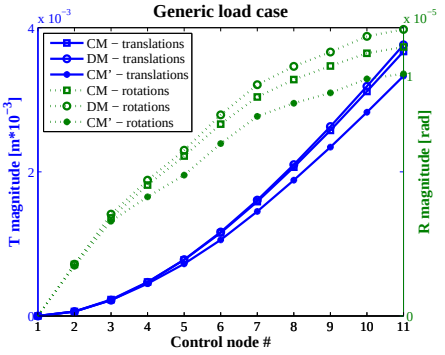

Figure 3.11: **T**, **R** – case 6.

counterparts CM_4, CM_5 and CM_6. This effect is due to their different and often higher area MOI J_{xx} and J_{yy}, and torsional stiffness parameter J_{zz} (Tables 3.1, 3.2 and 3.3, column ref).

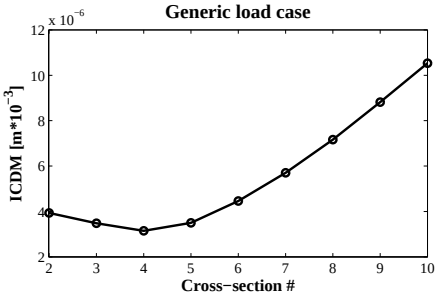

Figure 3.12: **ICDM** for $\mathbf{DM_{1\_ref}}$.

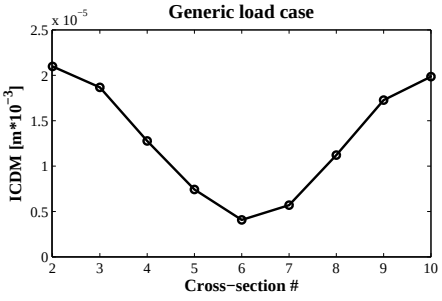

Figure 3.13: **ICDM** for $\mathbf{DM_{2\_ref}}$.

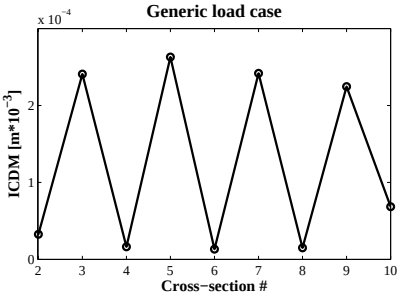

Figure 3.14: **ICDM** for $\mathbf{DM_{3\_ref}}$.

Tables 3.4 and 3.5 summarize the relative percentage errors Δ_T and Δ_R be-

tween all concept-detailed model pairs (cases 1 to 6, reference and resized configurations) regarding the translation and rotation magnitudes in the generic load case. For the sake of briefness, the reported values are the average of the relative errors for all control nodes (Δ_{T_avg} and Δ_{R_avg}). In the resized configurations (columns 3 to 6 in both tables) similar trends can be observed as for the previously discussed reference models (Figs. 3.6 to 3.11). Both Δ_{T_avg} and Δ_{R_avg} have negative signs (i.e. stiffness overestimation), except for some small error values under 1.2% and for two CM'_6 modifications. In addition, Δ_{R_avg} tends to be bigger than Δ_{T_avg}. The stiffness underestimation of $CM'_{6\_1.5h_{\mathbf{ref}}}$ and $CM'_{6\_0.5w_{\mathbf{ref}}}$ is due to the decreased J_{yy} and J_{zz} of the open cross-sections (Table 3.2 and 3.3) with respect to their actual values ($CM_{6\_1.5h_{\mathbf{ref}}}$ and $CM_{6\_0.5w_{\mathbf{ref}}}$).

Table 3.4: $\Delta_{\mathbf{T\_avg}}$[%], generic load case.

Case	ref	$0.5h_{ref}$	$1.5h_{ref}$	$0.5w_{ref}$	$1.5w_{ref}$
1	0.01	-0.27	0.05	-0.26	0.25
2	-1.16	-0.49	-1.76	-2.84	-0.37
3	-11.54	-4.59	-21.26	-2.80	-12.27
4	-0.13	-0.11	-0.54	-0.48	0.21
$4'$	-42.06	-46.05	-42.18	-45.71	-42.95
5	1.10	1.21	0.43	0.44	0.42
$5'$	-32.03	-32.62	-35.87	-43.49	-38.30
6	-0.36	-4.84	-2.78	-3.00	0.91
$6'$	-7.44	-22.36	8.04	16.94	-17.78

Table 3.5: $\Delta_{\mathbf{R\_avg}}$[%], generic load case.

Case	ref	$0.5h_{ref}$	$1.5h_{ref}$	$0.5w_{ref}$	$1.5w_{ref}$
1	0.08	-0.94	0.51	0.02	0.05
2	-2.45	-3.12	-3.47	-4.97	-1.69
3	-40.38	-14.54	-31.42	-7.10	-52.99
4	-0.04	-0.22	0.02	-0.46	0.13
$4'$	-43.76	-47.22	-43.98	-46.58	-45.18
5	-3.87	-8.56	-1.90	-3.92	-3.52
$5'$	-50.37	-37.13	-48.27	-24.02	-61.36
6	-4.40	-4.81	-5.11	-6.36	-2.01
$6'$	-12.72	-31.33	2.94	9.84	-21.60

Similarly to the reference models, the lowest errors (less than 1%) are observed for the closed beams (CM_1 and CM_4), for all resized configurations. The errors increase for CM_2, CM_5 and CM_6 but they are still less than 10%. On its turn, CM_3 results again the most erroneous because of the abrupt change in the cross-sectional properties at the transitions. Although such a difference still persists in CM_6, it is smaller, resulting thus in a smaller error. Finally, CM'_4, CM'_5 and CM'_6

for the resized configurations increase the error significantly with respect to CM_4, CM_5 and CM_6 because of their J_{xx}, J_{yy} and J_{zz}, differing considerably from the real ones (Table 3.1, 3.2 and 3.3).

Tables 3.6 and 3.7 show the loads that resulted in the biggest error contributions for each beam case. Δ_{T_avg} and Δ_{R_avg} were calculated for each of the 6 load cases (F_x, F_y, F_z, M_x, M_y, M_z - Fig. 3.5) and the dominant load was selected as the one with the highest unsigned value of Δ_{T_avg}, respectively Δ_{R_avg}. The loads with the biggest influence on the error are undoubtedly torsional (M_z) and in much fewer cases bending (F_x, F_y). However, as in this study F_x and F_y are not applied in the shear center (except for case 1), the beam structures will not only bend but also twist. The single occurrence of M_x for case $5'$ (resized configuration $0.5w_{ref}$) is due to the prevalence of the difference with respect to the reference cross-section geometry.

Table 3.6: $\Delta_{\mathbf{T\_avg}}$ – dominant loads.

Case	ref	$0.5h_{ref}$	$1.5h_{ref}$	$0.5w_{ref}$	$1.5w_{ref}$
1	M_z	M_z	M_z	M_z	M_z
2	M_z	M_z	M_z	M_z	M_z
3	M_z	M_z	M_z	M_z	M_z
4	M_z	M_z	M_z	M_z	M_z
$4'$	M_z	M_z	M_z	M_z	M_z
5	M_z	M_z	M_z	M_z	M_z
$5'$	M_z	F_x	M_z	M_x	M_z
6	M_z	M_z	M_z	M_z	M_z
$6'$	M_z	M_z	M_z	M_z	M_z

Table 3.7: $\Delta_{\mathbf{R\_avg}}$ – dominant loads.

Case	ref	$0.5h_{ref}$	$1.5h_{ref}$	$0.5w_{ref}$	$1.5w_{ref}$
1	M_z	M_z	M_z	M_z	M_z
2	M_z	F_x	M_z	F_x	M_z
3	M_z	M_z	M_z	M_z	M_z
4	M_z	M_z	M_z	M_z	M_z
$4'$	M_z	M_z	M_z	M_z	M_z
5	F_y	M_z	M_z	M_z	M_z
$5'$	F_x	F_x	M_z	M_x	F_x
6	M_z	M_z	M_z	M_z	M_z
$6'$	M_z	M_z	M_z	M_z	M_z

Tables 3.8 and 3.9 summarize the forces and respectively moments that resulted in the highest in-plane cross-section deformations for each beam case. To obtain them, the sum of the $ICDM$ for all 9 non-rigid cross-sections was calculated for each of the 6 load cases (F_x, F_y, F_z, M_x, M_y, M_z - Fig. 3.5). To avoid dependence

on the load values, $ICDM$ was always computed per load unit ($1N$ and $1Nmm$ respectively) for each load component. The highest $ICDM$ sums resulting from the first three load cases determined the dominant forces (Table 3.8), while the highest $ICDM$ sums resulting from the latter three load cases determined the dominant moments (Table 3.9). As for the highest error contributions (Tables 3.6 and 3.7), the loads with the biggest influence on the $ICDM$ are M_z, F_x and F_y, all three having torsion in common. For all beams with open only or both open and closed cross-sections, torsion is the cause for the highest in-plane cross-section deformations and also for the highest errors with the used beam theory. Its influence on the concept model precision will be discussed for an industrial case-study in Section 3.4.2. On the other hand, not only M_z, but also M_x and M_y resulted dominant for cases 1 and 4. However, these were also the cases with the lowest and almost negligible errors (Tables 3.4 and 3.5).

Table 3.8: ICDM – dominant forces.

Case	ref	$0.5h_{ref}$	$1.5h_{ref}$	$0.5w_{ref}$	$1.5w_{ref}$
1	F_y	F_y	F_y	F_y	F_y
2	F_y	F_y	F_x	F_x	F_y
3	F_x	F_y	F_x	F_x	F_x
4	F_y	F_y	F_x	F_x	F_y
5	F_x	F_y	F_x	F_x	F_y
6	F_y	F_y	F_y	F_y	F_y

Table 3.9: ICDM – dominant moments.

Case	ref	$0.5h_{ref}$	$1.5h_{ref}$	$0.5w_{ref}$	$1.5w_{ref}$
1	M_x	M_x	M_x	M_x	M_z
2	M_z	M_z	M_z	M_z	M_z
3	M_z	M_z	M_z	M_z	M_z
4	M_y	M_y	M_x	M_x	M_z
5	M_z	M_z	M_z	M_z	M_z
6	M_z	M_z	M_z	M_z	M_z

Discussion

The results showed that the in-plane cross-section deformations, the cross-section type and the discontinuities can deteriorate the concept model precision to a different extent. The following guidelines can be given:

- **In-plane cross-section deformations.** If unaccounted for in the employed beam theory, they are partially responsible for the overestimation of the beam stiffness. They are of significant importance for 1D beams subject to torsion and can be the cause for model imprecision. In this regard, 1D beams

with open cross-sections can become a source for errors in the concept model, because of their lower torsional stiffness and bigger in-plane distortions with respect to closed profiles. For these reasons the quantification of the in-plane deformation is important and must be applied where possible. Measures as $ICDM$ can be used to determine the load resulting in the highest cross-section deformations. $ICDM$ can be used as an additional tool for detailed analysis of problematic cases at single beam level (e.g. structures with abrupt cross-section change). Finally, the cross-section distortion can be not only quantified but also visualized (Fig. 3.1).

- **Beam cross-section geometry.** STCSs are appropriate for space frame structures and simple academic case-studies with regular beam geometry. They can be also used for beams with non-standard cross-section profile, but only if the difference between the properties of the actual cross-section and the STCS is negligible. The usage of STCSs in the general case of non-standard cross-section shape is inappropriate and it can lead to significant difference with respect to the actual structural stiffness which can be both under- or overestimated. For such structures, ABCSs are the preferable choice as they give better approximation of the real geometry and higher precision.
- **Discontinuities.** As a general rule, the smoother the change in the cross-section properties, the better the precision of the 1D beam structure. Big discontinuities resulting in very different adjacent cross-section properties can be the cause for considerable modeling errors. For detailed models with such parts of the structure, special attention must be paid when creating the concept model and its precision must be controlled afterwards. If the number and type of the discontinuities in the same model cannot be considered negligible, advanced modeling improvements must be developed and applied. One possible solution with the currently used beam theory could be the use of additional beam elements at both sides of the transition with interpolated cross-section properties in order to provide a smoother change from open to closed geometry and vice-versa. The more these auxiliary 1D elements, the less the problems with the 7^{th} warping DOF of the transition node and the better the model precision in general. On one hand such workaround will allow a more realistic structural behavior of the 1D beam model, but on the other hand it could cause geometrical dissimilarities as the additional cross-section properties at the transition will not be actually present in the reference model. Thus this solution and its side effects must be further studied before recommending it as a good general practice for handling discontinuities.

3.3.2 Non-idealized beams

Case-study definition

The A-pillar, the windshield header and the B-pillar of a Toyota Rav4 (Fig. 3.20) were subject to simplification with 1D beams. All three of them are non-

prismatic steel structures with complex geometry and varying properties. The corresponding detailed models (DM) and concept models (CM) are displayed in Fig. 3.15. Similarly to the idealized beam structures, closed (7), open (8) and mixed open/closed (9) cases can be distinguished.

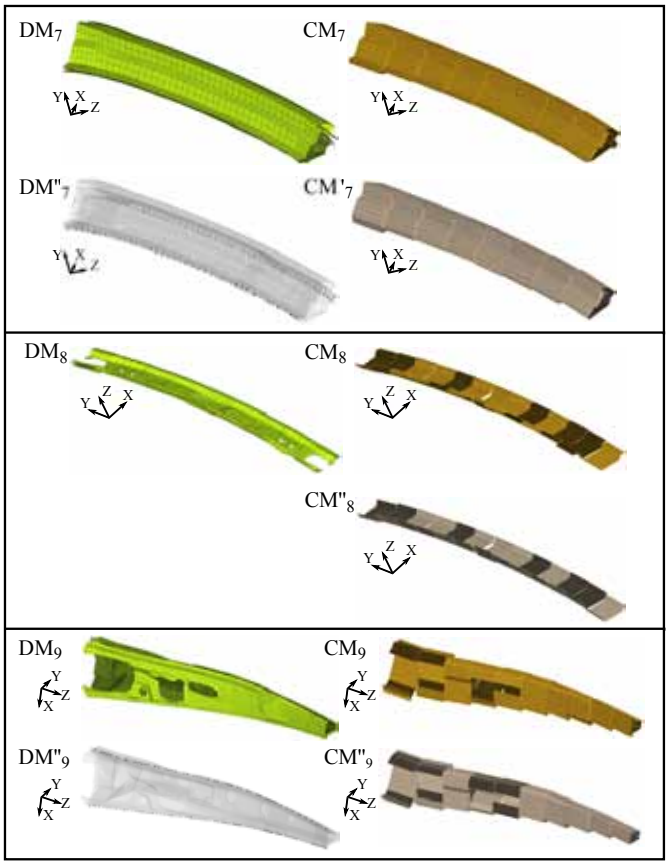

Figure 3.15: Non-idealized beam case-studies.

Based on the conclusions made in Section 3.3.1, 1D beams with ABCSs were used to represent the non-standard profiles of the real cross-sections and guarantee a good match. In this regard, a generally applicable rule-of-thumb was defined and used to decrease the cross-section complexity of the ABCS where needed by creating equivalent shell layers. Let L_1 and L_2 be two adjacent stamped sheets such as the ones in the upper part of Fig. 3.2(a), which have similar dimensions and are made of the same material. Let L_1 be the external layer and let L_2 be the internal one. Moreover, let t_1, S_1 and V_1 be the thickness, area and volume of the entire L_1 stamped sheet, while similarly t_2, S_2 and V_2 are the thickness, area and volume of the entire L_2 stamped sheet. To simplify the ABCS, L_2 must be removed and its equivalent thickness must be added to t_1. The thickness, area and volume of the new equivalent layer are noted as t_1^*, S_1^* and V_1^*. To have

the same mass of the reference structure $V_1^* = V_1 + V_2$ must hold. In addition $S_1^* = S_1$ as there is no change in the area of L_1. The new thickness t_1^* is defined as $t_1^* = t_1 + t_{eqv}$, where t_{eqv} is the unknown equivalent thickness of L_2. Taking into account all the above, t_{eqv} can be defined as:

$$t_{eqv} = (V_1 + V_2)/S_1 - t_1 = V_2/S_1 \tag{3.7}$$

The merits of this technique will be further illustrated in Section 3.4.1.

In order to study the influence of the flanges, three additional concept models were created – CM_7'' to CM_9''. As it can be seen in Fig. 3.15, the flanges of the detailed FE models were not modeled in the corresponding simplified ones. Furthermore, two modified detailed FE models were also considered – DM_7'' and DM_9''. They are in transparent view to evidence better the difference with respect to the reference structures DM_7 and DM_9. The aim was to see how much the simplifications concerning spot welds could influence the precision of the concept models. To make the detailed models as close as possible to the concept ones in this regard, spot welds were added in DM_7'' and DM_9''. Thus the gaps between the flange borders became as if they were closed, given that all nodes belonging to them were connected. DM_8'' was not considered as DM_8 contained just a few spot welds connecting the main stamped sheet to a stiffener.

Tables 3.10 and 3.11 compare the mass and the principal MOI (I_{XX}, I_{YY}, I_{ZZ}) for the models of Fig. 3.15. In these tables Δ_{CM-DM} and $\Delta_{CM''-DM}$ stay for the relative percentage errors introduced by the concept models (Table 3.10) and respectively the concept models without flanges (Table 3.11), both with regard to the corresponding detailed FE models. The results for DM_7'' and DM_9'' are not reported as they coincide with the results for DM_7 and DM_9. The concept models CM_7 to CM_9 have different precision because of their different complexity. The biggest errors are observed for the windshield header, but still they are under 5% which is acceptable for the purposes of a concept study. The smaller discrepancies for the A- and the B-pillar confirm the feasibility of the above defined rule for creating equivalent shell layers (Eq. 3.7). However the relative percentage errors increase considerably for the concept models without flanges (CM_7'' to CM_9'') which are logically expected to be more imprecise.

Table 3.10: Δ_{CM-DM} [%].

Case	$Mass$	I_{XX}	I_{YY}	I_{ZZ}
7	-0.54	-0.06	-0.63	-0.71
8	-4.75	-4.81	-4.72	-4.87
9	1.97	3.39	2.03	1.99

A generic static load case was defined both for the detailed FE and the concept models. It contained the same load types shown in Fig. 3.5: three moments (M_x, M_y, M_z) and three forces (F_x, F_y, F_z). The same characteristic ratios were used for their values as explained in Section 3.3.2. The loads were applied on the neutral axis of the end cross-section and were parallel to the axes of the local coordinate

Table 3.11: $\Delta_{CM''-DM}$ [%].

Case	$Mass$	I_{XX}	I_{YY}	I_{ZZ}
7	-24.93	-25.03	-25.20	-24.82
8	-25.98	-26.36	-26.01	-26.07
9	-11.34	-11.18	-11.76	-11.29

system O_{xyz} of the end beam element. Each 1D beam structure had different number of control nodes, the resulting translations and rotations of which were measured. To match the DOFs of the detailed and the concept models the same technique was applied as in Section 3.3.1. Each detailed model was modified so that rigid elements connected the nodes of the cross-sections at both beam ends, while interpolation elements connected the nodes of the intermediate cross-sections along the beam. Thus the control nodes in the detailed model were defined again as the independent nodes of the RBE2 and the dependent ones of the RBE3 elements.

Results

As for the idealized beam cases, linear static analysis was performed for all reference and concept structures (Fig. 3.15), applying the same loads. $ICDM$ was calculated for the cross-sections corresponding to the control node locations. The translational and rotational components of the displacement vectors were extracted for the control nodes in each model. The results for the three cases under study are shown in Figs. 3.16 to 3.18. Again double Y-axis plots are used. These graphics compare not only the behavior of DM and CM, but also of their modified versions DM'' and CM''.

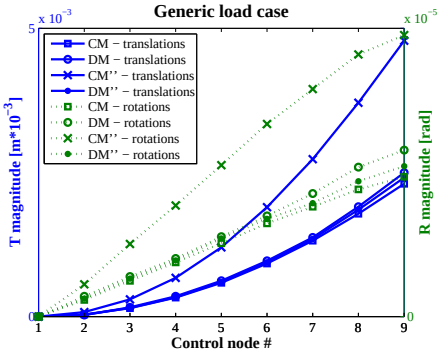

Figure 3.16: T, R – case 7.

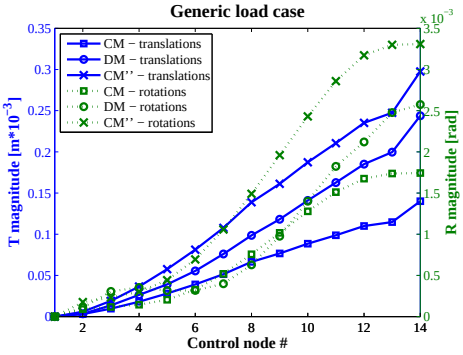

Figure 3.17: T, R – case 8.

Predictably, CM_7 to CM_9 overestimate the reference structural stiffness up to a different extent. This erroneous behavior is due to the mixed influence of the applied beam theory (CM_7, CM_8, CM_9), the concept representation of the spot welds (CM_7, CM_9), the presence of abrupt discontinuities (CM_9), and in part

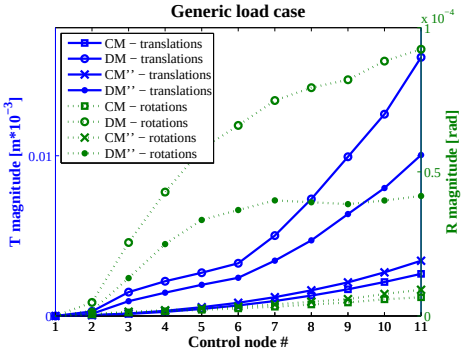

Figure 3.18: **T**, **R** – case 9.

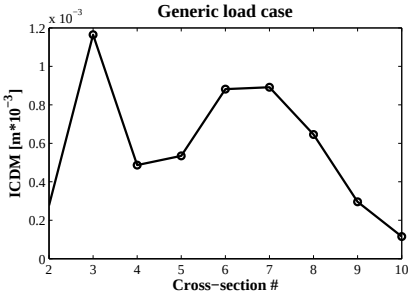

Figure 3.19: **ICDM** for **DM9**.

the complex beam geometry (CM_7, CM_9). A quantitative comparison between the $CM - DM$ pairs of cases 7, 8 and 9 is given in Tables 3.12 and 3.13, which summarize the average of the relative errors for all control nodes regarding the translations (Δ_{T_avg}), and respectively the rotations (Δ_{R_avg}). While the actual structural behavior (DM_7 and DM_8) is approximated relatively well by CM_7 and CM_8 and the main trends for the translations and rotations are followed, the performance of the concept B-pillar is not satisfactory. There are large discrepancies between the detailed and the concept model, as all error factors are present, including the transition from open to closed cross-sections. As for the idealized beams the latter factor proved to be a significant one, a similar methodology was applied for its study by computing the variation of the $ICDM$ along the B-pillar (Fig. 3.19). $ICDM$ is zero for the first cross-section corresponding to the constraint, as well as for the last cross-section because of the rigid element connecting its nodes. The transitions between open and closed cross-sections in DM_9 occur at control nodes 3, 4 and 6. Similarly to DM_{3_ref} (Fig. 3.14), also in Fig. 3.19 the abrupt transitions correspond to peaks in the graphics. For the B-pillar the biggest $ICDM$ value is observed for node 3 which also corresponds to the biggest difference in the properties of the adjacent cross-sections. As at nodes 4 and 6 these transitions are smoother, the $ICDM$ values are smaller too.

Table 3.12: $\Delta_{\mathbf{T\_avg}}$[%], generic load case.

Case	$CM - DM$	$CM'' - DM$	$DM'' - DM$
7	-6.34	93.30	-3.55
8	-35.03	35.59	-
9	-84.19	-80.05	-33.72

The results for all concept models without flanges CM'' are also displayed in Figs. 3.16 to 3.18. A quantitative comparison between all $CM'' - DM$ pairs is given in Tables 3.12 and 3.13. Due to the elimination of the flanges, CM'' are more flexible than the corresponding CM both in terms of translations and

Table 3.13: $\Delta_{\mathbf{R\_avg}}$[%], generic load case.

Case	$CM - DM$	$CM'' - DM$	$DM'' - DM$
7	-10.65	83.33	-5.79
8	-17.33	63.71	-
9	-95.05	-93.67	-48.48

rotations. Moreover, for the control node translations and rotations of case 7 and 8, the concept models without flanges are even more flexible than the detailed ones. This reduced stiffness can be explained with the difference with respect to the actual cross-sectional properties of the various beam parts. On the other hand, while this effect is considerable for cases 7 and 8, it is less influential for case 9, where other error factors are predominant such as the in-plane cross-section deformations, the discontinuities and the spot welds.

Finally, Figs. 3.16 and 3.18 show also the results for the modified detailed models DM''. In addition, a quantitative comparison between all $DM'' - DM$ pairs is given in Tables 3.12 and 3.13. DM_7'' is even closer to CM_7 than DM_7, which confirms the importance of the error factor due to spot welds. The same trend is observed for DM_9'' which results much stiffer than DM_9, thus explaining partially the big discrepancy between the concept and the detailed model of the B-pillar.

Discussion

The improper modeling of the spot welds, the exclusion of the flanges as well as the high degree of cross-section complexity can all decrease the quality of the concept model, as confirmed in Section 3.3.2. Being closely related to all industrial case studies, these three factors are discussed hereafter.

- **Beam cross-section geometry.** The results from Section 3.3.1 clearly demonstrated that when it comes to the general case of complex real structures GNCSs and STCSs are inappropriate and the ABCS approach should be used instead. However, depending on the complexity of the cross-section geometry, some simplification choices must be still made. Beam-like structures like the A- or the B-pillar are often made by more than two stamped metal sheets and can also have internal stiffeners (Fig. 3.2(a)). Including all the details in the concept model could be unnecessary, it could require too much modeling efforts or it could be even impossible due to technical limitations of the existing tools (e.g. not more than one internal layer allowed [100]). The ABCSs in the concept model must be the right compromise between simplification and precision. A rule-of-thumb was defined to decrease the number of adjacent internal layers without changing the mass. It was successfully applied during the creation of both the A- and the B-pillar concept models.
- **Spot welds.** By closing the gaps between the flanges, the detailed models

result stiffer (Tables 3.12 and 3.13). As such an approach is also applied during the creation of the concept models, it contributes to their increased stiffness with respect to the reference structures. As in a detailed FE model of the BIW there are thousands of spot weld connections, this becomes an important factor to consider. Unfortunately, there are no alternative methods to use during the model creation phase. An approach based on model updating/correction coefficients could be subsequently applied. In such an adjustment process, the modeling errors are corrected but on their turn they are due to the mixed influence of all factors. The prediction capabilities of such forcibly changed concept model are therefore not guaranteed.

- **Flanges.** Not considering the flanges in the concept model leads to significant discrepancies in the stiffness with respect to the reference structure. The concept models are typically less stiff than their counterparts with flanges, and in some cases also than the detailed ones (Tables 3.12 and 3.13). Moreover, considerable errors are introduced regarding the mass and the principal MOI of the beam structures (Table 3.11). Having different mass consequently deteriorates the concept model precision for dynamic load cases. Finally, it is not advisable to remove the flanges in the concept model not only because of the resultant erroneous static and dynamic behavior but also because of the geometrical differences that arise. ABCSs are the most appropriate choice to model the flanges. However, during optimization the entire cross-section is rescaled which is undesirable. In this regard, proper methodologies for 1D beam optimization handling must be developed, that take into account the flanges but do not resize them.

3.4 Industrial case-studies

In this section two industrial cases are considered and the previously derived guidelines are employed. Firstly, the established good practices for concept modeling are applied in order to create a hybrid detailed-concept FE model of a BIW. Secondly, the quality of an existing BIW concept model is assessed.

3.4.1 Hybrid BIW

The Toyota Rav4 BIW, year 1997, shown in Fig. 3.20 was used as reference FE model. It was initially developed by the National Crash Analysis Center (NCAC) for crash impact simulations. In this dissertation it was adapted accordingly after some minor modifications so that it can be used for the purposes of static and low frequency dynamic analysis. The front and rear windshields were also taken into consideration although they are not part of the BIW as they strongly influence the car stiffness. The structure is made of steel having Young's modulus $E = 210GPa$, Poisson's ratio $\nu = 0.3$ and mass density $\rho = 7890kg/m^3$. The model has 249 640 nodes (253 406 elements).

To study the modeling error due to the use of 1D beams at global scale, a hybrid FE model of the BIW was created. For this purpose, several beam-like parts of the body were substituted with ABCS concept beams – A-,B-,C-pillar,

windscreen header rail and side roof rail (Fig. 3.21). Consequently, the resulting hybrid model (Fig. 3.22) was a mix of detailed and concept components.

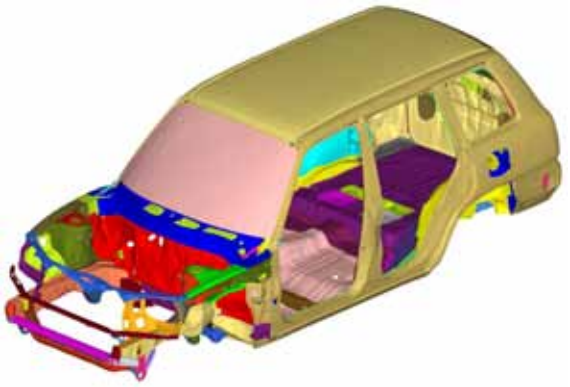

Figure 3.20: Toyota Rav4 BIW FE model.

Figure 3.21: Toyota Rav4 1D beam parts.

During the creation of the hybrid FE model incompatible elements had to be connected – 1D beam to 2D shell elements. Where relevant, the connections between the shell elements belonging to the panel-like parts (e.g. windshield, roof) and the 1D beam parts were created following the original spot weld layout of the reference FE model (shell to shell connections). In addition, each of the 1D beam structures was connected at its both ends to the adjacent shell elements of the detailed FE model through rigids (Nastran RBE2 elements [100]). As discussed in Chapter 2, although such a solution introduces some additional stiffness in the model [23], it is among the popular and recommended approaches because of its simplicity [10, 36, 123, 131]. To assess the stiffening effect of the rigid beam to shell connections a stiffened detailed model was created. The only difference with respect to the reference model (Fig. 3.20) is that the stiffened one had also rigid

elements connecting the same nodes as in the hybrid model. The stiffened BIW is shown in transparent view in Fig. 3.23, where all rigid connections are evidenced in red.

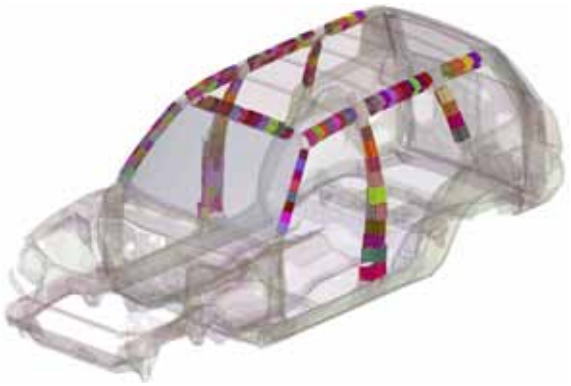

Figure 3.22: Toyota Rav4 hybrid BIW.

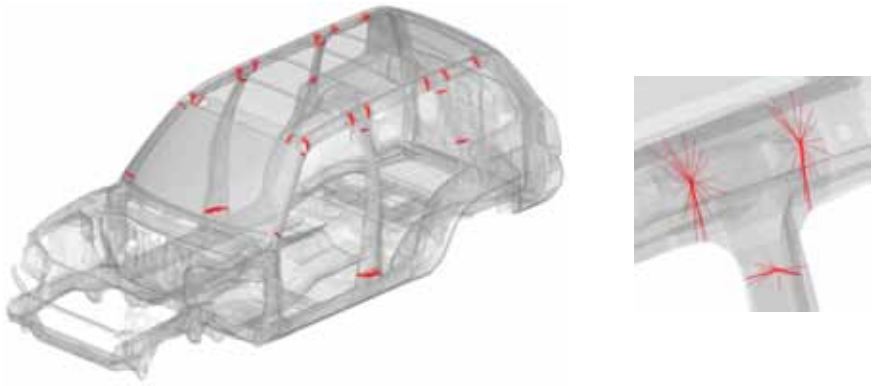

Figure 3.23: Toyota Rav4 with RBE2 at all connections – BIW (left) and B-pillar to roof rail joint (right).

To evaluate the global static performance of the reference, hybrid and stiffened BIW two load cases were used for bending and torsion respectively. They were defined according to the static test benches most often used in the industry [9, 11, 14, 18] (Section 1.2.2). These load cases are represented schematically in Fig. 3.24 and 3.25. In these figures the constraints are marked with blue triangles and the forces - with red arrows.

In the static bending load case (Fig. 3.24) the BIW was constrained at the front and rear suspensions and eight forces F were applied on the front seats. In the static torsion load case (Fig. 3.25) the BIW was constrained at the rear

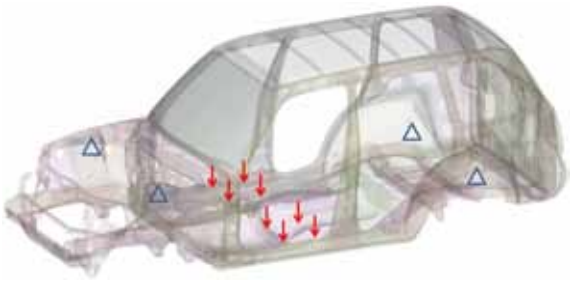

Figure 3.24: Static bending load case.

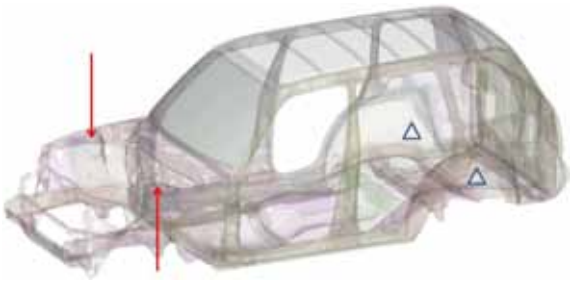

Figure 3.25: Static torsion load case.

suspensions and torque was applied at the front suspensions. Thus the global static bending and torsional stiffness, K_b and K_t, can be defined as follows:

$$K_b = \frac{8F}{\max\left(t_{z\_door\_sill}\right)} \tag{3.8}$$

where $t_{z\_door\_sill}$ are the absolute values of the vertical displacements of all nodes belonging to the two door sills,

$$K_t = \frac{FW}{\arctan\left(\Delta t_z / W\right)} \tag{3.9}$$

where Δt_z is the difference between the vertical displacements of the nodes where the two opposite forces F were applied, and W is the distance between these nodes.

For the evaluation of the global dynamic performance modal analysis was performed for the three BIW models under free-free conditions. The first 6 modes were considered (after excluding the 6 rigid body modes).

The results regarding the total BIW mass, the static bending and torsional stiffness (K_b and K_t), as well as the eigenfrequencies of the first bending and first torsional mode ($f_{1^{st}b}$ and $f_{1^{st}t}$) are reported in Table 3.14. In this table BIW_{ref}, BIW_{rgd} and BIW_{hyb} correspond to the reference (Fig. 3.20), stiffened (Fig. 3.23) and respectively hybrid (Fig. 3.22) FE models. The relative percentage errors for the responses of BIW_{rgd} with respect to the reference ones (BIW_{ref}) are marked

with $\Delta_{rgd-ref}$. Similarly, the values of $\Delta_{hyb-ref}$ give the errors introduced by the hybrid structure (BIW_{hyb}).

Table 3.14: Toyota Rav4 reference, stiffened and hybrid BIW.

Response	BIW_{ref}	BIW_{rgd}	$\Delta_{rgd-ref}$[%]	BIW_{hyb}	$\Delta_{hyb-ref}$[%]
$Mass$ [kg]	304.20	304.20	0.00	304.20	0.00
K_b [N/m]	3.08E6	3.36E6	9.22	3.50E6	13.79
K_t [Nm/rad]	2.68E5	2.93E5	9.21	3.08E5	14.87
$f_{1^{st}b}$ [Hz]	26.26	27.45	4.52	28.30	7.73
$f_{1^{st}t}$ [Hz]	29.87	32.28	8.07	33.18	11.11

Both $\Delta_{rgd-ref}$ and $\Delta_{hyb-ref}$ are zero for the mass. In the first case this is due to the fact that the rigid elements added in BIW_{rgd} have no mass. As for the second case, the concept beams in the hybrid model were created as precisely as possible from geometrical point of view, following all the guidelines derived in Sections 3.3.1 and 3.3.2. ABCS beams were used and all flanges were considered. Where relevant, equivalent layers were created according to the defined rule-of-thumb (Eq. 3.7).

On the other hand, BIW_{rgd} results in overestimation with an average of 9.2% for the static stiffness and with an average of 6.3% for the eigenfrequencies. Although the stiffening effect of using rigid connections was expected, these errors resulted too high, given that just part of the structure was considered. The connection between dissimilar elements is thus an important error factor for hybrid models, which has to be studied into detail and treated properly. Various attempts have been made to resolve the problem [23, 32, 43, 193] (Section 2.2.2), but still no established solution exists. However, this is not an issue for fully conceptual BJP models with 1D beams and parametric simplified joints.

The errors regarding the static and dynamic performance of BIW_{hyb} are even bigger. The average overestimation is 14.3% for the static stiffness and 9.4% for the eigenfrequencies. In Figs. 3.26 and 3.27 the first bending and first torsional modes of BIW_{ref} and BIW_{hyb} are compared. The contour plots in Figs. 3.26(a) and 3.26(b) use the same color scale, as well as the ones in Figs. 3.27(a) and 3.27(b). Despite the big discrepancies in the eigenfrequencies, the mode shapes are still quite similar. The errors $\Delta_{hyb-ref}$ have three main sources: the cross-section distortion, the spot welds and the rigid beam to shell connections. The used beam theory has a direct impact on the model precision, as in-plane cross-section deformations are not considered and each beam structure could result stiffer. Unfortunately, there is still a lack of advanced beam theories which can successfully face the challenges posed by the typical automotive industry problems. In accordance with the conclusions made in Section 3.3.2, closing the cross-sections of the 1D beams to represent the spot welds results in further increase of the model stiffness. However, there are no alternative approaches acting during the model creation. Only the disadvantageous model updating or correction coefficients can be applied. On the other hand, both these factors taken together (spot welds and local deformations) result less influential than the third one. As confirmed

by the results for BIW_{rgd}, the biggest portion of the error in the hybrid model can be attributed to the rigid element connections. This factor turns out to be a promising field of research for all similar problems having incompatible elements.

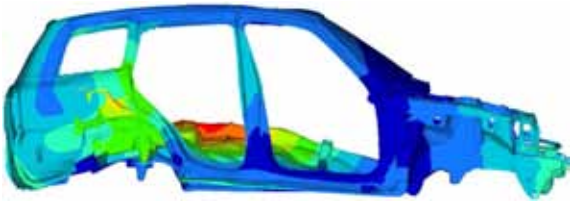

(a) $\mathbf{BIW_{ref}}$.

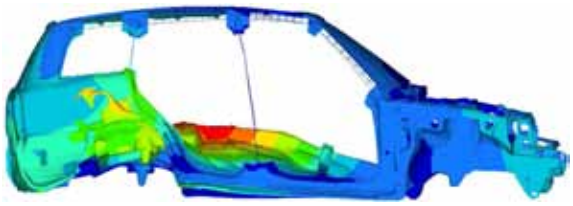

(b) $\mathbf{BIW_{hyb}}$.

Figure 3.26: First bending mode.

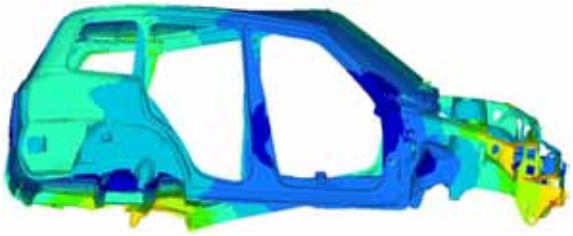

(a) $\mathbf{BIW_{ref}}$.

(b) $\mathbf{BIW_{hyb}}$.

Figure 3.27: First torsional mode.

3.4.2 Concept BIW

The concept FE model of the BMW 3 series BIW is shown in Fig. 3.28 (detailed 1D element display). It has been developed at the BMW Group. The model has 13137 nodes (13675 elements). 1D beams with ABCSs are used to represent the reference structure. In total, there are 319 different ABCSs, out of which 115 are open cross-sections and the remaining ones are closed. Such a concept FE model is small-sized and parametric. As ABCSs are used instead of STCSs, the model is not only as close as possible to the real geometry, but also more precise.

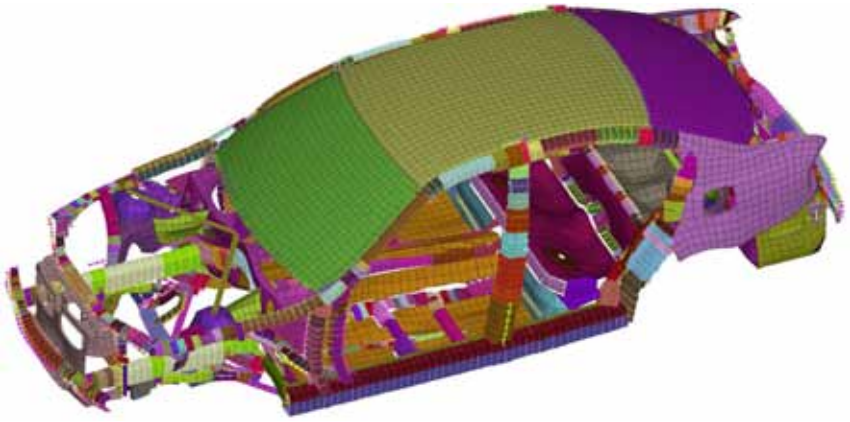

Figure 3.28: BMW 3 series BIW.

The global static performance of the vehicle BIW was evaluated on the base of a bending (K_b) and torsion (K_t) load case similar to the ones defined in Section 3.4.1 (refer to Chapter 6 for a detailed definition). It was thus possible to obtain the following components of the internal forces and moments in each 1D beam element: bending moments in the two reference planes at the neutral axis, shear forces in the two reference planes at the shear center, axial force at the neutral axis, total torque about the beam shear center axis and component of this torque due to warping. Because of the confirmed influence of torsion generated in 1D beams on the model precision (Section 3.3.1), the total and warping torques are discussed hereafter.

As there was a considerable number of open cross-sections in this concept model, the warping DOF was activated for all 1D beams in order to approximate the effect of out-of-plane cross-section distortion. Figs. 3.29(a) and 3.29(b) show the total and warping torque respectively, both at end A for all 1D beam elements. These color plots were obtained from the K_b load case. Similarly, Figs. 3.30(a) and 3.30(b) represent the total and warping torques resulting from the K_t load case.

As discussed in Section 3.3.1, the error is expected to be bigger for the 1D beam structures subject to torsion which are open or have discontinuities. Moreover, the bigger the generated torque, the bigger will be the in-plane cross-section

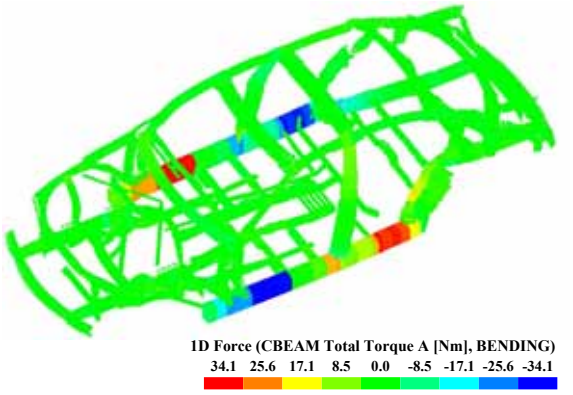

(a) Total torque.

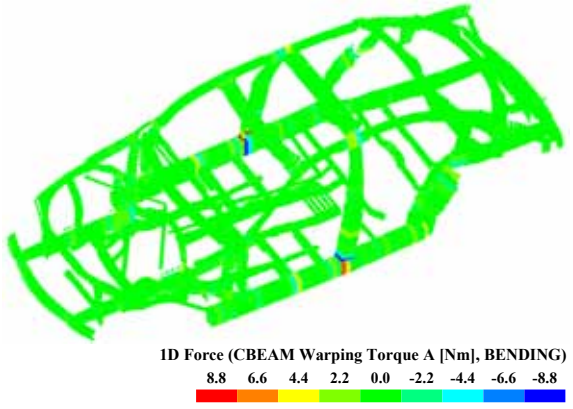

(b) Warping torque.

Figure 3.29: BMW 3 series BIW, $\mathbf{K_b}$ load case.

deformations unaccounted for and the error. As it can be seen from Figs. 3.29(a) and 3.30(a) the torques with the highest absolute values are concentrated in a relatively small part of the structure. For the K_b load case this is mainly the door-sill and for the K_t load case - the rear part of the vehicle. However, all 1D beam cross-sections corresponding to these parts are closed. Thus, the reasonable assumption can be made that a low modeling error can be expected relative to the in-plane cross-section distortion. Regarding the warping torque, its highest absolute values are concentrated in an even smaller part of the structure (Figs. 3.29(b) and 3.30(b)). These parts are mainly related to structural joints, e.g. the base of the B-pillar. In this model the joints are represented as junction of 1D beams and the resulting complex structures have both open and closed cross-sections [41]. This makes the warping activation mandatory. A similar analysis can be made for any other concept model of the vehicle structure. As result, either its adequacy can be confirmed (as in this case study), or better insight can be given for the causes of the modeling errors (Section 3.4.1).

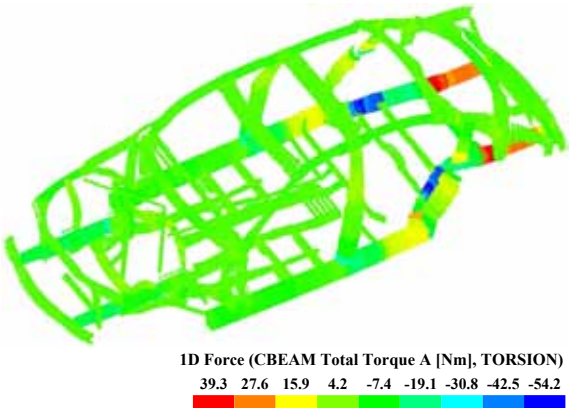

(a) Total torque.

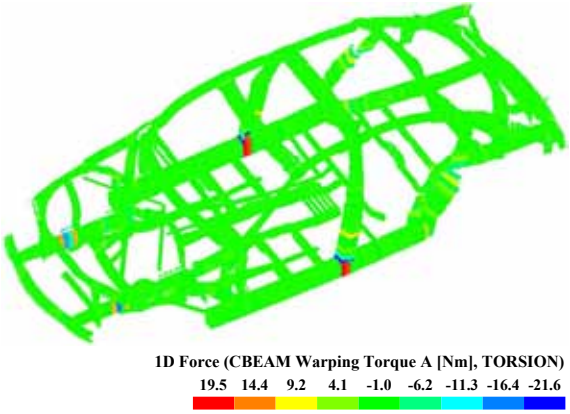

(b) Warping torque.

Figure 3.30: BMW 3 series BIW, $\mathbf{K_t}$ load case.

3.5 Conclusions

This chapter deals with the main factors that can cause errors in 1D beam concept models: the beam cross-section geometry, the incorrect approximation of spot welds and flanges, the presence of discontinuities and the lack of local cross-section deformations. As demonstrated on a set of idealized and non-idealized case-studies, these factors can generate significant discrepancies with respect to the detailed FE model in terms of geometrical similarity and structural behavior. Their better understanding is mandatory both in order to create better concept models, and to assess the performance of the existing ones. In this regard, the guidelines derived from the current study have been successfully applied for the qualitative analysis of a BIW concept model and for the quantitative analysis of a BIW hybrid model.

Chapter 4

A novel approach for beam concept modeling and optimization handling

4.1 Introduction

Together with the concept joints and panels, 1D beams are one of the constituent parts of the BJP simplified models. As they represent the main load-carrying structure, they are the predominant type of elements in such a BIW concept model. This makes them of primary interest for the predecessor-based concept modeling methods. As seen in Chapter 3, a lot of efforts are dedicated in order to overcome the current limitations of 1D beams and to reduce the modeling error due to their use.

In this regard, the cross-section geometry and the way it is represented in the concept model is of decisive importance. It is related both to the structural behavior and to the similarity with the actual structure. Here this factor is considered not only from the point of view of modeling, but also of optimization. In fact, the main purpose of most BJP models is to be involved in structural optimization studies (Fig. 2.2(a)). This means multiple evaluations of the same model (typically hundreds or thousands). Considering that an eventual improvement in the optimization handling of 1D beams would be multiplied by the number of OF calls involved, a big potential gain could be achieved.

Consequently the following aspects must be considered when evaluating the existing approaches for cross-section description or developing new ones:

- Precision:

  A good level of precision must be achieved – the properties of the concept cross-section must be as close as possible to the reference ones.

- Relation to the real structure:

  The link to the actual geometry must be preserved.

- Design variables:

  Enough design parameters must be available for optimization. Their definition and handling must be easy and flexible.

- Efficiency:

  The cross-section description must be efficient, i.e. it must be fast and easy to generate.

- Performance:

  If cross-section computations are involved at some point, they must not in any way slow down the optimization process.

These major modeling and optimization aspects should be addressed in the best possible way. On the other hand, each of the existing state-of-the-art methods faces problems in regard to one or more of these criteria. The current approaches are either not able to maintain the similarity with the detailed FE model (reference and/or optimized) or are suffering some flexibility and performance issues.

The need to address the current problems and fill in the existing gap motivated the study presented in this chapter. In the next sections a novel approach for 1D beam modeling and optimization handling is presented that combines the advantages of the state-of-the-art techniques. The objective is not only to develop and validate a new method, but to propose a better design alternative. The proposed approach keeps the reference cross-sectional shapes of all 1D beams, but when each of them is rescaled during optimization, the beam is represented by means of GNCS properties. Thus a lighter and simpler representation of the concept beams is created and at the same time the connection with the detailed FE model is not broken. The proposed method can be easily implemented and then applied to make concept modeling for the vehicle structure faster and more flexible.

This chapter is organized as follows. The strengths and weaknesses of the current approaches for beam concept modeling and optimization handling are discussed in Section 4.2. In Section 4.3 the novel method is developed and its feasibility is verified for a set of representative beam cross-sections. It is then validated on an industrial case-study in Section 4.4. The advantages of the proposed approach in terms of time gain during optimization are demonstrated in Section 4.5. Finally, the extension capabilities of the 3B method are discussed in Section 4.6.

4.2 1D beam cross-section techniques – current status

The various aspects of 1D beam modeling were thoroughly studied in Chapter 3. The emphasis of this work is on the representation of the 1D beam cross-sections. The three main state-of-the-art approaches related to it (Sections 2.2.2 and 3.2.1) are critically reviewed hereby so that their advantages can be evidenced and their deficiencies can be identified.

4.2.1 Standard cross-section approach

In regard to the modeling and optimization aspects listed in Section 4.1, the STCS method can be evaluated as follows:

- Precision:

As demonstrated in Section 3.3.1, STCSs are mainly suitable for case-studies with regular beam geometry when the difference between the properties of the actual cross-section and the STCS is negligible. If however STCSs are employed in other applications, the actual structural stiffness can be both under- or overestimated significantly. This automatically limits their usage for industrial problems to space frame constructions. Sometimes they are also employed to perform concept design under lack of knowledge in the very early vehicle development phase.

- Relation to the real structure:

  With STCSs the link to the actual geometry is preserved, as long as the initial STCS approximation is at least similar to the real structure. Naturally, if this requirement is fulfilled or not, depends on the structure itself and on the irregularity of the reference cross-sections in particular.

- Design variables:

  The typical design parameters of the various STCSs are their width, height and one or more plate thicknesses (Fig. 4.1). They become automatically available with the creation of the model and can be easily handled in a sizing optimization study.

- Efficiency:

  STCSs are described in terms of their characteristic parameters like material, type of cross-section shape and basic dimensions. This results in a simple and compact representation.

- Performance:

  Before FEA of the model can be performed, all STCSs that it contains are automatically transformed to GNCSs (Fig. 4.1). This transition is required by the structural analysis which works in terms of GNCSs only (areas, MOI). The generation of GNCS properties for a STCS is performed either by means of FE formulation, or by using the original beam equations. As the latter are based on the assumption for thin walls, FEM is considered more exact and is therefore preferred. Even if small, a certain computational effort is required. The transformation process from STCSs to GNCSs is repeated for each newly generated design during optimization.

In brief, STCSs can be considered as a way between GNCSs and ABCSs. They seem only partially appropriate for real-world automotive problems.

4.2.2 Arbitrary cross-section approach

The ABCS approach is hereby assessed, again in terms of modeling and optimization capabilities:

- Precision:

  The maximum possible precision level can be reached. ABCSs are not limited to a set of predefined profiles. They can match perfectly any reference cross-section geometry.

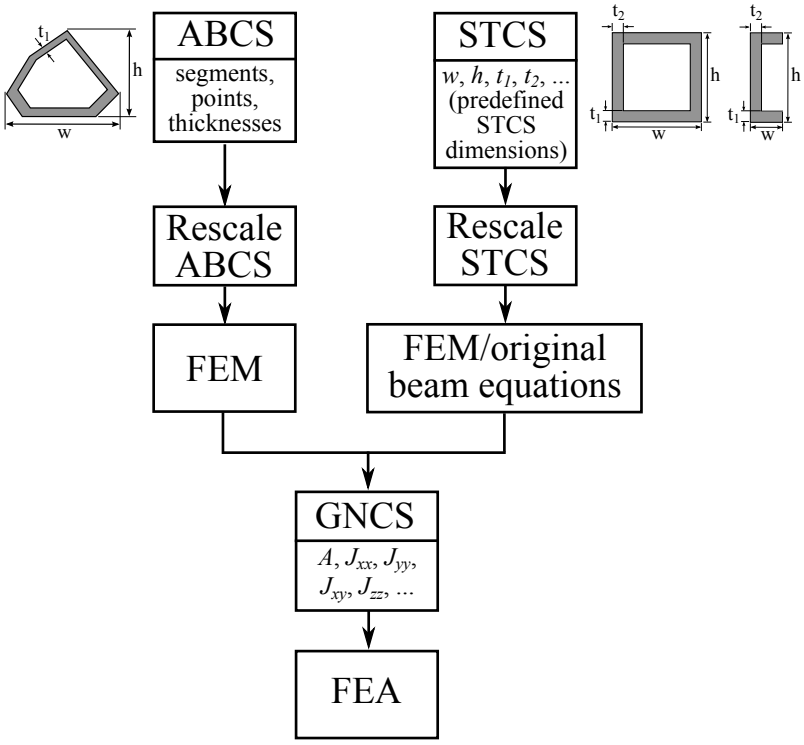

Figure 4.1: Optimization handling of 1D beam cross-sections.

- Relation to the real structure:

  Thanks to the high precision that can be achieved, the transition back from optimized simplified to optimized detailed FE model is greatly facilitated. In a completely detailed ABCS description the link to the actual geometry can be fully preserved, i.e. there will be a one to one correspondence between concept and actual cross-section.

- Design variables:

  There can be various approaches to change an ABCS during optimization. The cross-sectional shape can be changed by moving the positions of the points defining it. Alternatively, the cross-section can be rescaled and the thicknesses of all segments can be modified in a sizing optimization process (Fig. 4.1). In case of many ABCSs, the first approach involves a high number of design variables which are difficult to manage. For this reason the rescaling technique is usually preferred. Both approaches require dedicated scripts for the automatic generation of modified cross-sections.

- Efficiency:

  The cross-section description in terms of points, segments and thicknesses is considerably more complex and less compact compared to STCSs. If

possible, automated tools must be employed for its creation.

- Performance:

  As with STCSs, FEM is used to compute the cross-sectional properties of the ABCSs. Similarly, the transition from ABCS down to GNCS is performed each time before a new design is analyzed (Fig. 4.1). In an optimization process requiring hundreds or more OF evaluations, the cost of this repeated transformation can become prohibitively high [100].

In summary, the ABCS approach is the best available so far. Still, it is by no means perfect and has various problems to face.

4.2.3 Generic cross-section approach

The modeling and optimization features of the GNCS approach are evaluated hereafter:

- Precision:

  As with ABCSs, a high level of precision can be achieved. The GNCS properties can be practically the same as those of the actual cross-sections.

- Relation to the real structure:

  Once the GNCS concept model is created and then modified, the link between simplified and detailed model is completely broken. This is highly undesirable, especially for concept optimization studies.

- Design variables:

  All GNCS properties are directly available as design parameters for modification including the cross-section area, the area MOI, the area product of inertia, the torsional stiffness parameter, etc. (Fig. 4.1). All of them can be easily changed. However, without the relation to the problem geometry, this advantage is of significantly smaller value.

- Efficiency:

  GNCSs are described in terms of their characteristic parameters like material and inertia properties. Similarly to STCSs, this results in a simple and compact cross-section description.

- Performance:

  In contrast to ABCSs and STCSs, GNCSs do not involve any additional computational burden as they are directly used in the subsequent structural analysis. In a 1D beam model consisting only of GNCSs no preliminary transformation is needed before FEA can be performed (Fig. 4.1).

Despite being the least advanced of the three approaches, GNCSs offer good level of simplicity, efficiency and performance.

4.3 Beam Bounding Box approach

4.3.1 Method description

The overview of the state-of-the-art methodologies in Section4.2 clearly demonstrated that there is still room for improvement. While STCSs are not relevant for irregular structures (many of the real-world problems), GNCSs do not keep any geometry information. Even the most advanced of the three techniques – the ABCS method, is by no means without any deficiencies and suffers some flexibility and performance issues.

In this regard an advanced approach for beam concept modeling and optimization handling is presented hereby. Its name is Beam Bounding Box (3B) method because of the rectangular bounding box created around each cross-section of the reference beam structure. The main stages of the method are shown in Fig. 4.2.

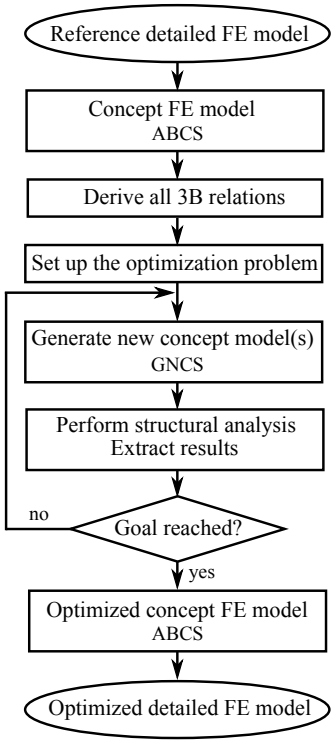

Figure 4.2: 3B method for beam concept modeling and optimization handling.

As in the state-of-the-art approaches, a validated full FE model of the vehicle structure is used as a reference. The beam-like parts of this model are identified and substituted with 1D concept beams having ABCSs. A rectangular bounding box is created around each of the ABCSs. If x and y are the axes of the beam local coordinate system lying in the plane of the cross-section, the width of the bounding

box is determined by the difference between the maximum and the minimum x coordinates of the points describing the cross-section, and its height — by the difference between the maximum and the minimum y coordinates. Before starting the sizing optimization, a 3B relation is defined between the dimensions of each bounding box and the equivalent cross-sectional properties of its corresponding ABCS by means of RS model (discussed in detail in Section 4.3.2). During the subsequent optimization the design variables controlled by the algorithm are the widths and heights of all bounding boxes. However in the concept model the cross-sections are represented as generic and not as arbitrary due to the 3B relations derived earlier. For the sake of simplicity all plate thicknesses are kept constant. Nevertheless, they can be added as design variables in a further step of the method development.

After the end condition of the optimization cycle has been satisfied, all cross-sections of the optimized structure can be transformed back from generic to arbitrary. To obtain the optimized ABCS model one has to rescale the reference ABCS according to the optimal dimensions of their corresponding bounding boxes. These ABCSs can be visualized and the concept model will resemble a real structure. Thus a better insight can be given to the design engineers on how the real optimized model should look like. Eventually the corresponding detailed FE model can be built on the basis of the reference one by using mesh morphing techniques. The bounding boxes of the ABCSs can be used to construct bounding volumes around each corresponding beam-like part. Then these volumes can be transformed to morphing volumes in order to be able to scale the reference FE model accordingly.

The 3B relations are a key element in the new approach as they result in a lighter but at the same time enhanced cross-sectional description. In spite of the use of GNCSs the relation to the real cross-sectional geometry is preserved. On the other hand, the 3B method results faster than a STCS- or ABCS approach, as for both of them each cross-section has to be always transformed to a GNCS description before starting the structural analysis (Fig. 4.1). For a concept model with hundreds of different cross-sections, e.g. for the whole car body, the time needed for this transformation can become a substantial part of the time needed for the whole analysis, given that typically a single static or modal analysis on a BIW concept model takes seconds. This slow-down can become an important factor during optimization, considering the hundreds or even thousands OF calls and thus CAE analyses.

4.3.2 Deriving the 3B relations

In the following sections the methodology used to derive the 3B relations is discussed in detail. Its feasibility is also checked as preliminary validation before applying the 3B method on industrial case-studies.

Let x, y and z be the axes of the beam local coordinate system. Let z be aligned with the beam axis and let the x–y plane be the plane perpendicular to the axis (Fig. 4.3). Then the equivalent cross-sectional properties are:

- A — area of the beam cross-section;
- J_{xx}, J_{yy} — area MOI about the neutral axis;

- J_{xy} — area product of inertia;
- J_{zz} — torsional stiffness parameter;
- N_x, N_y — (x,y) coordinates of the neutral axis with respect to the shear center.

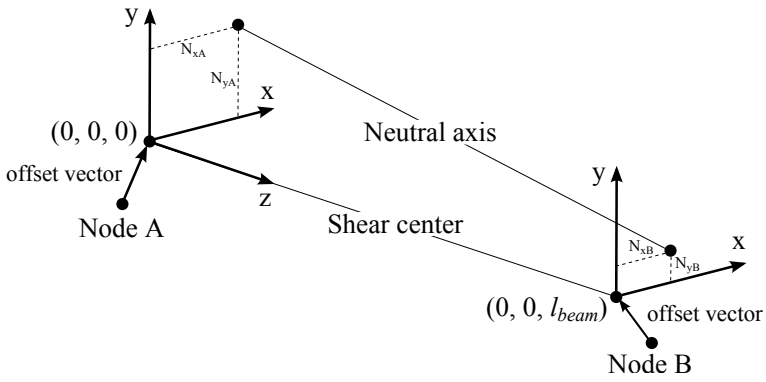

Figure 4.3: 1D beam element coordinate system.

The properties listed above are considered the same for both ends of the beam. The shear centers at both element ends have (x,y) coordinates of (0,0) and coincide with the nodes defining the beam. Therefore the relative positioning of each cross-section in the x–y plane depends on its shear center. To change this positioning, non-zero offsets can be defined between the nodes and the shear centers at both ends. Offsets are thus needed in the common case for which the beam nodes should coincide with the centroids of the end cross-sections [1, 8, 22, 23, 26, 41, 43]. In such a situation, the coordinates of the neutral axis must be used to compute the offsets, which was the reason to consider them in this work.

Response surface model

RS polynomial models are widely used in the engineering practice when it comes to relating an output variable (called also response) to the levels of a number of input variables that affect it [194]. In this chapter they were used to derive the 3B relations. For each separate ABCS the main stages of this process are as follows:

- Definition of the input variables: they are the width and the height of the ABCS bounding box. A decision must be taken also regarding their range.
- Definition of the output variables: they are the seven equivalent cross-sectional properties mentioned in the paragraph above – A, J_{xx}, J_{yy}, J_{xy}, J_{zz}, N_x, N_y. Each of them has to be approximated by a different RS polynomial.
- Selection and execution of a DOE plan: each planned experiment corresponds to different bounding box dimensions and thus to a rescaled ABCS.

All generated cross-sections are then analyzed and their equivalent cross-sectional properties are extracted. The cross-sectional properties of a beam can be calculated either by dedicated software accepting text input or by in-house code, both using FEM.

- Fitting of the RS polynomials on the basis of the DOE results: the unknown coefficients of the polynomials approximating all seven responses are found using the least squares criterion in order to minimize the sum of all squared differences between their actual and predicted values.

Feasibility study

The derivation of the 3B relations was tested on a set of 25 representative cross-sections. They are shown in Fig. 4.4 with their corresponding identifiers (ID). They include open and closed cross-sections with different geometries, corresponding to different beam-like parts of a vehicle BIW. The reference cross-sections have different (typically high) width-to-thickness and height-to-thickness ratios. In order to ensure better visualization and uniformity, the thicknesses for all of them are represented with lines having the same width (Fig. 4.4).

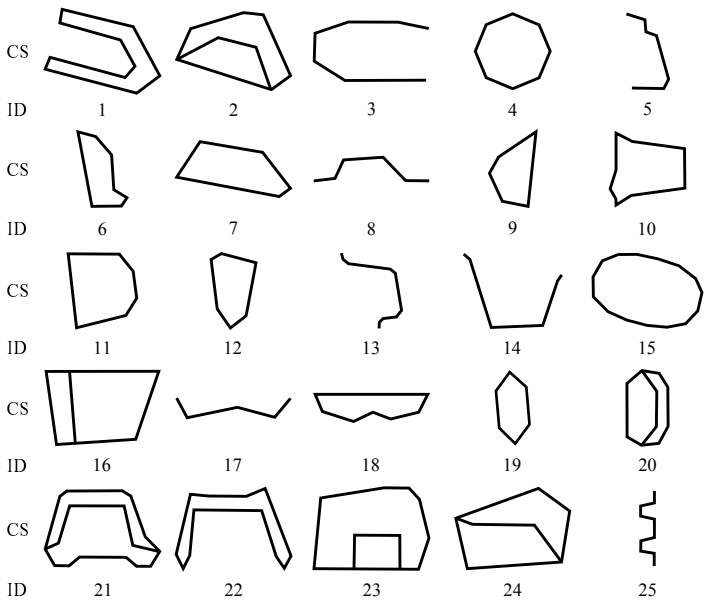

Figure 4.4: Representative cross-sections used for the feasibility study.

The width and the height of each cross-section were varied in the range $[0.5 * ref, 1.5 * ref]$, where ref is their respective reference (i.e. nominal) value. Such a variable range can be considered reasonable from industrial point of view, given the typical geometry constraints and production limitations.

The following approximating polynomials were defined for the cross-sectional

properties:

$$\hat{Y}^2 = \beta_0 + (\beta_1 w + \beta_2 h) + (\beta_{11} w^2 + \beta_{22} h^2 + \beta_{12} wh) \tag{4.1}$$

$$\hat{Y}^4 = \hat{Y}^2 + (\beta_{111} w^3 + \beta_{222} h^3 + \beta_{112} w^2 h + \beta_{122} wh^2) + (\beta_{1111} w^4 + \beta_{2222} h^4 + \beta_{1112} w^3 h + \beta_{1122} w^2 h^2 + \beta_{1222} wh^3) \tag{4.2}$$

In these equations w and h are the width and height of the ABCS, β are the unknown regression coefficients, and $\hat{Y}^2$ and $\hat{Y}^4$ are the estimated responses, where the upper index indicates the degree of the polynomial. The subscripts of the regression coefficients are defined according to their corresponding successive term. Thus a subscript of 1 stays for w and a subscript of 2 stays for h. The repetition of the subscript is defined by the degree of w and h in the term. Eq. 4.1 was used to approximate the cross-sectional area A, and Eq. 4.2 – for all other cross-sectional properties – J_{xx}, J_{yy}, J_{xy}, J_{zz}, N_x, N_y. As stated in [194], when the approximation needs to be made over limited regions usually a polynomial of first or second degree represents sufficiently well the true function. However, in this study polynomials of order lower than four resulted in unsatisfactory model fit and turned out to be inadequate approximations for all cross-sectional properties but the area A. Such a result was somewhat predictable based on the formulations of these quantities for cross-sections with standard profile given in the manuals of engineering.

Latin Hypercube Sampling (LHS) [195] was selected for the DOE phase. Space-filling designs such as LHS can be more useful than conventional ones (e.g. central-composite, Box-Behnken) when the nature of the RS is highly nonlinear either because the system is too complex or because of the relatively large range of the input variables [196]. They can provide more information about the design space and are thus useful for the approximation of computer experiments with deterministic output. In addition to its good space-filling property, LHS is also flexible. The number of experiments and thus the number of levels for the input variables can be controlled by the user. The designer has the freedom to balance between accuracy of the approximation and computational time for the DOE. Furthermore LHS can cope with many input variables and it is computationally cheap to generate. Thus additional variables for the plate thicknesses can be also added. In the current work there are only two input variables per cross-section but up to 14 regression coefficients, which means that at least 14 experiments need to be performed. For this study 30 experiments per cross-section were performed. The decrease of this number deteriorated the approximating models. Its increase did not bring any considerable improvement.

After finding the regression coefficients of all approximation models for each of the cross-sections, their performance needs to be assessed. The following criteria were used for this purpose:

- Determination coefficient R^2
- Adjusted determination coefficient R^2_{adj}
- F-statistic

Let n be the number of experimental designs used in fitting the polynomial and k be the number of regression coefficients (the constant term is not counted). For the i^{th} experiment let $\hat{Y}_i$ be the response predicted by the polynomial, let Y_i be the actual measured response and $\bar{Y}$ be the average of all actual responses over the n experiments. Then the following three quantities can be defined:

$$SSR = \sum_{i=1}^{n} (\hat{Y}_i - \bar{Y})^2 \tag{4.3}$$

$$SSE = \sum_{i=1}^{n} (Y_i - \hat{Y}_i)^2 \tag{4.4}$$

$$SST = \sum_{i=1}^{n} (Y_i - \bar{Y})^2 \tag{4.5}$$

In Eqs. 4.3, 4.4 and 4.5 SSR is the sum of squares due to regression (or also sum of squares explained by the fitted model), SSE is the sum of squares unaccounted for by the fitted model and SST is the total sum of squares which gives the total variation in the data set. Then the criteria mentioned above can be defined as:

$$R^2 = 1 - \frac{SSE}{SST} \tag{4.6}$$

$$R^2_{adj} = 1 - \left(\frac{n-1}{n-k-1} \right) \left(1 - R^2 \right) \tag{4.7}$$

$$F = \frac{SSR/k}{SSE/(n-k-1)} \tag{4.8}$$

The determination factor R^2 gives the proportion of the total variation explained by the fitted model. R^2_{adj} is a statistically unbiased version of R^2 that takes into account the number of regression coefficients k which can vary for different models. Both criteria measure the goodness of fit. Their values can be between zero and one, but should be preferably close to one which in other words means that the biggest portion of the total variation is explained by the polynomial model.

The F-statistic is used to test the significance of the fitted regression equation. Usually the so-called null hypothesis H_0 is tested — the hypothesis that all β_i (β_0 excluded) are zero. If H_0 is true the F-statistic follows a $F_{(\alpha,k,n-k-1)}$ distribution, where α is the significance level, usually chosen between 1% and 10%. Thus, if F, calculated with Eq. 4.8, exceeds the table value $F_{(\alpha,k,n-k-1)}$, H_0 is false and the variation explained by the fitted model is greater than the unexplained variation. Moreover, as recommended in [197], F should preferably exceed $F_{(\alpha,k,n-k-1)}$ by a factor of 10.

To make an additional assessment of the fitted polynomial models in practical engineering terms, the following standard deviation σ can be calculated [104]:

$$\sigma = \sqrt{\left(\sum_{i=1}^{n} \left(r_i - \bar{r} \right)^2 \right) / \left(n - 1 \right)} \tag{4.9}$$

In this formula $r_i = \hat{Y}_i / Y_i$ is the ratio between predicted and actual response for the i^{th} experiment and $\bar{r} \approx 1$ is the average of all r_i. The lower the standard deviation, the lower the prediction errors will be. In fact, according to the 3-sigma rule, about 99.7% of all r_i will be in the interval $[\bar{r} - 3\sigma, \bar{r} + 3\sigma]$.

Figs. 4.5(a) and 4.5(b) show R^2 and R^2_{adj} calculated for all the seven characteristics of each of the 25 cross-sections (Fig. 4.4). As it can be seen, all values for both criteria are practically equal to one or very close to one. Their lowest values correspond to the approximating polynomials of N_x and N_y for just a few of the cross-sections, but are however not below 0.998 (R^2_{adj}). It can be thus concluded that the biggest part of the total variation is explained by the proposed polynomial models (Eqs. 4.1 and 4.2).

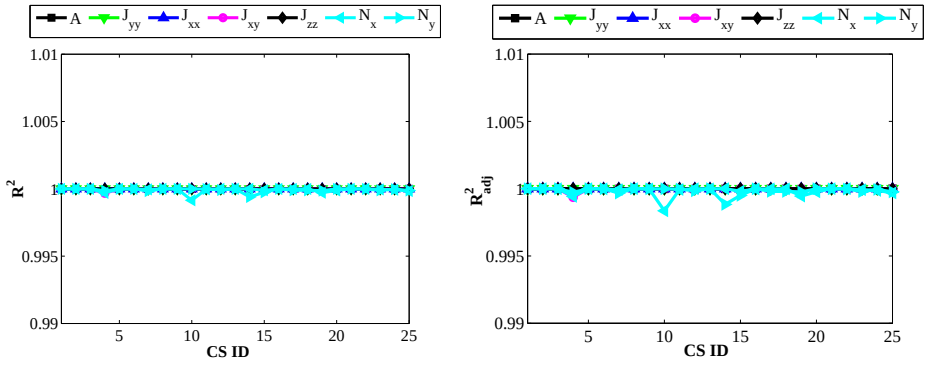

(a) $\mathbf{R^2}$. (b) $\mathbf{R^2_{adj}}$.

Figure 4.5: Determination factors.

Fig. 4.6(a) shows the F-statistic calculated for the area A and Fig. 4.6(b) for all the other properties, in both cases for each of the 25 cross-sections. A significance level α of 1% was chosen. Thus the table values of F used in testing the null hypothesis are $F_{(0.01,5,24)} = 3.895$ for the area A and $F_{(0.01,14,15)} = 3.564$ for all other properties, given that $k = 5$ and 14 respectively and $n = 30$ for both. In Fig. 4.6(a) and 4.6(b) these two values are abbreviated as F_{thr2} and F_{thr4} respectively and are multiplied by 10. From both figures it can be seen that for each of the seven cross-sectional properties the values of the F-statistic vary from cross-section to cross-section which can be explained with their different geometries (Fig. 4.4). However, all calculated F-statistic exceed the threshold values F_{thr2} and F_{thr4} by a factor much greater than 10. Consequently, the null hypothesis can be rejected and all fitted regression equations are significant.

Finally, the standard deviations of the ratios between predicted and actual responses were calculated according to Eq. 4.9. As discussed before, for all responses a prediction error of up to $\pm 3\sigma$ can be expected in 99.7% of the cases. As visible from Fig. 4.7, σ is higher than 0.005 just for J_{xy} of cross-section 22. This means a relative error of 3.3% in this case and a relative error less than 1.5% in all other cases. These results can be considered acceptable for the aims of a concept study.

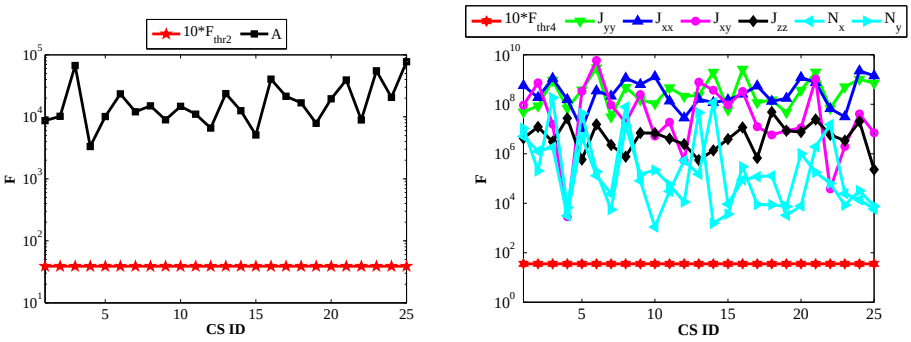

(a) F-statistic for **A**. (b) F-statistic for all other responses.

Figure 4.6: F-statistic.

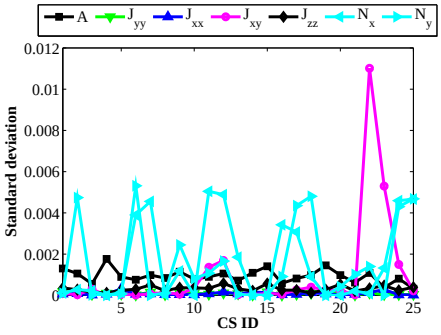

Figure 4.7: Standard deviation of predicted over actual responses.

The feasibility study terminated successfully as the approximating models were adequate. However, their derivation has a certain computational cost. It generally depends on the computational resources, on the program used for calculating the cross-sectional properties, on the number of experiments per cross-section, and finally on the total number of reference ABCSs. On the other hand, the 3B relations are derived just once for a specific concept model and a predefined design variable range (Fig. 4.2). The gain of using the 3B instead of the classical ABCS approach during sizing optimization is considerable and increases with the increase of the number of OF evaluations (Section 4.5). Moreover, as the results from the first optimization run are rarely satisfactory, the optimization algorithm is often restarted on the same concept model but with different setups of the optimization problem. This can be an additional pay-off for the computational cost of the initial phase.

The time for deriving all relations for the feasibility study in this section is negligible. Time considerations regarding more realistic cases are discussed in

Section 4.5.

4.4 Case study 1 – local optimization of a vehicle BIW

In this section the 3B approach was validated for an industrial case study. The Toyota Rav4 BIW, year 1997, shown in Fig. 3.20 was used as reference FE model. The model has been described in Section 3.4.1.

For the sake of simplicity only its B-pillar was simplified and optimized. As stated in [1], the design modifications of the B-pillar and its adjacent joints can largely influence the static and dynamic stiffness of the body. Therefore the effect of the local B-pillar optimization on the global structural behavior was also verified. MD Nastran 2010 [100] was used for the linear static and the modal analysis, as well as for the computation of the equivalent ABCS properties. Of course, instead of addressing the B-pillar design at component level, it could be performed at full vehicle level too in combination with reduction techniques such as WBS for the rest of the body (e.g. [1]).

4.4.1 B-pillar simplification

The B-pillar of the Toyota Rav4 (Fig. 3.20) was isolated from the rest of the model (Fig. 4.8(a)) and was then substituted with its concept equivalent (Fig. 4.8(b), detailed and simple 1D element display). Ten different beam groups with their respective ABCSs (Fig. 4.8(b)) were created so that a more accurate model could be obtained. The geometries of the reference ABCSs were saved as they were needed to create the 3B relations and later on in the transition back from concept to detailed optimized model.

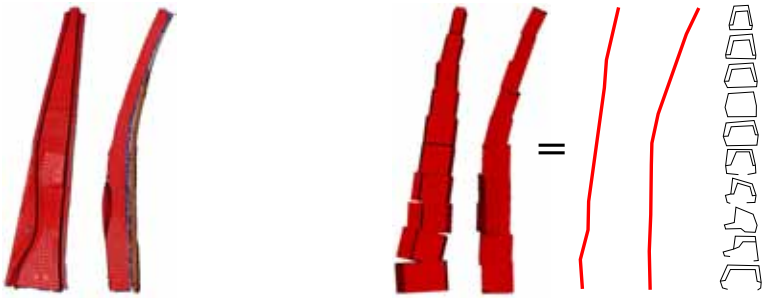

(a) Detailed FE model.

(b) ABCS concept model.

Figure 4.8: Toyota Rav4 B-pillar — frontal and side views.

The 3B relations for all reference ABCSs were automatically derived. For this purpose the same settings were used as in Section 4.3.2 (variable range, polynomials, number of experiments). To make sure that the RS models are adequate enough R^2, R^2_{adj}, the F-statistic and the standard deviation of the predicted over actual responses were calculated for all cross-sections (Fig. 4.9, 4.10 and 4.11).

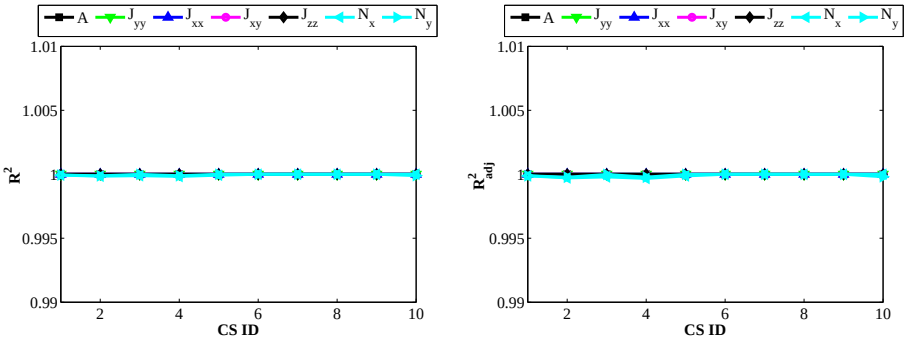

(a) $\mathbf{R^2}$. (b) $\mathbf{R^2_{adj}}$.

Figure 4.9: Determination factors.

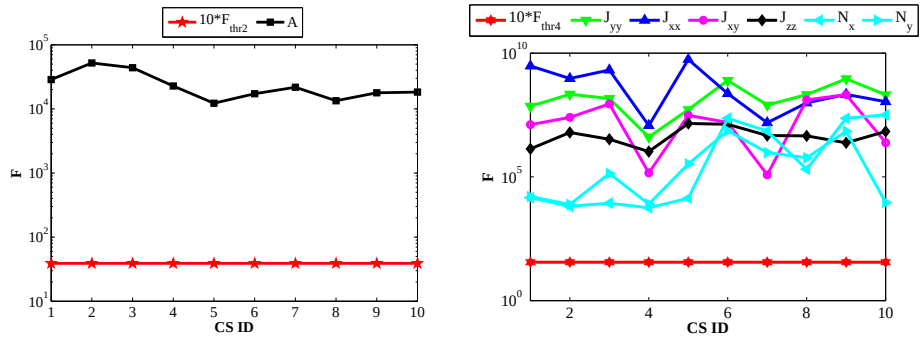

(a) F-statistic for **A**. (b) F-statistic for all other responses.

Figure 4.10: F-statistic.

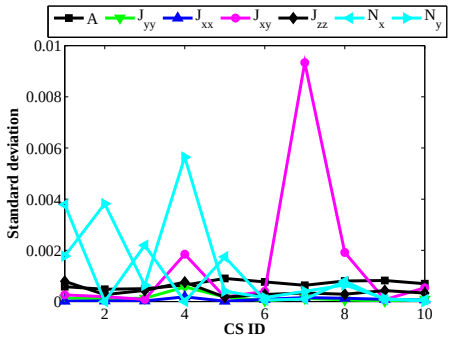

Figure 4.11: Standard deviations of predicted over actual responses.

The results for R^2 (Fig. 4.9(a)) and R^2_{adj} (Fig. 4.9(b)) are even better than those from the feasibility study — 99% of the total variation is explained by the

fitted models. Regarding the F-statistic, the table values of F remain unchanged (i.e. $F_{(0.01,5,24)} = 3.895$ and $F_{(0.01,14,15)} = 3.564$). As visible from Fig. 4.10(a) and 4.10(b) the F-statistic for all responses of the 10 cross-sections exceeds those values times more than the recommended factor of 10. As for the standard deviations, σ is higher than 0.006 just for J_{xy} of cross-section 7. As a possible remedy to decrease it, more experiments can be generated. For all other cases a relative error of less than 1.8% can be expected. Thus the proposed RS approximations can be considered appropriate for all cross-sections under study.

4.4.2 B-pillar optimization

After the concept model of the B-pillar was created, local sizing optimization was performed in order to increase its static stiffness. A simple static load case was defined. The B-pillar was constrained at its lower end and forces and moments were applied to its upper end (similarly to the load case setup in Section 3.3.2). The optimization problem can be briefly defined as follows:

- Design variables: the widths and the heights of all bounding boxes, i.e. 20 variables;
- Geometry constraints: 9 smoothness constraints (regarding the maximum allowable ratios between the widths and respectively the heights of each two adjacent bounding boxes) and 10 side ratio constraints (regarding the maximum allowable ratios between the width and the height of each bounding box);
- Response constraints: $M \leq 1.3M_{ref}$, where M_{ref} and M are the masses of the reference and the target concept B-pillar respectively. This constraint had to be imposed as all plate thicknesses were kept constant;
- OF: $(T_i \leq 0.5T_{i\_ref})$ and $(R_i \leq 0.5R_{i\_ref})$, where $i = 1..3$ are the X, Y and Z axis of the global coordinate system. The i^{th} translational and rotational component of the upper end tip node are denoted with T_{i_ref} and respectively R_{i_ref} for the reference concept B-pillar, and with T_i and respectively R_i – for the target concept B-pillar. When all geometry and response constraints, as well as these targets are satisfied, the OF is zero.

DE [198] was chosen as optimization algorithm (see Chapter 6). The number of population members was set to 10, the differential weight to 0.8 and the crossover probability to 0.9. Fig. 4.12 shows the convergence plot. It can be seen that DE converged after 323 OF calls. At the end of the optimization, all constraints were satisfied and at the same time the static stiffness of the B-pillar was improved. It must be noted that the 3B method can be successfully integrated also in a classical GB algorithm (e.g. Nastran SOL200 [100]).

Knowing the optimal dimensions of all bounding boxes, it was possible to transform the GNCSs in this model back to ABCS description by rescaling the nominal cross-sections accordingly. Table 4.1 shows the maximum absolute relative errors $|\Delta|_{max}$ between the predicted and the actual properties of all ABCSs. It

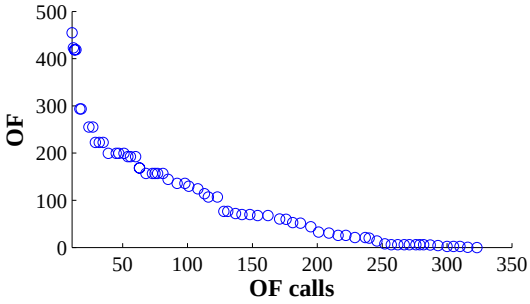

Figure 4.12: Convergence plot for the B-pillar optimization case-study.

Table 4.1: Maximum absolute relative errors between the GNCSs of the optimized B-pillar and their corresponding ABCSs.

	A	J_{xx}	J_{yy}	J_{xy}	J_{zz}	N_x	N_y
$\|\Delta\|_{max}[\%]$	0.00	0.00	0.00	0.00	0.00	0.33	0.03

can be seen that, as expected, these prediction errors are very low (the maximum is 0.33%). Furthermore they lie within the 3σ confidence interval.

Table 4.2 compares the reference ABCS model (Fig. 4.8(b)), the optimized GNCS model and the final ABCS model (Fig. 4.13(a)). In this table $\Delta_{opt-ref}$ stands for the relative difference between the optimized and the reference model, whereas $|\Delta_{opt-fnl}|$ is the absolute relative error between the optimized and the final model. The modulus of $\Delta_{opt-fnl}$ is given as its sign is irrelevant in this case. As imposed in the OF, all translational and rotational components of the tip node are reduced by more than 50% in the optimized GNCS model. On the other hand, the average relative error between the optimized GNCS model and its corresponding ABCS model is 1.95% for the translational components and 0.02% for the rotational components. This can be considered a sufficient accuracy for a concept study.

Table 4.2: Translational and rotational components of the upper end tip node.

	Reference model (ABCSs)	Optimized model (GNCSs)	Final model (ABCSs)	$\Delta_{opt-ref}$ [%]	$\|\Delta_{opt-fnl}\|$ [%]
$T_1[m*10^{-3}]$	-3.34	-1.66	-1.70	-50.25	2.39
$T_2[m*10^{-3}]$	5.69	2.26	2.32	-60.20	2.23
$T_3[m*10^{-3}]$	1.03	0.38	0.39	-62.92	1.22
R_1[rad]	-9.07E-3	-3.67E-3	-3.67E-3	-59.50	0.00
R_2[rad]	5.79E-4	2.73E-4	2.72E-4	-52.92	0.06
R_3[rad]	-1.55E-2	-7.07E-3	-7.07E-3	-54.33	0.00

Fig. 4.13(a) shows the final ABCS B-pillar. As the concept model is quite detailed it can give the designer a relatively good idea of the corresponding detailed FE model. If the optimized model is compared with the one from Fig. 4.8(b), it can be seen that almost all the widths increased, as well as the cross-sectional heights of the lower half of the B-pillar. At the same time the imposed smoothness and side ratio constraints were respected.

(a) Offsets considered. (b) Offsets not considered.

Figure 4.13: Optimized B-pillar – frontal and side views of the ABCSs.

Finally, Fig. 4.13 illustrates the importance of considering variable beam offsets during design modifications. Fig. 4.13(b) shows the result of an optimization with initial settings as the ones used to obtain the model from Fig. 4.13(a), but in this second case all beam offsets were kept unchanged. The side view of this model demonstrates the disadvantages of such an assumption. The ABCSs are rescaled and respect the geometry constraints but in practice if visualized they do not follow the main feature line of the B-pillar because of the constant offsets. This shift with respect to the feature line is more visible for open cross-sections and it can become a problem especially if mesh morphing should be performed after this stage in order to obtain the optimized detailed FE model.

4.4.3 Hybrid model

To see the effect of the B-pillar optimization on global scale, two FE models of the BIW were created. In both of these hybrid models the two B-pillars of the detailed reference FE model were replaced with their 1D beam counterparts. Because of symmetry reasons the right B-pillar was created by mirroring the 1D beam elements of the left one. Thus the ABCS B-pillars from Fig. 4.14(a) correspond to the reference 1D B-pillar (Fig. 4.8(b)), and the ones from Fig. 4.14(b) correspond to the optimized 1D B-pillar (Fig.4.13(a)).

To quantify the static performance of the vehicle BIW the values for the global bending and torsional stiffness, K_b and K_t, were obtained by means of the same load cases and formulas as in Section 3.4.1. For the evaluation of the global dynamic performance modal analysis was performed for the two hybrid models under free-free conditions. The first 6 non-rigid body modes were considered.

(a) Reference B-pillars. (b) Optimized B-pillars.

Figure 4.14: Hybrid FE model of the BIW.

For both hybrid models (Fig. 4.14) the results regarding the BIW mass, static bending and torsional stiffness are shown in Table 4.3. To measure the similarity between the j^{th} mode shape of the reference hybrid model ϕ_j^{ref} and the i^{th} mode shape of the optimized hybrid model ϕ_i^{opt}, the MAC was calculated according to Eq. 4.10 [156]. The results for the eigenfrequencies and the diagonal values of the MAC matrix can be seen in Table 4.4, where f_{ref} and f_{opt} stand for the eigenfrequencies of the reference and optimized model respectively. The relative difference between the optimized and the reference hybrid BIW is denoted with $\Delta_{opt-ref}$ in both tables.

$$MAC\left(\phi_i^{opt}, \phi_j^{ref}\right) = \frac{\left|\phi_i^{opt^{\mathsf{T}}}\, \phi_j^{ref}\right|^2}{\left(\phi_i^{opt^{\mathsf{T}}}\, \phi_i^{opt}\right)\left(\phi_j^{ref^{\mathsf{T}}}\, \phi_j^{ref}\right)} \tag{4.10}$$

Table 4.3: Mass, static bending and torsional stiffness for the hybrid BIW FE models.

	Reference hybrid BIW	Optimized hybrid BIW	$\Delta_{opt-ref}$ [%]
Mass [kg]	303.25	305.38	0.70
$K_b[N/m]$	3.20E6	3.26E6	1.69
$K_t[Nm/rad]$	2.78E5	2.82E5	1.37

As it can be seen from Table 4.3 and 4.4 the local optimization of the B-pillar improves the global static and dynamic behavior at the price of just a small increase of the mass (0.7%). The average increase of the eigenfrequencies is 0.55% and the maximum relative difference is 1.27%. The biggest improvements are achieved with regard to the first vertical bending and first torsional mode. There is no mode switching as it can be seen from the MAC. The static bending and torsional stiffness increase with 1.69% and 1.37% respectively. All these improvements do not drastically change the structure and its performance, but it must be also considered that just a small part of the BIW was optimized and all thicknesses were kept constant.

Most importantly these results confirm the feasibility of the 3B method also for industrial case studies. Once the methodology has been developed and validated,

Table 4.4: Eigenfrequencies and MAC values for the hybrid BIW FE models.

Mode #	Description	$f_{ref}[Hz]$	$f_{opt}[Hz]$	MAC	$\Delta_{opt-ref}$ [%]
1	1^{st} vertical bending	26.90	27.12	1.00	0.83
2	2^{nd} vertical bending	29.22	29.41	1.00	0.63
3	1^{st} torsion	31.06	31.46	1.00	1.27
4	2^{nd} torsion	36.40	36.49	0.99	0.24
5	lateral bending	37.69	37.82	0.99	0.35
6	mixed bending-torsion	39.39	39.37	1.00	-0.05

it is easy to apply it for any beam-like part of the detailed FE model – A-, B-, C-pillar, door sill, roof rail, etc. In contrast to the GNCS approach, the link with the detailed FE model is not broken, as the reference ABCS geometries are kept and then rescaled according to the optimal dimensions of their bounding boxes. An optimized concept model with ABCSs such as the one from Fig. 4.13(a) can give hints on how the optimized detailed FE model would look like and can be used as guidance in a subsequent mesh morphing. Thus the 3B method is more realistic than the GNCS approach and equally or more correct than the STCS approach. In addition, it is flexible and faster than the ABCS method. Because of the small number of cross-sections for the B-pillar model (only 10), time considerations regarding this last advantage will be discussed in depth in the next section.

4.5 Case study 2 – time considerations

The 3B method outperforms the GNCS and the STCS approaches in terms of similarity to the detailed FE model. Despite of that, its advantages with respect to the ABCS approach must be also evidenced. If compared only in terms of final results, both methods have an ABCS concept model as an output. However, the 3B approach can lead to a considerable time gain with respect to the ABCS approach during the optimization phase.

In the 3B method there is an initial time cost t_{init} related to the preliminary phase of deriving the approximating polynomials for all cross-sections. The concept model is then generated and evaluated many times till the end conditions for the optimization are met. Thus for every OF evaluation, a certain amount of time t_{prop} is spent for calculating all cross-sectional properties with the previously created RS models. After that the part of the input file regarding the changes in the model is generated for time t_{input}. Finally structural analysis is performed on this model, which takes time t_{anls}.

In the case of an ABCS approach $t_{init} = 0$. For every OF evaluation the points describing the ABCSs are recalculated and an input file is generated for time t_{input}. Before analyzing the concept model, the equivalent cross-sectional properties of all ABCSs need to be calculated for time t_{prop} using FEM (Fig. 4.1).

To compare the performance of the two approaches in terms of time, t_{init}, t_{prop} and t_{input} were measured for different number of cross-sections, corresponding thus

to different levels of detail, given that the number of beam elements was kept the same. For this purpose a cross-sectional database and its corresponding BIW concept model were used (Fig. 2.4). The model has 15678 nodes and the time t_{anls} needed to perform linear static analysis is 4.8s. All calculations were made on a desktop PC with the following technical characteristics: CPU Intel Core i5 760@2.8 GHz, 6 GB RAM, OS Windows 7 Pro X64. MD Nastran 2010 [100] was used for the computation of the equivalent ABCS properties.

Fig. 4.15 shows the values for t_{init} in function of the number of cross-sections. For the ABCS approach t_{init} is zero. Regarding the 3B method, even for the highest number of cross-sections t_{init} is in the order of a few minutes. This initial cost can be considered negligible in view of the expected pay-off during optimization.

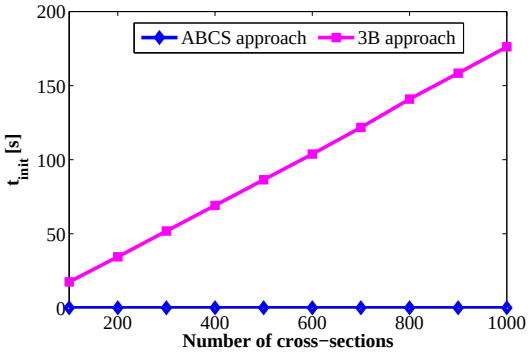

Figure 4.15: Time $\mathbf{t_{init}}$ for different number of cross-sections.

Fig. 4.16 and 4.17 show a comparison between t_{input} and t_{prop} for the 3B- and the classical ABCS approach. The time needed for the input file generation improves with the 3B method as result of the simpler description of the concept model. However, it remains negligible in both cases as it is in the order of less than half second. On the other hand, in the ABCS approach t_{prop} increases linearly with the increase of the number of cross-sections because of the FEM solution process (Fig. 4.17). The 3B approach clearly outperforms it (Fig. 4.17) as t_{prop} is practically zero, independently of the number of cross-sections. Its advantage is even bigger as this time gain is actually multiplied by the number of OF evaluations which can be hundreds or thousands. For example, to solve the simple optimization problem from Section 4.4, 323 OF calls were needed. In addition, in a typical scenario the optimization can be relaunched more than once with different settings, e.g. in the case that no convergence is reached or when the robustness of the algorithm is tested.

Fig. 4.18 summarizes all criteria by comparing the time cost needed for one OF call when using the 3B and the ABCS approach respectively. This time t_{OF} can be expressed as $t_{OF} = t_{input} + t_{prop} + t_{anls}$. It can be clearly seen that for the same number of beam elements, the greater the number of cross-sections assigned to them, the bigger will be the advantage of the 3B method. In fact, with the ABCS approach the sum of t_{input} and t_{prop} becomes commeasurable with t_{anls}

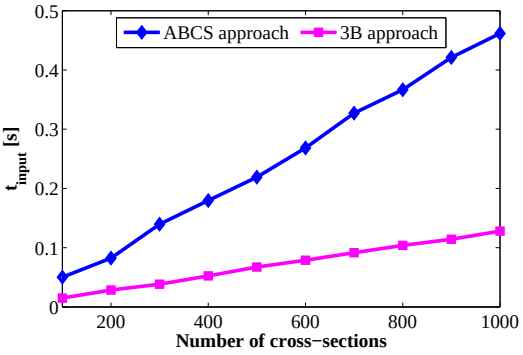

Figure 4.16: Time $\mathbf{t_{input}}$ for different number of cross-sections.

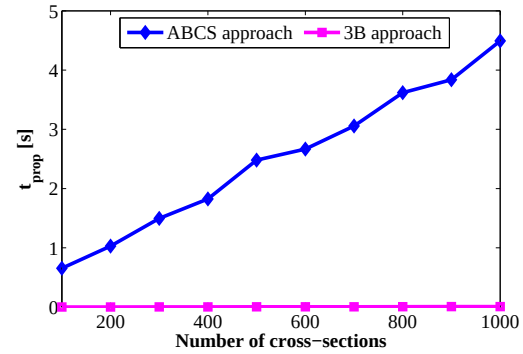

Figure 4.17: Time $\mathbf{t_{prop}}$ for different number of cross-sections.

when increasing the number of the cross-sections. On the other hand, with the 3B method t_{OF} remains practically unchanged and is very close to t_{anls}. Thus if the 3B approach is integrated in the optimization workflow a significant time gain can be achieved which will increase with the increase of the OF evaluations (OF_{eval}). Let the total cost of the optimization process be $t_{tot} = t_{init} + OF_{eval} * t_{OF}$. Then the following threshold number OF_{eval_thr} can be defined:

$$OF_{eval\_thr} = t_{init}^{3B} / \left(t_{input}^{ABCS} + t_{prop}^{ABCS}\right) \tag{4.11}$$

If $OF_{eval} > OF_{eval\_thr}$ the 3B method will have better performance than the ABCS approach. The threshold OF evaluations as function of the number of cross-sections can be seen in Fig. 4.19. For example, in the case of 300 cross-sections (common for BIW concept models, e.g. Fig. 3.28), the 3B method will outperform the ABCS approach after 32 OF calls. For an optimization problem of that scale the design space to explore is large. Consequently, there is a high probability that the actual number of OF calls will largely exceed the threshold (See Chapter 6). A similar reasoning can be made for the rest of the cases ranging from 100 to 1000 cross-sections.

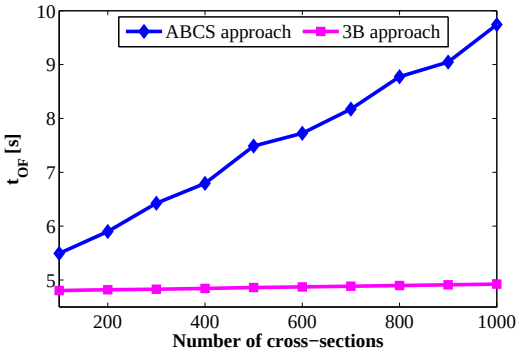

Figure 4.18: Time t_{OF} for different number of cross-sections.

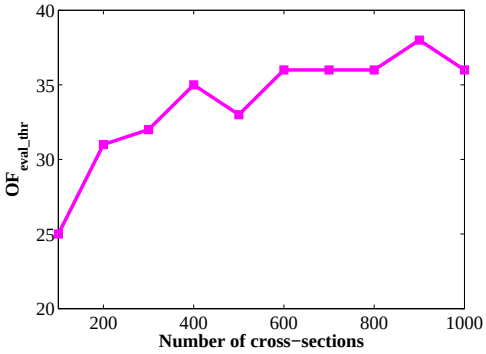

Figure 4.19: Threshold OF evaluations for the 3B method.

4.6 Discussion

From a practical point of view it is important to discuss the extension capabilities of the 3B method as additional design variables might be needed for its future application. In the case of conventional isotropic materials, plate thicknesses can be included for each cross-section. If beams with material mix or carbon reinforced materials have to be handled, other relevant design parameters will also be required in addition to the ABCS width and height. For both cases new design responses might be needed too, for example to take into account the shear stiffness factors in order to improve the accuracy of the concept models.

Two important aspects must be considered if the 3B method is to be extended. First of all, such improvement should be feasible, i.e. all the responses should be approximated well enough. As previously demonstrated in this chapter, the quality of the response surfaces can be easily checked. This step might be needed either when completely new responses are added or if the basic cross-sectional properties (A, J_{xx}, J_{yy}, J_{xy}, J_{zz}, N_x, N_y) are used in function of more design variables (not only the width and the height). If for some reason the accuracy

of the approximation has to be improved, possible countermeasures could be to increase the number of experiments, to decrease the limits of the factors and/or to change the type of the approximating polynomial. In any case, no difficulties are expected with the seven base responses as their physical nature remains the same.

The second key aspect to be considered is the eventual cost of a 3B method extension. This cost must remain such that the 3B method is still computationally more advantageous than the direct ABCS approach when used during optimization. An eventual extension in terms of new responses will not increase the cost of the initial preparation phase for creating the 3B relations if these responses do not require approximating polynomials of order higher than four, i.e. if the total number of experiments remains unchanged. On the other hand, although being straightforward, an extension in terms of additional design variables will unavoidably cause an increase of t_{init}^{3B} and therefrom of OF_{eval_thr}. The hypothetical case of including the plate thicknesses of the cross-section segments is illustrated hereby. Similar considerations can be easily made also in regard to other design parameters such as the orientation angles and the thicknesses of the various plies in a composite material.

As in Section 4.5, the cross-section database of a concept BIW is analyzed. There is a maximum of four different thicknesses per cross-section, i.e. from three up to six associated input variables. The characteristic ratios between the cross-sections with one, two, three and four thicknesses are taken into account. Actually, the cross-sections having one or two thicknesses are prevalent, accounting for 95% of all cases. Assuming that a full 4^{th} degree polynomial will be sufficient to approximate even the most complex responses, the regression coefficients and consequently the minimum required experiments are 35, 70, 124 or 205 depending on the number of design variables for each cross-section. Of course, it can also turn out that more experiments are needed for a good RS quality (e.g. twice as much). The expected performance of the extended 3B method for the best case scenario is shown in Figs. 4.20 and 4.21. In fact, a comparison is made with the original 3B formulation (no thicknesses included) regarding t_{init} and OF_{eval_thr}. No substantial difference is expected as far as t_{input}, t_{prop} and t_{OF} are concerned. Logically, t_{init} increases because of the additional design variables and thus experiments (Fig. 4.20). As a consequence also the efficiency threshold OF_{eval_thr} of the extended 3B method becomes higher than for its reference formulation (Fig. 4.21). On the other hand, it can be regarded as negligible in view of the optimization in a larger design space. When more design variables are involved, more OF evaluations will be needed to complete the search (e.g. see Chapter 6). On their turn, they will quickly compensate for the increased cost of the extended 3B method, so that it remains more efficient than the direct application of the ABCS approach. From that point of view, if OF_{eval_thr} becomes higher due to any additional cross-section parameters, it is likely to be exceeded many times thanks to the optimization of a problem with increased dimensionality. Thus it is reasonable to claim that for the typical automotive problems similar extensions of the 3B approach are achievable without compromising the method's computational benefit.

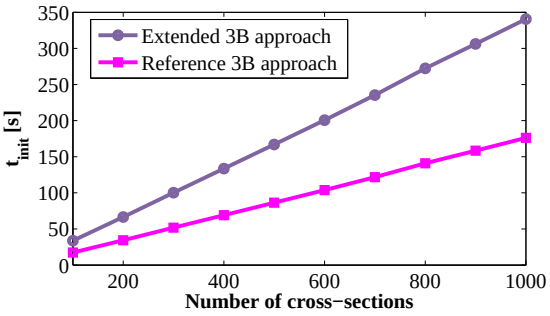

Figure 4.20: Time $\mathbf{t_{init}}$ – reference and extended 3B method.

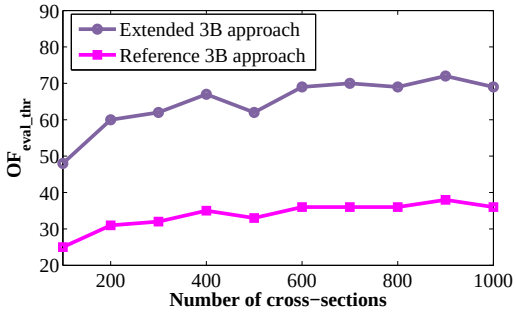

Figure 4.21: Threshold $\mathbf{OF_{eval\_thr}}$ – reference and extended 3B method.

4.7 Conclusions

The 3B approach is a novel methodology for modeling and optimization handling of concept beams. It combines some of the main advantages of the existing state-of-the-art approaches and offers some improvements to them. Each of the GNCSs in the 3B model has its corresponding ABCS description, which on its turn is considered precise and can have varying level of detail. The connection with the real cross-sectional geometry during and after sizing optimization is maintained thanks to the bounding box around each reference ABCS. At the same time, the 3B representation is simpler and more compact than the direct use of ABCSs. This becomes especially important during the optimization phase, where considerable time gains can be achieved.

The 3B method was applied for the creation and optimization of a concept B-pillar. The results confirmed the method appropriateness for beam concept modeling in industrial case studies. Moreover a study was performed on the time gain during optimization. As demonstrated, the 3B approach can lead to significant speed-up with respect to an ABCS representation.

Chapter 5

Concept modeling of joints

5.1 Introduction

The predecessor-based concept approaches for the creation of BJP FE models have the potential to offer the right balance between efficiency, simplicity and precision. This does not come without a cost – this group of methods has been a subject of active development during the last years. In addition to beams (Chapters 3 and 4), the structural joints are the second crucial aspect to consider when creating a new BJP model. Although they account for a relatively small part of the whole structure, their representation can influence the overall approximation and prediction capabilities of the different concept methods. As discussed in Chapter 2, the joints impact greatly the global static and dynamic behavior of the BIW [103].

Normally, after all beam-like parts in the BIW have been substituted with 1D beams, a concept representation must be employed also for its joints. As joints are even more complex structures than beams, there are more aspects to consider when creating their concept models. The following requirements must be taken into account both during the development of a new approach and when choosing an appropriate method among the existing ones:

- Modeling effort

  The time and expertise needed to create a concept joint are not always negligible, which makes the modeling effort an important factor to take into account. Whereas with beams it is not an issue, there are no fully automatic tools for the modeling of concept joints. This is a consequence of the various but quite different approaches for their handling.

- Repeatability

  Under the lack of automation during the creation of simplified joints, repeatability can become problematic. There is often no guarantee that the same result will be obtained by two different designers, as many of the decisions that have to be taken are the result of subjective judgment.

- Geometry

The availability of geometry information and its similarity with the real structure is important. If this condition is satisfied after the model creation, a better model accuracy is to be expected. In addition, the interpretation of optimization results becomes easier for the design engineers if the joints are realistic and close to what is actually expected.

- Numerical effort

  As BJP models are typically small-sized, it is important how the joint representation affects the number of elements and nodes, as well as the total time for simulation. Again, the right compromise must be found between accuracy and computational time.

- Accuracy

  Because of the pronounced influence of the joints on the global structural behavior, the more their concept representations are inaccurate, the more erroneous will result the simplified BIW model. Therefore, it is of extreme importance to reduce the errors due to joint modeling as much as possible.

- Ease of application for industrial problems

  The different methodologies must be suitable for any kind of joint – from the most simple academic examples to the structural nodes in a BIW. Even the most innovative and original approach that does not respect this prerequisite is doomed to limited use in VCM.

The goal of each BJP method is to satisfy these requirements in the best possible way. However, the concept modeling of joints represents a problem which has not yet found a single generally valid and acceptable solution. There is a wide variety of approaches (Section 2.2.2) which range from studying detailed FE models of joints at component level to simplified representations integrated in concept models of the whole car body. Nevertheless all of them have some disadvantages. A lot of efforts are put to overcome the limitations of the state-of-the-art techniques, testified also by the considerable amount of related research papers.

Considering the current concept modeling status in regard to joints, it seems impossible to have all good features combined in one method. A compromise must be always made between weaknesses and strengths. Usually the right method is chosen also taking into account its application. In this sense, an alternative approach for concept joint modeling is proposed hereby which is suited for complex structural nodes, such as those found in the BIW. It is based on dynamic reduction and results in a compact but realistic joint representation. It can be not only easily implemented and applied, but also combined with existing beam-only methods for the creation of simplified BIW models.

This chapter is organized as follows. To begin with, a critical overview is made of the state-of-the-art techniques for concept modeling of joints (Section 5.2). The proposed alternative approach is presented in Section 5.3. First the basics of dynamic SE reduction are summarized (Section 5.3.1. After that the integration of this technique in a typical method using simplified structure layout is discussed

into detail in Section 5.3.2. Finally, an industrial case study is considered in Section 5.4 to evidence the advantages of the dynamic SE joints with respect to one of the most popular state-of-the-art techniques for joint modeling.

5.2 Concept joint modeling techniques – current status

To understand better the necessities of the concept modeling for vehicle joints, the currently available techniques (Section 2.2.2) are evaluated according to the requirements defined in Section 5.1. A summary of this assessment is presented in Table 5.1. A plus sign indicates that the technique has advantages with respect to a certain requirement and satisfies it well, whereas the opposite holds in the case of a minus sign. The presence of a plus and a minus in one cell means that the method has both strengths and weaknesses in regard to the corresponding criterion. In Table 5.1 the main groups of concept joint modeling techniques are organized by columns. Detailed non-parametric and parametric joints are considered (columns 4 and 5) as well as the three main groups of simplified parametric joints: joints as junction of 1D beams (column 2), joints with spring elements and joints as combination of 2-joints. The latter two groups are considered together in column 3 – because of their similarity, the evaluation results for them coincided.

Table 5.1: Evaluation of methods for concept joint modeling.

	Junction of 1D beams	Springs/ 2-joints	Detailed non-parametric	Detailed parametric
Modeling effort	+	-	+	+/-
Repeatability	-	+/-	+	+
Geometry	-	-	+/-	+
Numerical effort	+	+	+	-
Accuracy	-	+/-	+	+
Ease of application	+	-	+	+/-

- Modeling effort

  The lowest modeling effort is usually needed for joints as junction of 1D beams – the concept beams have to be connected in the same node. More intricate in-house procedures have been reported [41, 42] that combine 1D beams with both open and closed cross-sections and require significant skills and experience. However, they can be considered more isolated cases than a general practice. Detailed non-parametric joints are also easily created. Normally, the only effort is related to the initial SE reduction which is quite standardized as procedure. Depending on their type, the detailed parametric joints can represent a greater difficulty. Parametric joints based on mesh morphing are relatively simple to define. On the contrary, the creation of a single fully parametric detailed joint could take months [106]. Finally, simplified joints with springs or 2-joints are also difficult to model as they

require an initial adjustment of the joint parameters. This means that a detailed FE joint model (or alternatively – test results) is also needed and an updating procedure must be performed to correct the concept joint with respect to the actual structural node.

- Repeatability

  Obtaining reliable results for various joints is not an issue in the case of detailed joints, as practically no precision is lost. On the contrary, various subjective decisions must be taken when creating a simplified joint. Joints with springs or 2-joints partially alleviate this issue if model updating is applied. However, with joints as junction of 1D beams there is no guarantee that the same result will be achieved by two different designers.

- Geometry

  The availability of geometry information and the possibility to vary it during optimization is of utmost importance for practical applications. However, these conditions are satisfied only by the detailed parametric joints. With detailed non-parametric joints the geometry is still kept but cannot be changed (SEs are used). All simplified FE joints lose completely the link to the geometry once they are modified. Although their parameters can be easily estimated from tests or detailed FE models, they represent conceptual rather than physical quantities [105]. Once updated, these parameters must be kept constant or the transition back to the detailed joint model will not be guaranteed.

- Numerical effort

  All groups of simplified joint models do not affect the total time for analysis of a BJP model as they have a low number of elements and nodes. The computational cost for detailed non-parametric joints is still low as usually SEs are used which condense the stiffness and mass of the joint to its end nodes. Detailed parametric models are the most problematic ones because they are computationally expensive (shell FE mesh with considerably more nodes).

- Accuracy

  Logically, detailed parametric and non-parametric joint models offer the highest accuracy. In contrast to them, the stiffness of beam-only joints results overestimated [112]. FE models with springs or 2-joints are more accurate simplified models [102] as the joint flexibility is considered. However, an updating process is usually needed to obtain satisfactory results.

- Ease of application for industrial problems

  Joints as junction of 1D beams and detailed non-parametric joints are the easiest to create in an industrial context – their modeling is straightforward and in the same time complex structures can be handled. In general joints with springs or 2-joints are not appropriate for real-world problems. In fact, most of the related methodologies have been developed for simple academic case studies only. How they should be applied for complex joints remains an

open question. Finally, detailed parametric joints can manage structures of arbitrary complexity, but the time for their creation is prohibitive.

The general conclusion which can be made from this critical review is that clearly none of the existing state-of-the-art methods is without deficiencies. Combining the strengths of the various approaches in a single methodology is not feasible. At this stage of concept modeling, further alternatives are needed to broaden the spectrum of available solutions.

5.3 Improved non-parametric concept joints

Based on the assessment made in Section 5.2, the methods for the creation of detailed non-parametric concept joints were identified as one of the most promising groups of approaches. Their main disadvantage is that the joint geometry cannot be changed, but efforts are being made also in this direction (e.g. [24]). Alternatively, taking into account that they are in general much more complex than the beam-like structures, the vehicle joints could be the subject of separate component level studies (e.g. [103]).

As discussed in Section 2.2.2 up to now mainly static reduction has been used [1, 8, 22–24, 26, 35, 45, 103, 112–115]. It does not introduce any approximation in static analysis but is less accurate for structural dynamics applications. In this second case the reduction of the stiffness is exact, but approximations occur during the reduction of the mass and damping matrices. The assumption is made that the components are very stiff and that local dynamic effects can be ignored. Satisfactory results can be obtained for the lowest modes of the system, but the higher frequency or local modes can be wrongly calculated or even entirely missed.

In this regard, the application of dynamic reduction has been identified as a step for further improvement of the state-of-the-art methods. It is a well known reduction approach which offers better accuracy than static condensation at insignificantly higher initial computational cost. In addition, dynamic reduction can be applied not only for joints but also for bigger and/or complex parts of the BIW which cannot be or are wrongly modeled with 1D beams. Thus, if combined with a BJP approach, it can extend the method's validity and applications. The dynamic reduction of joints as SEs has the following strengths:

- Straightforward approach;
- Computationally cheap concept joint models;
- Appropriate for structural statics and dynamics;
- Excellent accuracy, better than static condensation;
- Easy to integrate into existing concept methodologies (e.g. 1D beam only approaches);
- Reuse of the SEs in optimization studies;
- Geometry information is preserved;
- Realistic representation of the joint structural behavior;

- Facilitated practical application through commercial software solutions, e.g [199].

5.3.1 Dynamic reduction

Craig-Bampton CMS [200] was chosen for the dynamic reduction of detailed FE joints into SEs. It is one of the most popular CMS techniques, which has numerous applications reported and good accuracy [1].

With CMS techniques the dynamic behavior of a structure can be represented by a subset of the total DOFs. Let $\mathbf{M}^c$ and $\mathbf{K}^c$ be the mass and stiffness matrix of a component. Let $\mathbf{u}^c$ be the displacement vector and $\mathbf{f}^c$ - the force vector, including forces at the SE boundary. Then the equation of motion in case of undamped component has the form:

$$\mathbf{M}^c\ddot{\mathbf{u}}^c + \mathbf{K}^c\mathbf{u}^c = \mathbf{f}^c \tag{5.1}$$

or in terms of internal (i) and boundary (b) nodes of a SE:

$$\begin{bmatrix} \mathbf{M}_{ii} & \mathbf{M}_{ib} \\ \mathbf{M}_{bi} & \mathbf{M}_{bb} \end{bmatrix} \begin{bmatrix} \ddot{\mathbf{u}}_i \\ \ddot{\mathbf{u}}_b \end{bmatrix} + \begin{bmatrix} \mathbf{K}_{ii} & \mathbf{K}_{ib} \\ \mathbf{K}_{bi} & \mathbf{K}_{bb} \end{bmatrix} \begin{bmatrix} \mathbf{u}_i \\ \mathbf{u}_b \end{bmatrix} = \begin{bmatrix} 0 \\ \mathbf{f}_b \end{bmatrix} \tag{5.2}$$

As in CMS the component physical coordinates ($\mathbf{u}^c$) are expressed in terms of generalized coordinates ($\mathbf{p}^c$), using the relationship

$$\mathbf{u}^c = \mathbf{\Psi}^c\mathbf{p}^c \tag{5.3}$$

Eq. 5.1 can be rewritten in generalized coordinates, if the component mode matrix $\mathbf{\Psi}^c$ is known:

$$\mathbf{\Psi}^{cT}\mathbf{M}^c\mathbf{\Psi}^c\ddot{\mathbf{p}}^c + \mathbf{\Psi}^{cT}\mathbf{K}^c\mathbf{\Psi}^c\mathbf{p}^c = \mathbf{\Psi}^{cT}\mathbf{f}^c \tag{5.4}$$

In the case of Craig-Bampton CMS the transformation matrix $\mathbf{\Psi}^c$ includes fixed-interface normal modes and interface constraint modes [161]. The former are found by restraining all boundary nodes of the SE and solving the eigenproblem in the first equation obtained from Eq. 5.2:

$$\left[\mathbf{K}_{ii} - \omega_j^2\mathbf{M}_{ii}\right]\phi_j = 0, j = 1, 2, \ldots, N_i \tag{5.5}$$

where ω_j are the eigenfrequency values, ϕ_j are the normal mode shapes and N_i is the number of internal nodes. For the complete set of N_i normal modes the fixed-interface normal modes are given by

$$\underset{N\times N_\mathbf{i}}{\mathbf{\Phi}_{norm}} = \begin{bmatrix} \mathbf{\Phi}_{inorm} \\ 0_{bnorm} \end{bmatrix} \tag{5.6}$$

where N is the total number of nodes. The constraint modes are found by using the first equation obtained from the static form of Eq. 5.2:

$$\mathbf{K}_{ii}\mathbf{u}_i + \mathbf{K}_{ib}\mathbf{u}_b = 0 \tag{5.7}$$

By successively applying unit displacement for each of the boundary coordinates and fixing the remaining boundary DOFs, the constraint mode matrix becomes

$$\underset{N\times N_\mathbf{b}}{\mathbf{\Psi}_{cstr}} = \begin{bmatrix} \mathbf{\Psi}_{ib} \\ \mathbf{I}_{bb} \end{bmatrix} = \begin{bmatrix} -\mathbf{K}_{ii}^{-1}\mathbf{K}_{ib} \\ \mathbf{I}_{bb} \end{bmatrix} \tag{5.8}$$

where N_b is the number of boundary nodes and $\mathbf{I}_{bb}$ is identity matrix.

Usually only a smaller set $\mathbf{\Phi}_{kept}$ is kept from the normal mode set $\mathbf{\Phi}_{norm}$. Taking into account Eqs. 5.6, 5.8 and the reduction of $\mathbf{\Phi}_{norm}$ to $\mathbf{\Phi}_{kept}$, the transformation matrix $\mathbf{\Psi}^c$ in the case of Craig-Bampton CMS can be written as

$$\mathbf{\Psi}^c = \begin{bmatrix} \mathbf{\Phi}_{ikept} & \mathbf{\Psi}_{ib} \\ 0 & \mathbf{I}_{bb} \end{bmatrix} \tag{5.9}$$

Thus the mass and stiffness matrices in generalized coordinates – $\mathbf{\Psi}^{cT}\mathbf{M}^c\mathbf{\Psi}^c$ and $\mathbf{\Psi}^{cT}\mathbf{K}^c\mathbf{\Psi}^c$ respectively, will be reduced because of $\mathbf{\Phi}_{kept} < \mathbf{\Phi}_{norm}$. In addition, it should be noted that Craig-Bampton CMS facilitates the enforcement of geometric compatibility at the substructure interfaces, as all physical boundary coordinates are kept as component generalized coordinates [161]. It must be also mentioned that this method is most effective when the coupling interface is small with respect to the component size [1]. In this case the resulting reduced model is significantly smaller than the original FE model.

In practical terms, the application of Craig-Bampton CMS for the dynamic reduction of structural joints is achieved in two basic steps:

- Each joint SE is separated from the rest of the structure. Its boundary (or interface) nodes are defined. Decision is made on how many modes $\mathbf{\Phi}_{kept}$ to keep. In general, the more component modes are used, the more accurate results can be obtained. Finally, reduced matrices are generated from the detailed physical model, which will be used in the follow-up assembly run;
- All joint SEs created in the previous step are assembled together with the residual structure (e.g. beam-like and panel-like parts), so that the completed concept model can be analyzed.

This type of SEs are commonly referred to as external SEs [199]. Their main advantage is that, once dynamic reduction has been performed for all components of interest, they can be reused multiple times. This can be extremely useful in the case of optimization or any repetitive analysis.

5.3.2 Integration in methods based on simplified structure layout

The dynamic reduction of detailed non-parametric joints can be easily integrated in a concept approach for the creation of simplified structural layout (Fig. 5.1). The starting point is a validated, complete FE model (i.e. a reference model). First all panels, joints and the beams between them must be localized. The joints are usually defined as inscribed in a sphere with diameter fitting all structural nodes in a car body (e.g. 250 mm) [114, 117]. The center of the sphere is placed in the approximate joint center and the legs are cut where the sphere bisects them. Alternatively the incoming load-carrying beams can be cut at the point near the joint center where their structure becomes increasingly complex and has little similarity to the rest of the beam. After that, all beam-like parts are divided into groups with similar geometry characteristics. Each group is substituted with 1D beam elements having the same cross-section properties. To assure the fit between

joints and beams, all nodes at the end cross-sections of the joints are connected to the corresponding 1D beams (Fig. 5.2). For this purpose one of the techniques for joining dissimilar elements can be employed (Section 2.2.2), e.g. rigid connection. After that dynamic reduction of all joints is performed by means of Craig-Bampton CMS, following the two-steps procedure defined in Section 5.3.1. The final result is that the joint is reduced to its end nodes, i.e. to the connection nodes with the 1D beams at its end cross-sections. It is for the same reason that first the beams must be simplified and only then the joints. The subsequently generated simplified model is an assembly of the SE joints and the residual 1D beam structure. Concept panels with coarsened mesh can be also added to it, if present in the reference model.

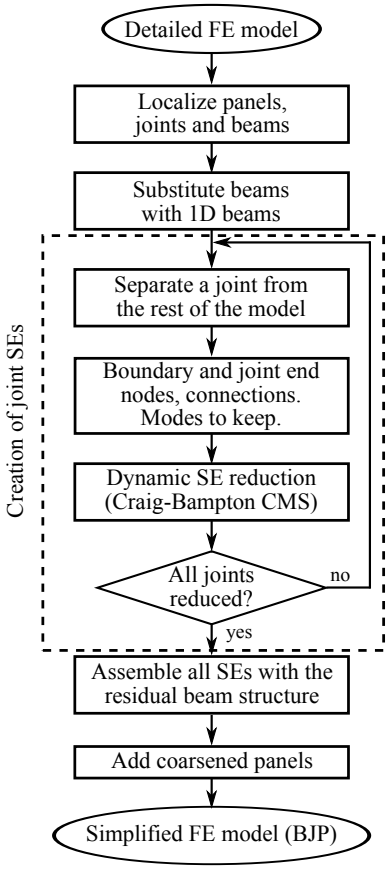

Figure 5.1: Creation of BJP models.

The created BJP model can be used to obtain either an optimized detailed FE model (Fig. 2.2(a)) or an equivalent simplified FE model (Fig. 2.2(b)). Whereas the first case is a classical application of structural optimization in the concept stage, the second one is related to model updating of initially inaccurate BJP models. In practice, model updating resolves an optimization problem too, but

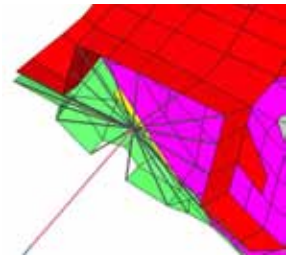

Figure 5.2: Connection between joints and 1D beams.

the objective is to maximize the similarity of the simplified model with respect to the detailed one (Fig. 2.10). Typically, model updating of BJP models is to be expected when STCSs are employed as they result in gross approximations (Chapter 3). On the other hand, models with ABCSs can be often used directly in optimization studies (Fig. 2.2(a)) because of their good performance and better precision [41, 42, 131]. In both cases the design variables are related to the cross-section dimensions. Eventually the panel thicknesses can be also changed. It must be noted that once created, the SE joints remain constant during model updating or optimization.

5.4 Industrial case study

In this section the proposed improved non-parametric concept joints are applied to an industrial case study. A beam and joint simplified model is created for a vehicle subframe. A beam-only representation of the same structure is also built. Thus the performance of the two most popular methods for joint concept modeling is investigated – joints as junction of 1D beams and non-parametric detailed joints.

An existing method for the creation of simplified structure layouts is used as a basis of this work [27, 28, 30]. In its original formulation the approach uses 1D beams only, while for the purposes of this study it has been successfully extended with joint SEs according to the flowchart shown in Fig. 5.1. The employed 1D beams have STCSs which normally result in a rough approximation of the actual cross-section characteristics for a structure with non-standard geometry. Hence the typical application of this methodology is to create equivalent simplified FE models through model updating (Fig. 2.2(b)). The influence of the type of simplified model (joints as junction of 1D beams or dynamic SE joints) on the performance of an updating procedure similar to the one presented in Section 2.2.5 will be studied.

5.4.1 Reference model

The engine subframe of a Lancia K was taken as reference detailed FE model (Fig. 5.3). It consists of 6725 shell elements. The objective of this study is to obtain a simplified FE model with dynamic behavior equivalent to the reference one. To be able to make the comparison detailed-simplified model later on, modal

analysis was performed for the validated FE model. The following results were saved for the purposes of subsequent correlation: the first nine eigenfrequencies (Table 5.2) and mode shapes, the total mass and the principal MOI (Table 5.3).

Figure 5.3: Engine subframe – reference model.

Table 5.2: Eigenfrequencies of the reference model.

Mode#	Eigenfrequency [Hz]
1	43.14
2	99.09
3	126.58
4	141.59
5	147.93
6	180.72
7	208.30
8	237.15
9	249.27

Table 5.3: Total mass and principal MOI for the reference model.

Property	Value
$Mass[kg]$	19.07
$I_{XX}[kg * m^2]$	2.43
$I_{YY}[kg * m^2]$	2.24
$I_{ZZ}[kg * m^2]$	4.6

5.4.2 Initial simplified FE models

Model creation

According to the general procedure for the creation of BJP models (Fig. 5.1), the detailed subframe was divided in beam-like parts and joints as shown in Fig.

5.4. Two parametric simplified models were created on its basis – a beam-only model and an improved beam model with SE joints. The workflow of Fig. 5.1 was respected and first the beam-like parts were simplified by means of STCS 1D beams. However for the beam-only model, the stage related to the creation of joint SEs was logically replaced with the creation of joints as junction of 1D beams. Such a model is a rough approximation of the actual joints in terms both of geometry and stiffness. On the other hand, in the improved model dynamic reduction is performed for each of the joints identified in Fig. 5.4. The joints are taken as small as possible because, once reduced to SEs, they cannot be modified, as it will be possible for the rest of the model. The boundary nodes of each joint end cross-section are connected to the end node of the incoming beam through rigid elements similarly to Fig. 5.2. As discussed in 2.2.2, this technique has been chosen because of its reliability, its extensive validation as well as its ease of application for both academic and industrial case studies. For each of the SEs 36 normal modes are included, which is sufficient for the frequency range of interest.

Figure 5.4: Partition of the full assembly in joints and beams.

The two simplified FE models are shown in Fig. 5.5. They are both superposed with the detailed FE model. The color of the 1D beam elements is determined in accordance to their properties, so the various 1D beam groups are shown in different colors.

In order to verify the quality of the SE joints and the approximations introduced, the following check was performed. Before being connected to the 1D beams, the joints were reduced to the boundary nodes at their end cross-sections and they were thus attached to the rest of the original structure. Modal analysis was performed for the new model consisting of detailed beam-like structures and SE joints. The results for the first nine eigenfrequencies are shown in Table 5.4. The average error for the eigenfrequencies is 0.83% and is considered negligible for the purposes of a concept study. Moreover, such an error is incomparable in regard to the stiffness overestimation introduced by joints as junction of 1D beams. If however better accuracy is needed, alternative CMS techniques can be investigated with different mode sets.

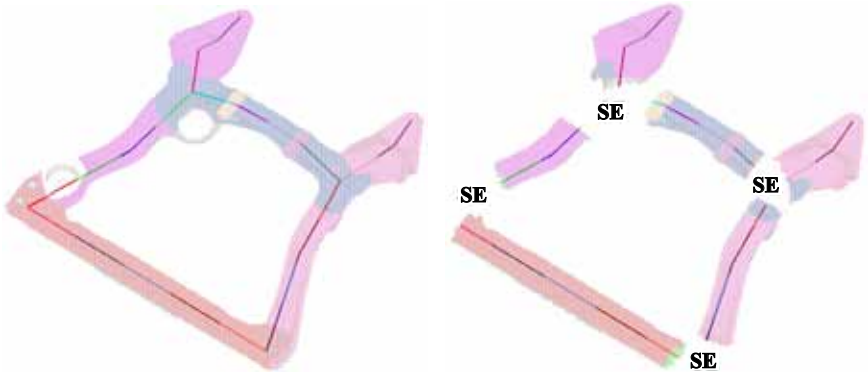

(a) No joints considered. (b) With SE joints.

Figure 5.5: Superposed reference and simplified model.

Table 5.4: Error introduced with SE joints.

	Eigenfrequency [Hz]		
Mode#	Reference model	Reference model + SE	Error [%]
1	43.14	42.85	0.67
2	99.09	98.19	0.91
3	126.58	123.74	2.24
4	141.59	141.54	0.04
5	147.93	147.28	0.44
6	180.72	179.92	0.44
7	208.30	207.57	0.35
8	237.15	232.87	1.80
9	249.27	247.82	0.58

Choice of updating parameters

The results regarding the dynamic behavior of the initial simplified models (Fig. 5.5) are not presented hereby as there was a huge mismatch with the reference model. Not only was its dynamic stiffness strongly overestimated, but some of the higher modes were entirely missed. As already mentioned, and as demonstrated in Chapter 3, this effect was expected because of the use of 1D beams with STCSs in both models. In the beam-only model the mismatch was also due to the non-realistic joint representation.

Thus model updating had to be performed in order to correct the inexact initial simplifications. The same algorithm as in Fig. 2.10 was used. Consequently, updating parameters had to be chosen. For both models they were the heights, widths and thicknesses of the various beam cross-sections. This allowed for an easy set-up of the optimization problem. In addition, whereas the joints in the beam-only model were changed during the updating, the SE joints remained unmodified.

5.4.3 Model matching

As the detailed and the simplified FE models differ in terms of DOFs and FE mesh, model matching must be performed. For this purpose, measurement nodes in each of the simplified models are selected uniformly along the beam elements groups, including the most significant locations. For each of these nodes a group of nodes in its proximity is selected in the reference model (e.g. nodes from adjacent cross-section planes – Fig.5.6). The values of the eigenvector components for all these proximity nodes are averaged and then compared with the corresponding eigenvector component in the simplified model. With such matching technique local deformation effects (difficult to reproduce with simplified models) can be reduced. MAC (See Eq. 4.10) is used to assess the similarity between simplified and detailed FE model. The combination MAC-eigenfrequencies is useful for mode tracking.

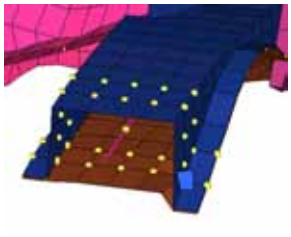

Figure 5.6: Sample measurement node and corresponding MAC control group.

5.4.4 Correlation

To measure the difference between the validated detailed FE model and its concept representation and to decide if they can be considered equivalent in terms of structural behavior, a correlation check must be performed. In the current study this check was made in terms of total mass, principal MOI, MAC (modeshape similarity) and eigenfrequencies.

Actually, the model updating procedure in Fig. 2.10 represents an optimization problem that minimizes the differences between detailed and concept FE model. The design variables are the updating parameters with their lower and upper bounds. Geometry constraints for smooth transitions between the contiguous beam groups can be also imposed. Logically, the OF must be an integral measure for the correlation. An optimization algorithm can then be used to update the simplified model repeatedly until a correlation with the reference model is reached. In the context of the problem at hand the following four OF modules were needed:

$$p_1 = \left| \frac{m^{ref} - m^{simp}}{m^{ref}} \right| \tag{5.10}$$

$$p_2 = \sqrt[n]{\frac{1}{3}\left(\left|\frac{I_{XX}^{ref} - I_{XX}^{simp}}{I_{XX}^{ref}}\right|^n + \left|\frac{I_{YY}^{ref} - I_{YY}^{simp}}{I_{YY}^{ref}}\right|^n + \left|\frac{I_{ZZ}^{ref} - I_{ZZ}^{simp}}{I_{zz}^{ref}}\right|^n\right)} \tag{5.11}$$

$$p_3 = \sqrt[n]{\frac{1}{\#freq}\sum_{i=1}^{\#freq}\left|\frac{f_i^{ref} - f_i^{simp}}{f_i^{ref}}\right|^n} \tag{5.12}$$

$$p_4 = 1 - \sqrt[n]{\frac{1}{\#modes}\sum_{j=1}^{\#modes} MAC(j,j)^n} \tag{5.13}$$

The subscript "ref" in the above equations is used to denote the data extracted from the reference model – the total mass m, the eigenfrequencies f_i and the principal MOI I_{XX}, I_{YY}, I_{ZZ}. In a similar way the subscript "$simp$" refers to the data extracted from the simplified model. The diagonal elements of the MAC matrix are denoted as $MAC(j,j)$. In Eqs. 5.11, 5.12 and 5.13 exponential average is used in order to minimize the dispersion around the mean value. The exponent n is determined in such a way that if all the averaged values but one are 20% below the mean acceptable value, that value cannot exceed the threshold by more than 20%.

Only the diagonal elements of the MAC matrix are used in Eq. 5.13 (i.e. there should be no mode switching in the equivalent simplified model). Their average value should not be less than 0.75. As far as it concerns the other modules, the maximum acceptable errors for them are given in Table 5.5. These thresholds can be set even more restrictive depending on the required level of precision for the concept model.

Table 5.5: Weights and maximum allowed errors for the four criteria.

Criteria	Weight in the OF	Max. acceptable error
p_1	0.15	5%
p_2	0.15	8%
p_3	0.3	5%
p_4	0.4	-

Each of the four modules is normalized (p_{norm_k}) and multiplied by its corresponding weighting factor (Table 5.5). The final OF is then obtained as a sum of these contributions (Eq. 5.14). Once all limits are satisfied, the value of the OF becomes -10000.

$$OF = \sum_{k=1}^{4} w_k * p_{norm\_k} \tag{5.14}$$

where w_k are the weights from Table 5.5.

GA (see Appendix C) was used as main optimization algorithm to improve the correlation simplified-reference model. Despite its undoubted strengths, GA is often not able to reach 100% of the predefined minimum value for a certain reasonable number of generations. If for several generations there is no considerable improvement in the OF, it is preferable to continue with deterministic algorithm, that will converge faster. In this work pattern search was used [201]. The advantages of such a hybrid global-local approach are confirmed in Section 5.4.5.

5.4.5 Results

All model updating procedures have been performed on a desktop PC with the following technical characteristics: CPU Intel Core2 Quad Q6600 @ 2.4 GHz, 4 GB RAM, OS Windows 7 Pro x64. When GA was used in the model updating, each population was thus processed in parallel, as the OF evaluations are independent. The average time required for 1000 OF evaluations in parallel was around 30 minutes.

Four simplified models were created, updated and compared. The differences between them are given in Table 5.6. As it can be seen, in cases 1A and 1B all beam thicknesses are fixed. Because of including them, cases 2A and 2B have twice more variables. For all four cases the thicknesses for the opposite sides of the cross-sections are taken as equal. In addition, cases 1A and 2A have 23 beam sections and cases 1B and 2B – 22. In the latter, a whole group is eliminated because of the lower left joint SE. This difference was taken into account in the GA where the size of the population was defined proportionally to the number of design variables, with a coefficient of about 4.5 for each variable. Bigger populations did not improve the final results.

Table 5.6: Basic differences between the simplified models to be updated.

Case	Description	Type of design variables	Total number of design variables
1A	Beam-only model	height, width	46
1B	Improved model, beams and SE joints	height, width	44
2A	Beam-only model	height, width, 2 thicknesses	92
2B	Improved model, beams and SE joints	height, width, 2 thicknesses	88

As the initial simplified models in all four cases differed from the dynamic behavior of the reference, they passed a model updating procedure. For each case, the computations were repeated three times with the same input parameters, except for the state of the random number generator used in the GA. The best optimization runs (lowest number of OF calls) are reported in Table 5.7.

As expected, the improved simplified models 1B and 2B exceed the performance of the beam-only models (1A, 2A) in terms of OF calls needed for the model

updating. The number of the OF evaluations was reduced between two and three times. Moreover, when only GA was used in the model updating, 100% of the predefined minimum OF value was reached for both 1B and 2B without the help of pattern search.

Due to the inaccuracies in the joint geometry and stiffness, the equivalent beam-only models were obtained with more difficulties and the model updating procedure was slowed down. Apparently, it was difficult for the optimization algorithm to tweak the dynamic performance of the concept model by rescaling the cross-sections belonging to the joints. In contrast to that, the convergence was positively influenced in the case of the improved models. By adding SE joints to the initial simplified model, its quality was improved considerably as it was made more realistic. Consequently, the time-consuming model updating procedure needed times fewer OF evaluations. Of course, this speed-up comes at the price of the initial effort needed for performing the dynamic reduction. However, considering the time gain achieved, the cost of this single computation is negligible.

Finally it should be noted that, although the model updating for cases 1A and 1B is faster than for 2A and 2B respectively, this may not always be the case if the initial estimations of the thicknesses (fixed in the first two cases) are not good.

Table 5.7: Number of OF calls for the four cases.

Case	Best run, GA only		Best run, hybrid approach	
	OF calls	% of OF	OF calls	% of OF
1A	21008	93%	11744	100%
1B	13600	100%	6119	100%
2A	42420	96%	33021	100%
2B	14000	100%	11240	100%

Figs. 5.7 and 5.8 compare the convergence for cases 1A, 1B and cases 2A, 2B respectively. Apart from the improved performance of 1B and 2B, the advantage of using pattern search after the GA is also clearly visible for all the cases.

Table 5.8 compares the mass and inertia properties for the two best runs of 1B and 2B (hybrid approach) to the reference configuration. The errors are tolerable and respect the limits imposed in Section 5.4.4.

Table 5.8: Reference and optimized models – mass and MOI.

Property	Reference	Case 1B	Error [%]	Case 2B	Error [%]
$Mass[kg]$	19.07	19.62	2.88	19.13	0.31
$I_{XX}[kg*m^2]$	2.43	2.51	3.29	2.46	1.23
$I_{YY}[kg*m^2]$	2.24	2.27	1.34	2.39	6.7
$I_{ZZ}[kg*m^2]$	4.6	4.72	2.61	4.78	3.91

In Fig. 5.9 the MAC between the reference model and the two best runs of 1B and 2B is shown. Table 5.9 gives a comparison of the first nine eigenfrequencies

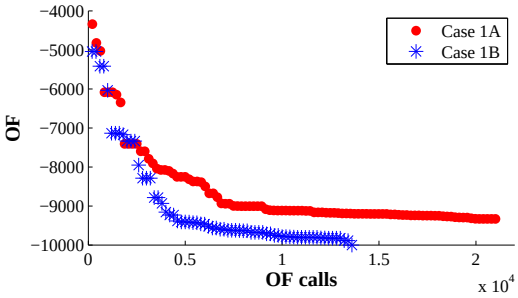

(a) GA only.

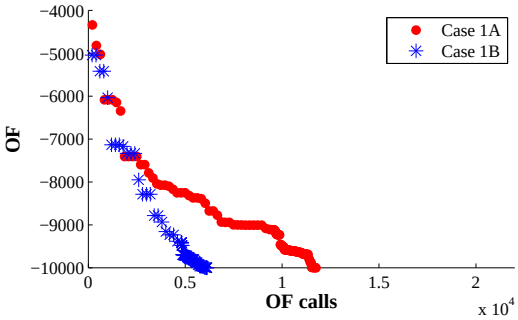

(b) Hybrid approach.

Figure 5.7: Convergence for cases 1A and 1B.

and the corresponding diagonal MAC values in addition. In both 1B and 2B the average error for the eigenfrequencies was within the specified limit of 5% and good correspondence of the mode shapes was obtained – exponential average of 0.75 for the MAC diagonal. Only modes 7 and 8 have lower diagonal MAC values. This can be explained with the more complex mode shapes for the higher modes which are more difficult to reproduce with simplified models (See Appendix A, Section A.1, Figs. A.1 to A.9). For example, in mode 8 only the two rear elongations move, which is hard to describe with the current models. As a countermeasure, the number of beam groups can be increased, but at the cost of more design variables.

In 1B as well as in 2B most of the off-diagonal terms in the MAC matrix are almost negligible. There are just a few terms bigger than 0.1, the biggest one of which 0.17 (1B and 2B). In order to obtain lower off-diagonal terms the number of MAC control groups in the original model and the measurement points in the simplified model can be increased (Fig. 5.6).

The mode shapes for the first and the seventh eigenmode can be seen in Figs. 5.10 and 5.11 respectively. The simplified model corresponds to the results from the fastest run for case 2B (hybrid approach). The undeformed shape is in gray lines and the deformed shape is in color. The correspondence between reference

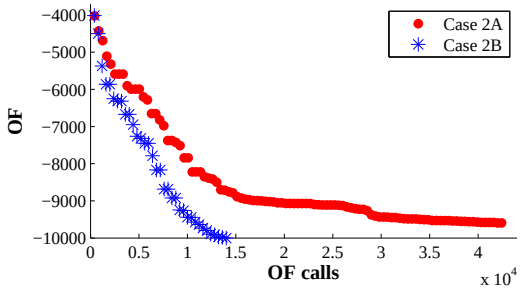

(a) GA only.

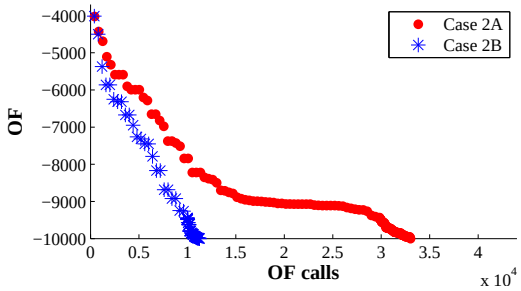

(b) Hybrid approach.

Figure 5.8: Convergence for cases 2A and 2B.

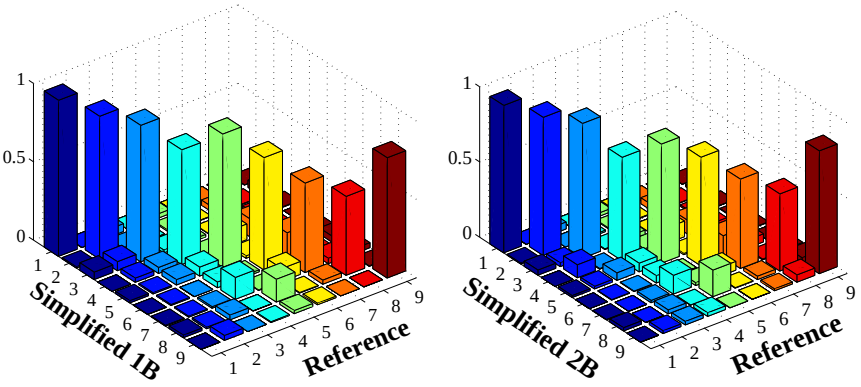

(a) 1B. (b) 2B.

Figure 5.9: MAC for the best cases.

and simplified model is clearly visible in Fig. 5.10, as confirmed by the high MAC value. There is still some similarity between the deformed shapes in Fig. 5.11 in spite of the low MAC value for the seventh mode (0.59). A similar comparison for all modes of the same models is made in the Appendix A, Section A.1 (Figs. A.1

Table 5.9: Reference and optimized models – eigenfrequencies and MAC.

Mode#	Reference [Hz]	Case 1B [Hz]	Error [%]	MAC	Case 2B [Hz]	Error [%]	MAC
1	43.14	44.64	3.48	1.00	45.27	4.94	0.98
2	99.09	104.78	5.74	0.91	104.11	5.07	0.92
3	126.58	132.99	5.06	0.87	126.76	0.14	0.89
4	141.59	138.31	2.32	0.73	133.83	5.48	0.69
5	147.93	154.33	4.33	0.85	153.61	3.84	0.79
6	180.72	171.33	5.20	0.72	171.43	5.14	0.72
7	208.30	219.29	5.28	0.57	205.53	1.33	0.59
8	237.15	226.64	4.43	0.50	231.55	2.36	0.51
9	249.27	257.04	3.12	0.77	250.54	0.51	0.82

to A.9).

(a) Reference model. (b) Simplified model.

Figure 5.10: Mode 1 with MAC=0.98.

(a) Reference model. (b) Simplified model.

Figure 5.11: Mode 7 with MAC=0.59.

5.5 Conclusions

In this chapter the current problems of concept joint modeling have been treated. A critical overview has been made on the state-of-the-art approaches.

As it seems, non-parametric detailed joints offer an excellent compromise between strengths and weaknesses. The existing methods of these group relying mainly on static condensation have been hereby extended with dynamic reduction of all joints into SEs by means of Craig-Bampton CMS. Such an approach is more accurate and more suitable both for statics and dynamics. It can handle joints of arbitrary complexity and is computationally efficient. Moreover, the proposed technique is not only valid for joints, but can be used also for complex parts of the structure which cannot be simplified with 1D beams. The dynamic reduction can be easily integrated into existing concept methods as it was also demonstrated in practice. The proposed technique showed excellent performance on an industrial case study in comparison with the classical joints as junction of 1D beams. The improved simplified model proved to be more realistic and accurate. The presented approach does not claim to resolve completely all problems of joint concept modeling but it is meant to be a useful alternative to the state-of-the-art methods with the least possible disadvantages.

Chapter 6

Advanced sizing optimization

6.1 Introduction

Structural optimization is a crucial part in the automotive virtual prototyping process, which on one side requires considerable efforts and expertise but on the other can bring worthy improvements. The vehicle must be optimized as early as possible in the product development time-line starting from the concept stage [8]. The earlier the design modifications are made, the lower is the related cost. Moreover, the improvement phase must be short enough for an industrial context and possibly a design near the global optimum must be found.

Among the various approaches in the concept phase, the predecessor-based methods for the creation of simplified BIW models are widely popular and applied for the design of the vehicle structure. The resulting small-sized and parametric BJP models are extremely suited for sizing optimization in which the design variables are the cross-section parameters of the 1D beams. Typical goals include decreasing the mass and achieving better vehicle static and dynamic performance.

In general, most of the structural optimization problems can have more than one local optimum and are not convex [162, 164]. Nevertheless, sizing optimization problems are usually considered less difficult to solve compared to topology or shape optimization. The conventional mathematical programming techniques often perform sufficiently well and give satisfactory results. They have become practically a standard in sizing optimization and are without any doubt the most widely applied group of approaches. Although the classical GB approaches can be used for fast optimization, only speed is not sufficient. There are some cases which can represent a more serious obstacle or can even make the classical approaches fail. The sizing optimization of a BJP vehicle body is a typical example – with hundreds or even thousands of design variables and constraints as well as various, sometimes conflicting performance targets [41]. Under such conditions the computational effort to solve the global optimization problem increases enormously ("the curse of dimensionality" [202]). The feasible domain can be severely constrained and discontinuous and it is possible that only small islands of acceptable solutions exist in the search space [44]. Although some preliminary information from similar problems might exist, in simulated-based optimization the nature of the design responses is often a black-box, but most likely they are multimodal, non separable

and non differentiable.

On the other hand, the standardly used GB methods are point-to-point search algorithms which use the derivatives of the OFs and/or constraints to guide the search through the feasible decision space. Their convergence and the final solution depend upon the selection of the initial design to be optimized (the so-called starting point), i.e. they are local-search strategies [44, 164, 165, 175, 176]. In case of inappropriate starting point the algorithm can often get stuck in sub-optimal regions of the decision space [165]. The possibility that it misses the global optimum is high, especially for large-scale problems [164]. Although in practical industrial applications an improved final solution is often sufficient [183], better and/or radically different design alternatives can be overlooked.

Under these circumstances it becomes less certain that GB algorithms are acceptable also for more complex automotive problems. In the context typical for the concept stage, their ubiquitous use and reliability are put into question. Apparently, an improved alternative for sizing optimization is needed. To overcome the biggest disadvantage of the GB methods (getting trapped in local optima), advanced global-search techniques for large-scale structural optimization problems must be identified and/or developed, and validated.

Many authors recommend a multi-start approach for global optimization by launching a local optimizer from a number of randomly selected starting points [44, 164, 165]. The best local minimum point found is then taken as the global minimum. This approach is simple, but not very efficient. It can be difficult or even impossible to estimate the number of local minima and consequently starting points needed. Moreover some sample points can lead to the same local minimum or end with infeasible final solutions.

Stochastic methods can undoubtedly produce creative results and lead to radically different designs. This makes them an appealing alternative to GB algorithms. Heuristic optimization methods such as GA are able to locate near-global solutions. On the other hand, they are inherently much slower than the GB algorithms. Moreover, the absence of the approximation concept leads to less efficient, direct communication FEA-optimizer. Most heuristic algorithms suffer poor scalability and their performance deteriorates significantly with increasing the dimensions of the search space. This explains why so far their use has been limited mainly to small-scale and eventually to medium-scale problems. In fact, EC is becoming increasingly popular in sizing optimization and applications of GA, PSO and SA have been reported [174], but mostly for simple and small-scale problems. A comprehensive study on stochastic global-search strategies for large-scale structural optimization problems has not been made yet.

In [203] an interesting consideration is made on structural optimization complexity. It seems that it is currently impossible to reach the maximum levels of complexity for model, analysis and optimization in the same time, mainly because these limits are being continuously increased. As global heuristic optimization strategies are much more complex than local GB techniques, to employ them means to make compromise with the complexity of the model and/or the analysis.

In this sense, VCM offers a new, unexplored opportunity – to apply heuristic algorithms for structural optimization problems in the concept stage involving

small-sized simplified FE models. It is expected that a similar research can help to improve the quality of the final results significantly. In a wider sense it can be used for identification of reliable large-scale global optimization strategies and for their validation on real-world engineering problems.

The purpose of this chapter is to explore the potential of global-search strategies in the concept stage of vehicle development with regard to sizing optimization of BJP FE models. A new feasible alternative to the classical GB algorithms will be identified, improved if needed, implemented and validated on complex medium- and large-scale engineering problems. In addition to its importance and originality, such a study can undoubtedly claim to be at the cutting edge of both VCM and structural optimization.

This chapter is organized as follows. Section 6.2 deals with the algorithms for advanced sizing optimization. First the performance of two promising heuristic approaches (GA and DE) is compared in Section 6.2.1. As DE outperforms GA in terms of speed of convergence, it is chosen for further development, enhancements and validation. A single-run and a multi-start GB approach are also taken into further consideration. The basics of DE (Section 6.2.2) as well as different strategies for handling of constraints (Section 6.2.3) and multiple objectives (Section 6.2.4) are discussed. The classical local-search GB algorithm, the multi-start GB approach and different DE variants are then tested on two case-studies (Section 6.3 and 6.4) using BJP models.

6.2 Advanced sizing optimization

6.2.1 Choice of optimization algorithm

As stated in [204], there is a clear gap between the theory and practice of structural optimization. In the literature there are few examples of its application on complex real cases [170]. On one side, the classical algorithms are restricted to small changes and may even lead to an infeasible design [172]. On the other, heuristic methods can undoubtedly produce creative results and lead to radically different designs, but require too much computational time [183]. It seems that the mathematical programming methods have reached their limits but the stochastic strategies are far from maturity [174]. In this sense, the challenge posed by sizing optimization in the concept stage is to perform a paradigm change to global-search strategies for large-scale problems.

The right choice of a search strategy becomes crucial. As discussed in Section 2.3.5 this is an uneasy task. Benchmarks with well-known analytical functions can be helpful and can give some guidelines, but in general the conclusions made can be misleading when extrapolated for real-world problems. It must be also taken into account that no algorithm performs equally well for all classes of problems. Thus it is more reasonable to make tests for a certain group of engineering problems, in this case – sizing optimization of BJP models. The main problem is that the maximum number of OF evaluations in simulation-based optimization is limited, even when simplified concept models are analyzed. The situation becomes even worse taking into account the curse of dimensionality and the typical number of

design variables and constraints involved in sizing optimization of the vehicle BIW. As it was clearly impossible to test all major algorithms for the class of problems under consideration, a limited number of strategies had to be identified and then tested, based on an extensive literature review. After a detailed survey on global-search algorithms for large-scale optimization, two candidates were chosen as most promising – GA and DE. Their essentials are explained in Appendix C and Section 6.2.2 respectively.

According to [146] the GA is the most popular algorithmic approach in engineering design optimization. Moreover, GA is claimed to be the most widely used heuristic method in structural optimization [146, 167, 174]. It is traditionally applied for topology and shape optimization, but also some applications in sizing optimization have been reported [205–222]. However, GA is typically employed for small- or at most medium-scale sizing problems. Promising new horizons were open in the original research paper by Will et al. [44], where GA was used for large-scale sizing optimization of a simplified BIW model (approximately 1500 design variables). In this case-study a small population size of 50/100 individuals was set and GA was stopped after a limited number of 100 generations. The idea was to identify as many as possible feasible solutions through GA, to cluster them in "islands" of different design alternatives and to perform fast GB optimization on each of these "islands".

DE has been successfully applied to many engineering optimization problems related to electrical power systems, electromagnetism, propagation and microwave engineering, control systems and robotics, bioinformatics, chemical engineering, pattern recognition and image processing, artificial neural networks (ANNs), signal processing and others [223]. In [146] DE was identified as one of the emergent computing techniques with great potential for application in design optimization. Although it has found extremely limited application for structural optimization problems so far [8, 224], a number of advantages over other heuristic algorithms make DE a prospective candidate to be used in this field. Compared to other stochastic approaches, DE demonstrates better search efficiency and finds global optimal solutions in many cases [198, 223, 225]. In addition DE has only few control parameters to adjust. It is simpler than other evolutionary-based strategies, as well as easy to implement and suitable for parallel applications. In the context of sizing optimization with BJP models of the BIW, DE has an important strength – it shows good scalability [223], i.e. its performance does not tend to deteriorate much when increasing the problem dimensions. Variants of DE have won the front ranks at optimization competitions in multiobjective optimization, EC in dynamic and uncertain environments, but most importantly also in large-scale global optimization (CEC 2008 - third rank) [223]. Its ability to handle problems with high number of design variables is further testified by a number of related research papers [226–232].

A first preliminary assessment was performed to check the ability of GA and DE to handle sizing optimization problems in the vehicle concept stage. In addition to these two global optimization strategies, a multi-start GB approach was also employed. The classical single-run GB approach for local search was used as reference. The objective was to make a choice between GA and DE in view of a

more detailed subsequent study. The single- and multi-start GB strategies were considered in this section and throughout the rest of this chapter because despite their deficiencies GB algorithms are still the most widely used approach to sizing optimization, also at industrial level. A research not including these classical methods will be incomplete. The basics of the GB approach have been discussed in Section 2.3.

A medium-scale practical engineering problem was taken as benchmark. Actually, it corresponds to the model updating problem presented in Section 5.4. A simplified vehicle subframe consisting of 1D beams with STCSs and SE joints (Fig. 5.5(b)) had to be optimized in order to match the dynamic behavior of the reference FE model (Fig. 5.3). As in case 2B defined in Section 5.4, there were 88 design variables corresponding to the widths, heights and thicknesses of the different 1D beam cross-sections. The SE joints were not modified during the updating. No constraints were defined. As in Chapter 5, the matching between detailed and simplified FE model was measured in terms of mass, principal MOI, eigenfrequencies and modeshapes. These similarity criteria were then used to form the OF. It was considered that the equivalent simplified model had been obtained and that convergence had been reached for a value of the OF equal to -10000. For the GB algorithm a solution widely recognized in the automotive field was used – MD Nastran SOL200 [100]. A commercial software solution was employed also for GA – MATLAB®. As the problem at hand was unconstrained, the classical DE [198, 233] was implemented in MATLAB® in its $DE/rand\text{-}to\text{-}best/1$ version (See Section 6.2.2).

First the performance of the classical GB algorithm was checked for this problem. A single run only was performed, as well as 10 runs from randomly initialized starting points. For both approaches the same issue was encountered. If all the nine mode shapes were followed, i.e. "tracked", throughout the optimization process, the run terminated prematurely due to mode tracking failure. The reason is that as the mode shapes vary between one design iteration and the next, some of them might become too different from the tracked physical behavior. In that case the corresponding eigenfrequency is considered as undefined, i.e. there is a discontinuity in this design response and consequently in the OF. As the GB algorithm is unable to handle discontinuities, a mode tracking failure occurs. This problem is often encountered for the higher modes which was also the case of the current study. In the same time, if only the first two mode shapes were tracked, GB converged successfully. Logically, if there was no mode tracking at all but the similarity with the detailed model was searched only in terms of mass, MOI and eigenfrequencies, there was again no error termination. However, tracking no modes or just the first two did not respect the original problem formulation and was not acceptable. A reliable optimization algorithm for NVH problems must be able to follow the relevant eigenmodes of the structure identified in the initial design as they change throughout the design iterations. As stressed in [176, 182], mode tracking is of utmost importance, especially in the automotive field. It is the physical nature of the original mode shape that counts and not merely the mode number. The intent is to control a particular physical mode (e.g. the first global bending mode). The frequency of the physical mode shape is optimized

while the mode number can vary due to the redesign. Despite that its basic idea is quite clear, mode tracking can often encounter difficulties [176, 182] or even fail completely as in the current case. At a first glance, it can be concluded that Nastran SOL200 is not appropriate for tracking higher modes and/or more than 2-3 modes. If one or more of the tracked mode shapes temporarily "disappears" in the current design variant, a failure occurs and the algorithm stops. For this reason the results of GB are not reported hereby.

After that the robustness of DE was checked for this problem within a limited number of 4000 OF evaluations. It was important to choose the right size of the population. It had to be large enough to avoid local optima or stagnation, but small enough so that the computational effort is not increased unreasonably [234]. In general, the recommended population size is between $5 * D$ and $10 * D$ [198, 233, 234], but it must be at least 4 to ensure that DE will have enough mutually different vectors to work with [198, 233, 234]. According to an empirical rule-of-thumb raising the population size above 40 or 50 does not substantially improve the convergence, independent of the number of parameters [225]. Considering that the problem at hand was a medium-scale one with 88 design variables and that applying the rule $10 * D$ would have resulted in unreasonably large population (880 individuals), a population size of 20 individuals was chosen. DE was launched 10 times with different initial states of the random number and with a predefined maximum number of OF calls. The results are shown Fig. 6.1. Excellent search performance and robustness were demonstrated. The target OF value was achieved within only 4000 OF evaluations for 8 out of 10 runs. The other 2 managed to exceed 90% of it and were still converging when the optimization was stopped.

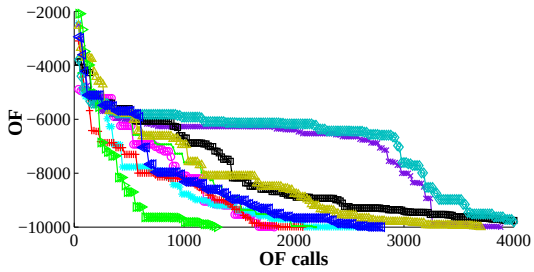

Figure 6.1: DE robustness for population of 20 individuals.

After that the robustness of GA was checked under the same conditions as for DE – for 4000 OF evaluations and for a population of 20 individuals. Similarly, GA was relaunched 10 times. As shown in Fig. 6.2, this seems to be an extremely undersized population for an algorithm like GA and its convergence is deteriorated considerably. In fact, after the first few hundreds of OF calls, stagnation was observed for all 10 cases and not more than 65% of the target OF value was reached. Apparently, when the number of individuals is too low with respect to the design variables, the sample is insufficient and GA performs poorly.

In this regard, an additional check was also made on the performance of GA.

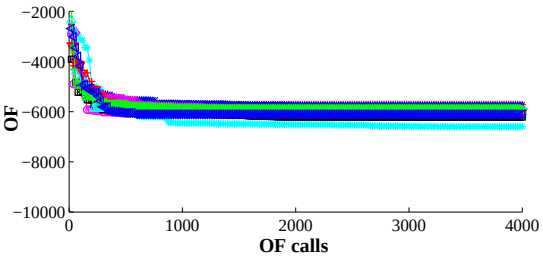

Figure 6.2: GA robustness for population of 20 individuals.

A population of 400 individuals was used, as in the original study from Section 5.4. The number of OF calls was limited to 25000. As in the case of DE, GA was launched 10 times with different initial states of the random number generator. The results are shown in Fig. 6.3. As it can be seen, in all cases but one at least 90% of the target OF value was reached within 25000 OF calls. GA can be thus considered robust enough. Nevertheless, the advantage of DE over GA is clear. The performance of DE resulted times better than GA.

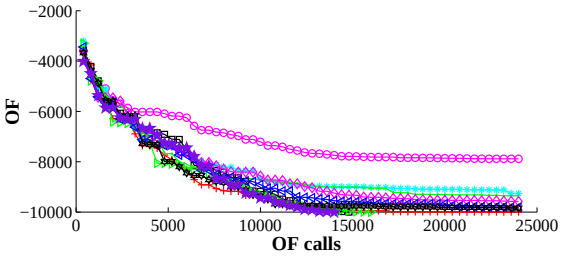

Figure 6.3: GA robustness for population of 400 individuals.

Finally, the results of Figs.6.3 and 6.1 have been summarized in Fig. 6.4 to evidence better the advantage of DE over GA. As after a certain number of generations the convergence of GA was extremely slow, the X-axis was limited up to 15000 OF calls for better visualization. From this figure it is clear that even the worst performing DE run is converging faster than the best GA run. Moreover, the best DE run was around 7 times faster than the best GA run.

In comparison to GA, DE offers scalability and greater simplicity (See Section 6.2.2). It can work well also with a very small population size and is robust. Most importantly, it turned out to be times faster than GA for the real-world sizing optimization problem considered in this section. Considering the attributes of a good optimization algorithm defined in Section 2.3.2 and in view of the results obtained in the current section, DE can be preliminarily assessed as efficient (for a heuristic algorithm), robust, accurate and able to deal with real-world problems. However, it must be also taken into account that in contrast to GA and other

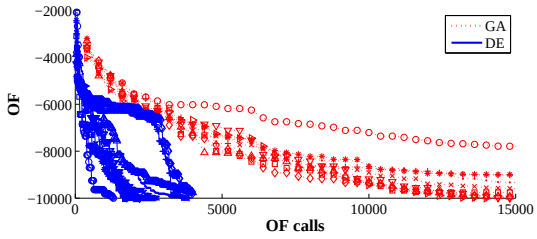

Figure 6.4: GA (population size = 400) versus DE (population size = 20), robustness comparison.

heuristic techniques, DE is immature, not fully validated and still under active development. In its classical version DE is not able to handle multiple constraints and objectives. As with GA, the adjustment of its control parameters is often problem dependent.

Because of its undoubted advantages with respect to GA in solving a sample sizing optimization problem of a BJP model, DE was identified as more promising than GA for further research and development. The aim was to apply it for even more complex tasks such as the optimization of a vehicle subframe and the whole BIW. It was for the first time possible to perform such a study as the inherently slower convergence of DE (compared to the classical methods) was compensated by a faster FEA (small-sized BJP models were used). For this purpose the classical DE (Section 6.2.2) had to be extended with strategies for handling constraints (Section 6.2.3) and multiple objectives (Section 6.2.4). In this way it was possible to consider the general multi-objective constrained optimization problem given in Eq. 2.1.

6.2.2 Differential Evolution

DE is an evolutionary-based direct search algorithm which is relatively new [198]. It comprises the stages of initialization, mutation, crossover and selection, which are briefly summarized hereafter.

In the original DE formulation [198], the problem from Eq. 2.1 is simplified to a single-objective unconstrained problem. In the initialization stage (generation number $G = 0$) a population of NP individuals is generated, each of them being a D-dimensional parameter vector:

$$\mathbf{X}_{i,G} = [x_{i,1,G}, x_{i,2,G}, ..., x_{i,D,G}], i = 1..NP \tag{6.1}$$

where the vector components $x_{i,j,G}$ are generated as a random numbers. The individual $\mathbf{X}_{i,G}$ is also called target vector.

Till a termination criteria is met, the phases of mutation, crossover and selection are repeated. In each next generation $G + 1$, NP mutant vectors $\mathbf{V}_{i,G+1}$ are generated, such that:

$$\mathbf{V}_{i,G+1} = \mathbf{X}_{r_1,G} + F(\mathbf{X}_{r_2,G} - \mathbf{X}_{r_3,G}) \tag{6.2}$$

where r_1,r_2,$r_3 \in \{1..NP\}$ are random integers $\neq i$. The DE control parameter $F \in [0, 2]$ is called differential weight. Another possibility to form the mutant vector is:

$$\mathbf{V}_{i,G+1} = \mathbf{X}_{i,G} + \lambda(\mathbf{X}_{best,G} - \mathbf{X}_{i,G}) + F(\mathbf{X}_{r_2,G} - \mathbf{X}_{r_3,G}) \tag{6.3}$$

As it can be seen from Eq. 6.3 the mutation vector $\mathbf{V}_{i,G+1}$ is created using two randomly selected population members $\mathbf{X}_{r_2,G}$ and $\mathbf{X}_{r_3,G}$, as well as the vector $\mathbf{X}_{best,G}$ which results in the best OF value in the current generation. λ is another control parameter of DE in the range $[0, 2]$, which is usually set $\lambda = F$.

In each generation a set of NP D-dimensional trial vectors $\mathbf{U}_{i,G+1}$ is generated. Their components are derived according to the crossover rule:

$$u_{i,j,G+1} = \begin{cases} v_{i,j,G+1} & if\ (rand_{i,j} \leq CR)\ \vee\ (j = I_{rand}) \\ x_{i,j,G} & otherwise \end{cases} \tag{6.4}$$

where the random number $rand_{i,j} \in [0, 1]$ and the random integer number $I_{rand} \in \{1..D\}$. The additional condition $j = I_{rand}$ ensures that at least one parameter of the mutant vector will be taken over in the trial vector. The DE control parameter $CR \in [0, 1]$ is called crossover probability.

Finally, a comparison is made between all corresponding pairs of target and trial vectors based on their OF. The selection rule is:

$$\mathbf{X}_{i,G+1} = \begin{cases} \mathbf{U}_{i,G+1} & if\ better \\ \mathbf{X}_{i,G} & otherwise \end{cases} \tag{6.5}$$

The vector $\mathbf{U}_{i,G+1}$ is better when:

$$OF(\mathbf{U}_{i,G+1}) \leq OF(\mathbf{X}_{i,G}) \tag{6.6}$$

Different variants of DE exist and they are usually notated according to the convention $DE/x/y/z$, where x specifies the choice of the vector to be perturbed during mutation, y is the number of weighted difference vectors used during this perturbation, and z is the type of crossover. Thus the above description of DE corresponds to the classical $DE/rand/1$ scheme if Eq. 6.2 is used and to $DE/rand\text{-}to\text{-}best/1$ if Eq. 6.3 is used. Throughout this study a $DE/rand\text{-}to\text{-}best/1$ scheme was preferred as it balances robustness and fast convergence [225], which makes it appropriate for engineering problems.

Many researchers have studied the influence of the control parameters (NP, F and CR) on the performance of DE and have tried to determine their most appropriate values or at least give some rules of thumb [198, 225, 233, 234]. Attempts have been also made to create variants of DE with adaptive behavioral parameters in order to avoid manual tweaking and to achieve better performance [235, 236]. Some authors even propose meta-optimization, i.e. optimization of the control parameters before starting DE [237, 238].

In this work fixed values have been used. Their values were determined in result of quick manual adjustment. For this purpose several trials with different

values were performed on the problem from Section 6.3 for a small number of OF evaluations. The ones which resulted in the fastest convergence were chosen. Manual adjustment was preferred instead of other approaches for several reasons. As discussed in [237], adaptation of the behavioral parameters does not bring much advantages with respect to keeping their values to the ones recommended in the literature [225, 234, 237]. On the other hand, performing meta-optimization as proposed by [237] would have resulted in unacceptably high time already in this preliminary tweaking phase.

6.2.3 Constraint handling

The classical DE [198] can deal only with unconstrained optimization problems. In contrast to that the majority of engineering problems need to satisfy some boundary, equality and inequality constraints. Thus they must be considered so that DE can be used in the vehicle concept stage. On the other hand, finding an efficient and robust constraint handling strategy is not so simple task. In fact, [174] identify the development of such methods as one of the future research directions regarding evolutionary design. An extensive state-of-the-art survey is given in [171]. Different strategies regarding DE in particular can be found in [225] and [234].

Boundary constraints are the easiest to satisfy. If they are violated by the trial vector after crossover, a simple bounce-back approach is often used [225]. It has been adopted in this study too (Eq. 6.7):

$$u_{i,j,G+1} = \begin{cases} x_j^{(LB)} + rand_j * (x_{base\_i,j,G} - x_j^{(LB)}) & if\ u_{i,j,G+1} < x_j^{LB} \\ x_j^{(UB)} + rand_j * (x_{base\_i,j,G} - x_j^{(UB)}) & if\ u_{i,j,G+1} > x_j^{UB} \\ u_{i,j,G+1} & otherwise \end{cases} \tag{6.7}$$

where $rand_j$ is a random number in the interval $[0, 1]$ and $\mathbf{X}_{base\_i,G}$ is the vector to which the random vector differential is added during mutation, i.e. $\mathbf{X}_{r_1,G}$ (Eq. 6.2) or $\mathbf{X}_{i,G}$ (Eq. 6.3).

On their turn, equality constraints are usually transformed to the more general inequality constraints [225]. Some representative techniques for handling inequality constraints are explained hereafter together with the corresponding modifications in the DE algorithm.

Penalty functions

Undoubtedly, the penalty function approach is the most commonly used in EC [171, 174]. There are different variations of the method but the basic idea is to eliminate the inequality constraints g_l from Eq. 2.1 and transform the OF so that it is penalized when one or more of them is violated. Thus Eq. 6.5 is still used for

selection but Eq. 6.6 is replaced with Eq. 6.8:

$$OF(\mathbf{U}_{i,G+1}) + \sum_{l=1}^{M} p_l * max(g_l(\mathbf{U}_{i,G+1}), 0)^{\beta} \leq$$
$$OF(\mathbf{X}_{i,G}) + \sum_{l=1}^{M} p_l * max(g_l(\mathbf{X}_{i,G}), 0)^{\beta} \tag{6.8}$$

where p_l are positive constants called penalty factors, and β is normally 1 or 2. Various authors show that the method has some difficulties, especially for highly constrained optimization problems [174]. The OF is evaluated also for infeasible designs, which is not very efficient if FEA is involved. Moreover, setting the right values for p_l can be laborious as both under- and over-penalization must be avoided.

Modified selection rule

Two direct constraint handling strategies are considered. In both of them the selection rule from Eq. 6.5 is modified so that Eq. 6.6 is replaced by Eq. 6.9 [225]:

$$\begin{aligned}((\forall l \in \{1..M\} : g_l(\mathbf{U}_{i,G+1}) \leq 0 \wedge g_l(\mathbf{X}_{i,G}) \leq 0) \wedge (\text{Compare feasible})) \vee \\ ((\forall l \in \{1..M\} : g_l(\mathbf{U}_{i,G+1}) \leq 0) \wedge (\exists l \in \{1..M\} : g_l(\mathbf{X}_{i,G}) > 0)) \vee \\ ((\exists l \in \{1..M\} : g_l(\mathbf{U}_{i,G+1}) > 0) \wedge (\text{Compare infeasible}))\end{aligned} \tag{6.9}$$

The logical expression for comparing feasible individuals is true when Eq. 6.6 holds. The two strategies differ in the logical expression for comparing infeasible individuals. For the first approach it is true when Eq. 6.10 is valid, and with the second one – when Eq. 6.11 holds. The first method was proposed by Lampinen [225]. As for the second strategy, it was initially developed for GA by Deb [239], but here it has been adapted for DE by integrating it in Eq. 6.9.

$$\forall l \in \{1..M\} : max(g_l(\mathbf{U}_{i,G+1}), 0) \leq max(g_l(\mathbf{X}_{i,G}), 0) \tag{6.10}$$

$$\sum_{l=1}^{M} max(g_l(\mathbf{U}_{i,G+1}), 0) \leq \sum_{l=1}^{M} max(g_l(\mathbf{X}_{i,G}), 0) \tag{6.11}$$

For both approaches if the compared individuals are feasible they are evaluated on the basis of their OF. In addition a feasible individual is preferred than an infeasible one. Finally, if both are infeasible they are compared based on the individual values of all violated constraints – Eq. 6.10 [225], or on their sum – Eq. 6.11 [239]. The advantage of using these direct constraint handling techniques is evident – no OF evaluations are made for infeasible designs in contrast to Eq. 6.8.

6.2.4 Multiple objectives

Engineering problems with more than one OF are quite common. Two different multi-objective approaches to be integrated in the classical DE were chosen.

Weighted sum approach

A simple to implement and widely used approach is to compute the weighted sum of all objectives and thus transform them into a single one. To combine this technique with the previously defined constraint handling strategies, the OF in Eqs. 6.6, 6.8 and 6.9 is substituted with OF' such that:

$$OF' = \sum_{k=1}^{K} w_k * OF_k \tag{6.12}$$

where the sum of all weights w_k is usually equal to 1.

No special modification of the DE algorithm is needed. On the other hand, it is difficult to define the right weights without having prior information about the problem and the relative importance of the OFs. In addition, if the Pareto front is non-convex, some solutions might not be accessible with this technique.

Pareto-based optimality

This second approach was proposed specifically for DE in [225]. It works similarly to Lampinen's dominance-based criterion for constrained optimization (Eq. 6.10) that pressures the individuals toward feasible regions.

To integrate the technique in the direct constraint handling strategies from Section 6.2.3 the logical expression for comparing feasible individuals (Eq. 6.9) is determined by the validity of Eq. 6.13 [225] instead of Eq. 6.6:

$$\forall k \in \{1..K\} : OF_k(\mathbf{U}_{i,G+1}) \leq OF_k(\mathbf{X}_{i,G}) \tag{6.13}$$

To combine this approach with the penalty-based constraint handling, again Eq. 6.13 is used, but OF_1 is penalized according to Eq. 6.8.

By using the proposed Pareto-dominance-based selection rule, the population can be driven towards the Pareto front. To obtain its approximation all dominated individuals in the last generation are removed. However it is not guaranteed that this approximation will be close enough to the true Pareto front. In addition, the found non-dominated individuals might not be enough and might not cover the entire Pareto front.

6.3 Case study 1 – simplified vehicle frame

6.3.1 FE model

In this case study the concept FE model of a vehicle frame (Fig. 6.5, detailed 1D element display) was subject to sizing optimization. The model had 62 nodes (52 elements). 1D beam elements with rectangular (Fig. 6.6(a)) and C-type (Fig. 6.6(b)) STCSs were used to represent the reference structure. The FE model was small-sized and most importantly – parametric. For each cross-section the width (w), height (h) and the plate thicknesses of each two opposite sides (t_1, t_2) were changed, resulting thus in 4 design variables (Figs. 6.6(a) and 6.6(b)).

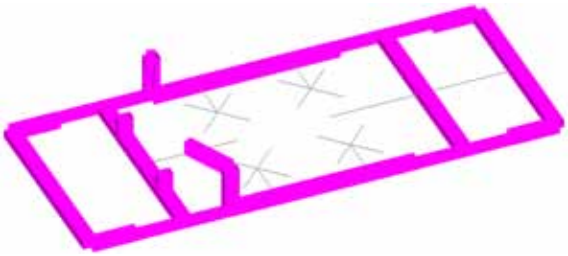

Figure 6.5: Simplified frame.

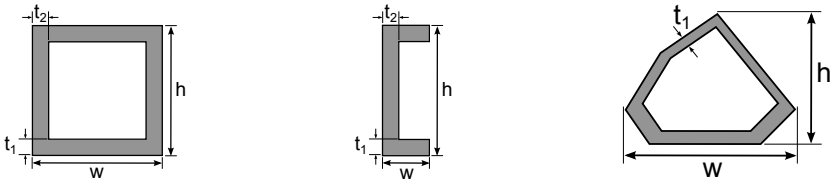

(a) Box STCS. (b) C-shape STCS. (c) ABCS.

Figure 6.6: STCS and ABCS sizing parameters.

6.3.2 Problem definition

As there were 21 different STCSs, the design variables were 84 ($D = 84$), which can be considered a medium-scale problem for the vehicle concept stage [41]. On the other hand such a number can become a challenge for many stochastic algorithms as the search space increases enormously.

Lower and upper bounds were defined for each of the design variables x_j such that $x_j \in [0.1 * x_{j\_nom}, 30 * x_{j\_nom}]$, where x_{j_nom} is the nominal value of the design variable as defined in the reference FE model. From an engineering point of view this design variable range was quite large, so additional geometry constraints had to be imposed ($M = 87$). The maximum allowable ratios between the parameters of each cross-section were considered, as well as the smoothness, i.e. the avoidance of abrupt changes in the parameters of two adjacent cross-sections. It must be noted that the reference FE model did not satisfy them, i.e. it was an infeasible design.

For this problem 10 OFs had to be simultaneously satisfied ($K = 10$). The mass m had to be minimized while maximizing the static and dynamic stiffness. The 10 structural responses R_k needed to compute the OFs are given in Table 6.1 with their reference (R_{k_ref}) and target (R_{k_tgt}) values. The relation column gives the desired change with respect to R_{k_ref}. As mentioned in [240] such a multi-objective optimization problem can be easily reformulated to a constrained one. However, in this study all analysis-based responses were considered as soft objectives and their transformation to constraints was consciously avoided in order

to minimize the time needed for optimization.

Table 6.1: Simplified frame – structural responses.

k	*Response*	R_{k_ref}	*Relation*	R_{k_tgt}	*Description*
1	m [kg]	65.11	$\leq$	38	structural mass
2	K_{b1} [N/m]	9.19E4	$\geq$	1.5E5	vert. bending stiffness, LC_1
3	K_{b2} [N/m]	5.19E5	$\geq$	7.5E5	vert. bending stiffness, LC_1
4	K_{b3} [N/m]	1.15E5	$\geq$	1.5E5	vert. bending stiffness, LC_2
5	K_{b4} [N/m]	5.88E4	$\geq$	8E4	vert. bending stiffness, LC_2
6	K_{b5} [N/m]	1.60E6	$\geq$	2E6	lat. bending stiffness, LC_3
7	K_{t1} [Nm/rad]	5.29E4	$\geq$	8.59E4	torsional stiffness, LC_4
8	K_{t2} [Nm/rad]	5.32E4	$\geq$	8.59E4	torsional stiffness, LC_5
9	$f_{1^{st}t}$ [Hz]	11.28	$\geq$	15	1^{st} torsional mode
10	$f_{1^{st}b}$ [Hz]	13.76	$\geq$	20	1^{st} bending mode

To evaluate the global static bending and torsional performance of the frame, five load cases (LC_1 to LC_5) were defined according to the static test benches most often used in the industry [18]. They are represented schematically in Figs. 6.7 to 6.11 (simple 1D element display), in which the constraints are marked with blue triangles, the forces – with red arrows, and the measurement nodes – with yellow circles. The general formula to compute the static bending stiffness is given in Eq. 6.14, where F is the applied load and t_{Ai} is the displacement of the measurement node A_i in vertical (Figs. 6.7, 6.8) or lateral direction (Fig. 6.9).

$$K_{bi} = F/|t_{Ai}|, i = 1..5 \tag{6.14}$$

The general formula to calculate the static torsional stiffness is given in Eq. 6.15, where t_{Bi} and t_{Ci} are the vertical displacements of the measurement nodes B_i and C_i, and D_i is the distance between the nodes in which the two opposite forces F are applied.

$$K_{ti} = \frac{FD_i}{\arctan\left(|t_{Bi} - t_{Ci}|/D_i\right)}, i = 1..2 \tag{6.15}$$

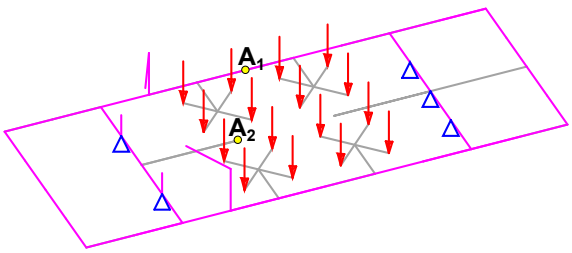

Figure 6.7: $\mathbf{LC_1}$: $\mathbf{K_{b1}}$ and $\mathbf{K_{b2}}$.

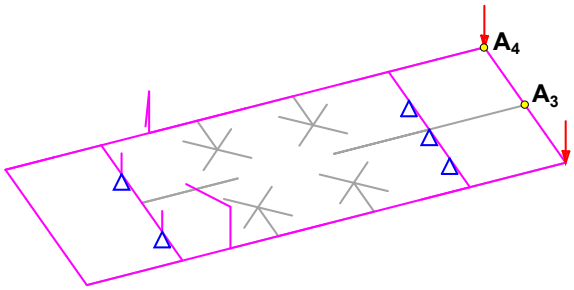

Figure 6.8: LC_2: K_{b3} and K_{b4}.

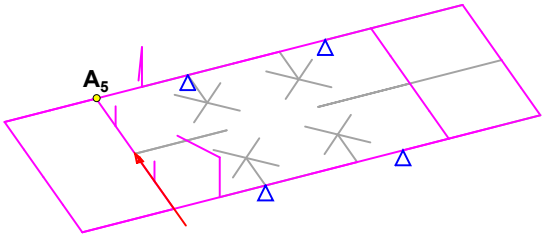

Figure 6.9: LC_3: K_{b5}.

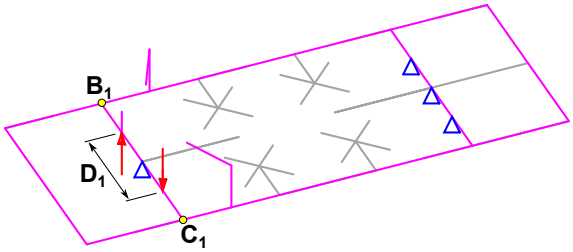

Figure 6.10: LC_4: K_{t1}.

For the evaluation of the global dynamic performance modal analysis was performed under free-free conditions. The first 4 modes were considered (excluding the 6 rigid body modes). The mode shapes of the first torsional and bending modes are shown in Figs. 6.12 and 6.13. The eigenfrequencies $f_{1^{st}t}$ and $f_{1^{st}b}$ of these global modes had to be increased while in the same time tracking the corresponding reference mode shapes. This second task was important because mode switching can occur between two iterations due to structural modifications. As stressed by [176], the mode tracking algorithms in dynamic cases must be considered with special attention. The inappropriate algorithm choice may lead

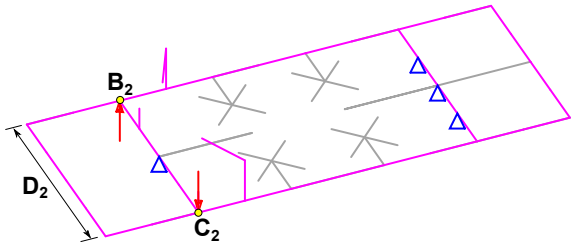

Figure 6.11: LC_5: K_{t2}.

to suboptimal solutions or mode tracking failures and premature stopping of the optimization process.

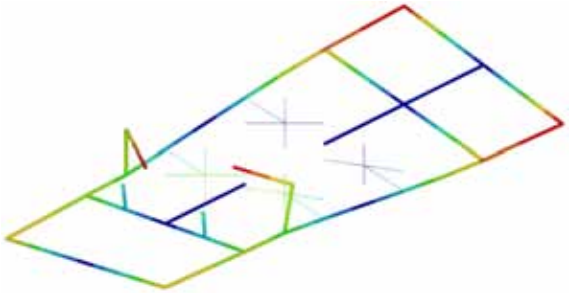

Figure 6.12: Simplified frame, 1st torsional mode at 11.28 Hz.

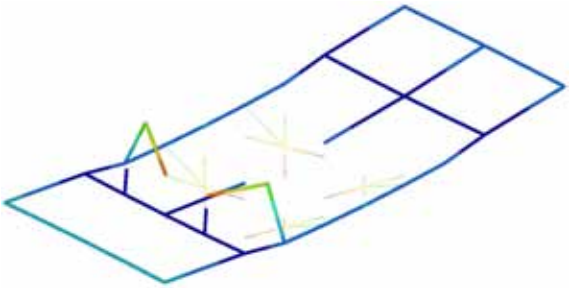

Figure 6.13: Simplified frame, 1st bending mode at 13.76 Hz.

In this work the used GB approach was implemented in commercial software. There was only one possible mode tracking strategy based on cross-orthogonality check with updating of the reference mode shapes at each design cycle [100]. In this approach the cross-orthogonality check is performed between the current design

cycle i and the previous one $i-1$ in accordance with Eq. 6.16.

$$t_i = \Phi_i'^T M_i \Phi'_{i-1} \tag{6.16}$$

where Φ' denotes the mass-normalized eigenvectors. In case of unchanged mode-shapes and mass of the system, t_i is a diagonal matrix. In the process of optimization, it is more likely that the mode shapes of the current design cycle change as a result of stiffness and/or mass variation, and their correlation is less than 1.0. It can also happen that the mode numbers change. In that case dominant off-diagonal terms are found in t_i. If the values of these terms are above a certain predefined threshold and sufficient correlation exists, mode switching has occurred and the modes which have switched can be identified. This mode tracking strategy has the advantage of favoring the changes in the structural behavior due to redesign, as such changes are natural and expected during optimization. On the other hand, in some cases it could turn out misleading and can have adverse effects. If, for example, there are many design cycles and/or the similarity threshold is relatively low, some of the mode shapes can change too much and the final results can be too far or even not similar at all to the actual physical modes that had to be tracked. Moreover, in certain situations this strategy tends to favor the temporary "disappearance" of some mode shapes in the current design, which on its turn causes the GB method to fail as it cannot handle discontinuities.

As an alternative, an improved strategy based on the MAC was combined with DE, close to the one reported in [241]. The MAC measured the similarity between the i^{th} mode shape of the design resulting from the current optimization iteration ϕ_i^{opt} and the j^{th} mode shape of the reference model ϕ_j^{ref} according to Eq. 4.10. No updating was made of the reference mode shapes throughout the optimization, despite that this approach allowed it and could have been easily adapted. Such a mode tracking strategy was considered more correct in terms of mode shapes of the optimal solution. The N_m mode shapes ϕ_i^{opt} obtained at the current design iteration were compared with each of the reference eigenvectors. The mode tracking consisted in finding the objective eigenvector ϕ_i^{obj} for each of the reference ones ϕ_j^{ref} satisfying:

$$\phi_i^{obj} = \phi_i^{opt} \text{ such that } \underset{i=1..N_{\mathbf{m}}}{max} \left[MAC\left(\phi_i^{opt}, \phi_j^{ref}\right)\right] \tag{6.17}$$

Actually, among all eigenvectors ϕ_i^{opt}, the one with the MAC value closest to 1.0 with respect to the reference eigenvector ϕ_j^{ref} determines (i.e. tracks) the followed physical mode shape in the current configuration. Normally a lower bound is set for the MAC value of ϕ_i^{obj}. If it is under this correlation threshold, then the tracked mode shape is missing in the current design and its eigenfrequency is not defined. As such cases are undesirable, the OF is penalized with a high cost.

Finally, the 10 OFs were defined as follows:

$$OF_k = max(\alpha_k(R_{k\_tgt} - R_{k\_act})/(R_{k\_tgt}), 0), k = 1..10 \tag{6.18}$$

In Eq. 6.18 R_{k_tgt} is the target value of each response as defined in Table 6.1, and R_{k_act} is its actual value after the current OF call. Additionally, $\alpha_1 = -1$, and $\alpha_k = 1$ for $k \in \{2..10\}$, so that all OFs had to be minimized.

6.3.3 Optimization algorithms

Based on the simple frame model, a comparison was made between a classical GB algorithm and DE. All computations were made on a desktop PC with the following technical characteristics: CPU Intel Core i5 760@2.8 GHz, 6 GB RAM, OS Windows 7 Pro X64.

Both single-run and multi-start GB strategies were tested. In the first case the reference configuration was analyzed (GB_{ref}). For the multi-start approach the GB algorithm was launched from 50 randomly generated starting points (GB_{rnd}). The used mathematical programming technique was implemented in a commercial software and was based on MMFD. As for the approximation, mixed method was used and, based on the response type, direct, reciprocal or convex linearization was applied.

Six different DE variants DE_1 to DE_6 (Table 6.2) were tested based on the combinations between the strategies for handling constraints (CNSTR) and multiple objectives (MULTIOBJ) (Sections 6.2.3 and 6.2.4). A *DE/rand-to-best/1* scheme (Section 6.2.2) was used. A maximum number of 50000 OF calls was set with additional stopping condition in case of no considerable OF improvement over 50 generations.

Special attention was put on the proper choice of the DE settings which were the same for the six compared DE variants. The DE control parameters were manually adjusted considering the general recommendations given in [198, 225, 234, 237]. In the literature NP between five to ten times the number of the design variables is given as a reasonable choice [198, 233]. Moreover, it must not be lower than four (so that enough mutually different vectors exist) [198]. According to an empirical rule NP should not be higher than 40 or 50 independent of the number of design variables, as raising it above these values does not improve the convergence [225]. Inline with the above and taking into account the problem dimensions, $NP = 40$ was chosen as a population size big enough to provide sufficient exploration of the design space and to avoid stagnation. As for the differential weight, F is often chosen $\in [0.5, 1]$. Values outside this interval are only occasionally effective [198, 233]. It must be also noted that small values of F could lead to premature convergence, while high ones could slow down the search process [234]. Hence a value of $F = 0.8$ was chosen and used in the current study. Finally, a good first choice for the crossover probability CR is said to be a value considerably lower than one (e.g. 0.1 or 0.3) [198, 233]. However, a high CR (e.g. 0.9 or 1.0) speeds up the search in case of convergence issues [198, 233] and can thus prove to be helpful, e.g. for real-world engineering problems. Based on these recommendations and after a quick manual adjustment phase, $CR = 0.9$ was selected as the most appropriate value. Thus $NP = 40$, $F = 0.8$ and $CR = 0.9$ were used as DE control parameters throughout the rest of this chapter. As seen later on (Subsections 6.3.4 and 6.4.4), these settings together with the

DE/rand-to-best/1 scheme proved to be appropriate for handling the two complex case studies at hand. Although it is true that the best values of the control variables are problem dependent, the ones used in this study can be recommended at least as a first initial guess for similar structural optimization cases from the automotive industry.

Table 6.2: DE variants.

MULTIOBJ / CNSTR	Weighted sum	Pareto-based
Penalty	DE_1	DE_2
Lampinen	DE_3	DE_4
Deb	DE_5	DE_6

6.3.4 Results

The results for GB_{ref} and for the best run of GB_{rnd} are given in Table 6.3. Both final designs are feasible and satisfy the imposed target values for all responses but the mass. With GB_{ref} it decreases to 54.85 kg. With GB_{rnd} a significantly better final solution is found of just 42.64 kg. It remains hidden for GB_{ref} as it is trapped in a local minimum.

A multi-start approach can turn out more successful, as in this case, but it is difficult to decide how many random starting points to be used. The more they are, the bigger are the chances to find a better solution, but even then there is no guarantee that it will not be missed. Indeed, for the frame case study only 7 out of all 50 runs terminate successfully due to convergence. They are feasible and all response targets are reached but the mass which varies between 42.64 kg (best run) and 63.78 kg (worst run). For this reason the cycles and timings for GB_{rnd} are given for all 50 runs. Not only is the variability of the mass too big, but the remaining 43 runs fail due to wrongly tracked mode shapes of interest. This faulty behavior is on one hand due to the inability of the GB algorithm to handle discontinuities. On the other hand it can be explained with the tracking mechanism which relies on the updating of the reference mode shapes. In contrast to that, there are no mode tracking failures with DE_1 to DE_6, which confirms the appropriateness of the used tracking strategy (Section 6.3.2).

The results for the different strategies DE_1 to DE_6 are reported in Table 6.4. The optimization history of all design responses is given in the Appendix A, Section A.2 (Figs. A.10 to A.15). Where applicable (DE_1, DE_3 and DE_5) also the history of OF' (as defined in Eq. 6.12) is shown. Similarly to the results obtained with GB_{ref} and GB_{rnd}, the target which is the most difficult one to reach is the mass. All the other target thresholds are satisfied. As expected, all DE variants are much slower than GB_{ref} and GB_{rnd}. A hybrid DE-GB strategy seemed a logical choice to combine the advantages of both. However, despite the popularity of the hybrid global-local approaches for structural optimization [44, 170, 175], in this case they were completely unsuccessful. Similarly to the multi-start GB approach,

Table 6.3: Results GB.

Result	GB_{ref}	GB_{rnd}
m [kg]	54.85	42.64
K_{b1} [N/m]	2.23E5	2.29E5
K_{b2} [N/m]	7.48E5	7.51E5
K_{b3} [N/m]	1.68E5	1.50E5
K_{b4} [N/m]	8.63E4	8.31E4
K_{b5} [N/m]	2.00E6	2.01E6
K_{t1} [Nm/rad]	8.59E4	8.59E4
K_{t2} [Nm/rad]	8.65E4	8.65E4
$f_{1^{st}t}$ [Hz]	16.03	18.37
$MAC_{1^{st}t}$	0.8267	0.7243
$f_{1^{st}b}$ [Hz]	22.31	26.36
$MAC_{1^{st}b}$	0.8308	0.6720
Feasible	Yes	Yes
Cycles	19	1783
Time [s]	206	16260

the GB solver suffered repetitive mode tracking failures when started from the final solution obtained with DE. It must be also noted, that although DE_2, DE_4 and DE_6 use selection based on Pareto-dominance (Section 6.2.4), they all end with a single non-dominated final solution.

Table 6.4: Results DE.

Result	DE_1	DE_2	DE_3	DE_4	DE_5	DE_6
m [kg]	46.97	52.46	41.72	55.68	51.00	72.44
K_{b1} [N/m]	2.26E5	2.07E5	1.94E5	3.02E5	1.90E5	3.21E5
K_{b2} [N/m]	7.72E5	7.53E5	7.50E5	8.45E5	8.08E5	8.07E5
K_{b3} [N/m]	1.55E5	1.52E5	1.50E5	1.52E5	1.55E5	1.90E5
K_{b4} [N/m]	8.52E4	8.47E4	8.56E4	8.21E4	8.79E4	9.13E4
K_{b5} [N/m]	2.00E6	2.03E6	2.00E6	2.01E6	2.00E6	2.11E6
K_{t1} [Nm/rad]	8.59E4	8.77E4	8.59E4	8.59E4	8.71E4	9.45E4
K_{t2} [Nm/rad]	8.65E4	8.77E4	8.65E4	8.65E4	8.77E4	9.51E4
$f_{1^{st}t}$ [Hz]	17.22	16.89	18.73	15.95	16.97	15.02
$MAC_{1^{st}t}$	0.8762	0.7948	0.8110	0.7797	0.8320	0.6376
$f_{1^{st}b}$ [Hz]	23.23	28.52	25.23	20.76	20.38	21.46
$MAC_{1^{st}b}$	0.6144	0.6531	0.6009	0.6091	0.6036	0.7394
Feasible	No	No	Yes	Yes	Yes	Yes
OF calls	32600	50000	31022	14983	26418	8003
Time [s]	165486	252023	156924	76098	133794	40835

Because of the use of penalties neither DE_1, nor DE_2 lead to a feasible final

solution. In fact, the sum of all violated constraints was minimized considerably throughout the optimization and was negligibly small for the final configuration, but still greater than 0. Such infeasible solutions are directly excluded from further consideration because the satisfaction of all geometry constraints is an important engineering prerequisite which can rarely be relaxed. Moreover, DE_1 and DE_2 required the highest number of OF calls.

The OF calls for DE_4 and DE_6 are much lower than for their counterparts based on a weighted-sum strategy for handling the objectives (DE_3 and DE_5), but they converged prematurely, resulting in end designs with relatively high mass. This behavior can be explained with the low NP – i.e. 40, with respect to the recommended value of $10 * D$ [198], i.e. 840. On the other hand, setting NP to 840 was not feasible from a practical point of view. Finally, DE_5 also converged prematurely, which can be explained with the poor population diversity after a certain number of OF calls, reported also by [239] for GA applications.

Based on the feasibility criteria and the fulfillment of the response targets, the strategy identified undoubtedly as the best performing one is DE_3. The end configuration has mass of only 41.72 kg which is lower even than the best GB_{rnd} run. On the other hand, the time needed for GB_{rnd} (all 50 runs) is 16260 s, while DE_3 finishes in 156924 s. However, not only the speed, but also the quality of the end results must be considered, when comparing both. As demonstrated, with GB_{rnd} finding the global optimum is by far not guaranteed. In contrast to that, even if slower, DE_3 approaches it and in the same time provides more information. During the optimization process 6534 feasible design alternatives are found with mass ranging from 398.42 to 41.72 kg. Moreover, there are 5861 feasible configurations with mass under the reference value of 65.11 kg. A summary of their response values with respect to the target levels is given in Fig. 6.14(a). Fig. 6.14(b) shows the generated alternative designs with mass ranging from 41.72 to 42.72 kg. Even in this small range, the number of different configurations is considerable. In both figures the quantities for all axes are the relative percentage differences Δ between actual and reference values (R_{k_act} and R_{k_ref}) – respectively for K_{bi} and K_{ti} (X-axis), $f_{1\mathbf{st}b}$ and $f_{1\mathbf{st}t}$ (Y-axis) and m (Z-axis). The final optimum is marked with a big black asterisk symbol. Actually, ΔK_{bi} was calculated as the average of the relative differences for all five bending stiffnesses (i.e. $i = 1..5$), whereas ΔK_{ti} was taken as the average of the relative differences for the two torsional stiffnesses (i.e. $i = 1..2$).

Finally, it can be concluded that the strategy to handle constraints and multiple objectives influences a lot the performance of DE and the choice of the right one is decisive. A similar study has never been performed on real engineering problems in the field of sizing optimization. Such a comparison can be extremely useful to push forward the use of global-search strategies like DE by identifying the best performing approach for a certain class of problems. For the sizing optimization of automotive structures this turned out to be DE_3 which employed a weighted sum for the OFs together with a selection rule modified according to Lampinen for direct handling of all constraints.

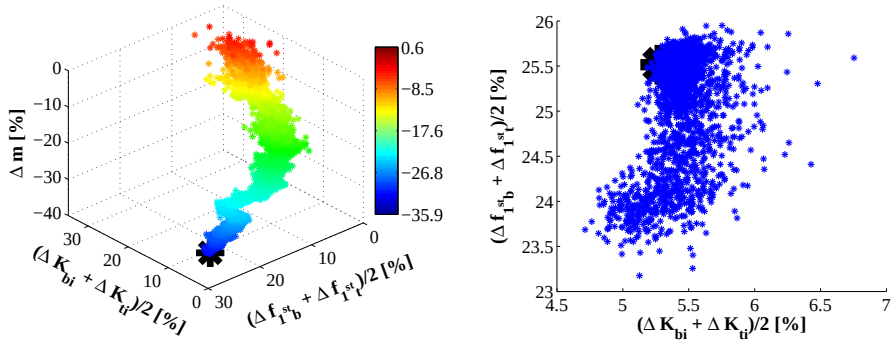

(a) 3D view.

(b) Zoomed 2D view.

Figure 6.14: DE$_3$ feasible solutions.

6.4 Case study 2 – simplified vehicle body

6.4.1 FE model

In this case study the concept FE model of the BMW 3 series BIW (Fig. 3.28, detailed 1D element display) was subject to sizing optimization. The model was described in Section 3.4.2, where also its quality was checked. 1D beam elements with ABCSs were used to represent the reference structure (Fig. 6.6(c)). As in Section 6.3, the resulting FE model was small-sized and parametric. In the same time the ABCSs gave a precise description of the real geometry compared to STCSs [41]. Each ABCS was rescaled by changing the width (w) and height (h) of the rectangular bounding box around it. In addition, the plate thicknesses t_i of each ABCS segment were varied. Thus there was a minimum of 3 design variables per ABCS (Fig. 6.6(c)).

6.4.2 Problem definition

There were 1154 design variables in total corresponding to the 319 different ABCSs. The design variable range was narrowed to a more realistic one compared to Section 6.3, i.e. $x_j \in [0.5 * x_{j\_nom}, 1.5 * x_{j\_nom}]$. In addition, there were 1346 geometry constraints related to the allowable ratios of the cross-section parameters. This problem can be classified as highly constrained large-scale sizing optimization typical for the vehicle concept stage. It was expected to pose a greater challenge both for GB and DE.

Two similar optimization problems with increasing difficulty were defined. For problem I four OFs had to be simultaneously satisfied ($K = 4$). The mass m had to be minimized while maximizing the static bending and torsional stiffness, K_b and K_t, as well as the eigenfrequency of the first bending mode $f_{1\mathbf{st}_b}$. For problem II the eigenfrequency of the first torsional mode $f_{1\mathbf{st}_t}$ had to be increased too ($K = 5$). In addition, the target thresholds for both eigenfrequencies were increased. All structural responses needed for the computation of the OFs are

given in Table 6.5 with their reference values R_{k_ref}. The two sets of target values R_{k_tgtI} and R_{k_tgtII} correspond to optimization problem I and II respectively.

Table 6.5: Concept BIW – structural responses.

k	Response	R_{k_ref}	Relation	R_{k_tgtI}	R_{k_tgtII}	Description
1	m [kg]	362.20	$\leq$	250.00	250.00	structural mass
2	K_b [N/m]	1.80E7	$\geq$	2.57E7	2.57E7	vertical bending
3	K_t [Nm/rad]	1.45E6	$\geq$	1.89E6	1.89E6	torsion
4	$f_{1^{st}b}$ [Hz]	50.65	$\geq$	53.00	56.00	1^{st} bending mode
5	$f_{1^{st}t}$ [Hz]	55.13	$\geq$	-	60.00	1^{st} torsional mode

To evaluate the global static performance of the vehicle BIW two load cases were used for bending and torsion respectively (Figs. 6.15 and 6.16, simple 1D element display). The notation is the same as in Section 6.3.2. Eqs. 6.14 and 6.15 were used to calculate the bending and torsional stiffness, K_b and K_t, of the BIW. The only difference is that in Eq. 6.14 $|t_A|$ was replaced by the maximum absolute value among the vertical displacements of all nodes belonging to the two door sills. These nodes are evidenced in yellow in Fig. 6.15. For the evaluation of the global dynamic performance modal analysis was performed under free-free conditions. The first 6 modes were considered (excluding the 6 rigid body modes). The same mode tracking strategies were used as in Section 6.3.2. The tracked mode shapes are shown in Figs. 6.17 and 6.18.

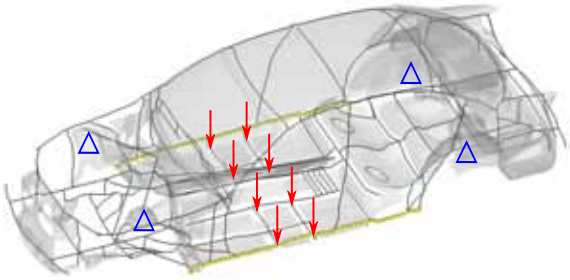

Figure 6.15: BMW 3 series, $\mathbf{K_b}$ load case.

All OFs were defined on the basis of the responses from Table 6.5 and Eq. 6.18. In both optimization problems $\alpha_1 = -1$ and $\alpha_k = 1$ for $k \in \{2..4\}$ (problem I) and respectively for $k \in \{2..5\}$ (problem II).

6.4.3 Optimization algorithms

The same PC and algorithm settings were used as in Section 6.3.3 but a maximum number of 30000 OF calls was set for DE because of the bigger FE model. GB_{ref} and GB_{rnd} were compared only with DE_3 as it proved to be the best performing DE variant (Section 6.3.4).

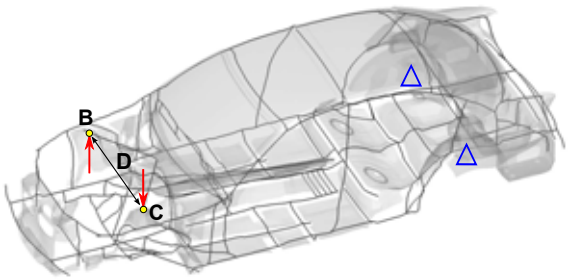

Figure 6.16: BMW 3 series, $\mathbf{K_t}$ load case.

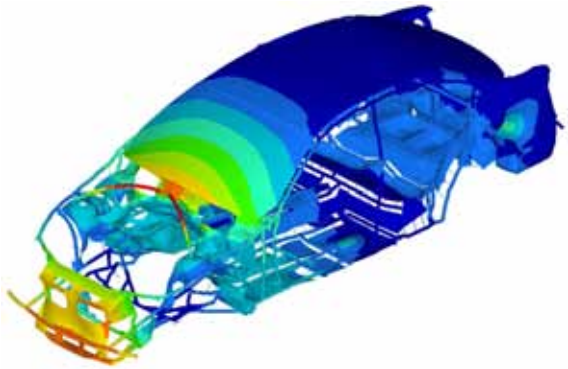

Figure 6.17: BMW 3 series, 1$^{\mathbf{st}}$ bending mode at 50.65 Hz.

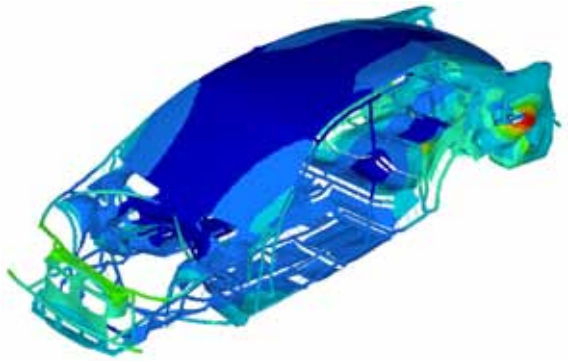

Figure 6.18: BMW 3 series, 1$^{\mathbf{st}}$ torsional mode at 55.13 Hz.

6.4.4 Results

The results both for problem I and II are summarized in Table 6.6. The results of the multi-start approach (GB_{rnd}) are reported for the best of all 50 runs in

both cases. However, the cycles and timings correspond to all 50 random runs.

Table 6.6: Results **GB** and **DE$_3$** for problem I and II.

Result	GB_{ref_I}	GB_{rnd_I}	DE_{3_I}	GB_{ref_II}	GB_{rnd_II}	DE_{3_II}
m [kg]	308.14	304.61	339.31	307.12	349.16	344.51
K_b [N/m]	2.57E7	2.57E7	2.58E7	2.57E7	2.57E7	2.57E7
K_t [Nm/rad]	1.89E6	1.89E6	1.89E6	1.89E6	1.89E6	1.89E6
$f_{1^{st}b}$ [Hz]	53.78	53.81	54.79	56.02	56.67	56.04
$MAC_{1^{st}b}$	0.9254	0.9381	0.9570	0.9456	0.9725	0.9597
$f_{1^{st}t}$ [Hz]	-	-	-	Failed	61.52	61.08
$MAC_{1^{st}t}$	-	-	-	Failed	0.7045	0.6208
Feasible	Yes	Yes	Yes	Yes	Yes	Yes
Cycles/OF	21	1115	30000	21	1084	30000
Time [s]	5241	197400	556620	5755	194400	567752

All three final configurations for problem I (GB_{ref_I}, GB_{rnd_I} and DE_{3_I}) are feasible. Moreover, the thresholds for all targets are achieved except for the mass. In terms of performance attributes the solutions found with GB_{ref_I} and GB_{rnd_I} are similar, but the final design for GB_{rnd_I} is 3.5 kg lighter. On the other hand, the results of GB_{rnd_I} are obtained on the basis of 50 runs. Only one of them results in an infeasible design. The remaining 49 runs reach $R_{k\_tgtI}, k = 2..4$ and have mass varying between 304.6 and 365.2 kg. This high variability of the end results proves that the problem has multiple optima. Thus GB_{rnd_I} outperforms slightly GB_{ref_I} in terms of final results, but GB_{ref_I} requires times less computational time. As in Section 6.3, a hybrid DE-GB strategy was unsuccessful because of mode tracking issues. Therefore only the results for DE are reported hereafter.

The final configuration obtained with DE_{3_I} has higher K_b and $f_{1^{st}b}$ than GB_{ref_I} and GB_{rnd_I}, but it is in the same time heavier. Actually, DE was still converging and it stopped because the maximum number of OF calls was reached. A higher threshold for the OF evaluations would have allowed DE to come closer to the global optimum. However, it was kept to 30000 as it corresponded to a computational time reasonable in an industrial context (around 1 week). As expected, DE is much slower than a single GB run. This difference becomes less evident when comparing DE with the multi-start approach, for both of which the magnitude of the computational time is in days. On the other hand, DE not only provides the final configuration but also 8925 feasible designs recorded during the optimization process. For all of them the thresholds for K_b, K_t and $f_{1^{st}b}$ are reached, while the mass varies from 339.3 kg to 409 kg. Fig. 6.19(a) shows a scatter plot of all these solutions. The design alternatives with mass from 339.3 kg to 340.3 kg are shown in Fig. 6.19(b). In both figures the quantities for all axes are the relative percentage differences Δ between actual and reference values (R_{k_actI} and R_{k_ref}) – respectively for K_b and K_t (X-axis), $f_{1^{st}b}$ (Y-axis) and m (Z-axis). The final optimum is marked with a big black asterisk symbol. Even for the small range of 1 kg a lot of configurations are found and recorded, different both in terms of design variables and structural responses (Fig. 6.19(b)).

From this point of view, the lower speed of DE is compensated by the wealth of information gathered during the search process.

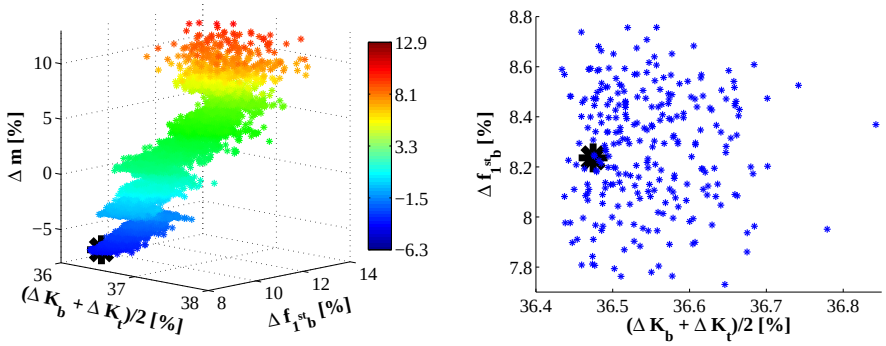

(a) 3D view.

(b) Zoomed 2D view.

Figure 6.19: DE_{3_I} solutions.

Also for problem II the three final configurations (GB_{ref_II}, GB_{rnd_II} and DE_{3_II}) respect the geometry constraints. The target for the mass is again the most difficult one to reach, but the tracking of $f_{1^{st}t}$ creates some problems too. Although the mass found with GB_{ref_II} is the lowest one, the final design is not considered valid because of the failed tracking of $f_{1^{st}t}$. Moreover, it is exceptionally problematic also for GB_{rnd_II} – 49 out of the 50 runs fail due to mode tracking issues. They are mainly caused by the inability of GB to deal with design responses that are not defined, i.e. that are discontinuous. The combination of GB search and cross-orthogonality check with updating of the reference mode shape does not seem a good choice for mode tracking in the case of complex, highly constrained problems. Thus, although GB_{rnd} gives good final results for problem I, its success rate decreases considerably for problem II. In this sense the advantage of GB in terms of computational time becomes less relevant. On the other hand, DE_3 moves slowly but steadily towards the global optimum and provides a better design for problem II. The final configuration is 4.7 kg lighter than the one found with GB_{rnd_II}. The resulting structures for both GB_{rnd_II} and DE_{3_II} are shown in Figs. 6.20, 6.22 and 6.24, and respectively in Figs. 6.21, 6.23 and 6.25. All figures are in detailed 1D element display. They demonstrate not only the changed BIW but also the ratios between the width, height and plate thicknesses of each cross-section in the optimized and respectively in the reference model. As it can be seen, GB and DE act differently on the structure. GB tends to make uniform changes, especially regarding the widths and the heights – entire parts of the body are changed with the same or very similar scaling factor. In contrast to that, DE does not group the design variables and demonstrates creativity. In fact DE is expected to lead to more innovative designs with respect to GB, especially for problems with multiple optima or disjoint feasible region. Similarly to problem I, DE provides not only the final optimal configuration, but a set of 8610 feasible solutions recorded during the optimization with mass between 405.7 and 344.5 kg

– Fig. 6.26(a). The designs with mass from 344.5 to 346.5 kg are shown in Fig. 6.26(b). Based on this wealth of information, the design engineer can be given a much better insight into the problem and can even choose alternative designs out of the available ones. This can be a valuable tool, especially during the concept stage of vehicle development.

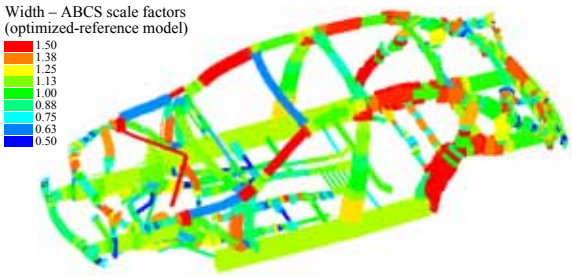

Figure 6.20: $\mathbf{GB_{rnd\_II}}$ - width ratios.

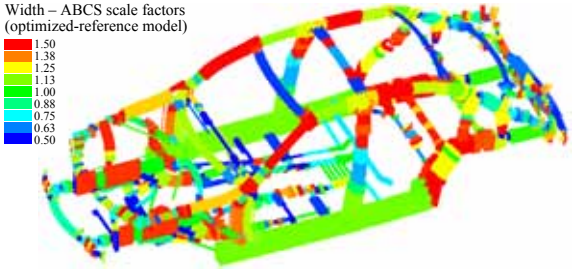

Figure 6.21: $\mathbf{DE_{3\_II}}$ - width ratios.

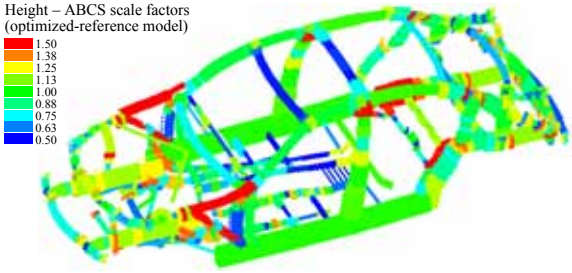

Figure 6.22: $\mathbf{GB_{rnd\_II}}$ - height ratios.

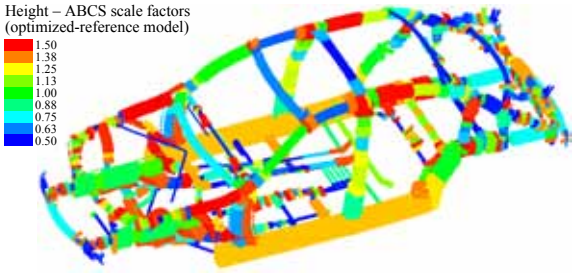

Figure 6.23: $\mathbf{DE_{3\_II}}$ - height ratios.

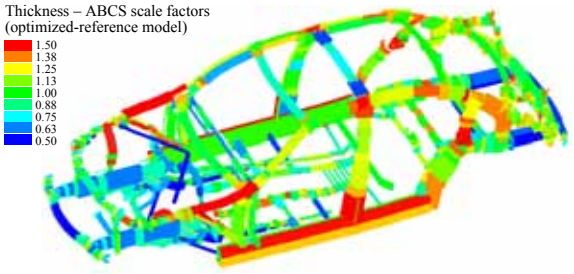

Figure 6.24: $\mathbf{GB_{rnd\_II}}$ - thickness ratios.

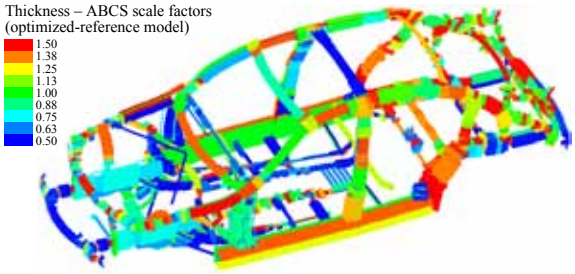

Figure 6.25: $\mathbf{DE_{3\_II}}$ - thickness ratios.

6.5 Conclusions

This chapter treated some aspects with regard to advanced sizing optimization of BJP concept models. The performance of a single-run and a multi-start GB approach was compared to that of a heuristic method. DE was proposed as an advanced global-search alternative to the multi-start GB technique. It was improved to meet the demands of real world engineering problems in the concept phase of vehicle development. The results from this study showed that there is clearly a need for global-search techniques to solve the sizing optimization problems typical for the concept stage. The multi-start GB approach proved more successful than

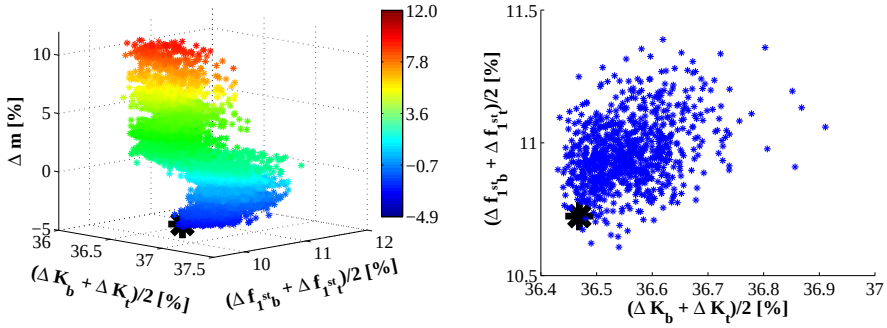

(a) 3D view.

(b) Zoomed 2D view.

Figure 6.26: DE_{3_II} solutions.

the single-run GB method for all cases. Although slower, it managed to identify significantly better solutions. On the other hand, DE not only provided good final designs, but also an immense quantity of additional feasible configurations to choose from. Moreover, it was more stable than the GB algorithm, especially in regard to dealing with mode tracking issues. DE can be potentially integrated at industrial level as it is robust, easy to tweak and requires reasonable time. It deals successfully with problems having varying difficulty, large-scale sizing optimization included. DE approaches the global optimum in reasonable time while providing information also for alternative design configurations.

Chapter 7

Surrogate modeling based on mesh morphing

7.1 Introduction

As discussed in Chapter 2, the predecessor-based methods constitute the most frequently applied class of approaches. Naturally, this is not without a reason. In the VDP variant or incremental improvements of existing vehicles are often created. Even if a completely new vehicle is designed, predecessor knowledge is always needed. The two sub-classes of this popular group rely on different techniques and offer different capabilities. The methods based on simplified structure layout were the main subject of Chapters 3 to 6. Both novel methodologies and improvements of existing ones were proposed in order to overcome the intrinsic limitations of these approaches. Partially as the result of these recent enhancements, the most advanced methods of this sub-class can be currently considered sufficiently accurate in regard to the modeling and fast enough in regard to the optimization of BJP models. However, expertise in concept modeling for the vehicle structure is fundamental, or else too many approximations could be introduced and the models would not be reliable. Good knowledge of the most recent and advanced techniques is necessary, as most of them are not implemented in commercial software solutions. A well-established, standardized methodology for the concept model creation must be available at company level. These requirements can sometimes result too high for the everyday practice, especially if there are no dedicated tools and/or no engineers with previous experience in VCM.

From this point of view, the methods based on mesh morphing are more immediate. The morphing setup results much easier compared even to the semi-automatic creation of a simplified BIW model. Moreover, the direct use of detailed FE models guarantees precision without much additional effort. Compared to the BJP models which are typically used for statics and low frequency dynamics, a much wider range of performance attributes can be assessed on a detailed model, e.g. crashworthiness, ride and handling, NVH, structural integrity and durability, aerodynamics. In contrast to Fig. 2.2(a), no time and accuracy is lost in the transition detailed-simplified model before optimization and in the backward transformation simplified-detailed model after optimization. Undoubtedly, giving

the possibility to work with the detailed FE model is one of the crucial strengths of this second class of predecessor-based methods. It is also the reason for a big disadvantage – the high and usually not affordable computational cost of directly involving a detailed model during optimization.

This problem gave the motivation of the current chapter. Its objective is to circumvent the computational burden of using detailed FE models by means of RS metamodels based on mesh morphing structural modifications (Fig. 7.1). Such mathematical representation is a feasible alternative for the concept stage as optimization becomes fast and does not require FEA. This idea corresponds to shifting from the paradigm illustrated in Fig. 2.1(c) to the one from Fig. 2.1(d). While with the first concept mainly simple "what-if" studies can be performed (e.g. [3, 53, 125, 129]), in the second one numerous OF evaluations are possible. The focus in this work is on approximating the static and dynamic behavior of the vehicle structure, but metamodels for other design responses can be created in a similar manner. With the proposed methodology it is also possible to perform local joints modifications on the optimized detailed FE model so that the design engineer has more flexibility for changes. Joints were considered as means of additional tweaking because of their strong influence on the global vehicle performance.

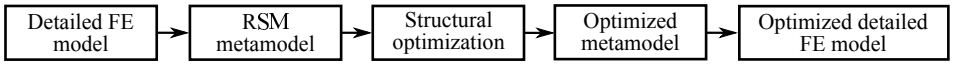

Figure 7.1: Methods based on mesh morphing.

This chapter is organized as follows. First the methodology used for deriving the RS models is described (Section 7.2). It is then applied to an industrial case study and two optimization problems are solved (Section 7.3). Their final solutions are presented and compared in terms of structural modifications and resulting responses. After that the advantages and limitations of the proposed approach are discussed (Section 7.4).

7.2 Methodology

RS models are widely used in the engineering practice when it comes to relating an output variable (called also response) to the levels of a number of input variables (called also factors) that affect it [194]. The methodology proposed in this work relies on such mathematical models. It consists in the creation of morphing-based RS models of the global static and dynamic behavior of the vehicle. They are subsequently used for fast optimization studies after which additional local joint modifications can be applied if needed. A flowchart of the approach is shown in Fig. 7.2. The various steps are explained hereafter:

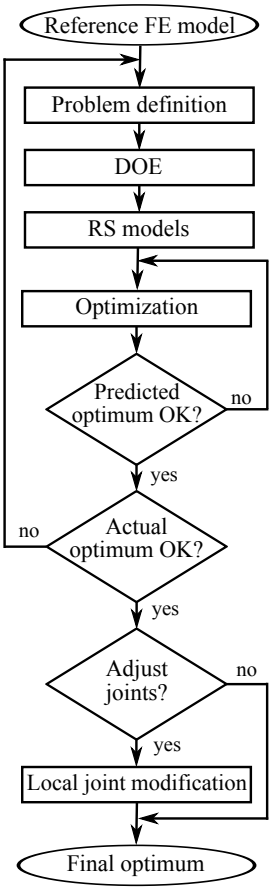

Figure 7.2: Methodology.

Reference FE model

The reference FE model of an existing vehicle structure is the starting point. This is a validated, full FE model.

Problem definition

At this stage it must be decided which will be the structural modifications to perform. Both the morphing and the joint setup have to be defined, as well as the responses needed during optimization which will be approximated (e.g. node displacement, eigenfrequency of the first bending mode, etc.).

Indirect morphing via morph volumes is a good choice for the automatic creation of parametric FE models as it is repeatable, flexible and fast (Section 2.2.2). Each morph volume envelopes part of the existing FE mesh. When morphing operations such as translation, rotation, scaling and similar are applied to the volumes,

the mesh inside them is automatically morphed on its turn and a new FE model is generated. The morphing setup includes the definition of these operations, also called morphing parameters, and of their lower and upper bounds. If they are too much (more than 6-8), the less important ones can be screened out.

The joint setup includes defining the main pairs of structural joints and, if relevant, performing sensitivity analysis to identify the most influential ones of them. After the end of the optimization loop, they can be used for complementary adjustment of the optimized FE model. The choice of such local modification is motivated by the fact that the car body joints can impact greatly the global vehicle stiffness. However, they have complex geometry and although their basic topology repeats (T-type and corner-type joints), detailed designs can differ significantly. This makes the creation of parametric models for tweaking the joint stiffness a difficult task, which can take months [106]. The most straightforward method, adopted also in this work, is to change the thicknesses of the shell elements belonging to the joint structure. Alternatively, one can apply more elaborate approaches such as adding additional internal stiffeners and changing the joint geometry by mesh morphing techniques.

Design of Experiment

The next step consists in the selection and execution of a DOE plan (Fig. 7.3). It is decisive for the creation of the RS models at a cost which is as low as possible. As in Chapter 4, LHS [195] is used also in the current study. Designed specifically for computer experiments, LHS not only has a good space-filling property, but is also flexible - the number of experiments and thus the number of levels for the input variables can be controlled by the user. This means that the designer has the freedom to balance between accuracy of the approximation and computational time for executing the DOE experiments. Furthermore, LHS can cope with many factors and it is computationally cheap to generate. Additional input variables can be easily added.

The factors varied in the LHS plan are the previously defined morphing parameters. Thus each experiment corresponds to a different morphed FE model (Fig. 7.3). All generated models are analyzed and the responses of interest are extracted from the output.

Response Surface models

As it can be difficult to define the most appropriate polynomial model for each response a priori (before the DOE phase), analysis of variance (ANOVA) is performed to determine it according to various criteria (e.g. F-test, R^2). Thus, in the end of this step each response can be represented with the RS model that best approximates it on the basis of the DOE results. The unknown coefficients of each polynomial are found using the least squares criterion in order to minimize the sum of all squared differences between the actual and the predicted values of the response.

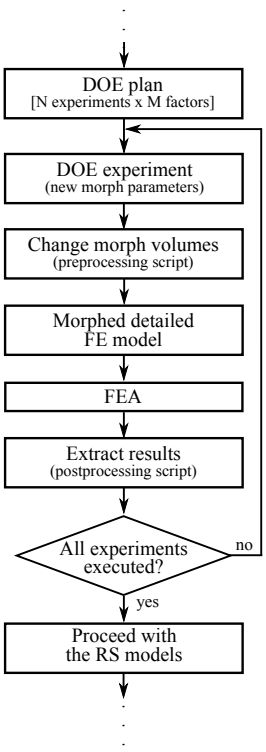

Figure 7.3: DOE stage.

Optimization

The design variables of the optimization problem are the DOE factors, i.e. the morphing parameters with their corresponding lower and upper bounds as defined during the DOE. If the range of the design variables is extended, the validity of the RS models is not guaranteed. The OF and all constraints must be defined in this step. The optimization algorithm can be chosen independently of the previous two phases. As computationally cheap mathematical models are used for the OF and the constraints, not only local, but also global-search algorithms can be applied. This can become an advantage especially if the design space is severely constrained or in the case of highly non-linear responses (e.g. crashworthiness performance). Finally, the control parameters of the optimization algorithm must be set up. Fast optimization can be then started during which each of the responses of interest is replaced by its best approximating mathematical model.

Predicted optimum

If the optimum found after optimization over the RS models is not satisfactory, the problem can be redefined. Possible solutions include, but are not limited to,

reformulating the OF in alternative way where possible, loosening the constraints, setting new control parameter values of the optimization algorithm if they influence the convergence, etc.

Actual optimum

On the basis of the optimal configuration predicted by the approximating models, the corresponding morphed FE model is generated and consequently analyzed. The results of both models are compared. A difference between them, which is not negligible, signals a problem with the RS models. Various countermeasures can be taken such as for example to narrow the range of the DOE factors, to perform more experiments in the LHS DOE, to use polynomials of higher degree for the approximations, etc. In addition, the actual morphed FE model can be included to the experimental points thus contributing information about the design space.

Local joint modifications

Local joint modifications can be optionally made if the designer wants to increase the vehicle stiffness at the cost of small mass increase. For this purpose the plate thicknesses of the most influential joints pairs identified previously are set to their maximum values.

Final optimum

The final optimum is the optimized morphed FE model eventually with some joint pairs made stiffer. This model can be used later on during the creation of the CAD model for the optimized concept.

7.3 Industrial case study

In this section the previously described methodology was applied to an industrial case study. The Toyota Rav4 BIW, year 1997, shown in Fig. 3.20 was used as reference FE model. The model was described in Section 3.4.1.

7.3.1 Problem definition

Responses

Two types of responses were defined – geometry-based and requiring analysis. The geometry-based responses taken into account were 10: the BIW mass (m), the wheelbase length (WB), the overall length (L), width (W) and height (H), the volume of the engine compartment (Vol_0), the volume of the passenger compartment up to the front seats (Vol_1), between the front and rear seats (Vol_2) and behind the rear seats (Vol_3), and, finally, the windshield angle ($\measuredangle_{ws}$). Except for the mass, they are all visualized in Fig. 7.4. On their turn the analysis-based responses were 4 and included the global static bending and torsional stiffness (K_b and K_t), and the eigenfrequencies of the first bending and torsional mode ($f_{1\mathbf{st}_b}$

and $f_{1^{st}t}$). The purpose was to approximate both groups with RS polynomial models. This was especially important for the analysis-based responses as in this way fast optimization studies were made possible. As for the geometry-based responses, their calculation was also possible with a FE preprocessor, but RS models were preferred as a faster and equally precise alternative.

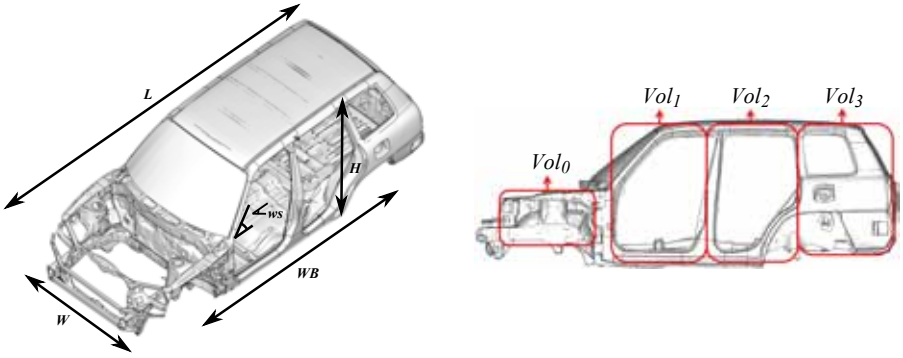

Figure 7.4: Geometry-based responses.

To evaluate the global static performance of the vehicle BIW the same two load cases were used for bending and torsion as defined in Section 3.4.1 (Figs. 3.24 and 3.25). K_b and K_t were thus calculated with Eqs. 3.8 and 3.9. For the evaluation of the global dynamic performance modal analysis was performed under free-free conditions. The first 4 non-rigid body modes were considered.

The results for all geometry- and analysis-based responses of the reference FE model (Fig. 3.20) are given in Tables 7.1 and 7.2.

Table 7.1: Geometry-based responses.

Response	Value
m [kg]	304.20
WB $[m * 10^{-3}]$	2413.03
L $[m * 10^{-3}]$	3909.86
W $[m * 10^{-3}]$	1700.27
H $[m * 10^{-3}]$	1367.66
Vol_0 [l]	371.53
Vol_1 [l]	1459.20
Vol_2 [l]	931.19
Vol_3 [l]	761.10
$\measuredangle_{ws}$ [rad]	0.8461

Table 7.2: Analysis-based responses.

Response	Value
K_b [N/m]	3.08E6
K_t [Nm/rad]	2.68E5
$f_{1^{st}b}$ [Hz]	26.26
$f_{1^{st}t}$ [Hz]	29.87

Morphing setup

For the morphing setup a set of morph volumes was defined (Fig. 7.5) which splits the vehicle BIW in different parts. 6 morphing parameters were chosen as factors in the LHS DOE and consequently as design variables in the optimization. Their lower and upper bounds are listed in Table 7.3. The first parameter is dimensionless as it is a scaling factor. All the others are translations in meters.

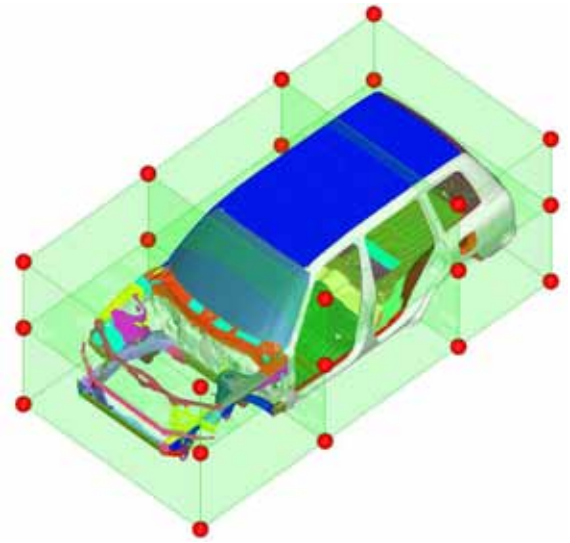

Figure 7.5: Morph volumes definition.

The FE models resulting from changing one morphing parameter at a time in the order from 1 to 6 are shown in Fig. 7.6, 7.7, 7.8, 7.9, 7.10 and 7.11 respectively. The reference structure is shown in grey and the morphed one - in magenta. The morphed models are the result of scaling in lateral direction (Fig. 7.6), translation in vertical (Fig. 7.7, 7.8) and longitudinal direction (Fig. 7.9, 7.10, 7.11). All morphing operations were applied to the respective morph volume handles (Fig. 7.5) - e.g. vertical translation of all handles belonging to the upper side of the

Table 7.3: Factors.

Factor #	Unit	LB	UB
1	-	0.9412	1.0588
2	$m * 10^{-3}$	-119	119
3	$m * 10^{-3}$	-124	124
4	$m * 10^{-3}$	-150	150
5	$m * 10^{-3}$	-140	140
6	$m * 10^{-3}$	-150	150

morph volume matrix for changes of factor 2. The sample structural modifications correspond to decreasing the overall width (Fig. 7.6), the height of the upper (Fig. 7.7) and lower (Fig. 7.8) half of the vehicle, the length of the front (Fig. 7.9) and rear (Fig. 7.11) part of the vehicle and the length of the passenger compartment (Fig. 7.10). Preference was given to morphing parameters resulting in global changes instead of local ones in order to reduce the number of factors as much as possible.

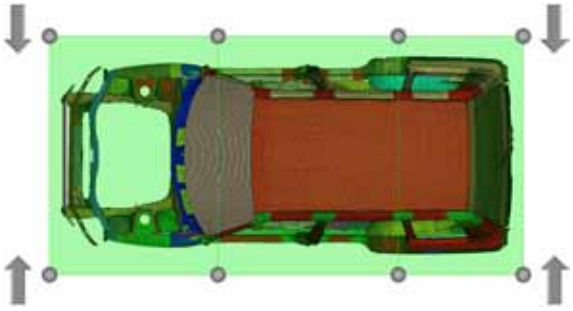

(a) Affected morph handles.

(b) Width change.

Figure 7.6: Factor 1.

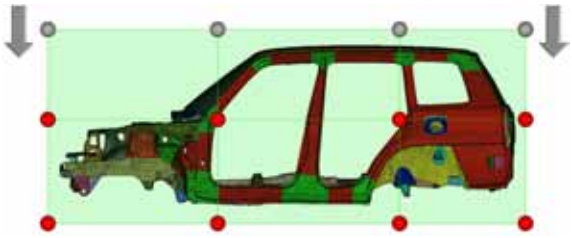

(a) Affected morph handles.

(b) Height change, upper half.

Figure 7.7: Factor 2.

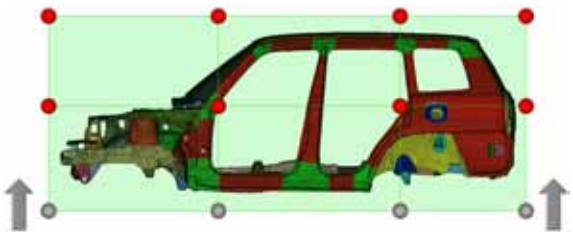

(a) Affected morph handles.

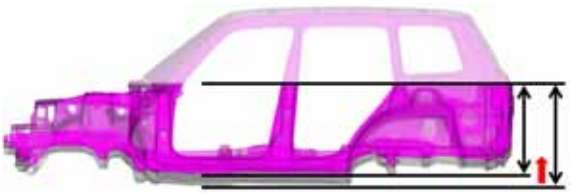

(b) Height change, lower half.

Figure 7.8: Factor 3.

Joint setup

The eight joint pairs which were chosen for optional structural modifications after the optimization ends are shown in Fig. 7.12. They correspond to the major BIW joints in Fig. 2.6. The approach adopted for the change of their stiffness consisted in multiplying the thicknesses of all internal layers of shell elements belonging to the joint structures by a scaling factor.

Sensitivity analysis based on the one-factor-at-a-time (OFAT) method was used

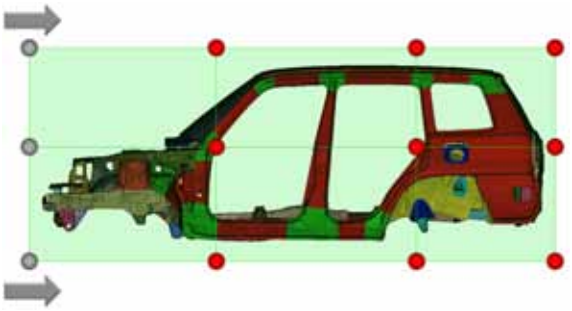

(a) Affected morph handles.

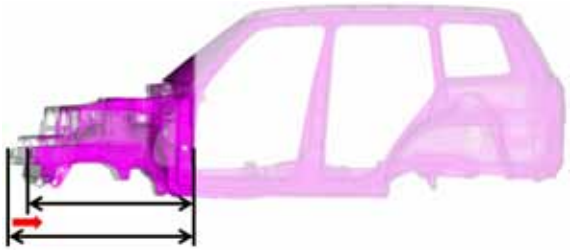

(b) Length change, front part.

Figure 7.9: Factor 4.

to identify the joints with the biggest influence on the global static and dynamic performance. Although such a sensitivity analysis does not take into account any factor interactions, it is computationally cheap as it requires just 8 runs. On the other hand a resolution V fractional factorial DOE for eight factors with unbiased main effects requires a minimum of 64 runs.

At each run the scaling factor for one joint pair at a time was set to 1.5 while keeping all other scaling factors at 1. The results from the sensitivity analysis are shown in Fig. 7.13. The individual effects were evaluated as $\Delta Resp = (Resp - Resp_{ref})$, where $Resp$ refers to K_b, K_t, $f_{1^{st}b}$ and $f_{1^{st}t}$ obtained after the individual joint pair modifications, and $Resp_{ref}$ refers to their corresponding reference values (Table 7.2). The three most influential joint pairs were identified from the performed sensitivity analysis - 1, 4 and 5.

As it can be seen from Fig. 7.13 with such local structural modifications it is possible to improve the global static and dynamic performance of the vehicle structure at the cost of small increase of mass. On the other hand, the effect of the increased thicknesses was predictable - the stiffer the joints, the stiffer the whole BIW. For this reason the three most influential joint pairs were not included in the DOE phase. Keeping the number of factors to 6 and not to 9 required less numerical experiments to perform.

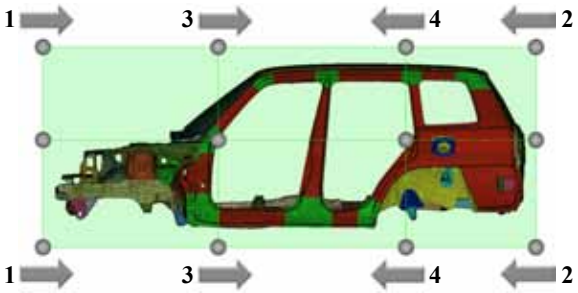

(a) Affected morph handles.

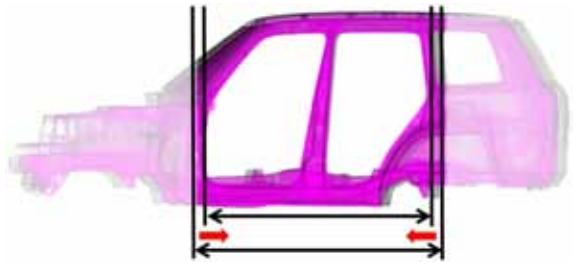

(b) Length change, cabin.

Figure 7.10: Factor 5.

7.3.2 Response Surface models

The parametrization of the reference FE model was defined by means of morph volumes during the morphing setup. Thus all experiments for the DOE phase corresponding to different morphed models were generated automatically with dedicated in-house scripts. As LHS DOE plan was used, it was possible to choose the number of experiments considering the number of factors, the expected nonlinearity of the approximated responses, the maximum allowable time for the DOE (from industrial point of view), the available computational resources, etc. For this study a number of 40 experiments was chosen as reasonable in order to gather more information about the design space and ensure lower prediction errors. Consequently, 40 static and modal analyses were involved. For less than 40 experiments the approximation of the analysis-based responses was not good enough. It must be noted that after each modal analysis, $f_{1^{st}b}$ and $f_{1^{st}t}$ were tracked in the new configuration based on the MAC (Eq. 4.10). This was necessary as due to the structural modifications mode switching was possible and it was not enough to follow the same mode numbers as in the reference configuration.

Given the 40 DOE runs, the following regression models were checked for each of the 14 responses in order to choose the one that best approximates its relation with the input variables (Table 7.3):

- linear – constant and linear terms (Eq. 7.1);
- interaction – constant, linear and interaction terms (Eq. 7.2);
- quadratic – constant, linear, interaction and squared terms (Eq. 7.3);

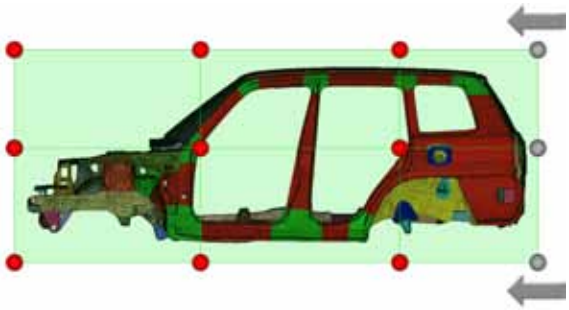

(a) Affected morph handles.

(b) Length change, rear part.

Figure 7.11: Factor 6.

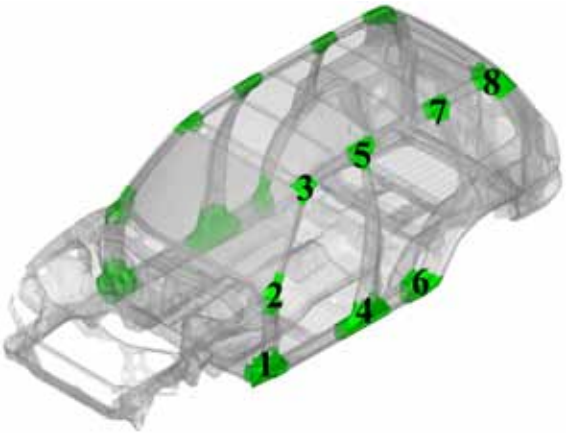

Figure 7.12: Modified joints.

- pure quadratic – constant, linear and squared terms (Eq. 7.4).

Given the number of factors - 6, there were respectively a maximum of 7, 22, 28 and 13 unknown coefficients β in the approximating polynomials.

$$Resp_{lin} = \beta_0 + \beta_1 x_1 + \beta_2 x_2 + \beta_3 x_3 + \beta_4 x_4 + \beta_5 x_5 + \beta_6 x_6 \tag{7.1}$$

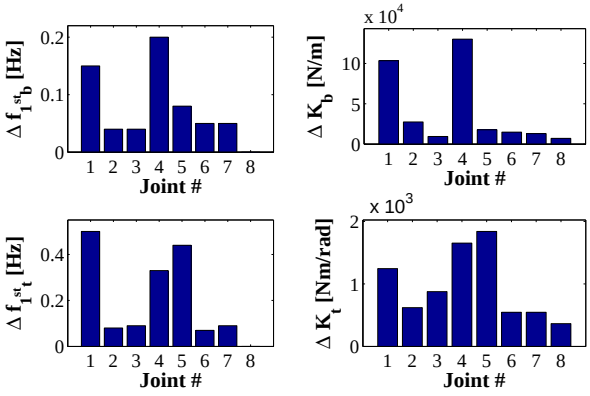

Figure 7.13: Joints – sensitivity analysis.

$$Resp_{interact} = Resp_{lin} + \beta_{12}x_1x_2 + \beta_{13}x_1x_3 + \beta_{14}x_1x_4 + \beta_{15}x_1x_5 + \beta_{16}x_1x_6 + \beta_{23}x_2x_3 + \beta_{24}x_2x_4 + \beta_{25}x_2x_5 + \beta_{26}x_2x_6 + \beta_{34}x_3x_4 + \beta_{35}x_3x_5 + \beta_{36}x_3x_6 + \beta_{45}x_4x_5 + \beta_{46}x_4x_6 + \beta_{56}x_5x_6 \quad (7.2)$$

$$Resp_{quad} = Resp_{interact} + \beta_{11}x_1^2 + \beta_{22}x_2^2 + \beta_{33}x_3^2 + \beta_{44}x_4^2 + \beta_{55}x_5^2 + \beta_{66}x_6^2 \quad (7.3)$$

$$Resp_{purequad} = Resp_{lin} + \beta_{11}x_1^2 + \beta_{22}x_2^2 + \beta_{33}x_3^2 + \beta_{44}x_4^2 + \beta_{55}x_5^2 + \beta_{66}x_6^2 \quad (7.4)$$

All calculations were made on a desktop PC with the following technical characteristics: CPU Intel Core i5 760@2.8 GHz, 6 GB RAM, OS Windows 7 Pro X64. For the FE model of Fig. 3.20 a single linear static analysis took 390 s and a single modal analysis - 660 s. The parallel computation on 2 cores took 22446 s in total for the whole DOE plan.

The best polynomial models for the analysis-based responses are given in Table 7.4. For briefness just the type of the regression model is given without the values of the different coefficients. The values of the determination criteria R^2, the adjusted determination criteria R^2_{adj} and the result of the F-test are also reported.

R^2 and R^2_{adj} are measures of the goodness of fit and can have values between 0 and 1. A value close to 1 shows good quality of the approximating polynomial. R^2_{adj} is a statistically unbiased version of R^2 that takes into account the number of regression coefficients which can vary for different models. It is typically lower than R^2. From Table 7.4 it can be seen that the adequacy of the best RS models is excellent - both R^2 and R^2_{adj} are 1 or very close to 1. In addition, all the chosen models passed the F-test for significance successfully. Thus the approximations of the global static and dynamic performance of the vehicle were considered reliable and were used in the next phase during the optimization process, eliminating the need for further CAE analysis.

Table 7.4: Best regression models.

Response	Model type	R^2	R^2_{adj}	F-test
K_b	quadratic	1.0000	1.0000	OK
K_t	quadratic	1.0000	1.0000	OK
$f_{1^{st}b}$	quadratic	0.9999	0.9996	OK
$f_{1^{st}t}$	interaction	0.9938	0.9866	OK

All geometry-based responses were also approximated to avoid the need of calling a FE preprocessor at each OF evaluation. The obtained best fitting RS models were as follows: linear for WB, L, W, H, interaction for Vol_0, Vol_3, and quadratic for m, Vol_1, Vol_2, $\measuredangle_{ws}$. As expected, the nature of this responses was much simpler than the analysis-based ones. Consequently, the F-test for all was passed and all R^2 and R^2_{adj} values were practically 1.

The obtained RS models are not visualized hereby as the plot of the responses is possible for up to three factors at a time, while the factors in the current study are six.

7.3.3 Optimization

The design variables at this stage were the 6 morphing parameters (Table 7.3). Two different constrained optimization problems were defined for the Toyota Rav4 BIW - Tables 7.5 and 7.6. The objectives were respectively to minimize the total BIW mass (problem 1) and to maximize the volume of the passenger and luggage compartment (problem 2), while not deteriorating the vehicle static and dynamic performance too much (problem 1, 2). The first problem aimed to address the constant need to reduce production costs and fuel consumption. On the other hand, nowadays there is also demand for more spacious vehicles (e.g. Toyota Rav4, year 2011), which motivated the definition of the second problem. For both problems additional geometry constraints had to be also satisfied. The constraint concerning $\measuredangle_{ws}$ aimed to serve as an intuitive control of the aerodynamic performance, although CFD simulations were not considered in this study.

Augmented Lagrangian Genetic Algorithm (ALGA) was chosen as optimization strategy in order to ensure better exploration of the design space on one hand and be able to handle nonlinear constraints on the other. Population size of 60 individuals was used. A maximum number of 50 generations was set. The optimization finished in only 17 s (problem 1) and 14 s (problem 2) which in both cases was times less than a single OF evaluation involving the detailed FE model. 17932 OF calls (7 generations) were needed to solve problem 1, and 15390 OF calls (6 generations) - to solve problem 2. In both cases the number of OF calls was higher than the number of generations multiplied by the population size because of the way the nonlinear constraint solver works. Solving the same optimization problems by directly involving FE analysis at each OF call (linear static analysis

Table 7.5: Optimization problem 1.

Problem 1
$min(m)$
while
$K_b \geq K_{b\_ref}$
$K_t \geq K_{t\_ref}$
$f_{1^{st}b} \geq f_{1^{st}b\_ref}$
$f_{1^{st}t} \geq f_{1^{st}t\_ref}$
$Vol_0 \geq 0.9Vol_{0\_ref}$
$Vol_1 \geq 0.9Vol_{1\_ref}$
$Vol_2 \geq 0.9Vol_{2\_ref}$
$Vol_3 \geq 0.9Vol_{3\_ref}$
$\measuredangle_{ws} - \measuredangle_{ws\_ref} \leq 26.18rad * 10^{-3}$
$\lvert WB - WB_{ref}\rvert \leq 150m * 10^{-3}$
$\lvert L - L_{ref}\rvert \leq 300m * 10^{-3}$
$\lvert H - H_{ref}\rvert \leq 100m * 10^{-3}$
$\lvert W - W_{ref}\rvert \leq 100m * 10^{-3}$

Table 7.6: Optimization problem 2.

Problem 2
$max(Vol_{1,2,3})$
while
$K_b \geq 0.95K_{b\_ref}$
$K_t \geq 0.95K_{t\_ref}$
$f_{1^{st}b} \geq f_{1^{st}b\_ref} - 1Hz$
$f_{1^{st}t} \geq f_{1^{st}t\_ref} - 1Hz$
$m \leq 1.05m_{ref}$
$Vol_0 \geq Vol_{0\_ref}$
$\measuredangle_{ws} - \measuredangle_{ws\_ref} \leq 26.18rad * 10^{-3}$
$\lvert WB - WB_{ref}\rvert \leq 150m * 10^{-3}$
$\lvert L - L_{ref}\rvert \leq 300m * 10^{-3}$
$\lvert H - H_{ref}\rvert \leq 100m * 10^{-3}$
$\lvert W - W_{ref}\rvert \leq 100m * 10^{-3}$

and modal analysis in parallel) would have taken 12283420 s for problem 1 (around 3412 hours) and 10542150 s for problem 2 (around 2928 hours). In contrast to that, using the proposed methodology the same task took respectively 22463 s (problem 1) and 22460 s (problem 2) in total, considering also the cost of the DOE phase.

The resulting optimal values of the 6 factors (i.e. design variables) are listed in Table 7.7. The results for the predicted (Opt_{RS}), actual (Opt_{FE}) and final (Opt_{jnt}) optima of both problems are given in Tables 7.8, 7.9, 7.10 and 7.11. In these tables Δ_{RS-FE} is the prediction error, i.e. the error due to the usage of RS instead of FE models. The improvements with respect to the reference configuration (Tables 7.1, 7.2) are denoted as Δ_{FE-ref} for the actual optimum Opt_{FE} and as $\Delta_{jnt-ref}$ for the final optimum Opt_{jnt} (i.e. Opt_{FE} with additional joint adjustments). All Δ-s were calculated as relative percentage changes.

Table 7.7: Optimal values of the 6 factors .

Factor #	Unit	Problem 1	Problem 2
1	-	0.95	1.05
2	$m * 10^{-3}$	-29.00	15.98
3	$m * 10^{-3}$	61.85	56.02
4	$m * 10^{-3}$	-149.79	-123.33
5	$m * 10^{-3}$	-79.30	5.94
6	$m * 10^{-3}$	-66.35	-3.89

In both optimization problems the prediction error for all geometry-based responses was practically 0. The maximum prediction error was for $f_{1^{st}t}$, but was still lower than 1%. These results proved the reliability of all RS models in practice and confirmed the appropriate setup of the DOE- and RS model creation phases. The optimized designs derived from Opt_{RS} and used to compute Opt_{FE} are shown in Figs. 7.14 and 7.15.

The total BIW mass was decreased with 17.3 kg for Opt_{FE} of problem 1. In the same time all response constraints were satisfied. The corresponding morphed FE model is shown in Fig. 7.14. As it can be seen, there was a slight height increase, but in the same time the length and the width decreased. Given that the cross-sections of the beam-like parts were not changed, the partially decreased global vehicle dimensions explain the improved static and dynamic performance (Table 7.8). To improve it additionally, the plate thicknesses of joint pairs 1, 4 and 5 were scaled by a factor of 1.5. Thus at the cost of a small mass increase, an even better final optimum Opt_{jnt} was obtained (Table 7.9).

As a result of optimizing the second problem, the volumes of the passenger and luggage compartment were increased with an average of 9.3%. The static performance was also improved considerably, but $f_{1^{st}b}$ and $f_{1^{st}t}$ remained below their reference values (Table 7.10). Although the corresponding constraints from Table 7.6 were satisfied (i.e. not decreasing the two eigenfrequencies by more than 1 Hz), similar effects deteriorating the vehicle dynamic behavior should be possibly avoided. Reformulating the optimization problem did not help to resolve this. The corresponding morphed FE model is shown in Fig. 7.15. The total width and height were increased resulting in a more spacious vehicle, and, on the other side, the length of the front part was decreased. In attempt to improve the

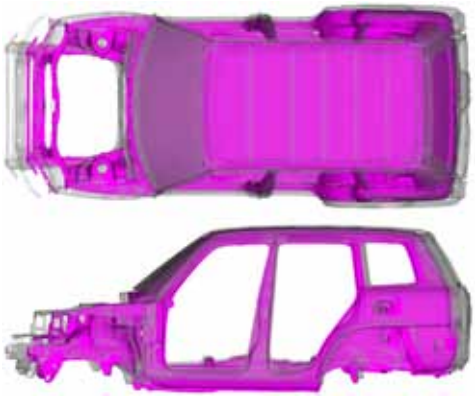

Figure 7.14: Optimal design – problem 1.

Table 7.8: Results – problem 1.

Response	Opt_{RS}	Opt_{FE}	Δ[%] RS-FE	Δ[%] FE-ref
m [kg]	286.88	286.87	0.00	-5.70
WB $[m * 10^{-3}]$	2263.39	2263.39	0.00	-6.20
L $[m * 10^{-3}]$	3632.15	3632.16	0.00	-7.10
W $[m * 10^{-3}]$	1611.70	1611.69	0.00	-5.21
H $[m * 10^{-3}]$	1393.11	1393.11	0.00	1.86
Vol_0 [l]	334.38	334.51	-0.04	-9.96
Vol_1 [l]	1327.06	1327.10	0.00	-9.05
Vol_2 [l]	853.70	853.44	0.03	-8.35
Vol_3 [l]	685.03	684.95	0.01	-10.00
$\measuredangle_{ws}$ [rad]	0.8681	0.8683	-0.02	2.61
K_b [N/m]	3.83E6	3.84E6	-0.18	24.67
K_t [Nm/rad]	2.84E5	2.84E5	0.01	5.93
$f_{1^{\mathbf{st}}b}$ [Hz]	28.99	29.02	-0.11	10.53
$f_{1^{\mathbf{st}}t}$ [Hz]	32.15	32.42	-0.83	8.55

deteriorated dynamic performance of Opt_{FE}, again local joint modifications were performed for the most influential joint pairs (1, 4 and 5) with a factor of 1.5. However, this structural change was insufficient for shifting $f_{1^{\mathbf{st}}b}$ to its reference value or above. Thus, a second attempt was made with a factor of 2. The results for the final optimum Opt_{jnt} (Table 7.11) confirm the usefulness of a combined global-local modification approach. The local joint adjustments can give the design engineer additional flexibility to improve the vehicle static and dynamic stiffness in exchange of slight mass increase. In any case, it must be also considered which

Table 7.9: Joint modification – problem 1.

Response	Opt_{jnt}	$\Delta_{jnt-ref}[\%]$
m [kg]	293.86	-3.40
K_b [N/m]	4.15E6	34.99
K_t [Nm/rad]	2.95E5	9.96
$f_{1^{st}b}$ [Hz]	29.45	12.15
$f_{1^{st}t}$ [Hz]	33.89	13.47

are the maximum allowable values for the thicknesses of the thin metal sheets from a manufacturing point of view.

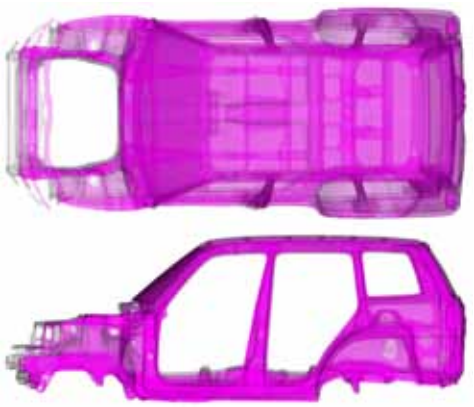

Figure 7.15: Optimal design – problem 2.

The results for both final optima (Tables 7.9 and 7.11) justify the exclusion of the joints during the DOE and optimization phases as the effect of making them stiffer was predictable. On the other hand, it was important to identify the most influential joints in order to keep the resultant mass increase as low as possible.

Both optimization problems were successfully solved with the proposed approach. Thanks to the usage of RS models the GA optimization took less than half a minute, while in the same time the errors due to the approximation proved to be negligible. However, these are just two examples of the method application. Numerous additional what-if or optimization studies can be performed as the methodology is both fast and precise.

7.4 Discussion

In a detailed FE model normally just the plate thicknesses are automatically available as design parameters but the achieved improvements are often unsatis-

Table 7.10: Results – problem 2.

Response	Opt_{RS}	Opt_{FE}	Δ[%] RS-FE	Δ[%] FE-ref
m [kg]	319.19	319.19	0.00	4.93
WB $[m * 10^{-3}]$	2377.03	2377.06	0.00	-1.49
L $[m * 10^{-3}]$	3800.41	3800.42	0.00	-2.80
W $[m * 10^{-3}]$	1781.47	1781.37	0.01	4.77
H $[m * 10^{-3}]$	1426.26	1426.26	0.00	4.28
Vol_0 [l]	376.49	376.32	0.05	1.29
Vol_1 [l]	1584.03	1583.75	0.02	8.54
Vol_2 [l]	1030.89	1030.97	-0.01	10.72
Vol_3 [l]	826.97	826.87	0.01	8.64
$\measuredangle_{ws}$ [rad]	0.8709	0.8707	0.02	2.90
K_b [N/m]	3.33E6	3.33E6	0.00	8.18
K_t [Nm/rad]	3.01E5	3.01E5	0.02	12.17
$f_{1^{st}b}$ [Hz]	25.64	25.59	0.18	-2.54
$f_{1^{st}t}$ [Hz]	28.89	29.17	-0.96	-2.35

Table 7.11: Joint modification – problem 2.

Response	Opt_{jnt}	$\Delta_{jnt-ref}$[%]
m [kg]	334.21	9.87
K_b [N/m]	3.79E6	23.02
K_t [Nm/rad]	3.20E5	19.33
$f_{1^{st}b}$ [Hz]	26.24	-0.09
$f_{1^{st}t}$ [Hz]	31.27	4.69

factory [53]. Mesh morphing gives the design engineer more freedom as with its help both local and global modifications can be performed [3, 53, 125, 128, 129]. The morphing setup is simple and results can be obtained with relatively small effort. If mesh morphing is combined with RS models as in this work, various modification/optimization studies can be performed, given that the design responses have been previously approximated. As proved by the results of the industrial case-study, the use of mesh morphing-enabled global structural modifications and RS models on one hand, and local joint stiffening on the other, can be a successful and reliable strategy for optimization in the concept phase.

It is preferable to apply the proposed approach in the very early stage of concept development when it is possible to make changes in the BIW layout at global level (changing the shape, the overall dimensions, etc.). It must be taken into consideration that in the industrial automotive context the overall outer dimensions

and proportions are generally very quickly fixed in the design process and after that they are rarely modified. In that sense, the presented methodology would be even more useful if a multi-objective multi-disciplinary optimization is performed which takes into account not only the static and dynamic stiffness but also the crash performance, the aerodynamics, the ergonomics, the durability, the acoustic behavior. Nevertheless, the proposed approach can prove helpful also in the later stages of concept development as it allows to setup parametric studies easily and to investigate the influence of the design parameters on the responses, e.g. the relation between the wheelbase, the vehicle width or a combination thereof and the global static stiffness.

Of course, local morphing-based modifications are also possible but if they are too many, considering them in the RS models might increase the cost of the DOE phase unreasonably. It is up to the design engineer to decide which is the maximum allowable number of factors and consequently design variables. In this sense, while the morphing setup is quite straightforward, some more experience with DOE and RSM is needed for the creation of good metamodels. A proper DOE plan must be chosen and decision must be made on the number of experiments. The right balance must be found between the reusability of the RS models and the cost for their creation. As the preliminary DOE phase is also the most time-consuming one, wrong decisions must be avoided at any cost. It must be also considered that RSM might not be fully appropriate for all types of responses (e.g. highly non-linear), so the quality of the approximation must be always checked.

Joints were modified after the optimization phase mainly because considering them in the surrogate models would have increased the time needed to perform the DOE. Nevertheless, this made the presented method more flexible. Instead of varying their thicknesses, changing the joints through more elaborate techniques such as design-oriented translators [104–106, 108] or tools for design at component level [103, 113, 114, 117–120] could result in an even bigger added value.

It is important to underline that the surrogate modeling based on mesh morphing and the concept approaches based on simplified structure layout are not interchangeable. The former can be used for shape and sizing optimization with regard to various performance attributes but for a limited number of design variables. The latter can be employed for sizing optimization in regard to BIW statics and dynamics with extremely high number of design parameters. Both approaches have their limitations and different typical applications. Thus both of them can be useful in the concept stage of vehicle development.

7.5 Conclusions

In this chapter an alternative to the state-of-the-art concept approaches is presented that speeds up the virtual prototyping process while introducing negligible modeling errors. The detailed FE model of a vehicle BIW is made parametric by means of mesh morphing techniques. The static and dynamic behavior of the BIW as functions of the morphing modifications are approximated by means of RS models. The creation of the meta-models is performed at the cost for the initial execution of a LHS DOE. This phase is on its turn flexible as the number

of needed experiments can vary taking into account the problem complexity on one hand and the maximum available computational time on the other. Once the RS models are created, fast optimization and what-if studies can be performed without the need of CAE analysis. Additional flexibility is introduced by the optional usage of local joint modifications. The approach presented in this chapter was successfully applied on an example case-study for which it proved to be both reliable and fast while in the same time avoiding some of the problems typical for simplified models. Thanks to its good accuracy, flexibility and efficiency, the methodology can be successfully integrated in an industrial environment. It can be used either for concept optimization before the structural dimensions have been fixed, or to perform parametric studies of the design responses at a later stage.

Chapter 8

Conclusions

In this chapter the major contributions of the dissertation are summarized. Conclusions are made and directions for future research are given.

8.1 General conclusions

Among the various problems that have to be faced by the virtual prototyping of the automotive body and chassis, the need of analysis that leads the design process from the concept stage onward is critical. Efficient and accurate holistic concept methodologies suitable both for simpler cases and for industrial applications are still missing. The objective of this dissertation is to answer this need by introducing novel CAE techniques in the concept phase, as well as improvements of existing ones. The focus is on the vehicle structure and the representation of its global static and dynamic performance by means of concept FE models. As demonstrated throughout the dissertation and as testified by the numerous related publications, this is a field of active research. Even more, it is of high practical importance and of leading interest for the automotive industry. In this regard, the concept modeling techniques for the design of automotive structures must not only have sound theoretical basis, but must be also applicable on realistic case studies of possibly higher complexity.

In line with the objectives defined in Chapter 1, an in-depth study was performed on the state-of-the-art approaches for VCM and structural optimization. Such a preliminary step was considered fundamental in order to evidence both their strengths and limitations, as well as to be able to identify the current needs and the existing gaps. While knowing the existing methods is decisive for the engineering practice, it is of even greater importance to propose new enhancements. As seen in Chapter 2, there is a wide spectrum of methods for concept modeling and optimization which vary in capabilities, validity and typical applications. Being a relatively new field of research, there are no firmly established and fully recognized approaches. Each of them has some disadvantages and/or needs improvement. Among the others, the appealing group of the predecessor-based methods has been chosen for further research throughout this dissertation. On the other hand, the heuristic search strategies have been identified as insufficiently

studied but promising in regard to structural optimization applications. These two choices determined the framework of the research presented hereby. The main focus of the dissertation was on the creation and optimization of simplified FE models of the vehicle structure (Chapter 3, 4, 5 and 6). Nevertheless, some efforts were dedicated also to the methods based on mesh morphing of predecessor FE models (Chapter 7). The contributions in regard to these two major groups of approaches are summarized hereafter.

- Methods based on simplified FE models of the vehicle structure
  - Concept beams

    Whereas in the VDP it is important to achieve "design right the first time", for VCM it is also essential to create the "concept model right the first time" as otherwise its subsequent use might be limited. Despite that various possibilities for 1D beam concept modeling exist in terms of beam theories and geometry representations, they all have some limitations. In particular, there is a number of error factors which can potentially decrease the accuracy of the concept models. They include (but are not limited to) the beam cross-section geometry, the incorrect approximation of spot welds and flanges, the presence of discontinuities and the lack of local cross-section deformations. These factors can be the reason for significant discrepancies with respect to the actual structure in terms of geometrical similarity and structural behavior. In this sense their profound understanding becomes mandatory both for the creation of better concept models, and for the performance assessment of the existing ones. To overcome the limitations of the existing 1D beam techniques, a systematic study of the potential error factors has been performed. On its basis guidelines for good modeling practices have been derived. Among the other contributions, an in-plane cross-section deformation measure has been proposed. In addition, a rule-of-thumb has been introduced in regard to simplifying the cross-section geometry, without compromising the model precision.

    As the natural application of BJP models is to serve for structural optimization purposes, not only accuracy, but also efficiency is important. A detailed study of the methodologies for modeling and optimization handling of the 1D beam cross-sections was therefore performed. It turned out that even the best-in-class ABCS approach can be subject to further improvements. The deficiencies of the state-of-the-art methods motivated the development of the novel 3B approach. The idea is to keep the reference cross-sectional shapes of all 1D beams. When each of them is rescaled during optimization, the beam is represented by means of GNCS properties. This makes the method computationally beneficial (if the models are used during optimization) and accurate at the same time. The representation of the concept beams is lighter and simpler while the connection with the actual structure is preserved.
  - Concept joints

Similarly to beams, there is no all-in-one solution for the concept modeling of joints. On the other hand, their incorrect representation can cause various problems among which compromised model accuracy at the first place. Considering the main groups of currently available techniques, detailed non-parametric joints were chosen for further development because of the good balance between weaknesses and strengths. An alternative approach for concept joint modeling was proposed, suited equally well for simple and for highly complex structural nodes, but also for the general case of other structural parts which cannot be substituted appropriately with 1D beams. It is based on dynamic reduction of all joints into SEs which results in more accurate simplified models. In addition, such joint representation is both compact and realistic. Taking into account also its ease of implementation, application and integration in existing methods, the dynamic reduction approach results undoubtedly more advantageous than other techniques such as for example joints as junction of 1D beams.

– Sizing optimization with BJP models

  The development of optimization algorithms is not directly related to VCM. On the other hand, the various optimization techniques perform well for certain classes of problems, while for others they are more inappropriate. Moreover, their application in regard to simulation-based optimization is often determined by the size of the FE model used. Being faster and requiring less OF calls, the traditional GB algorithms have been so far regarded as the state-of-the-art in structural optimization at industrial level, even if they do not seem completely suitable in all situations. Alternative methods like the group of heuristic approaches exist. However their potential to solve real-world structural and especially sizing optimization problems has not been fully revealed yet. While the high computational cost of detailed FE models has been one of the main reasons not to employ stochastic techniques, the recent emergence of small-sized BJP concept models opened new horizons. Based on an extensive state-of-the-art on heuristic approaches for large-scale problems, DE has been identified as one of the most promising candidates for further development. It has been extended, improved and validated for the purposes of advanced sizing optimization of BJP models. Its performance has been compared with that of a single-run and a multi-start GB approach. For a relatively simple medium-scale problem the multi-start GB strategy outperformed DE in terms of computational time (as expected) and partially in terms of final results. However, for an extremely complex highly constrained large-scale problem, DE proved to be the most advantageous choice. It not only provided a better final configuration but also a great number of alternative feasible designs. In similar situations the lower speed of DE (with respect to GB algorithms) is fully compensated by the wealth of information gathered during the search process. Naturally, the advantage of using BJP models can be exploited also by other heuristic

methods. In this sense the methods based on simplified structural layout have opened a new field of research – global sizing optimization in the concept phase of vehicle development.

- Methods based on mesh morphing of predecessor FE models

  As alternative to the simplified BJP models, surrogate representations of detailed FE models can be obtained. As demonstrated, mesh morphing techniques can be easily combined with DOE and RSM to create mathematical models of the global BIW static and dynamic behavior. Surrogate-based optimization is incomparably faster with respect to a simulation-based one. Metamodels require even less computational time than the small-sized BJP representations. Of course, the initial cost for performing the DOE must be also taken into account. However, if an economical DOE plan is chosen, if the number of factors is not excessive and if the metamodel is reused more times, this cost becomes often negligible. Apart from being efficient, such an approach has another big advantage – the transition from the optimized metamodel to the optimized detailed FE model is quite straightforward. The accuracy of the method depends on the quality of the RSs and if not sufficient it might be improved through changing the problem definition (e.g. polynomial type, DOE plan, different factor ranges, etc.). After the final detailed model has been obtained, local joint modifications can be also applied for optional tweaking of the global structural performance.

  Although such a methodology might seem appealing and less intricate compared to the approaches based on simplified structural layout, it can be by no means a replacement of these techniques. Both groups are not interchangeable and differ in their strengths, limitations and typical applications. Surrogate modeling based on mesh morphing can be used for shape and sizing optimization with regard to various performance attributes but for a limited number of design variables. Such strategy is more oriented towards global structural modifications which might not be always possible or needed. In the same time the methods for creation of BJP models can be employed for sizing optimization in regard to statics and dynamics with extremely high number of design parameters. This makes both techniques useful in the concept stage of vehicle development.

The presented approaches have been developed and validated on the basis of FE models with varying complexity. Highly simplified academic cases have been employed mostly during the methodological development. All contributions proposed in this dissertation have been applied for at least one problem of industrial relevance involving FE models such as the vehicle subframe of a Lancia K (Chapters 5 and 6), the simplified BMW frame (Chapter 6), the BMW 3 series concept BIW (Chapters 3 and 6), as well as the Toyota Rav4 BIW (Chapters 3, 4 and 7). This increased additionally the value of the developed methodologies as their potential suitability for an industrial context was demonstrated.

8.2 Future work

The complexity of the VDP, and of VCM in particular, is such that it is impossible to address and resolve all existing issues in a single study. In this regard, an eventual continuation of the research presented in this dissertation can be focused on the following directions:

- Concept beams

  The future work with regard to 1D beam modeling could include one or all of the following research topics:

  - The study on the potential error factors in 1D beam FE modeling has been performed only with regard to the beam static behavior. As a next step dynamic validation can be made in terms of mode shapes and eigenfrequencies of the concept and of the reference models.
  - Advanced beam theories (e.g. generalized beam theories, higher-order beam models) are needed to account for the cross-section deformations so that a concept model with better accuracy can be achieved. Most importantly, they must be generally valid not only for academic but also for industrial case studies.
  - The behavior of 1D beam composite structures should be investigated, because of the increased problem complexity on one hand and of their relevance to the automotive industry on the other. In relation to this, the Variational Asymptotic Method (VAM) can easily find its application into VCM.

- 3B method

  The 3B approach can be improved too. An important possible extension is to include handling different plate thicknesses for the ABCS segments. There should be no major obstacles to do this, as LHS allows changing the number of factors and experiments in a flexible way. As discussed in Section 4.6, such improvement should not deteriorate the 3B method performance either. A step even further would be to create 3B relations for managing complex beam structures with material mix and carbon reinforced materials. Additional improvements can be introduced also in regard to the flanges. They should be considered and modeled but must remain unchanged while the rest of the cross-section is rescaled during sizing optimization.

- Concept joints

  Because of their extreme complexity joints can be the subject of a separate dissertation. In regard to continuing the current work, various improvements can be made. If the idea of concept joints as SEs is kept, efforts must be dedicated to improving the connection between dissimilar elements, i.e. the shell elements of the joint end cross-section and the incoming 1D beam. To retain all the benefits of the detailed FE joints, they must be appropriately integrated in the concept model. Their connections to the 1D beams must

not be too flexible, but they must not make the model stiffer either. In this view, either MPCs or some variation of RBE2 (e.g. RBE2 in combination with springs) have the potential of becoming a promising topic for future research.

It must be taken into consideration that if the structural joints need to be varied during the optimization sequence, detailed parametric joints must be used instead of SEs. As an alternative to detailed FE models, simplified joints can be developed too, but a translator detailed-concept joint and vice versa must be created for this purpose. Various studies have shown that a concept joint without strong relation to the actual structural node is often useless. On the other hand, creating parametric detailed joints is difficult and it can turn out to be even more difficult to find out the right simplified joint model. If the translator is also dependent on the joint typology, the problem becomes highly intricate. In this sense the development and use of simplified FE joints in BJP models is still an open question.

- Sizing optimization

  Various improvements and new developments can be made in regard to sizing optimization with DE. They include but are not limited to the following:

  - Parallel implementation of the best performing DE strategy for additional speed-up.
  - Alternative mode tracking strategies to combine with DE and GB.
  - A hybrid DE-GB approach.
  - Optimization with 1D composite beams.

  The use of promising alternative optimizers such as SA, PSO, ACO and Quantum Computing could be also further investigated. Moreover, an optimization can be performed where in addition to resizing the cross-section dimensions also its typology is changed by choosing among a set of predefined ABCS (e.g. a database with the most common cross-sections of different car structures). Special attention must be dedicated to strategies for easy transition from the optimized simplified model to its corresponding detailed FE model. For such transformations morphing techniques can be extremely useful. Finally, the static and dynamic stiffness should be ideally optimized in a multi-disciplinary context together with other performance attributes such as crashworthiness, ride and handling, aerodynamics, durability.

- Surrogate modeling based on mesh morphing

  Improvements in regard to the presented methodology can be introduced in two directions. Firstly, more elaborate approaches for local joint modification must be developed and employed such as parametric detailed FE joints. The most influential joint parameters must be eventually added in the DOE and consequently in the optimization phase. Secondly, it is of even greater interest to attempt performing a multidisciplinary meta-model optimization considering also the vehicle crashworthiness performance. Some attempts

have been made in this direction but the complexity of such problems is much higher with respect to statics or low frequency NVH only. The existing methodologies have not reached maturity yet.

Appendix A

Additional figures

A.1 Vehicle subframe eigenmodes

(a) Reference model. (b) Simplified model.

Figure A.1: Mode 1 with MAC=0.98.

(a) Reference model. (b) Simplified model.

Figure A.2: Mode 2 with MAC=0.92.

(a) Reference model. (b) Simplified model.

Figure A.3: Mode 3 with MAC=0.89.

(a) Reference model. (b) Simplified model.

Figure A.4: Mode 4 with MAC=0.69.

(a) Reference model. (b) Simplified model.

Figure A.5: Mode 5 with MAC=0.79.

(a) Reference model. (b) Simplified model.

Figure A.6: Mode 6 with MAC=0.72.

(a) Reference model. (b) Simplified model.

Figure A.7: Mode 7 with MAC=0.59.

(a) Reference model. (b) Simplified model.

Figure A.8: Mode 8 with MAC=0.51.

(a) Reference model. (b) Simplified model.

Figure A.9: Mode 9 with MAC=0.82.

A.2 Optimization

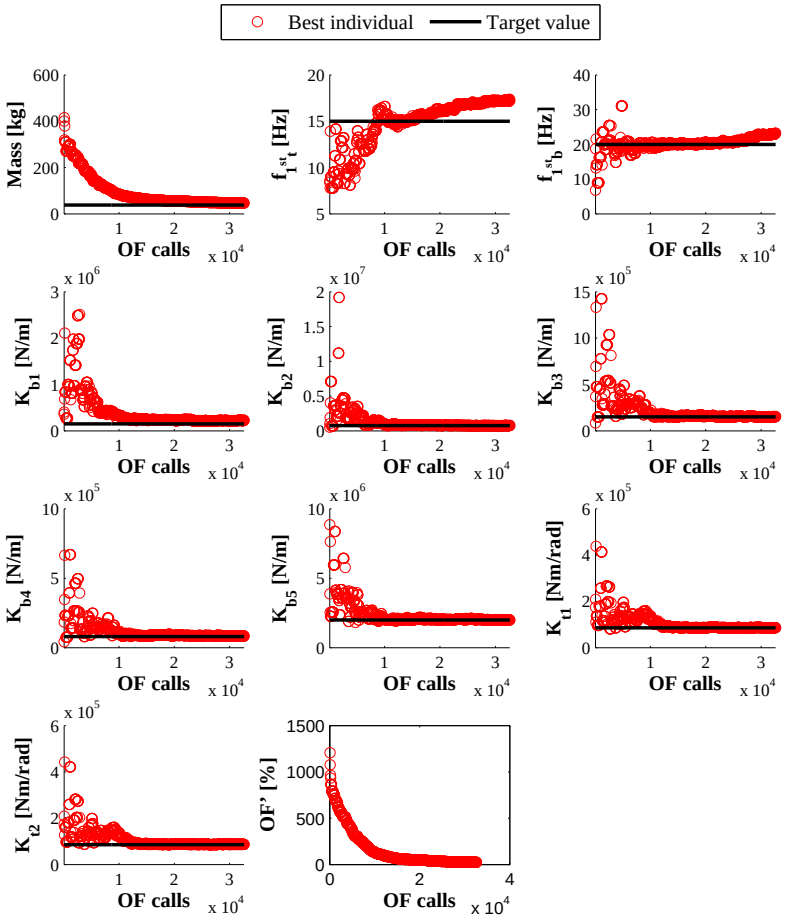

Figure A.10: Vehicle frame, $\mathbf{DE_1}$ OF' and responses.

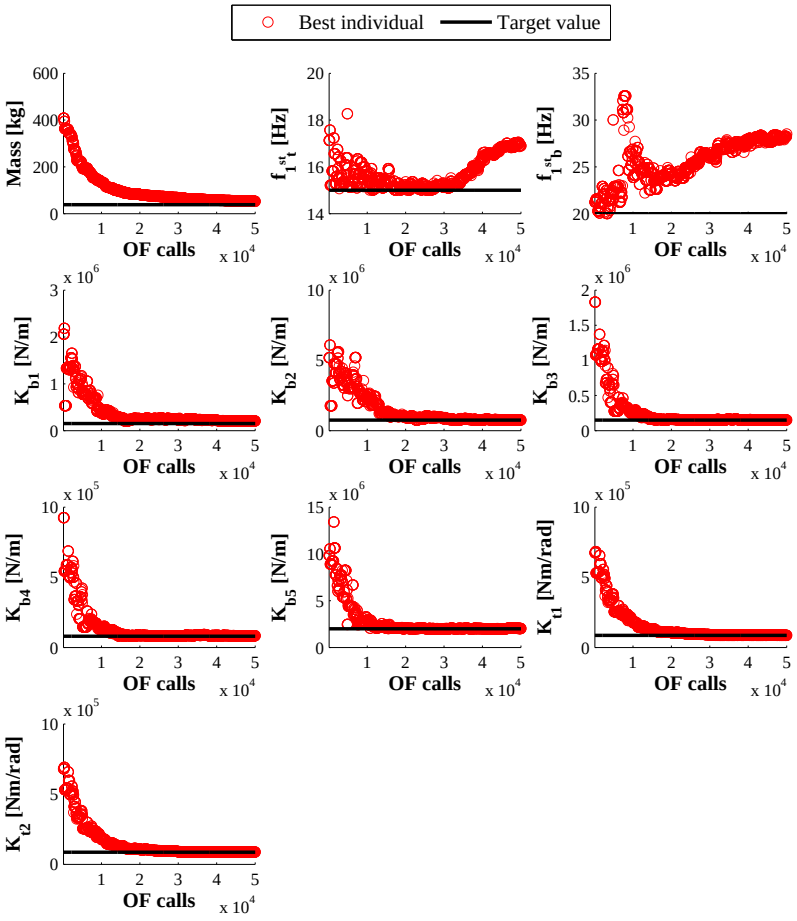

Figure A.11: Vehicle frame, $\mathbf{DE_2}$ responses.

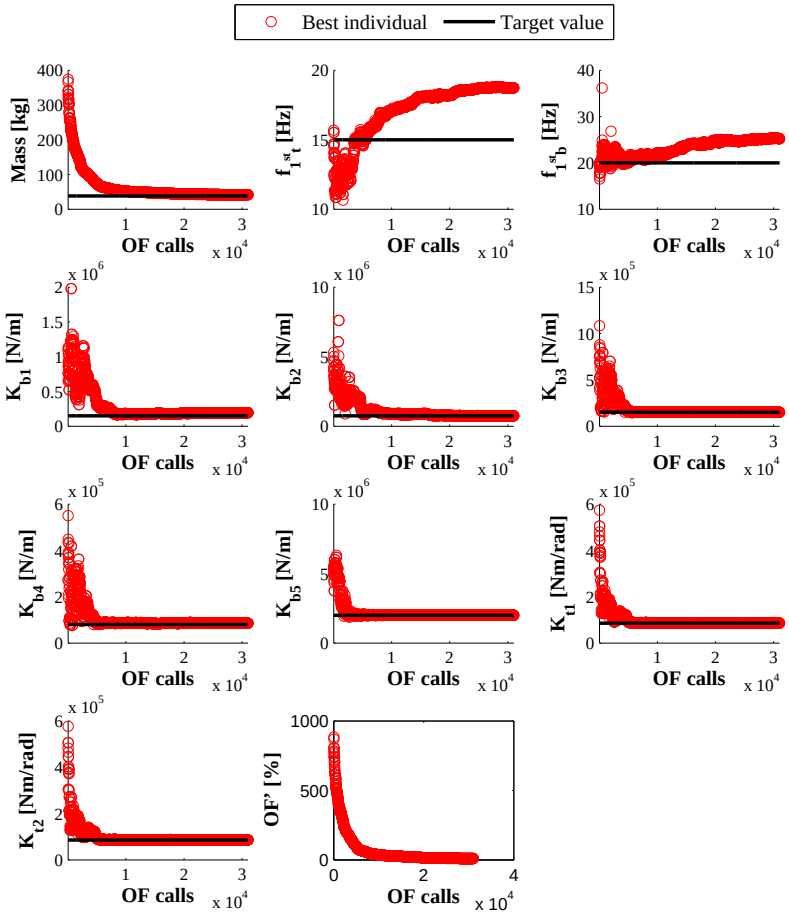

Figure A.12: Vehicle frame, $\mathbf{DE_3}$ OF' and responses.

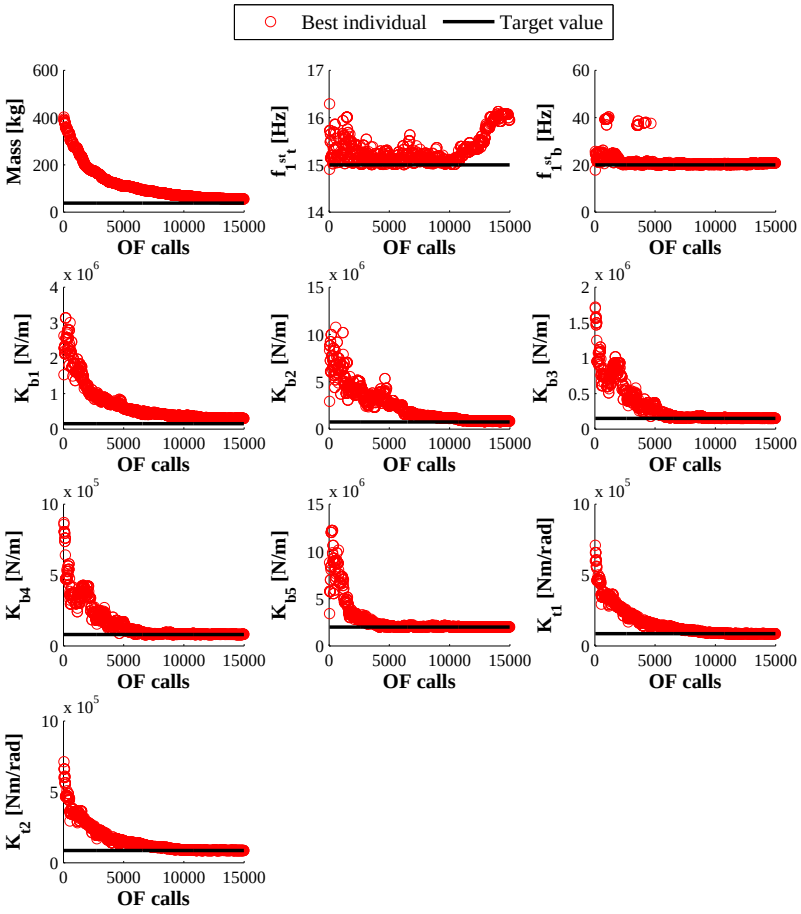

Figure A.13: Vehicle frame, **DE$_4$** responses.

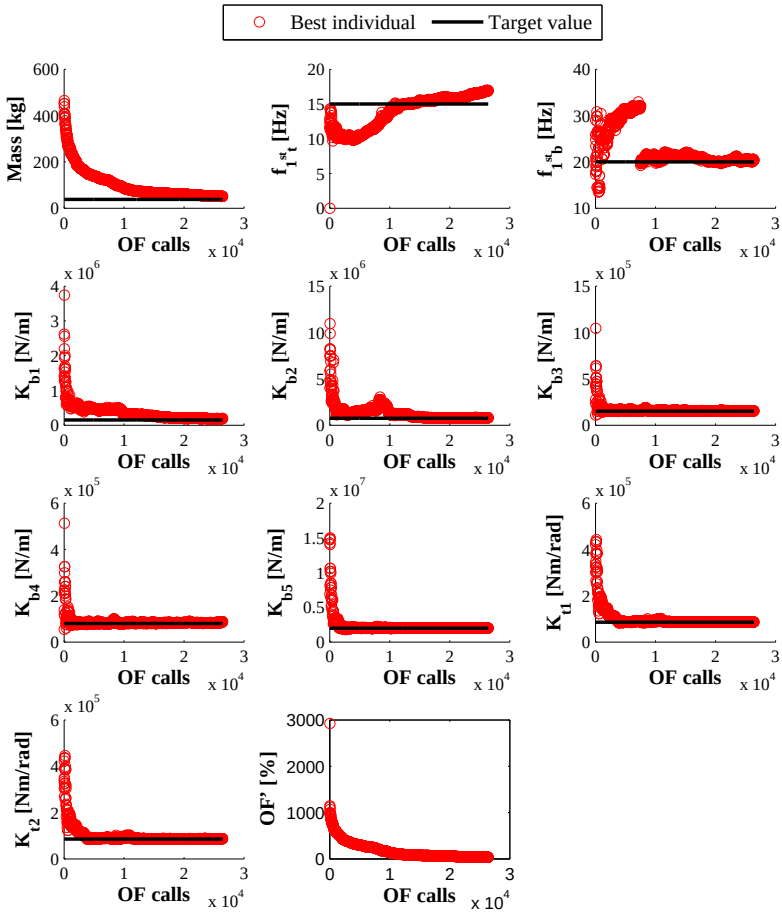

Figure A.14: Vehicle frame, $\mathbf{DE_5}$ OF' and responses.

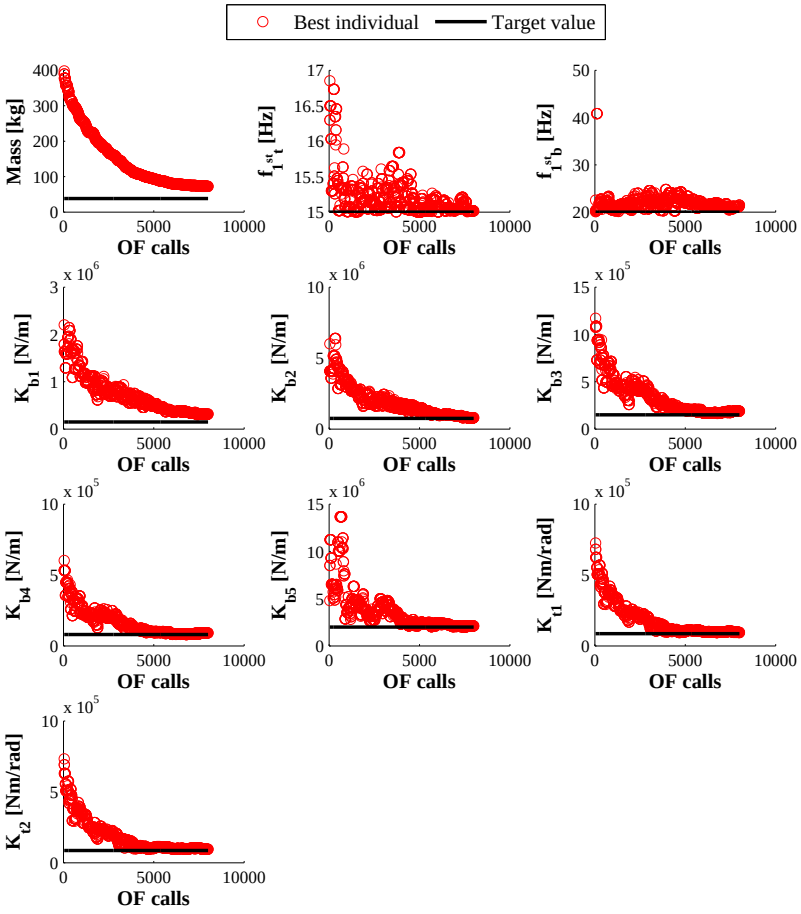

Figure A.15: Vehicle frame, $\mathbf{DE_6}$ responses.

Appendix B

Classical beam theories

A beam is a structure whose axial extension l_{beam} is predominant when compared to any other dimension orthogonal to it [54]. Its cross-section Ω lies in the plane perpendicular to this axis. As shown in Fig. 4.3, the beam displacements, stresses and strains are determined with respect to a Cartesian reference coordinate frame, where z is along the beam axis, while x and y are the in-plane coordinates. The classical beam theories of Euler-Bernoulli [55, 56] and Timoshenko [59, 60] are briefly discussed hereafter. The displacement field, strains, stresses, and resulting forces are derived according to both theories, starting from the a priori hypotheses for the kinematics of slender homogeneous structures under bending loads.

B.1 The Euler-Bernoulli beam theory

The Euler-Bernoulli beam theory (EBBT) is based on the following a priori assumptions [54] (Fig. B.1(a)):

1. The cross-section is rigid on its plane.
2. The cross-section rotates around a neutral surface remaining plane.
3. The cross-section remains perpendicular to the neutral surface during deformation.

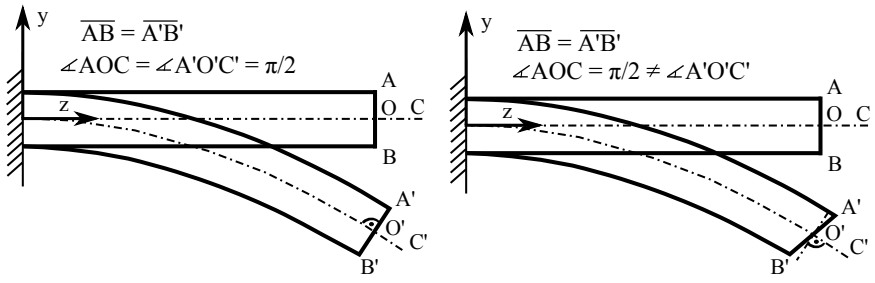

(a) Euler-Bernoulli. (b) Timoshenko.

Figure B.1: Bending of a beam according to different kinematic hypotheses.

As in-plane deformations are not considered according to the first hypothesis, the in-plane displacements u_x and u_y depend only on the axial coordinate z:

$$\begin{cases} \varepsilon_{xx} = \dfrac{\partial u_x}{\partial x} = 0 \\ \varepsilon_{yy} = \dfrac{\partial u_y}{\partial y} = 0 \\ \gamma_{xy} = \dfrac{\partial u_x}{\partial y} + \dfrac{\partial u_y}{\partial x} = 0 \end{cases} \Rightarrow \begin{cases} u_x(x,y,z) = u_{x_1}(z) \\ u_y(x,y,z) = u_{y_1}(z) \end{cases} \tag{B.1}$$

where ε_{xx} and ε_{yy} are the normal strains, and γ_{xy} is the shear strain. Moreover, the out-of-plane displacement u_z is linear versus the in-plane coordinates in consequence of the second hypothesis:

$$u_z(x,y,z) = u_{z_1}(z) + \theta_y(z)x + \theta_x(z)y \tag{B.2}$$

where θ_y and θ_x are the rotation angles along the y- and x-axis respectively. Finally, the shear strains γ_{zy} and γ_{zx} are disregarded, as result of the third hypothesis:

$$\gamma_{zy} = \gamma_{zx} = 0 \tag{B.3}$$

Based on Eqs. B.1, B.2 and B.3, θ_y and θ_x can be obtained as functions of the derivatives of the in-plane displacements:

$$\begin{cases} \gamma_{zx} = \dfrac{\partial u_z}{\partial x} + \dfrac{\partial u_x}{\partial z} = \theta_y + \dfrac{\partial u_{x_1}}{\partial z} = 0 \\ \gamma_{zy} = \dfrac{\partial u_z}{\partial y} + \dfrac{\partial u_y}{\partial z} = \theta_x + \dfrac{\partial u_{y_1}}{\partial z} = 0 \end{cases} \Rightarrow \begin{cases} \theta_y = -\dfrac{\partial u_{x_1}}{\partial z} \\ \theta_x = -\dfrac{\partial u_{y_1}}{\partial z} \end{cases} \tag{B.4}$$

The displacement field of the EBBT can be expressed as:

$$\begin{aligned} u_x &= u_{x_1} \\ u_y &= u_{y_1} \\ u_z &= u_{z_1} - \frac{\partial u_{x_1}}{\partial z}x - \frac{\partial u_{y_1}}{\partial z}y \end{aligned} \tag{B.5}$$

In regard to strains, only the axial strain ε_{zz} is accounted for in the EBBT according to the kinematic hypotheses. Based on its definition and Eq. B.5, ε_{zz} can be expressed as:

$$\varepsilon_{zz} = \frac{\partial u_z}{\partial z} = \frac{\partial u_{z_1}}{\partial z} - \frac{\partial^2 u_{x_1}}{\partial z^2}x - \frac{\partial^2 u_{y_1}}{\partial z^2}y \tag{B.6}$$

Hence, the axial stress σ_{zz} can be obtained:

$$\sigma_{zz} = E\varepsilon_{zz} = E\left(\frac{\partial u_{z_1}}{\partial z} - \frac{\partial^2 u_{x_1}}{\partial z^2}x - \frac{\partial^2 u_{y_1}}{\partial z^2}y\right) \tag{B.7}$$

The stress resultants (Eqs. B.8 to B.10) are obtained after integrating the axial stress on the cross-section. In these equations N is the axial force, whereas M_y

and M_x are the bending moments versus the y-and x-axis respectively. Moreover, S_x and S_y are the first moments of area.

$$N(z) = \int_\Omega \sigma_{zz} d\Omega = E\left(\frac{\partial u_{z_1}}{\partial z}A - \frac{\partial^2 u_{x_1}}{\partial z^2}S_y - \frac{\partial^2 u_{y_1}}{\partial z^2}S_x\right) \tag{B.8}$$

$$M_y(z) = \int_\Omega \sigma_{zz} x d\Omega = E\left(\frac{\partial u_{z_1}}{\partial z}S_y - \frac{\partial^2 u_{x_1}}{\partial z^2}J_{yy} - \frac{\partial^2 u_{y_1}}{\partial z^2}J_{xy}\right) \tag{B.9}$$

$$M_x(z) = -\int_\Omega \sigma_{zz} y d\Omega = -E\left(\frac{\partial u_{z_1}}{\partial z}S_x - \frac{\partial^2 u_{x_1}}{\partial z^2}J_{xy} - \frac{\partial^2 u_{y_1}}{\partial z^2}J_{xx}\right) \tag{B.10}$$

B.2 The Timoshenko beam theory

In the Timoshenko beam theory (TBT) the cross-section is still rigid on its plane and it rotates around a neutral surface remaining plane. However, it is no longer constrained to remain perpendicular to it (Fig. B.1(b)). In this sense, the third kinematic a priori assumption of the EBBT is relaxed [54]. Shear deformations are taken into account.

The displacement field of the TBT is given by:

$$\begin{aligned} u_x(x,y,z) &= u_{x_1}(z) \\ u_y(x,y,z) &= u_{y_1}(z) \\ u_z(x,y,z) &= u_{z_1}(z) + \theta_y(z)x + \theta_x(z)y \end{aligned} \tag{B.11}$$

The non-zero normal and shear strain components are:

$$\begin{aligned} \varepsilon_{zz} &= \frac{\partial u_z}{\partial z} = \frac{\partial u_{z_1}}{\partial z} + \frac{\partial \theta_y}{\partial z}x + \frac{\partial \theta_x}{\partial z}y \\ \gamma_{zx} &= \frac{\partial u_z}{\partial x} + \frac{\partial u_x}{\partial z} = \theta_y + \frac{\partial u_{x_1}}{\partial z} \\ \gamma_{zy} &= \frac{\partial u_z}{\partial y} + \frac{\partial u_y}{\partial z} = \theta_x + \frac{\partial u_{y_1}}{\partial z} \end{aligned} \tag{B.12}$$

The axial and shear stresses can be expressed as:

$$\begin{aligned} \sigma_{zz} &= E\varepsilon_{zz} = E\left(\frac{\partial u_{z_1}}{\partial z} + \frac{\partial \theta_y}{\partial z}x + \frac{\partial \theta_x}{\partial z}y\right) \\ \tau_{zx} &= \kappa G\left(\theta_y + \frac{\partial u_{x_1}}{\partial z}\right) \\ \tau_{zy} &= \kappa G\left(\theta_x + \frac{\partial u_{y_1}}{\partial z}\right) \end{aligned} \tag{B.13}$$

where κ is the shear correction factor, which is related mainly to the cross-section geometry. The shear predictions need to be corrected since the TBT model yields a constant value above the cross-section, whereas it is at least parabolic in order

to satisfy the stress-free boundary conditions on the unloaded edges of the cross-section [54].

Finally, the stress resultants can be obtained. They are given in Eqs. B.14 to B.18, where N is the axial force, M_y and M_x are the bending moments versus the y- and the x-axis respectively, while V_x and V_y are the shear forces along the x- and the y-axis respectively.

$$N = \int_\Omega \sigma_{zz} d\Omega = E \int_\Omega \left(\frac{\partial u_{z_1}}{\partial z} + \frac{\partial \theta_y}{\partial z} x + \frac{\partial \theta_x}{\partial z} y \right) d\Omega \tag{B.14}$$

$$M_y = \int_\Omega \sigma_{zz} x d\Omega = E \int_\Omega \left(\frac{\partial u_{z_1}}{\partial z} x + \frac{\partial \theta_y}{\partial z} x^2 + \frac{\partial \theta_x}{\partial z} xy \right) d\Omega \tag{B.15}$$

$$M_x = -\int_\Omega \sigma_{zz} y d\Omega = -E \int_\Omega \left(\frac{\partial u_{z_1}}{\partial z} y + \frac{\partial \theta_y}{\partial z} xy + \frac{\partial \theta_x}{\partial z} y^2 \right) d\Omega \tag{B.16}$$

$$V_x = \int_\Omega \tau_{zx} d\Omega = \int_\Omega \kappa G \left(\theta_y + \frac{\partial u_{x_1}}{\partial z} \right) d\Omega = \kappa G \left(\theta_y + \frac{\partial u_{x_1}}{\partial z} \right) A \tag{B.17}$$

$$V_y = \int_\Omega \tau_{zy} d\Omega = \int_\Omega \kappa G \left(\theta_x + \frac{\partial u_{y_1}}{\partial z} \right) d\Omega = \kappa G \left(\theta_x + \frac{\partial u_{y_1}}{\partial z} \right) A \tag{B.18}$$

Appendix C

Genetic Algorithm

The GA is a stochastic optimization method that simulates some of the processes observed in natural biological evolution. It modifies repeatedly a population of individual solutions using three main types of rules – selection, crossover and mutation. Over successive generations, the population evolves toward an optimal solution by applying the principle of survival of the fittest. The GA can be applied to solve a variety of optimization problems that are not well suited for standard optimization algorithms, such as problems in which the OF is discontinuous, highly nonlinear or with undefined derivatives. Actually, the GA differs in two key points from any GB method. Firstly, multiple points (individuals) are generated and evaluated at each iteration instead of a single one. The best individual in the population approaches the optimal solution. Secondly, random number generators are used in the creation of each generation in contrast to the rigorously deterministic computations in a GB approach.

The flowchart in Fig. C.1 summarizes how a typical GA works. At first a random initial population is created. It is actually an array of individuals which can be treated as different candidate solutions to the optimization problem. The population is scored and a fitness value is assigned to each individual by means of an OF. Thus the individual with the lowest OF value is considered the fittest one. While the stopping condition is not satisfied (e.g. time or OF value limit), the population is continuously changed and reevaluated, whereas each successive population is called a new generation.

At each step the GA selects certain individuals in the current population, called parents, who contribute their genes (i.e. the entries of their vectors) to create individuals in the next generation, called children. Usually, individuals that have better fitness values are more likely to be selected as parents. Two main types of children are produced. Either random changes are applied to the genes of a single parent (mutation children), or the vector entries (i.e. genes) of two parents are randomly combined (crossover children). Both genetic operators are essential to the GA. Crossover enables the algorithm to extract the best genes from different individuals and recombine them into potentially superior children. Mutation improves the population diversity and thereby increases the chances to obtain fitter individuals. Optionally, a third group of children can be also created – the so called elite children. They correspond to the individuals in the current

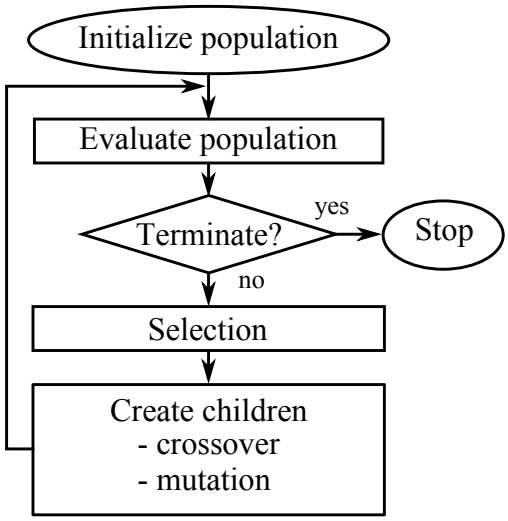

Figure C.1: Flowchart of a typical GA.

generation with the best fitness values. The elite children automatically survive to the next generation so that the best solutions so far are not lost. Finally, all produced children replace the current population and form the next generation to be evaluated. Although in principle the flowchart from Fig. C.1 is followed, the GA variants differ in the strategies applied for selection, mutation and crossover. Furthermore, they vary also in regard to the encoding. Whereas the classical binary GAs are appropriate for variables that are naturally quantized, real-valued GAs are a more logical choice when continuous variables are involved. Finally, GAs are often available not only as a sequential implementation, but they also take advantage of parallel computing which is closer to their nature.

Initially developed by John Holland in the early 1970s [242], the GA has found a wide range of practical applications including not only optimization, but also robotics, machine learning, signal processing, design, economics, bioinformatics and many others. Thanks to its strengths, it is still one of the most popular approaches for engineering optimization. The GA performs well for many types of problems as it does not make any assumptions about the underlying shape of the OF. In fact, it can be extremely useful in problem domains with a complex fitness landscape as mutation and crossover are designed to move the population away from local optima. The GA always results in an answer, which becomes better and better with time. It can cover large search spaces and, most importantly, it is capable of quickly finding promising regions within them. The GA not only has the potential to give a solution for a highly complex search space, but it is able to provide multiple ones and the final choice among them is left to the designer. If the optimization problem does not have a single solution, design alternatives can be identified simultaneously.

Bibliography

[1] S. Donders. *Computer-aided engineering methodologies for robust automotive NVH design*. PhD thesis, K. U. Leuven, 2008.

[2] H. Shiozaki, Y. Kamada, S. Kurita, S. Goossens, J. Van Herbruggen, V. Cibrario, and L. Poppelaars. CAE based vehicle development to reduce development time. In *Proceedings of the JSAE Annual Congress*, volume 20, Yokohama, Japan, May 20 2005.

[3] D. Talabă and A. Amditis, editors. *Product Engineering: Tools and Methods Based on Virtual Reality*, volume 35. Springer Verlag, 2008.

[4] J. Weber. *Automotive Development Processes: Processes for Successful Customer Oriented Vehicle Development*. Springer, July 2009.

[5] K. Ehrlenspiel. *Integrierte Produktentwicklung: Methoden für Prozeßorganisation, Produkterstellung und Konstruktion*. Hanser, 2. edition, 2003.

[6] K. Ehrlenspiel, A. Kiewert, and U. Lindemann. *Kostengünstig Entwickeln und Konstruieren: Kostenmanagement bei der integrierten Produktentwicklung*. Springer, 6. aufl. 2007 edition, September 2007.

[7] T. J. R. Hughes, J. A. Cottrell, and Y. Bazilevs. Isogeometric analysis: CAD, finite elements, NURBS, exact geometry and mesh refinement. *Computer Methods in Applied Mechanics and Engineering*, 194(39–41):4135–4195, 2005.

[8] S. Donders, Y. Takahashi, R. Hadjit, T. Van Langenhove, M. Brughmans, B. Van Genechten, and W. Desmet. A reduced beam and joint concept modeling approach to optimize global vehicle body dynamics. *Finite Elements in Analysis and Design*, 45(6-7):439–455, 2009.

[9] D. Crolla. *Automotive Engineering: Powertrain, Chassis System and Vehicle Body*. Butterworth-Heinemann, July 2009.

[10] L. Morello, L. R. Rossini, G. Pia, and A. Tonoli. *The Automotive Body: Volume I: Components Design*. Springer, 1st edition. edition, December 2010.

[11] L. Morello, L. R. Rossini, G. Pia, and A. Tonoli. *The Automotive Body: Volume II: System Design*. Springer, 1st edition. edition, December 2010.

[12] H. Heisler. *Advanced Vehicle Technology*. Butterworth-Heinemann Ltd, 2nd revised edition edition, July 2002.

[13] G. Genta and L. Morello. *The Automotive Chassis: Volume 2: System Design*. Springer, 1 edition, February 2009.

[14] G. Genta and L. Morello. *The Automotive Chassis: Volume 1: Components Design*. Springer, February 2009.

[15] J. C. Brown, A. J. Robertson, and S. T. Serpento. *Motor Vehicle Structures: Concepts and Fundamentals*. Butterworth-Heinemann Ltd, October 2001.

[16] J. Happian-Smith. *An Introduction to Modern Vehicle Design*. Elsevier, July 2001.

[17] E. Baumgart. Stiffness – an unknown world of mechanical science? *Injury*, 31:14–84, 2000.

[18] J. Helsen, L. Cremers, P. Mas, and P. Sas. Global static and dynamic car body stiffness based on a single experimental modal analysis test. In *Proceedings of the International Conference on Noise and Vibration Engineering ISMA 2010*, Leuven, Belgium, September 20–22 2010.

[19] A. E. Duncan, F. Su, and W. Wolf. Understanding NVH basics. In *International Body Engineering Conference Proceedings, IBEC*, Detroit, Michigan, USA, October 1–3 1996.

[20] G. Osborne, G. Prater, R. Lesiv, D. Lamb, and M. Castanier. Vehicle concept model abstractions for integrated geometric, inertial, rigid body, powertrain, and FE analysis. In *Proceedings of the ASME 2011 International Mechanical Engineering Congress & Exposition*, Denver, Colorado, USA, November 11–17 2011.

[21] M. Carpinelli, D. Mundo, T. Tamarozzi, M. Gubitosa, S. Donders, and W. Desmet. Integrating vehicle body concept modelling and flexible multibody techniques for ride and handling simulations. In *Proceedings of the ESDA Biennial Conference on Engineering Systems Design and Analysis*, Nantes, France, July 2–4 2012.

[22] D. Mundo, R. Hadjit, S. Donders, M. Brughmans, P. Mas, and W. Desmet. Simplified modelling of joints and beam-like structures for BIW optimization in a concept phase of the vehicle design process. *Finite Elements in Analysis and Design*, 45(6-7):456–462, 2009.

[23] G. Stigliano, D. Mundo, S. Donders, and T. Tamarozzi. Advanced vehicle body concept modeling approach using reduced models of beams and joints. In *Proceedings of the International Conference on Noise and Vibration Engineering ISMA 2010*, Leuven, Belgium, September 20–22 2010.

[24] D. Mundo, A. Maressa, N. Rizzo, S. Donders, and W. Desmet. A database framework for industrial vehicle body concept modelling. In *Proceedings of the 3rd WSEAS International Conference on Finite Differences - Finite Elements - Finite Volumes - Boundary Elements, F-and-B '10*, Bucharest, Romania, April 20–22 2010.

[25] A. Maressa, D. Mundo, S. Donders, and W. Desmet. A wave-based substructuring approach for concept modeling of vehicle joints. *Computers & Structures*, 89(23):2369–2376, 2011.

[26] D. Mundo, S. Donders, R. Hadjit, G. Stigliano, P. Mas, and H. Van Der Auweraer. Concept modelling of automotive beams, joints and panels. In *Proceedings of the 3rd WSEAS International Conference on Finite Differences - Finite Elements - Finite Volumes - Boundary Elements, (F-and-B '10)*, Bucharest, Romania, April 20–22 2010.

[27] N. Baldanzini and M. Pierini. Sviluppo di un metodo automatico di modal updating tramite algoritmi genetici. In *Proceedings of the 29th National Conference AIAS*, pages 47–56, Lucca, Italy, September 6–9 2000.

[28] N. Baldanzini, P. Citti, and M. Pierini. An improved method for updating simplified finite element models of mechanical systems. In *Proceedings of the 11th International Pacific Conference on Automotive Engineering*, Shanghai, China, November 6–9 2001.

[29] N. Baldanzini, D. Caprioli, and M. Pierini. Designing the dynamic behavior of an engine suspension system through genetic algorithms. *Journal of Vibration and Acoustics*, 123(4):480–486, 2001.

[30] N. Baldanzini. *Sviluppo di tecniche di ottimizzazione per la progettazione meccanica*. PhD thesis, Università degli Studi di Firenze, 2001.

[31] N. Baldanzini and A. Scippa. Shape and size optimization of an engine suspension system. In *Proceedings of the International Conference on Noise and Vibration Engineering – ISMA 2004*, pages 3539–3554, Leuven, Belgium, September 20–22 2004.

[32] T. M. Cameron, A. C. Thirunavukarasu, and M. E. M. El-Sayed. Optimization of frame structures with flexible joints. *Structural and Multidisciplinary Optimization*, 19(3):204–213, 2000.

[33] Y. Dai and C. Duan. Beam element modelling of vehicle body-in-white applying artificial neural network. *Applied Mathematical Modelling*, 33(6):2808–2817, 2009.

[34] G. De Gaetano, F.I. Cosco, C. Maletta, D. Mundo, and S. Donders. Dynamic FE-based method for concept modelling of vehicle beam-like structures. In *Proceedings of the International Conference on Noise and Vibration Engineering ISMA 2012*, pages 3725–3736, Leuven, Belgium, September 17–19 2012.

[35] M. Fard, N. Nasrollahzadeh, M. Tatari, and M. Mahjoob. Automotive body-in-white concept modeling method for the NVH performance optimization. In *Proceedings of the International Conference on Noise and Vibration Engineering ISMA 2012*, pages 3753–3763, Leuven, Belgium, September 17–19 2012.

[36] P. Mihaylova, N. Baldanzini, A. Pratellesi, and M. Pierini. On the improvement of concept modeling of joints within simplified finite element models with application to structural dynamics. In *Proceedings of the International Conference on Noise and Vibration Engineering ISMA 2010*, Leuven, Belgium, September 20–22 2010.

[37] P. Mihaylova, N. Baldanzini, A. Pratellesi, and M. Pierini. Beam Bounding Box – a novel approach for beam concept modeling and optimization handling. *Finite Elements in Analysis and Design*, 60:13–24, 2012.

[38] P. Mihaylova, N. Baldanzini, and M. Pierini. Considerations on 1D beam concept modelling for the vehicle structure. In *Proceedings of the International Conference on Noise and Vibration Engineering ISMA 2012*, pages 3793–3807, Leuven, Belgium, September 17–19 2012.

[39] P. Mihaylova, N. Baldanzini, and M. Pierini. Advanced sizing optimization of concept vehicle structures. Manuscript submitted for publication. *International Journal of Vehicle Design*, 2012.

[40] P. Mihaylova, N. Baldanzini, and M. Pierini. Potential error factors in 1D beam FE modeling for the early stage vehicle design. Manuscript submitted for publication. *Finite Elements in Analysis and Design*, 2012.

[41] A. Moroncini, L. Cremers, and M. Kroiss. NVH structural optimization using beams and shells FE concept models in the early car development phase at BMW. In *Proceedings of the International Conference on Noise and Vibration Engineering ISMA 2010*, Leuven, Belgium, September 20–22 2010.

[42] A. Moroncini, L. Cremers, and N. Baldanzini. Car body concept modeling for NVH optimization in the early design phase at BMW: a critical review and new advanced solutions. In *Proceedings of the International Conference on Noise and Vibration Engineering ISMA 2012*, pages 3809–3823, Leuven, Belgium, September 17–19 2012.

[43] G. M. Osborne, G. Prater, and A. M. Shahhosseini. Finite element concept modelling methodologies for pickup truck boxes. *International Journal of Heavy Vehicle Systems*, 17(1):1–17, 2010.

[44] J. Will, I. Raasch, C. Bucher, and J. Riedel. Suche nach alternativen Gesamtfahrzeugkonzepten mit OptiSLang. In *Proceedings Weimarer Optimierungs- und Stochastiktage*, volume 1, Weimar, Germany, December 2–3 2004.

[45] R. Hadjit, S. Donders, M. Brughmans, and L. Hermans. Analysis and optimization of vehicle body global dynamics using reduced model and concept modifications. In *Proceedings of the 12th International Congress on Sound and Vibration*, Lisbon, Portugal, July 11–14 2005.

[46] N. Lyu and K. Saitou. Decomposition-based assembly synthesis for structural stiffness. *Transactions of the ASME, Journal of Mechanical Design*, 125(3):452–463, 2003.

[47] N. Lyu and K. Saitou. Decomposition-based assembly synthesis of a three-dimensional body-in-white model for structural stiffness. *Journal of mechanical design*, 127(1):34–48, 2005.

[48] B. Yannou, A. Hamdi, and E. Landel. Une stratégie de modélisation conceptuelle pour la prise en compte de performances vibro-acoustiques en préconception d'un berceau automobile. *Mécanique & industries*, 4(4):365–376, 2003.

[49] C. Reed. Applications of Optistruct optimization to body in white design. *Proceedings of Altair Engineering Event, Coventry, UK*, 2002.

[50] T. Tamarozzi, G. Stigliano, M. Gubitosa, S. Donders, and W. Desmet. Investigating the use of reduction techniques in concept modeling for vehicle body design optimization. In *Proceedings of the International Conference on Noise and Vibration Engineering ISMA 2010*, Leuven, Belgium, September 20–22 2010.

[51] R. Hadjit, M. Brughmans, and H. Shiozaki. Application of fast body optimization procedures to shorten car development cycles. In *Proceedings of the JSAE Annual Congress*, volume 18, Yokohama, Japan, May 18–20 2005.

[52] N. Lyu, B. Lee, and K. Saitou. Optimal subassembly partitioning of space frame structures for in-process dimensional adjustability and stiffness. *Journal of Mechanical Design*, 128:527–535, 2006.

[53] M. Kaufmann, B. Lauber, Katzenschwanz C., J. Helsen, L. Cremers, P. Mas, and P. Sas. Optimization of a vehicle front part structure at Audi using ANSA morphing and OPTIMUS. In *Proceedings of the 2nd ANSA & mETA International Congress*, pages 159–168, Halkidiki, Greece, June 14–15 2007.

[54] E. Carrera, G. Giunta, and M. Petrolo. *Beam Structures: Classical and Advanced Theories*. Wiley, 2011.

[55] L. Euler. De curvis elasticis. *Lausanne und Genf*, pages 245–310, 1744.

[56] D. Bernoulli. De vibrationibus et sono laminarum elasticarum. *Commentarii Academiae Scientiarum Imperialis Petropolitanae*, 13:105–120, 1751.

[57] A. J. C. B. de Saint-Venant. Mémoire sur la flexion des prismes. *Journal de mathématiques pures et appliquées*, 1:89–189, 1856.

[58] A. J. C. B. de Saint-Venant. Mémoire sur la torsion des prismes. *Mémoires présentés par divers savants à l'Académie des Sciences de l'Institut Impérial de France*, 14:233–560, 1856.

[59] S. P. Timoshenko. On the transverse vibrations of bars of uniform cross-section. *Philosophical Magazine*, 43(6):125–131, 1922.

[60] S. P. Timoshenko. On the correction for shear of the differential equation for transverse vibrations of prismatic bars. *The London, Edinburgh, and Dublin Philosophical Magazine and Journal of Science*, 41(245):744–746, 1921.

[61] S. P. Timoshenko and J. M. Gere. *Theory of Elastic Stability*. McGraw-Hill, 1961.

[62] G. R. Cowper. The shear coefficient in Timoshenko's beam theory. *Journal of applied mechanics*, 33:335–340, 1966.

[63] F. Gruttmann, R. Sauer, and W. Wagner. Shear stresses in prismatic beams with arbitrary cross-sections. *International journal for numerical methods in engineering*, 45(7):865–889, 1999.

[64] F. Gruttmann and W. Wagner. Shear correction factors in Timoshenko's beam theory for arbitrary shaped cross-sections. *Computational mechanics*, 27(3):199–207, 2001.

[65] A. V. Krishna Murty. On the shear deformation theory for dynamic analysis of beams. *Journal of Sound and Vibration*, 101(1):1–12, 1985.

[66] I. Mechab, A. Tounsi, and M. A. Benatta. Deformation of short composite beam using refined theories. *Journal of Mathematical Analysis and Applications*, 346(2):468–479, 2008.

[67] P. F. Pai and M. J. Schulz. Shear correction factors and an energy-consistent beam theory. *International journal of solids and structures*, 36(10):1523–1540, 1999.

[68] I. S. Sokolnikoff and R. D. Specht. *Mathematical Theory of Elasticity*, volume 83. McGraw-Hill New York, 1956.

[69] W. Wagner and F. Gruttmann. A displacement method for the analysis of flexural shear stresses in thin-walled isotropic composite beams. *Computers & structures*, 80(24):1843–1851, 2002.

[70] R. El Fatmi and H. Zenzri. On the structural behavior and the saint venant solution in the exact beam theory: application to laminated composite beams. *Computers & structures*, 80(16):1441–1456, 2002.

[71] R. El Fatmi and H. Zenzri. A numerical method for the exact elastic beam theory. Applications to homogeneous and composite beams. *International Journal of Solids and Structures*, 41(9):2521–2537, 2004.

[72] R. El Fatmi. Non-uniform warping including the effects of torsion and shear forces. part II: analytical and numerical applications. *International journal of solids and structures*, 44(18):5930–5952, 2007.

[73] R. El Fatmi. Non-uniform warping including the effects of torsion and shear forces. part I: a general beam theory. *International journal of solids and structures*, 44(18):5912–5929, 2007.

[74] R. El Fatmi. A non-uniform warping theory for beams. *Comptes Rendus Mecanique*, 335(8):467–474, 2007.

[75] B. L. Krayterman and A. B. Krayterman. Generalized nonuniform torsion of beams and frames. *Journal of Structural Engineering*, 113(8):1772–1787, 1987.

[76] MSC.Software. *MSC.Nastran 2004 Reference Manual*. MSC.Software, 2004.

[77] V. Berdichevsky, E. Armanios, and A. Badir. Theory of anisotropic thin-walled closed-cross-section beams. *Composites Engineering*, 2(5):411–432, 1992.

[78] B. Popescu and D. H. Hodges. On asymptotically correct Timoshenko-like anisotropic beam theory. *International Journal of Solids and Structures*, 37(3):535–558, 2000.

[79] V. V. Volovoi, D. H. Hodges, V. L. Berdichevsky, and V. G. Sutyrin. Asymptotic theory for static behavior of elastic anisotropic I-beams. *International journal of solids and structures*, 36(7):1017–1043, 1999.

[80] V. V. Volovoi and D. H. Hodges. Theory of anisotropic thin-walled beams. *Transactions of the ASME, Journal of Applied Mechanics*, 67(3):453–459, 2000.

[81] W. Yu, D. H. Hodges, V. Volovoi, and C. E. S. Cesnik. On Timoshenko-like modeling of initially curved and twisted composite beams. *International Journal of Solids and Structures*, 39(19):5101–5121, 2002.

[82] W. Yu, V. V. Volovoi, D. H. Hodges, and X. Hong. Validation of the variational asymptotic beam sectional analysis (VABS). *AIAA journal*, 40(10):2105–2113, 2002.

[83] W. Yu and D. H. Hodges. Elasticity solutions versus asymptotic sectional analysis of homogeneous, isotropic, prismatic beams. *Journal of Applied Mechanics*, 71:15–23, 2004.

[84] W. Yu and D. H. Hodges. Generalized Timoshenko theory of the variational asymptotic beam sectional analysis. *Journal of the American Helicopter Society*, 50(1):46–55, 2005.

[85] P. B. Dinis, D. Camotim, and N. Silvestre. GBT formulation to analyse the buckling behaviour of thin-walled members with arbitrarily branched open cross-sections. *Thin-walled structures*, 44(1):20–38, 2006.

[86] R. Schardt. Eine Erweiterung der technischen Biegetheorie zur Berechnung prismatischer Faltwerke. *Der Stahlbau*, 35:161–171, 1966.

[87] R. Schardt. *Verallgemeinerte technische Biegetheorie*. Springer Berlin etc., 1989.

[88] R. Schardt. Generalized beam theory – an adequate method for coupled stability problems. *Thin-walled structures*, 19(2):161–180, 1994.

[89] N. Silvestre and D. Camotim. First-order generalised beam theory for arbitrary orthotropic materials. *Thin-Walled Structures*, 40(9):755–789, 2002.

[90] N. Silvestre and D. Camotim. Second-order generalised beam theory for arbitrary orthotropic materials. *Thin-Walled Structures*, 40(9):791–820, 2002.

[91] N. Silvestre and D. Camotim. GBT buckling analysis of pultruded FRP lipped channel members. *Computers & structures*, 81(18):1889–1904, 2003.

[92] N. Silvestre. Generalised beam theory to analyse the buckling behaviour of circular cylindrical shells and tubes. *Thin-walled structures*, 45(2):185–198, 2007.

[93] E. Carrera and E. Antona. *A Class of Two-Dimensional Theories for Anisotropic Multilayered Plates Analysis*. Accademia delle Scienze, 1995.

[94] E. Carrera. Theories and finite elements for multilayered, anisotropic, composite plates and shells. *Archives of Computational Methods in Engineering*, 9(2):87–140, 2002.

[95] E. Carrera. Theories and finite elements for multilayered plates and shells: a unified compact formulation with numerical assessment and benchmarking. *Archives of Computational Methods in Engineering*, 10(3):215–296, 2003.

[96] E. Carrera, S. Brischetto, A. Robaldo, O. Polit, T. Wallmersperger, and C. A. M. Soares. Variable kinematic model for the analysis of functionally graded material plates. *AIAA journal*, 46(1):194–203, 2008.

[97] E. Carrera and G. Giunta. Refined beam theories based on a unified formulation. *International Journal of Applied Mechanics*, 2(01):117–143, 2010.

[98] W. Kanok-Nukulchai and Y. S. Shin. Versatile and improved higher-order beam element. *Journal of Structural Engineering*, 110(9):2234–2249, 1984.

[99] K. Washizu. *Variational Methods in Elasticity and Plasticity*. Pergamon Press, New York, 1982.

[100] MSC.Software. *MD Nastran 2010 Design Sensitivity and Optimization User's Guide*. MSC.Software, 2010.

[101] A. M. Shahhosseini, G. Prater, G. M. Osborne, and E. Y. Kuo. Major compliance joint modelling survey for automotive body structures. *International Journal of Vehicle Systems Modelling and Testing*, 5(1):1–17, 2010.

[102] Y. -M. Moon, T. -H. Jee, and Y. -P. Park. Development of an automotive joint model using an analytically based formulation. *Journal of Sound and Vibration*, 220(4):625–640, 1999.

[103] N. Bylund. *Simulation driven product development applied to car body design.* PhD thesis, Lulea University of Technology, 2004.

[104] L. Long. *Design-oriented translators for automotive joints.* PhD thesis, Virginia Polytechnic Institute and State University, 1998.

[105] E. Nikolaidis and M. Zhu. Design of automotive joints: using neural networks and optimization to translate performance requirements to physical design parameters. *Computers and Structures*, 60(6):989–1001, 1996.

[106] E. Nikolaidis, L. Long, and Q. Ling. Neural networks and response surface polynomials for design of vehicle joints. *Computers & Structures*, 75(6):593–607, 2000.

[107] G. -W. Jang and Y. Y. Kim. Vibration analysis of piecewise straight thin-walled box beams without using artificial joint springs. *Journal of Sound and Vibration*, 326(3-5):647–670, 2009.

[108] K. Lee and E. Nikolaidis. Effect of member length on the parameter estimates of joints. *Computers and Structures*, 68(4):381–391, 1998.

[109] P. R. Marur. Analysis of thin-walled frames considering joint flexibilities. *Proceedings of the Institution of Mechanical Engineers, Part D: Journal of Automobile Engineering*, 221(10):1221–1230, 2007.

[110] H. Fredricson, T. Johansen, A. Klarbring, and J. Petersson. Topology optimization of frame structures with flexible joints. *Structural and multidisciplinary optimization*, 25(3):199–214, 2003.

[111] R. Guyan. Reduction of mass and stiffness matrices. *AIAA Journal*, 3(2):380, 1965.

[112] M. W. Suh, J. Suhr, and W. H. Yang. Condensed joint matrix method for the joint structure of a vehicle body. *Proceedings of the Institution of Mechanical Engineers, Part D: Journal of Automobile Engineering*, 216(1):35–41, 2002.

[113] N. Bylund and M. Eriksson. Simulation driven car body development using property based models. *SAE papers*, 2001.

[114] N. Bylund. ADRIAN: a software for computing the stiffness of automotive joints and its application in the product development process. *Journal of Computing and Information Science in Engineering*, 5(4):388–393, 2005.

[115] H. Sandström and M. Shamlo. Development of ADRIAN joint analysis software. Master's thesis, Chalmers University of Technology, 2002.

[116] S. B. Lee, J. R. Park, and H. J. Yim. Numerical approximation of vehicle joint stiffness by using response surface method. *International journal of automotive technology*, 3(3):117–122, 2002.

[117] N. Bylund. Fast and economic stiffness evaluation of mechanical joints. In *Proceedings of IBEC 2003 International Body Engineering Conference*, Chiba, Japan, October 27–29 2003.

[118] N. Bylund. Models, methods and tools for car body development. Master's thesis, Lulea University of Technology, 2002.

[119] N. Bylund, H. Fredericson, and G. Thompson. A design process for complex mechanical structures using property based models, with application to car bodies. In *Proceedings of the 7th International Design Conference*, pages 611–620, Dubrovnik, Croatia, May 14–17 2002.

[120] N. Bylund, O. Isaksson, V. Kalhori, and T. Larsson. Enhanced engineering design practice using knowledge enabled engineering with simulation methods. In *Proceedings of the 8th International Design Conference*, Dubrovnik, Croatia, May 18–21 2004.

[121] P. J. Wyatt Becker, R. H. Wynn Jr, E. J. Berger, and J. R. Blough. Using rigid-body dynamics to measure joint stiffness. *Mechanical systems and signal processing*, 13(5):789–801, 1999.

[122] MSC.Software. *MD/MSC Nastran 2010 Quick Reference Guide*. MSC.Software, 2010.

[123] S. Raghu. *Finite Element Modelling Techniques: in MSC. NASTRAN and LS/DYNA*. CreateSpace, September 2010.

[124] J. H. Kim, H. Seok Kim, D. Woon Kim, and Y. Y. Kim. New accurate efficient modeling techniques for the vibration analysis of T-joint thin-walled box structures. *International Journal of Solids and Structures*, 39(11):2893–2909, 2002.

[125] H. Van der Auweraer, T. Van Langenhove, M. Brughmans, I. Bosmans, N. Masri, and S. Donders. Application of mesh morphing technology in the concept phase of vehicle development. *International journal of vehicle design*, 43(1):281–305, 2007.

[126] H. Zimmer and M. Prabhuwaingankar. Implicitly parametric CRASH and NVH analysis models in the vehicle concept design phase. In *LS-DYNA Conference*, Bamberg, Germany, October 14–15 2005.

[127] M. Alexa. Recent advances in mesh morphing. *Computer Graphics Forum*, 21(2):173–198, 2002.

[128] M. Danti, M. Meneguzzo, R. Saponaro, and I. Kowarska. Multi-objective optimization in vehicle concept modeling. In *Proceedings of the International Conference on Noise and Vibration Engineering ISMA 2010*, pages 4095–4108, Leuven, Belgium, September 20–22 2010.

[129] H. Van der Auweraer, T. Van Langenhove, M. Brughmans, N. El Masri, and T. Olbrechts. Advanced mesh based design optimization for early-stage virtual prototyping. In *Proceedings of the International Conference on Noise and Vibration Engineering ISMA 2004*, pages 919–932, Leuven, Belgium, September 20–22 2004.

[130] M. Brughmans and S. Goossens. Cross-attribute optimization to support the vehicle development process by simulation-driven design. *SAE transactions*, 111(6):1882–1890, 2002.

[131] P. Mihaylova, A. Pratellesi, N. Baldanzini, and M. Pierini. Optimization of the global static and dynamic performance of a vehicle body by means of response surface models. In *ASME 2012 11th Biennial Conference on Engineering Systems Design and Analysis – ESDA2012*, Nantes, France, July 2–4 2012.

[132] P. Mihaylova, A. Pratellesi, N. Baldanzini, and M. Pierini. Surrogate-based optimization of the global static and dynamic performance of a vehicle body. In *Proceedings of the 8th European Solid Mechanics Conference ESMC2012*, Graz, Austria, July 9–13 2012.

[133] E. Schelkle and H. Elsenhans. Virtual vehicle development in the concept stage – current status of CAE and outlook on the future. In *Proceedings of the 3rd MSC worldwide aerospace conference and technology showcase*, Toulouse, France, September 24–26 2001.

[134] C. B. Chapman and M. Pinfold. The application of a knowledge based engineering approach to the rapid design and analysis of an automotive structure. *Advances in Engineering Software*, 32(12):903–912, 2001.

[135] M. Pinfold and C. Chapman. The application of KBE techniques to the FE model creation of an automotive body structure. *Computers in Industry*, 44(1):1–10, 2001.

[136] W. B. Hou, H. Z. Zhang, R. F. Chi, and P. Hu. Development of an intelligent CAE system for auto-body concept design. *International Journal of Automotive Technology*, 10(2):175–180, 2009.

[137] A. Hänschke, S. Zhou, M. Lee, J. Hilmann, E. Kaba, and M. Prabhuwaingankar. Parametric model knowledgebase for vehicle design to improve the early vehicle attribute assessments. In *Proceedings of the International Automotive Body Congress (IABC)*, Berlin, Germany, June 17–19 2007.

[138] J. Hilmann, M. Paas, A. Haenschke, and T. Vietor. Automatic concept model generation for optimisation and robust design of passenger cars. *Advances in Engineering Software*, 38(11):795–801, 2007.

[139] U. Lobenwein and M. Quadbeck. Multidisziplinäre Strukturoptimierung einer Motorhaube. Technical report, Technical report, Engineering and Design AG, EDAG, Sindelfingen, Germany, 2006.

[140] F. Duddeck, D. Heiserer, and J. Lescheticky. Stochastic methods for optimization of crash and NVH problems. In *Proceedings of the Second MIT Conference on Computational Fluid and Solid Mechanics*, Cambridge, Massachusetts, USA, June 17–20 2003.

[141] E. Schelkle and H. Elsenhans. Integration innovativer CAE-Werkzeuge in die PKW-Konzeptentwicklung. *Berechnung und Simulation im Fahrzeug*, 14:15, 2000.

[142] K. Volz. Car body design in the concept stage of vehicle development. In *Proceedings of the 2nd European LS-DYNA Conference*, pages 14–15, Gothenburg, Sweden, June 14–15 1999.

[143] K. Volz and F. Duddeck. Crash optimization of car bodies in the concept stage of vehicle development. In *3rd MIT Conference on Computational Fluid and Solid Mechanics*, pages 1315–1319, Boston, USA, June 14–17 2005.

[144] K. Volz, B. Frodl, F. Dirschmid, R. Stryczek, and H. Zimmer. Optimizing topology and shape for crashworthiness in vehicle product development. In *International Automotive Body Congress (IABC)*, Berlin, Germany, June 17–19 2007.

[145] H. Zimmer, A. Hövelmann, H. Schmidt, U. Umlauf, B. Frodl, and U. Hänle. Entwurfstool zur Generierung parametrischer, virtueller Prototypen im Fahrzeugbau. *VDI-Berichte*, 1559, 2000.

[146] R. Roy, S. Hinduja, and R. Teti. Recent advances in engineering design optimisation: Challenges and future trends. *CIRP Annals-Manufacturing Technology*, 57(2):697–715, 2008.

[147] P. Schreier. Modelling: CAD/CAE: closing the CAD/CAE gap. *Scientific Computing World*, (109):26–29, 2009.

[148] J. A. Cottrell, A. Reali, Y. Bazilevs, and T. J. R. Hughes. Isogeometric analysis of structural vibrations. *Computer methods in applied mechanics and engineering*, 195(41):5257–5296, 2006.

[149] Y. Bazilevs, L. B. Da Veiga, J. A. Cottrell, T. J. R. Hughes, and G. Sangalli. Isogeometric analysis: approximation, stability and error estimates for h-refined meshes. *Mathematical Models and Methods in Applied Sciences*, 16(07):1031–1090, 2006.

[150] Y. Bazilevs, V. M. Calo, Y. Zhang, and T. J. R. Hughes. Isogeometric fluid-structure interaction analysis with applications to arterial blood flow. *Computational Mechanics*, 38(4):310–322, 2006.

[151] J. A. Cottrell, T. J. R. Hughes, and A. Reali. Studies of refinement and continuity in isogeometric structural analysis. *Computer methods in applied mechanics and engineering*, 196(41):4160–4183, 2007.

[152] Y. Bazilevs, V. M. Calo, T. J. R. Hughes, and Y. Zhang. Isogeometric fluid-structure interaction: theory, algorithms, and computations. *Computational Mechanics*, 43(1):3–37, 2008.

[153] J. A. Cottrell, T. J. R. Hughes, and Y. Bazilevs. *Isogeometric Analysis: Toward Integration of CAD and FEA*. Wiley, 2009.

[154] Y. Bazilevs, V. M. Calo, J. A. Cottrell, J. A. Evans, T. J. R. Hughes, S. Lipton, M. A. Scott, and T. W. Sederberg. Isogeometric analysis using T-splines. *Computer Methods in Applied Mechanics and Engineering*, 199(5):229–263, 2010.

[155] T. J. R. Hughes, A. Reali, and G. Sangalli. Efficient quadrature for NURBS-based isogeometric analysis. *Computer methods in applied mechanics and engineering*, 199(5):301–313, 2010.

[156] W. Heylen, S. Lammens, and P. Sas. *Modal Analysis Theory and Testing*. Katholieke Universiteit Leuven, 1997.

[157] R. D'Ippolito, R. Raniolo, M. Olivero, M. Meneguzzo, V. Puleo, S. Donders, and M. Hack. Multi-disciplinary optimization of a vehicle spot weld layout under durability and NVH constraints. In *Proceedings of the International Conference on Noise and Vibration Engineering ISMA 2008*, pages 4111–4126, Leuven, Belgium, September 15–17 2008.

[158] R. R. Craig Jr and M. C. C. Bampton. Coupling of substructures for dynamic analyses. *AIAA Journal*, 6(7):1313–1319, 1968.

[159] R. R. Craig. A review of substructure coupling methods for dynamic analysis. *NASA Langley Res. Center Advan. in Eng. Sci.*, 2, 1976.

[160] R. R. Craig Jr and M. C. C. Bampton. Coupling of substructures for dynamic analyses: an overview. *AIAA Journal*, 6(7):3–14, 2000.

[161] R. R. Craig. A brief tutorial on substructure analysis and testing. In *Proceedings of IMAC XVIII - 18th International Modal Analysis Conference - Computational Challenges in Structural Dynamics*, pages 899–908, San Antonio, Texas, USA, February 7–10 2000.

[162] P. W. Christensen and A. Klarbring. *An Introduction to Structural Optimization*, volume 153. Springer Verlag, 2008.

[163] A. J. G. Schoofs. Structural optimization history and state-of-the-art. In *Topics in applied mechanics: integration of theory and applications in applied mechanics*, page 339, Kerkrade, The Netherlands, November 1992 1993.

[164] R. T. Haftka and Z. Gürdal. *Elements of Structural Optimization*. Springer, 3rd rev. and expanded ed. edition, November 1991.

[165] J. S. Arora, editor. *Optimization of Structural and Mechanical Systems*. World Scientific Pub Co Inc, 2007.

[166] D. H. Wolpert and W. G. Macready. No free lunch theorems for optimization. *IEEE Transactions on Evolutionary Computation*, 1(1):67–82, 1997.

[167] K. Saitou, K. Izui, S. Nishiwaki, and P. Papalambros. A survey of structural optimization in mechanical product development. *Journal of Computing and Information Science in Engineering*, 5(3):214–226, 2005.

[168] R. L. Haupt and S. E. Haupt. *Practical Genetic Algorithms*. Wiley-Interscience, 2 edition, May 2004.

[169] P. E. Gill, W. Murray, and M. H. Wright. *Practical Optimization*. Emerald Group Publishing Limited, January 1982.

[170] C. Bisagni and D. Terletti. Structural optimisation of composite elements of a Formula One racing car. *International Journal of Vehicle Design*, 48(1):149–170, 2008.

[171] C. A. Coello Coello. Theoretical and numerical constraint-handling techniques used with evolutionary algorithms: a survey of the state of the art. *Computer methods in applied mechanics and engineering*, 191(11–12):1245–1287, 2002.

[172] W. R. Spillers and K. M. MacBain. *Structural Optimization*. Springer Verlag, 2009.

[173] C.A. Coello Coello. A short tutorial on evolutionary multiobjective optimization. *Evolutionary Multi-Criterion Optimization*, 1993:21–40, 2001.

[174] R. Kicinger, T. Arciszewski, and K. D. Jong. Evolutionary computation and structural design: A survey of the state-of-the-art. *Computers & Structures*, 83(23):1943–1978, 2005.

[175] V. Plevris and M. Papadrakakis. A hybrid particle swarm-gradient algorithm for global structural optimization. *Computer-Aided Civil and Infrastructure Engineering*, 26(1):48–68, 2011.

[176] F. Duddeck. Multidisciplinary optimization of car bodies. *Structural and Multidisciplinary Optimization*, 35(4):375–389, 2008.

[177] K. J. Craig, N. Stander, D. A. Dooge, and S. Varadappa. Multidisciplinary design optimization of automotive crashworthiness and NVH using LS-Opt. In *7th International LS-DYNA Users Conference*, Dearborn, Michigan, USA, May 19–21 2002.

[178] S. Kodiyalam and J. Sobieszczanski-Sobieski. Multidisciplinary design optimisation – some formal methods, framework requirements, and application to vehicle design. *International journal of vehicle design*, 25(1):3–22, 2001.

[179] S. Kodiyalam, R. J. Yang, L. Gu, and C. H. Tho. Multidisciplinary design optimization of a vehicle system in a scalable, high performance computing environment. *Structural and Multidisciplinary Optimization*, 26(3):256–263, 2004.

[180] R. Padmanaban, R. Krishnan, M. Kayupov, S. Gogate, G. Kalpundi, N. Tumu, T. Wehner, and R. Yarlagadda. Multi-disciplinary optimization of a Sport Utility Vehicle. *SAE paper*, 5, 2004.

[181] J. Sobieszczanski-Sobieski, S. Kodiyalam, and R. Y. Yang. Optimization of car body under constraints of noise, vibration, and harshness (NVH), and crash. *Structural and Multidisciplinary Optimization*, 22(4):295–306, 2001.

[182] F. Duddeck. Multidisziplinäre Optimierung im Produktentwicklungsprozess der Automobilindustrie. In *Proceedings of Weimarer Optimierung-und Stochastiktage*, volume 2, Weimar, Germany, December 1–2 2005.

[183] M. Ohsaki. *Optimization of Finite Dimensional Structures*. CRC Press, July 2010.

[184] L. A. Schmit. Structural design by systematic synthesis. In *Proceedings of the 2nd ASCE Conference on Electronic Computation*, pages 105–122, Pittsburgh, Pennsylvania, USA, September 8–9 1960.

[185] O. Gartmeier and L. W. Dunne. Structural optimization in vehicle development. In *Proceedings of the 1999 MSC Worldwide Automotive Conference*, Munich, Germany, September 20–22 1999.

[186] N. Vanderplaats Garret. Structural optimization for statics, dynamics and beyond. *Journal of the Brazilian Society of Mechanical Sciences and Engineering*, 28(3):316–322, 2006.

[187] S. Dömök, A. Mach, and J. Merk. FE-OPTIM and MSC/NASTRAN for a frequency response optimization. In *MSC Americas Users' Conference*, Universal City, California, USA, October 5–8 1998.

[188] D. C. Lee and J. I. Lee. A structural optimization design for an aluminum-intensive vehicle. *Proceedings of the Institution of Mechanical Engineers, Part D: Journal of Automobile Engineering*, 217(9):771–779, 2003.

[189] J. Riedel. Weight optimization of a cruise liner under stress restrictions. In *Proceedings Weimarer Optimierungs-und Stochastiktage*, Weimar, Germany, 2000.

[190] G. G. Wang and S. Shan. Review of metamodeling techniques in support of engineering design optimization. *Journal of Mechanical Design*, 129(4):1–42, 2007.

[191] R. E. Bellman. *Dynamic Programming*. Princeton University Press, 1957.

[192] S. Donders, M. Brughmans, L. Hermans, C. Liefooghe, H. Van der Auweraer, and W. Desmet. The robustness of dynamic vehicle performance to spot weld failures. *Finite Elements in Analysis and Design*, 42(8–9):670–682, 2006.

[193] Y. Y. Kim and Y. Kim. A one-dimensional theory of thin-walled curved rectangular box beams under torsion and out-of-plane bending. *International Journal for Numerical Methods in Engineering*, 53(7):1675–1693, 2002.

[194] G. E. P. Box and N. R. Draper. *Response Surfaces, Mixtures, and Ridge Analyses*. Wiley-Interscience, 2 edition, March 2007.

[195] M.D. McKay, R.J. Beckman, and W.J. Conover. Comparison of three methods for selecting values of input variables in the analysis of output from a computer code. *Technometrics*, 21(2):239–245, 1979.

[196] D.R. Cox and N. Reid. *The Theory of the Design of Experiments*. Chapman and Hall/CRC, 1 edition, June 2000.

[197] G. E. P. Box and N. R. Draper. *Empirical Model-Building and Response Surfaces*. Wiley, January 1987.

[198] R. Storn and K. Price. Differential evolution - a simple and efficient heuristic for global optimization over continuous spaces. *Journal of Global Optimization*, 11(4):341–359, 1997.

[199] MSC.Software. *MD Nastran 2006 Superelement User's Guide*. MSC.Software, 2006.

[200] M. C. C. Bampton and R. R. Craig Jr. Coupling of substructures for dynamic analyses. *AIAA Journal*, 6(7), 2012.

[201] R. M. Lewis and V. Torczon. A globally convergent augmented Lagrangian pattern search algorithm for optimization with general constraints and simple bounds. *SIAM Journal on Optimization*, 12(4):1075–1089, 2002.

[202] R. E. Bellman. *Dynamic Programming*. Courier Dover Publications, March 2003.

[203] S. Venkataraman and R. T. Haftka. Structural optimization complexity: what has Moore's law done for us? *Structural and Multidisciplinary Optimization*, 28(6):375–387, 2004.

[204] Q. Q. Liang. *Performance-Based Optimization of Structures: Theory and Applications*. Spon Press, 1 edition, November 2004.

[205] H. Adeli and N. T. Cheng. Integrated genetic algorithm for optimization of space structures. *Journal of Aerospace Engineering*, 6(4):315–328, 1993.

[206] H. Adeli and N. T. Cheng. Augmented Lagrangian Genetic Algorithm for structural optimization. *Journal of Aerospace Engineering*, 7(1):104–118, 1994.

[207] C. Camp, S. Pezeshk, and G. Cao. Optimized design of two-dimensional structures using a genetic algorithm. *Journal of Structural Engineering*, 124(5):551–559, 1998.

[208] S. Y. Chen and S. D. Rajan. Improving the efficiency of genetic algorithms for frame designs. *Engineering optimization*, 30(3–4):281–307, 1998.

[209] C. A. Coello Coello, M. Rudnick, and A. D. Christiansen. Using genetic algorithms for optimal design of trusses. In *Proceedings of the 6th International Conference on Tools with Artificial Intelligence*, pages 88–94, New Orleans, Louisiana, USA, November 6–9 1994.

[210] K. Deb. Optimal design of a welded beam via genetic algorithms. *AIAA journal*, 29(11):2013–2015, 1991.

[211] C. K. Dimou and V. K. Koumousis. Genetic algorithms in competitive environments. *Journal of computing in civil engineering*, 17(3):142–149, 2003.

[212] D. E. Grierson and W. H. Pak. Discrete optimal design using a genetic algorithm. *Topology Design of Structures*, 227:89–102, 1993.

[213] P. Hajela and C. Y. Lin. Genetic search strategies in multicriterion optimal design. *Structural and Multidisciplinary Optimization*, 4(2):99–107, 1992.

[214] P. Hajela. Genetic algorithms in automated structural synthesis. *Optimization and artificial intelligence in civil and structural engineering*, 221:639–653, 1992.

[215] P. Hajela. Genetic search - an approach to the nonconvex optimization problem. *AIAA journal*, 28(7), 2012.

[216] J. P. B. Leite and B. H. V. Topping. Improved genetic operators for structural engineering optimization. *Advances in Engineering Software*, 29(7-9):529–562, 1998.

[217] P. Nanakorn and K. Meesomklin. An adaptive penalty function in genetic algorithms for structural design optimization. *Computers & Structures*, 79(29):2527–2539, 2001.

[218] S. Pezeshk, C. V. Camp, and D. Chen. Design of nonlinear framed structures using genetic optimization. *Journal of structural engineering*, 126(3):382–388, 2000.

[219] S. D. Rajan. Sizing, shape, and topology design optimization of trusses using genetic algorithm. *Journal of Structural Engineering*, 121(10):1480–1487, 1995.

[220] S. Rajeev and C. S. Krishnamoorthy. Discrete optimization of structures using genetic algorithms. *Journal of Structural Engineering*, 118(5):1233–1250, 1992.

[221] M. Schoenauer and S. Xanthakis. Constrained GA optimization. In *Proceedings of the 5th International Conference on Genetic Algorithms*, pages 573–580, Urbana-Champaign, Illinois, USA, July 17–21 1993.

[222] B. H. V. Topping and J. P. B. Leite. Parallel genetic models for structural optimization. *Engineering Optimization*, 31(1):65–99, 1998.

[223] S. Das and P. N. Suganthan. Differential evolution: A survey of the state-of-the-art. *Evolutionary Computation, IEEE Transactions on*, 15(1):4–31, 2011.

[224] J. Kilkki, J. Lampinen, and H. Martikka. Applying the differential evolution algorithm to the optimisation of cross sections of steel columns. *Computer Aided Optimum Design of Structures VII*, pages 63–72, 2001.

[225] K. Price, R. M. Storn, and J. A. Lampinen. *Differential Evolution: A Practical Approach to Global Optimization*. Springer, 1 edition, December 2005.

[226] J. Brest, A. Zamuda, B. Boskovic, M. S. Maucec, and V. Zumer. High-dimensional real-parameter optimization using self-adaptive differential evolution algorithm with population size reduction. In *IEEE Congress on Evolutionary Computation CEC 2008.*, pages 2032–2039, Hong Kong, China, June 1–6 2008.

[227] Y. Gao and Y. J. Wang. A memetic differential evolutionary algorithm for high dimensional functions' optimization. In *3rd International Conference on Natural Computation ICNC 2007*, volume 4, pages 188–192, Haikou, Hainan, China, August 24–27 2007.

[228] N. Noman and H. Iba. Enhancing differential evolution performance with local search for high dimensional function optimization. In *Proceedings of the Genetic and Evolutionary Computation Conference*, pages 967–974, Washington DC, USA, June 25–29 2005.

[229] A. K. Qin, V. L. Huang, and P. N. Suganthan. Differential evolution algorithm with strategy adaptation for global numerical optimization. *Evolutionary Computation, IEEE Transactions on*, 13(2):398–417, 2009.

[230] Z. Yang, K. Tang, and X. Yao. Differential evolution for high-dimensional function optimization. In *IEEE Congress on Evolutionary Computation CEC 2007*, pages 3523–3530, Singapore, Singapore, September 25–28 2007.

[231] Z. Yang, X. Yao, and J. He. Making a difference to differential evolution. *Advances in Metaheuristics for Hard Optimization*, pages 397–414, 2008.

[232] Z. Yang, K. Tang, and X. Yao. Large scale evolutionary optimization using cooperative coevolution. *Information Sciences*, 178(15):2985–2999, 2008.

[233] R. Storn. On the usage of differential evolution for function optimization. In *Biennial Conference of the North American Fuzzy Information Processing Society NAFIPS*, pages 519–523, Berkeley, California, USA, June 19–22 1996.

[234] V. Feoktistov. *Differential Evolution: In Search of Solutions*. Springer, 1 edition, October 2006.

[235] K. Zielinski and R. Laur. Parameter adaptation for differential evolution with design of experiments. In *Proceedings of the IASTED International Conference on Computational Intelligence*, pages 212–217, San Francisco, USA, November 20–22 2006.

[236] K. Zielinski and R. Laur. Differential evolution with adaptive parameter setting for multi-objective optimization. In *IEEE Congress on Evolutionary Computation CEC 2007*, pages 3585–3592, Singapore, Singapore, September 25–28 2007.

[237] M. E. H. Pedersen. *Tuning & simplifying heuristical optimization.* PhD thesis, University of Southampton, 2010.

[238] M. E. H. Pedersen. Good parameters for differential evolution. Technical report, Technical report, Hvass Computer Science Laboratories, 2010.

[239] K. Deb. An efficient constraint handling method for genetic algorithms. *Computer methods in applied mechanics and engineering*, 186(2-4):311–338, 2000.

[240] G. P. Liu, J. -B. Yang, and J. F. Whidborne. *Multiobjective Optimisation & Control.* Research Studies Pr, 1st edition, June 2002.

[241] T. S. Kim and Y. Y. Kim. MAC-based mode-tracking in structural topology optimization. *Computers & Structures*, 74(3):375–383, 2000.

[242] J. H. Holland. *Adaptation in natural and artificial systems.* University of Michigan Press, 1975.

Acknowledgments

The bigger part of the research presented in this dissertation has been carried out at the Department of Mechanics and Industrial Technologies, at the University of Florence, during my stay there as a Marie Curie fellow. I was hired as such after winning a fellowship from the VECOM project. Therefore, I want first of all to thank the European Commission for funding the VECOM ITN under the 7^{th} Framework Programme.

This work has been made possible by my tutor Dr. Niccolò Baldanzini, by my ex co-tutor Dr. Alessandro Pratellesi and by the head of our research group Prof. Marco Pierini. Thank you all for believing in me and for helping me constantly on my way to success.

Furthermore, I wish to express my gratitude to Dr. Luc Cremers from BMW AG, who as VECOM partner provided me detailed and concept FE models, as well as valuable technical support.

I would also like to thank Armando Mete, Daniele Catelani and Mauro Linari from MSC Software for their help and tips regarding MD Nastran.

In addition, I want to thank Dr. Manfred Kroiss, Dr. Stijn Donders, Dr. Bert Pluymers and Dr. Antonio Scippa for the technical advice, discussions and exchange of ideas.

I want to express special thanks to my co-workers from Via Rossi who were not merely colleagues, but also my close friends. In particular I want to thank Daniele, Giorgio and Giacomo for their constant technical and moral support.

Last but not least, I want to express my gratitude to my husband Kosta, who supported me online, offline, in person and in all other possible ways during these long years of separation. Without him this work would not have been possible.

Pavlina Brandiska
Sofia, December 2012

Curriculum Vitae

Pavlina Brandiska (maiden name Mihaylova) was born on October 18, 1982 in Sofia, Bulgaria. In 2007 she graduated with a M.Sc. degree in Computer Engineering at the Technical University of Sofia, with a thesis entitled "Software for mathematical optimization with application in Electromagnetics". From 2007 to 2009 she worked as R&D engineer and software integrator at Johnson Controls Electronics Bulgaria, where she was involved in the development of embedded software for the BMW 7 series instrument cluster.

In September 2009 Pavlina won a 3-years Marie Curie fellowship within the VECOM (Vehicle COncept Modeling) Initial Training Network (ITN) and started working as an early stage researcher at the University of Florence. A few months later Pavlina entered the Ph.D. program of the University of Florence, at the Department of Mechanics and Industrial Technologies, under the supervision of Dr. Niccolò Baldanzini. Both her Ph.D. and her work on the VECOM project focused on the concept modeling and optimization of automotive structures. After the end of her fellowship, Pavlina became a freelance engineer. Apart from vehicle concept modeling, her main research interests include numerical optimization, FEM, computer programming.

List of publications

International peer reviewed journal articles

P. Mihaylova, N. Baldanzini, A. Pratellesi, and M. Pierini. Beam Bounding Box – a novel approach for beam concept modeling and optimization handling. *Finite Elements in Analysis and Design*, 60:13–24, 2012.

P. Mihaylova, N. Baldanzini, and M. Pierini. Advanced sizing optimization of concept vehicle structures. Manuscript submitted for publication. *International Journal of Vehicle Design*, 2012.

P. Mihaylova, N. Baldanzini, and M. Pierini. Potential error factors in 1D beam FE modeling for the early stage vehicle design. Manuscript submitted for publication. *Finite Elements in Analysis and Design*, 2012.

Full papers in proceedings of international conferences

P. Mihaylova, N. Baldanzini, A. Pratellesi, and M. Pierini. On the improvement of concept modeling of joints within simplified finite element models with application to structural dynamics. In *Proceedings of the International Conference on Noise and Vibration Engineering ISMA 2010*, Leuven, Belgium, September 20–22 2010.

P. Mihaylova, A. Pratellesi, N. Baldanzini, and M. Pierini. Optimization of the global static and dynamic performance of a vehicle body by means of response surface models. In *ASME 2012 11th Biennial Conference on Engineering Systems Design and Analysis – ESDA2012*, Nantes, France, July 2–4 2012.

P. Mihaylova, N. Baldanzini, and M. Pierini. Considerations on 1D beam concept modelling for the vehicle structure. In *Proceedings of the International Conference on Noise and Vibration Engineering ISMA 2012*, pages 3793–3807, Leuven, Belgium, September 17–19 2012.

Abstracts in proceedings of international conferences

P. Mihaylova, A. Pratellesi, N. Baldanzini, and M. Pierini. Surrogate-based optimization of the global static and dynamic performance of a vehicle body. In *Proceedings of the 8th European Solid Mechanics Conference ESMC2012*, Graz, Austria, July 9–13 2012.